Investigation and Prediction of the Sound Transmission Loss of Plywood Constructions

Robin Richard Wareing

A thesis submitted in fulfilment of the requirements for the degree of:

Doctor of Philosophy

in Mechanical Engineering

at the University of Canterbury

University of Canterbury

Christchurch, New Zealand

2014

Abstract

The sound transmission loss of a range of plywood panels was measured to investigate the influence of the orthotropic stiffness of the plywood panels. The plywood panels were tested as single and also double leaf partitions, with a range of stud configurations. A new method was developed for predicting the sound transmission loss of single leaf partitions with both orthotropic and frequency dependent stiffness values.

The sound transmission loss was evaluated for two significantly different sample sizes. The observed influence of the sample size on the measured sound transmission loss was profound. The construction of the partition was shown to significantly affect the influence of the sample size on the sound transmission loss. A qualitative analysis based on existing published research of the contributing factors is presented, and methods for adjusting the results for the small sample size for comparison with the large results were developed.

The influence of a range of acoustic treatments of lightweight plywood partitions was investigated. The treatments involved internal viscoelastic materials and decoupled mass loaded barriers in various arrangements. The attachment between the treatment and the plywood panel was found to influence the sound transmission loss significantly. A prediction method based on published models was modified to allow the influence of the treatments to be included. Reasonable agreement was achieved between the predicted and measured results for a wide range of samples.

A prediction method was developed that accounts for the influence of orthotropic, frequency dependent material parameters. This method utilised an adaptive, numerical integration method to solve an analytical formulation for the sound transmission loss. The influence of the finite sample size was accounted for using an expression for the finite panel radiation impedance. The finite panel radiation impedance was predicted analytically and an approximation was also presented. The presence of a significant source room niche was accounted for by applying an appropriate limit to the integration range of the angle of incidence.

The prediction methods developed are compared with the measured transmission loss results from both the small and large test facilities. Good agreement was seen for some of the predicted results. Generally the agreement within the coincidence region was worse than for the rest of the transmission loss curve. The inclusion of orthotropic and frequency dependent stiffness values significantly improved the agreement within the coincidence region.

Table of Contents

List of Figures

List of Tables

Variables Used

Symbol	Definition	Units	Notes
τ	Field incidence transmission coefficient	N/A	
τ_d	Diffuse field incidence transmission coefficient	N/A	
$\tau_{\theta=0}$	Normal incidence transmission coefficient	N/A	
$W_{Transmitted}$	Transmitted sound power	w	
$W_{Incident}$	Incident sound power	w	
TL	Field incidence sound transmission loss	dB	
TL_N	Normal incidence sound transmission loss	dB	
TL_d	Diffuse incidence sound transmission loss	dB	
θ	Angle of incidence	deg	
P	Amplitude of pressure wave	Pa	
p	Time dependent pressure	Pa	
ω	Angular frequency	Rad/s	
t	Time	s	
k	Wavenumber	N/A	
x, y	Location	m	
ρ_0	Air density	kg/m^3	1.2004 kg/m^3
c_0	Speed of sound in air	m/s	340 m/s
w	Normal displacement of wall	m	
u	Normal velocity amplitude of wall	m/s	
Z_ω	Mechanical wave impedance	N/A	
C_r	Panel resistance coefficient	N/A	
m, m_1, m_2	Mass per unit area of wall leaves	kg/m^2	
c_f	Velocity of the flexural wave	m/s	
B	Bending stiffness	Pa	
$f_{c(\theta)}$	Coincidence condition	Hz	
f_c	Coincidence frequency	Hz	
f_{cs}	Coincidence frequency in soft direction	Hz	
f_{ch}	Coincidence frequency in hard direction	Hz	
l_x, l_y	Panel lengths	m	
η	Damping loss factor	N/A	
A	Characteristic area of panel	m^2	
θ_l	Limiting angle of incidence	deg	
σ	Single sided radiation efficiency	N/A	
E_x, E_y	Young's modulus in orthotropic directions	Pa	

ϕ	Azimuthal angle	deg	
ϕ_l	Integration limit on azimuthal angle	deg	90°
B_x, B_y	Orthotropic bending stiffness values	Pa	
H	Orthotropic stiffness parameter	Pa	
Γ	Integration constant	N/A	
d	Distance between wall leaves	m	
f_l	Limiting frequency	Hz	
r, r_i	Ratio between excitation frequency and coincidence frequency of (i^{th}) panel	N/A	
b	Stud spacing	m	
α	Absorption coefficient	dB/m	
χ	Modal frequency factor	N/A	
L_b	Length of beam	m	
E_b	Young's modulus of beam	Pa	
ρ_b	Density of beam	kg/m^3	
I_b	Second moment of area of beam	m^4	
w_b	Width of beam	m	
t_b	Thickness of beam	m	
η_b	Damping loss factor of beam	N/A	
ΔBW_{3dB}	Bandwidth of 3 dB down points	Hz	
T_{60}	Reverberation time	s	
I_n	Intensity of pressure wave	w/m^2	
d_I	Distance between intensity probe microphones	m	
u	Particle velocity	m/s	
L_P	Sound pressure level	dB	$20 \times 10^{-6} Pa$
L_I	Sound intensity level	dB	$1 \times 10^{-12} \frac{W}{m^2}$
PI_{index}	Pressure intensity index	dB	N/A
R_{index}	Repeatability index	dB	N/A
$\boldsymbol{k_b}$	Wavenumber in vector format	N/A	(k_x, k_y, k_z)
$\boldsymbol{r}$	Position vector	m	(x, y, z)
$g_\omega(\boldsymbol{r}, \boldsymbol{r}_0)$	Green's function for a point source on an infinite baffle	N/A	
S	Surface of panel for integration	N/A	
κ	Integration transformation variable	N/A	
ς	Integration transformation variable	N/A	
$\boldsymbol{Q}$	Rate of reduction of frequency dependent	Pa/Hz	

	stiffnesses		
β	Wavenumber factor of cavity of double leaf wall	1/m	
$\mathscr{p}$	Variable of convenience	N/A	
$\mathscr{q}$	Variable of convenience	N/A	
$\mathscr{k}$	Variable of convenience	N/A	
l_x	Shortest side length of finite panel	m	
l_y	Longest side length of finite panel	m	
$\mathscr{a}$	Half of shortest side length of finite panel	m	$l_x/2$
$\mathscr{b}$	Half of longest side length of finite panel	m	$l_y/2$

Acknowledgements

I would like to thank my supervisor Dr John Pearse for his support throughout my research. He provided me with a varied and supportive learning environment that allowed me to learn a wide range of new skills and challenged me frequently. Dr Pearse also provided valuable guidance and advice throughout this project.

I would like express my appreciation to Professor John Davy for his immense support and advice throughout this project. He provided me with unmatched technical advice, allowing me to vastly develop my understanding of building acoustics. Our long discussions on my research challenged me to a new level and were invaluable to my research.

To Jeffery Mahn, I greatly appreciated your advice on various aspects of building acoustics. Your knowledge, understanding and kindness were invaluable to me. To Mike Latimer, your assistance via our mutually beneficial projects and experiments was very helpful, furthermore your help with a range of practical problems was of great assistance.

I would like to extend my thanks and gratitude to my family; Angela, Richard and George. Your endless support and reassurance have kept me going throughout this project. You have all believed in me the whole way, even when I was struggling. Our long chats and your visits were a welcome break from my work and kept me going whenever times were tough.

I appreciate the company and friendship of the other members of the Acoustic Research Group. You all added so much fun and excitement to this journey. The discussions we all had about our research added a huge amount to my understanding and were highly enlightening. I wish you all the best in your future endeavours and hope you enjoyed your time studying together as much as I did.

Finally I would like to thank all the great friends I have had the good fortune to know during my time at the University of Canterbury. You are all wonderful people and I have learnt so many things from all of you. You all contributed to this in your own way, and for that I am truly grateful.

1. Introduction

This section presents the aim of the research described within this thesis. The project outline, scope, and facilities are presented and discussed. The novel contributions of the research are also discussed.

1.1. Research Outline

This research assessed the sound transmission loss of lightweight plywood partitions focusing upon the variation in the sound transmission loss as a consequence of the orthotropic nature of plywood. The majority of the existing research is focused on isotropic materials such as steel, concrete or gypsum plasterboard. The research presented in this thesis experimentally examines the acoustic behaviour of plywood, using the intensity method.

This research aimed to first quantify the sound transmission loss of plywood walls using the pressure-intensity method. This experimental data was utilised to develop an analytical model for the sound transmission loss of both single and double leaf wall systems. This resulting model is intended to form the basis for the development of an effective engineering tool.

The sound transmission loss of the plywood in both single and double leaf partitions was measured. The measurements were made in the University of Canterbury's transmission loss test facilities. The results of these measurements allowed an understanding of the behaviour of the orthotropic material to be developed. In conjunction with the sound transmission loss tests the material properties of the plywood were also measured and related to the measured sound transmission loss. The radiation efficiency of the partitions was also measured.

An investigation was made into the effect of the different sample sizes on the measured sound transmission loss. This research also assessed how the sample construction affected the variation caused by the changes in sample size. This was of importance when conclusions were to be made using the results from the small samples.

A number of methods were developed to predict the sound transmission loss of the orthotropic materials using classical models based on the bending wave impedance and the panel wave radiation impedance. The methods developed were compared to current prediction methods in terms of accuracy and computational effort.

Finally two sound transmission loss treatments were tested and evaluated. A decoupled mass loaded barrier was attached to the plywood panels. This system was evaluated and a prediction method was developed for this treatment. Damped plywood panels were constructed by inserting a

layer of viscoelastic material between two 6 mm plywood panels. Single and double leaf partitions constructed from these materials were evaluated. This damped system was tested to evaluate the effects that changes to the system damping had on the sound transmission loss.

1.2. Project Scope

The project was concerned with the airborne sound transmission loss of both single and double leaf partitions. Related aspects of building acoustics, such as flanking and impact noise, were not studied in this research.

1.3. Resources and Facilities

The primary facility utilised was the University of Canterbury's two transmission loss suites. The materials for testing were supplied by Carter Holt Harvey Ltd. and Pyrotek Noise Control. Measurement equipment was supplied by the University of Canterbury along with technical and academic support. Technical and academic support was provided by Professor John Davy.

1.4. Contributions

This section provides an overview of the novel contributions of the work. Several peer reviewed journal articles [1-3] and several conference papers [4-7] have been written, based on the research presented in this thesis. The material presented in these articles forms the basis for the novel contributions presented. Each contribution is briefly discussed below.

1.4.1. Sound Transmission Loss of Orthotropic Materials

The sound transmission loss of lightweight, moderately orthotropic materials has been studied to some extent. Despite this existing research there has not been a comprehensive study performed on the sound transmission loss behaviour of such materials. The research presented here covers a range of configurations which allows conclusions to be developed about the performance of such materials when used in partitions.

1.4.2. Effect of Decoupled Mass Loaded Barriers

The effect of the treatment of plywood panels with a decoupled mass loaded barrier was evaluated as an effective acoustic treatment method. From this evaluation a method for the prediction of the sound transmission loss of the treated systems was developed. Much of this research was presented at an international conference [4] and an associated journal article [2].

1.4.3. Prediction Methods for Orthotropic Materials

Several methods were developed for the prediction of the sound transmission loss of orthotropic single and double leaf partitions, combining the effects of the orthotropic stiffness and the finite radiation impedance. The inclusion of the orthotropic stiffness accounted for some of the transmission loss behaviour measured, and the finite radiation impedance accounted for some of the effects caused by the sample size. It was found that these measures were insufficient to entirely account for the behaviour observed in the measured results.

1.4.4. Influence of Frequency Dependent Stiffness

The stiffness of the plywood was found to depend on the frequency of excitation. A method was developed that allowed this stiffness to be incorporated into the orthotropic prediction scheme. It was found that this frequency dependant stiffness had a large influence on the predicted sound transmission loss, especially around the coincidence region. The frequency dependent stiffness caused a large widening of the coincidence region, often to a greater extent than the orthotropic stiffness.

1.4.5. Effect of Sample Size

The effect of altering the size and construction of a partition was explored. The results of this research was presented in a technical note [3] and a conference paper [5], which investigated the various effects that occur between the different sample sizes used in the two sound transmission loss facilities at the University of Canterbury. Furthermore the influence of several other test parameters was also investigated including the sample location, construction, and the niche effect.

2. Sound Transmission Loss Review

This section provides an overview of relevant research in the field of sound transmission loss. Published work, relevant theories, and published prediction methods are considered. This section provides a basis for the theoretical and experimental work that is presented in this thesis.

2.1. Introduction and Definitions

Sound transmission loss is a measure of the sound attenuation by a partition dividing two spaces and is often referred to as the sound reduction index. The sound transmission loss does not apply to incomplete partitions such as barriers where sound can diffract around the edges. When sound impinges on a partition most is reflected back into the room and some causes excitation of the structure. Of the sound that excites the partition structure some is dissipated within the structure, some is transmitted through the partition and some is transmitted to the surrounding structures. The behaviour of sound incident on a partition is depicted in Figure 2.1.

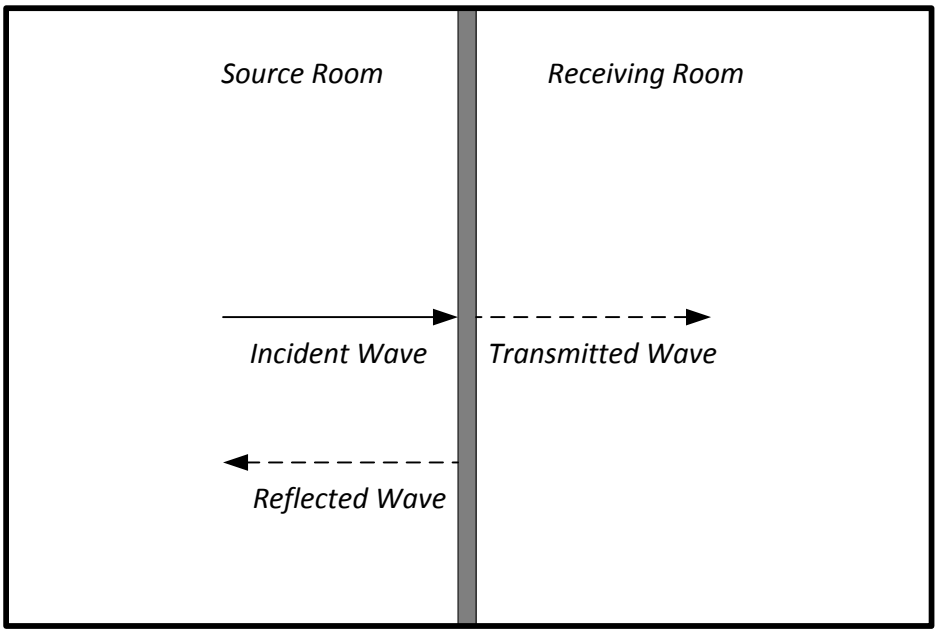

Figure 2.1: Sound transmission through a single leaf partition

The sound transmission coefficient (τ) is defined as the ratio sound power radiated directly receiving room side of the wall ($W_{Transmitted}$) and the sound power impinging on the partition ($W_{Incident}$). This definition allows the transmission coefficient (τ) to be expressed as in Equation 2.1

$$\tau = \frac{W_{Transmitted}}{W_{Incident}} \quad \textbf{2.1}$$

As the sound transmission coefficients are generally very small it is more convenient to use a logarithmic representation. The sound transmission loss (TL) is the representation used and is defined by Equation 2.2.

$$TL = -10 \log_{10} \tau \quad \textbf{2.2}$$

The sound transmission loss is dependent on the angle of incidence (θ) of the incident sound, and the azimuthal angle (ϕ) for non-isotropic materials. These angles are defined below (Figure 2.2)

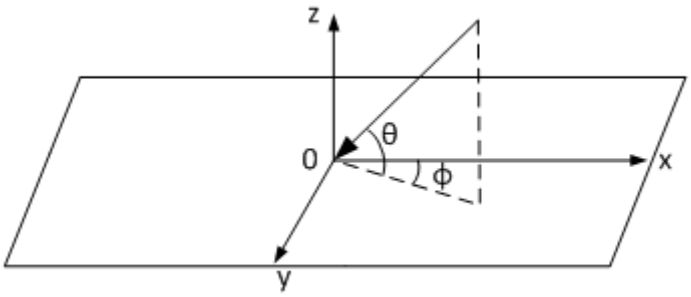

Figure 2.2: Angle of incidence and azimuthal angle

There are three forms of transmission loss that are typically referred to, these are the normal incidence sound transmission loss (TL_N), diffuse field incidence sound transmission loss (TL_d) and field incidence sound transmission loss (TL) [8]. Ideally the diffuse field transmission loss would be measured in all laboratory tests, but this can be limited by the laboratory construction. The location of the panel within the source room, the actual source room design, and the presence of any source room niches can alter the diffusivity of the field incident on the panel. Often, the field incidence transmission loss is closest to that measured in typical sound transmission loss test facilities. In this research, the field incidence transmission loss was measured and prediction models were developed to fit this data.

The normal incidence transmission loss is the transmission loss of a panel exposed to a normally incident plane wave. This normal incidence criterion assumes that the angle of incidence is zero. The normal incidence transmission loss can be expressed as Equation 2.3, where $\tau_{\theta=0}$ is the transmission coefficient at normal incidence.

$$TL_N = -10 \log_{10} \tau_{\theta=0} \quad \textbf{2.3}$$

The diffuse and field incidence transmission losses are calculated by integrating the plane wave transmission loss across a range of angles of incidence. The diffuse field transmission coefficient assumes that the sound incident on the source room side of the samples is completely diffuse, and

as such that waves are incident from 0 to 90 degrees. This is not always the case in reality because effects such as the finite extent of the panel, the presence of a niche, and the non-ideal diffusivity in real reverberation rooms cause deviations from the ideal diffusivity conditions [9]. The field incidence transmission loss accounts for these effects. This requires assumptions about the nature of the incident sound field.

The diffuse field transmission coefficient is given by Equation 2.4. Equation 2.4 can be expressed using a range of different formulations, the three presented below are utilised extensively in this thesis.

$$\tau_d = 2\int_0^{\pi/2} \tau(\theta)\cos\theta\sin\theta\, d\theta = \int_0^1 \tau(\theta) d(\cos^2\theta) = \int_0^1 \tau(\theta) d(\sin^2\theta) \qquad \textbf{2.4}$$

One method of calculating the field incidence transmission coefficient incorporates a limiting angle (θ_l) into the integration to account for the practical limitations of the system and is given by Equation 2.5. Other methods, such as the inclusion of a finite panel radiation impedance, will be discussed in the following sections.

$$\tau_f = 2\int_0^{\theta_l} \tau(\theta)\cos\theta\sin\theta\, d\theta = \int_{\cos^2\theta_l}^1 \tau(\theta) d(\cos^2\theta) = \int_0^{\sin^2\theta_l} \tau(\theta) d(\sin^2\theta) \qquad \textbf{2.5}$$

Section 2.2 presents analytical and empirical methods which can be used to calculate the sound transmission coefficient. The coefficients given by these methods are integrated using Equation 2.5, allowing the transmission loss to be calculated. In some cases this integration can be performed analytically, allowing an “exact” solution to be obtained. In general the integration cannot be achieved analytically; as such the solution is either calculated numerically or via a range of approximations.

A single panel’s sound transmission loss behaviour over a broad frequency range can separated into four main frequency regions [8]. The lowest frequency range is controlled primarily by the stiffness of the panel; this region ends at the first panel resonance. Within this low frequency region the sound transmission decreases towards a minimum at the first panel resonance. This first panel resonance can be calculated from the material properties and boundary conditions of the sample using the equations given in Chapter 18 of [10]. This low frequency sound transmission is also heavily influenced by the physical parameters of both the partition and the spaces around it [11-13]. This is due to the large amount of modal behaviour that can occur between the rooms that the panel is separating [14, 15]. The accurate measurement of sound transmission loss in this frequency range

is also difficult, due to the influence of the room parameters [16] and the limitations of existing measurement methods.

Between the first panel resonance and the critical frequency of the sample lies an intermediate region. This intermediate region is the often referred to as the mass law region as it is primarily controlled by the mass of the sample [17]; within this region the sound transmission loss typically increases at approximately six decibels per octave. Above the critical frequency the system enters a high frequency region where it's transmission loss behaviour is strongly influenced by the damping of the system [8]. This high frequency, damping controlled region typically shows an increase in the sound transmission loss of approximately nine decibels per octave.

Around the critical frequency there is a transitional region which is generally difficult to predict accurately, but there is typically a decrease in the transmission loss within this region. Within this region the panel is close to the grazing incidence coincidence condition. Coincidence occurs when the trace of the incident wave is equal to the wavelength of the bending wave within the partition; causing the partition to transmit sound between the adjacent spaces much more efficiently than the surrounding frequency range, resulting in a coincidence "dip"[17]. The behaviour of infinite and finite panels is very different at the coincidence condition [18, 19], but in both cases the coincidence behaviour results in a significant decrease in the sound insulation. The typical behaviour of a single panel is depicted in Figure 2.3.

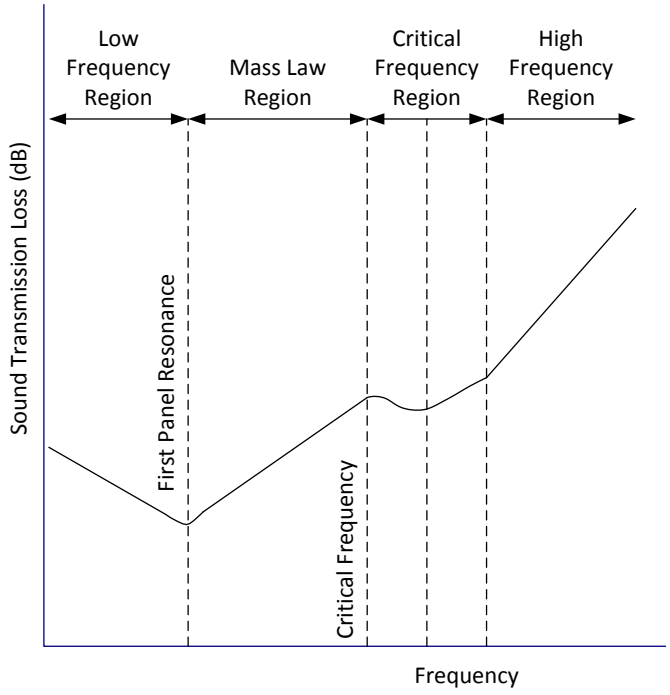

Figure 2.3: Typical sound transmission loss behaviour of single leaf partitions

Double leaf partitions exhibit more complex behaviour due to the interaction of several factors including the individual panels, structural connections (studs), and any absorptive material in the cavity. The behaviour of double leaf systems can be broken down into four broad frequency ranges [8]. The lowest frequency region lies below the mass-air-mass resonance of the double leaf system. This mass-air-mass resonance occurs in the low frequency range when the plates are acting as masses connected via the air cavity which acts like a spring. The mass-air-mass resonance results in a decrease in the sound transmission loss at this frequency [20, 21].

Between the mass-air-mass resonance and the lowest critical frequency of the two leaves is a region in which the sound transmission loss initially increases rapidly at approximately 18 decibels per octave then slows to approximately twelve decibels per octave. As the frequency approaches the lower of the two critical frequencies the transmission loss curve flattens and may decrease near the coincidence frequencies. Finally in the frequency range above the higher of the two critical frequencies the sound transmission loss increases at around 15 decibels per octave. The behaviour of a typical double leaf partition is shown in Figure 2.4 [8, 22].

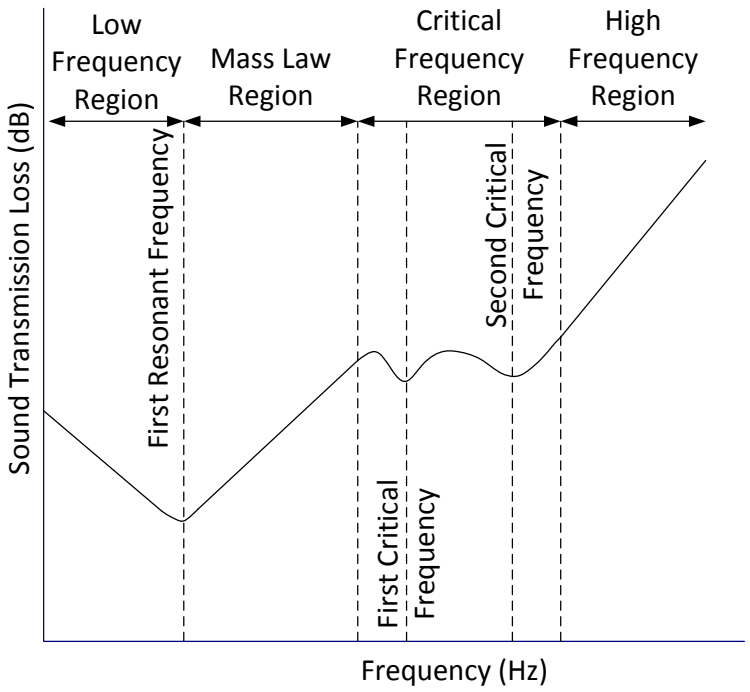

Figure 2.4: Typical sound transmission loss behaviour of double leaf partitions

A large body of work has been undertaken that explores analytical methods for predicting the sound transmission loss: these will be explored in Sections 2.2 – 2.5. Classical methods utilise the equations of motion for the plate and pressure variations in the acoustic mediums on either side to derive analytical equations for the transmission loss. These analytical equations have undergone

significant development with various approximations and correction factors applied in order to achieve better agreement with measured results.

A related technique is the transfer function method. This method is based on a technique initially developed for the prediction of waves through a solid medium [23]. These same techniques were then expanded for use with acoustic waves, focused on the behaviour of ultrasonic waves at interfaces [24, 25] and within layered materials [26]. More recently this method has been used to develop prediction methods for the propagation of sound through different solids and fluids [27, 28].

Finite element modelling techniques have also been applied to a range of both single and double leaf partitions with varying levels of success [29-38]. Computational requirements mean it is difficult to compute transmission loss problems above relatively low frequencies (100 – 500 Hz). As computational power becomes more readily available and affordable it becomes more viable to construct and solve numerical models for addressing the higher frequency behaviour.

Statistical energy analysis is another method for predicting the sound transmission loss of various systems. Statistical energy analysis is a broad topic that has been used for a wide range of applications; some of which are far from the field of building acoustics [39]. The system energy is expressed as a statistical variable, allowing the system to be expressed as weakly coupled oscillators [40, 41]. This was further expanded to include multiple subsystems, all of which could be expressed as weakly coupled oscillators [42]. The calculated energy transfer between these two oscillators can be used to calculate the sound transmission loss of a partition.

The sound transmission loss is commonly measured and usually predicted in one third octave bands. In order to provide a simple comparative measure of the effectiveness of a partition for sound insulation, several single number ratings have been developed. In New Zealand the ratings used are the STC [43] and R_w [44] ratings. Both these ratings use a standard curve that is fitted to the measured sound transmission loss, which yields a single number value for the sound transmission loss of the measured sample. The ISO method (R_w) also allows for the introduction of certain correction factors, C and C_{tr}. The correction factors allow the R_w curve to be adjusted based on the type of incident sound. The single number ratings and associated factors will be discussed in Section 2.6.

2.2. The Analytical Prediction of Sound Transmission Loss

2.2.1. Introduction

The sound transmission loss behaviour of single and double leaf partitions is investigated in this section. Several well-known analytical prediction methods for both single and double leaf partitions are presented. The sound transmission loss of single partitions has been studied extensively, and numerous publications have been presented that investigate aspects of the panel behaviour. In many cases the prediction methods presented are further extended to double leaf partitions. The prediction methods discussed are based on the research presented by London [45], Heckl [46], Sewell [47], Cremer [48], Sharp [22], Davy [49] and various other authors. Each of these models has seen a significant development from the form originally presented, by either the author or subsequent authors.

The transmission coefficient is defined as the ratio between the radiated sound power and the incident sound power (Equation 2.1). The transmission coefficient can be expressed as an equation which is dependent on the angle of incidence and the azimuthal angle of an incoming plane wave. All of the analytical models discussed seek to find an expression for this transmission coefficient and evaluate it in order to calculate the sound transmission loss of the partition.

The simplest prediction models consider a single leaf partition of infinite extent and assume that the panel is thin and that the panel impedance is a pure mass reactance [8, 17]. This results in a prediction model that neglects the effects of stiffness, damping, and the partition size. These models yield the so called “mass law” [50]. The result of this law is that increases in the mass of a partition will increase the sound transmission loss, primarily in the low frequency region where the transmission is forced and follows the mass law reasonably closely. This “mass law” has also been applied to double leaf partitions with less success than single leaf partitions [51, 52].

A double leaf partition will have a higher transmission loss across much of the frequency range than a single leaf partition of equivalent mass due to the presence of the cavity [53-56]. The prediction of the transmission loss of double leaf partitions is more complex than single leaf partitions. This added complexity is due to the addition of a number of factors [57, 58], including the presence of studs [59-61], the cavity [62], any absorptive material in the cavity [63-65], the attachment methodology [66, 67], and other minor factors [68].

The inclusion of stiffness into the prediction methods improved the performance of the models by introducing coincidence behaviour [8, 17] to the model. This results in a significantly better model of the overall system behaviour. The coincidence effect occurs in both single and double leaf

partitions. In double leaf partitions with mismatched leaves there are two different critical frequencies, whereas in matched double leaf partitions the coincidence criteria occurs at the same frequency for both leaves. The further inclusion of the internal damping loss factor allows the behaviour of the system to be predicted at and above the coincidence region; increases the damping loss factor increase the transmission loss in the higher frequency range [69, 70].

Double leaf partitions also exhibit a dip in the sound transmission loss due to a mass-air-mass resonance which occurs when the two partitions interact in a manner that maximises their combined transmission coefficient [20]. When the leaves of the partition are large compared with the gap between them the mass-air-mass frequency is given by Equation 2.6. Sharp did propose in the earlier versions of [22] that the numerator in Equation 2.6 be multiplied by 1.8 to account for the "effective mass" of the panels, which is somewhat less than their actual mass [8]. This correction factor is not utilised in this research.

$$f_0 = \frac{1}{2\pi}\left[\frac{\rho_0 {c_0}^2 (m_1 + m_2)}{d m_1 m_2}\right] \quad \textbf{2.6}$$

where m_1 and m_2 are the panel surface masses, ρ_0 is the density of the air, c_0 is the speed of sound in the air, and d is the cavity depth. Double leaf partitions also possess two further characteristic frequencies [8]; the lowest order acoustic resonance (f_2) and the limiting frequency (f_l). The lowest order acoustic resonance is given by Equation 2.7.

$$f_2 = c_0 / 2L_{cavity} \quad \textbf{2.7}$$

where L_{cavity} is the longest dimension of the cavity. The limiting frequency is given by Equation 2.8.

$$f_l = {}^{c}/_{2\pi d} \approx 55/d \quad \textbf{2.8}$$

This limiting is the lowest cavity resonance divided by π. This represents one-third the resonance frequency of the first acoustic mode in the direction through the cavity. According to Fahy and Gardonio [20], resonant frequencies below this can be effectively suppressed by the presence of cavity absorption.

The original models for the sound transmission of both single and double leaf partitions were based on infinite panels separating two infinite acoustic mediums. This allowed the systems to be evaluated with significantly more ease than would otherwise be the case. Later models incorporated the behaviour of finite panels into the prediction of the sound transmission loss. The alteration from a system of infinite extent to a finite system results in significant changes to the transmission loss

behaviour. Single leaf panels of finite extent have a significantly higher transmission loss than the equivalent infinite panel at low frequencies. This difference is reduced near the coincidence region where both finite and infinite partitions exhibit a similar coincidence dip.

2.2.2. London's Model

London [45] derived a formulation for the transmission coefficient (and transmission loss) of an infinite single leaf partition excited by an incident plane wave. The derivation presented was based on the model first developed by Cremer [17], who expressed the transmission loss of a partition when excited by an incident plane wave. Cremer's derivation expanded the system from a one dimensional system with the partition represented as an inert mass into a two dimensional formulation in which the plate can support bending waves. This derivation allowed an expression to be developed for the coincidence frequency depending on the angle of incidence ($f_{c(\theta)}$), given by Equation 2.9.

$$f_{c(\theta)} = \frac{{c_0}^2}{2\pi \sin^2\theta}\sqrt{\frac{\overline{m}}{B}} \qquad \textbf{2.9}$$

where m is the surface density of the plate, and B is the bending stiffness of the plate. The bending stiffness is related to the Young's modulus (E) via Equation 2.10.

$$B = \frac{Eh^3}{12(1-\nu^2)} \qquad \textbf{2.10}$$

where h is the thickness of the plate, and ν is the Poisson's ratio of the plate. The beginning of the coincidence condition occurs when the waves are at grazing incidence, yielding Equation 2.11 for the minimum frequency (f_c).

$$f_c = \frac{{c_0}^2}{2\pi}\sqrt{\frac{\overline{m}}{B}} \qquad \textbf{2.11}$$

London's expression for the transmission coefficient is averaged over all angles of incidence to yield an average transmission coefficient. The derivation defines the incident plane wave as represented in Figure 2.5.

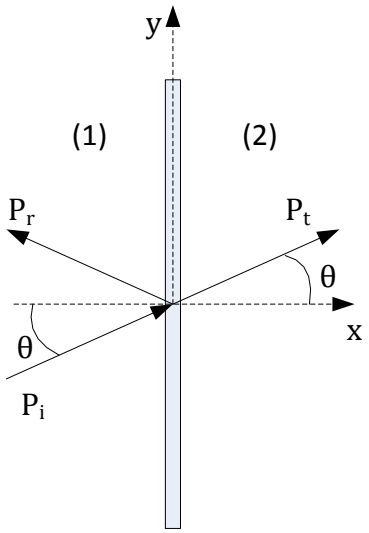

Figure 2.5: Plane wave incident on single leaf partition

The three pressure variables can be represented by Equation 2.12, where k is the wavenumber of the incident wave in air, ω is the frequency in radians, t is the time, x and y are the location variables, P_i is the magnitude of the incident acoustic pressure wave, P_r is the magnitude of the reflected acoustic pressure wave, P_t is the magnitude of the transmitted acoustic pressure wave, and p is the time and position dependent pressure.

$$p_i = P_i e^{i\omega t - ik(x\cos\theta + y\sin\theta)}$$

$$p_r = P_r e^{i\omega t - ik(-x\cos\theta + y\sin\theta)} \qquad \textbf{2.12}$$

$$p_t = P_t e^{i\omega t - ik(x\cos\theta + y\sin\theta)}$$

Two boundary conditions are applied to the system; continuity of particle velocity at the surface of the partition (Equation 2.13), and the relationship between the pressure difference across the partition and the partition motion (Equation 2.14).

$$P_i - P_r = P_t = \frac{\rho_0 c_0 \dot{x}}{\cos\theta} \qquad \textbf{2.13}$$

These boundary conditions allow an expression to be developed for the transmission coefficient, as shown in Equation 2.15.

$$(P_i + P_r) - P_t = Z_\omega \, \dot{x} \qquad \textbf{2.14}$$

$$\tau = \left|\frac{P_t}{P_i}\right|^{-2} = \left|1 + \frac{Z_\omega \cos\theta}{2\rho_0 c_0}\right|^{-2} \qquad \textbf{2.15}$$

where Z_ω is the mechanical wave impedance of the partition, and $\dot{x}$ is the velocity amplitude of the wall in the x-direction. If the wall is assumed to have a mass reactance only, the mechanical wave impedance can be expressed by Equation 2.16.

$$Z_\omega = i\omega m \tag{2.16}$$

This expression for the mechanical wave impedance can be used with Equation 2.15 to yield an expression for the plane wave transmission coefficient. The plane wave transmission coefficient is incorporated into Equation 2.4 for the diffuse field transmission coefficient, yielding Equation 2.17.

$$\tau_d = 2\int_0^{\pi/2} \frac{\cos\theta \sin\theta}{\left|1 + \frac{Z_\omega \cos\theta}{2\rho_0 c_0}\right|^2} d\theta \tag{2.17}$$

This integration provides an expression for the sound transmission loss, as given in Equation 2.18.

$$TL = 10\log_{10}\left[\left(\frac{\omega m}{2\rho_0 c_0}\right)^2\right] - 10\log_{10}\left[\ln\left\{1 + \left(\frac{\omega m}{2\rho_0 c_0}\right)^2\right\}\right] \tag{2.18}$$

This is the random incidence mass law which exhibits poor agreement with the measured sound transmission loss of lightweight partitions. This poor agreement has been shown to be due to the invalid assumption of a pure mass reactance for the velocity of a finite plate [71]. A resistive term can be added to the mechanical impedance (Equation 2.19) that yields a transmission loss coefficient given by Equation 2.20.

$$Z_\omega = \frac{2C_r}{\cos\theta} + i\omega m \tag{2.19}$$

where C_r is a resistance coefficient. This resistance coefficient adds an attenuation to the transmission coefficient; which decreases the effectiveness with which the partition transmits sound as the angle of incidence is increased. This has the effect of reducing the contribution from waves coming from near grazing angles of incidence.

$$TL = 10\log_{10}\left[\left(\frac{\omega m}{2\rho_0 c_0}\right)^2\right] - 10\log_{10}\left[\ln\left\{1 + \left(\frac{\frac{\omega m}{2\rho_0 c_0}}{1 + \frac{C_r}{\rho_0 c_0}}\right)^2\right\}\right] \tag{2.20}$$

The inclusion of the resistive term was found to improve the transmission loss predictions obtained. The resistance coefficient was chosen as an empirical fix to improve the agreement with

measured data. London also discusses the effect of including the flexural waves into the wave impedance. The inclusion of flexural waves was initially presented by Cremer [48] and London [56] showed that it resulted in the plate wave impedance that can be expressed by Equation 2.21.

$$Z_\omega = i\omega m\left[1 - \frac{B\omega^2}{mc_1}\right] = i\omega m\left[1 - \frac{f^2}{f_c^2}\sin^4\theta\right] \qquad \textbf{2.21}$$

where c_1 is the velocity of the flexural wave. Including the resistance coefficient used in Equation 2.19 yields an expression for the transmission coefficient, given by Equation 2.22.

$$\tau_d = 2\int_0^{\pi/2} \frac{\cos\theta\sin\theta}{\left|1 + \frac{2C_r}{\cos\theta} + \frac{i\omega m\cos\theta}{2\rho_0 c_0}\left[1 - \frac{f^2}{f_c^2}\sin^4\theta\right]\right|^2} d\theta \qquad \textbf{2.22}$$

The integral for this expression was found to be non-integrable but could be evaluated numerically. This formulation resulted in better agreement with the measured results, especially around the critical frequency. In London's research both C_r and f_c were chosen to ensure the best fit between the experimental and predicted data. Despite the use of empirical fixes to achieve better agreement this model provided a significant step in the prediction of the sound transmission loss of single leaf partitions.

London used the same method to developed a classical expression for the transmission coefficient of double leaf partitions [55]. This model has formed a basis for many of the subsequent models. The model assumes an infinite two dimensional partition between two infinite spaces. A brief overview of the derivation is presented, with a discussion of the limitations of the developed model.

Figure 2.6 shows the simplified double leaf partition that will be evaluated. It is important to note the absence of cavity absorption and connecting studs. In the derivation presented, the partition is assumed to be of infinite lateral extent.

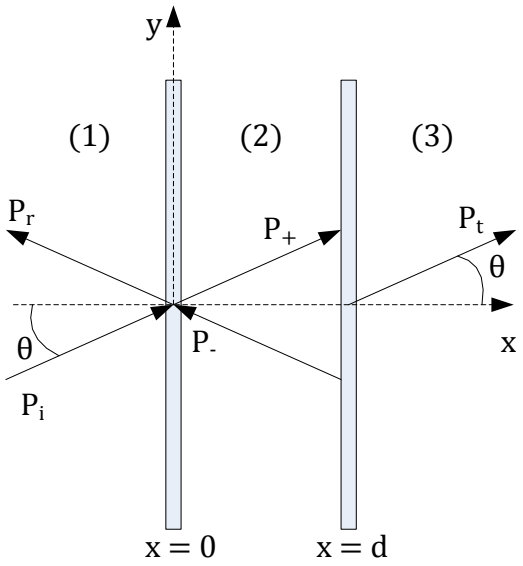

Figure 2.6: Double leaf partition excited by an incident plane wave

where P_+ is the magnitude of the internal acoustic pressure wave in the positive direction and P_- is the magnitude of the internal acoustic pressure wave in the negative direction.

Three separate acoustic spaces exist; the source room side, the cavity between the two panels, and the receiving room side. An equation can be derived for the acoustic pressure within each of these spaces, as presented in Equation 2.23.

$$\begin{aligned} p_1 &= P_i e^{i\omega t - ik(x\cos\theta + y\sin\theta)} + P_r e^{i\omega t - ik(-x\cos\theta + y\sin\theta)} && x \le 0 \\ p_2 &= P_+ e^{i\omega t - ik(x\cos\theta + y\sin\theta)} + P_- e^{i\omega t - ik(-x\cos\theta + y\sin\theta)} && 0 \le x \le d \\ p_3 &= P_t e^{i\omega t - ik(x\cos\theta + y\sin\theta)} && x \ge d \end{aligned} \qquad \textbf{2.23}$$

where the x direction is perpendicular to the panels. Of interest is the ratio $|P_t/P_i|$ which again represents the transmission coefficient of the partition. To evaluate this ratio a number of conditions are applied to the system to solve the corresponding equations. Continuity or boundary conditions are applied at each leaf of the partition. The gradient of the pressure at the surface of each leaf must be equal on either side of the partition; this is represented by Equations 2.24 and 2.25.

$$\left(\frac{\partial p_1}{\partial x}\right)_{x=0} = \left(\frac{\partial p_2}{\partial x}\right)_{x=0} \qquad \textbf{2.24}$$

$$P_i - P_r = P_+ - P_-$$

$$\left(\frac{\partial p_1}{\partial x}\right)_{x=d} = \left(\frac{\partial p_2}{\partial x}\right)_{x=d} \qquad \textbf{2.25}$$

$$P_+ e^{-ikd\cos\theta} - P_- e^{ikd\cos\theta} = P_t e^{-ikd\cos\theta}$$

Furthermore equations of motion can be developed for each panel, based on the pressure on either side (p_{1x}, p_{2x}) and the mechanical impedance of the partition (Z_ω). The equations of motion of the partition are presented in Equations 2.26 and 2.27.

$$p_{1(x=0)} - p_{2(x=0)} = Z_{\omega 1}\dot{x}_{x=0} \quad \textbf{2.26}$$

$$p_{2(x=d)} - p_{3(x=d)} = Z_{\omega 2}\dot{x}_{x=d} \quad \textbf{2.27}$$

Finally the normal partition velocity must be the same as the particle velocity on the panel surface, thus allowing Equation 2.28 and 2.29 to be developed.

$$\dot{x}_{x=0} = \frac{i}{\rho\omega}\left(\frac{\partial p_1}{\partial x}\right)_{x=0} = \frac{\cos\theta}{\rho c}(P_i - P_r)e^{i\omega t - iky\sin\theta} \quad \textbf{2.28}$$

$$\dot{x}_{x=d} = \frac{i}{\rho\omega}\left(\frac{\partial p_1}{\partial x}\right)_{x=d} = \frac{\cos\theta}{\rho c}P_t e^{i\omega t - ik(d\cos\theta + y\sin\theta)} \quad \textbf{2.29}$$

Assuming that the leaves are a pure mass reactance only; as defined earlier by Equation 2.16; an expression for the plane wave transmission coefficient can be derived.

$$|\tau|^2 = \left|\frac{P_i}{P_t}\right|^{-2}_{Z_{\omega=i\omega m}} = \frac{1}{1 + 4\left(\frac{\omega m}{2\rho_0 c_0}\right)^2 \cos^2\theta \times \left(\cos\mathcal{B} - \left(\frac{\omega m}{2\rho_0 c_0}\right)\cos\theta\sin\mathcal{B}\right)} \quad \textbf{2.30}$$

where $\mathcal{B}$ is given by the equation below.

$$\mathcal{B} = kd\cos\theta \quad \textbf{2.31}$$

The diffuse field transmission coefficient may then be calculated by integrating the plane wave incidence coefficient across the range of all possible incidence angles.

London compared the results of this calculation using several different experimental partitions. The systems tested had no mechanical ties between the two leaves and as such the sound transmission path between the two leaves was airborne. It was found that the predicted data agreed reasonably well with the measured data in the low frequency range (below 500 Hz). Above this frequency the predicted results deviated significantly from the measured results. It was also shown that the results of the prediction method were heavily dependent on the limiting angle of incidence applied during the integration of the transmission coefficient. This same limiting angle had a significant effect on the predicted single leaf partition transmission loss.

2.2.3. Sewell's Model

Sewell [47] developed a model for the prediction of the sound transmission loss of a single panel of finite extent. Sewell provided a detailed treatment of the transmission loss problem, which considered a panel of size $2l_{\mathrm{h}} \times 2l_{\mathrm{v}}$ surrounded by a rigid baffle of infinite extent. A brief overview of the derivation is presented, along with the resulting expression for the transmission coefficient.

In the case of an infinite panel there is no resonant transmission. This is because resonant transmission is controlled by the presence of edges in a system. Fahy [20] presents a simple explanation of this behaviour using the one dimensional case. The one dimensional case is reproduced in Figure 2.7 and Figure 2.8. The half pairs of positive and negative motions result in a cancellation of the radiated sound as they are 180 degrees out of phase. Only regions at the edges are not directly paired; for symmetric modes the edge components combine whereas for anti-symmetric modes the edge components cancel. Thus for resonant transmission to occur there must be edges or discontinuities present in the panel.

Figure 2.7: Symmetric mode of vibration of one dimensional plate (*This figure has been reproduced from Fahy* [20])

Figure 2.8: Anti-symmetric mode of vibration of one dimensional plate (*This figure has been reproduced from Fahy* [20])

The excitation of the panel by incident sound will result in the excitation of lower order modes by the sound at higher frequencies [8]. The excited modes are forced to vibrate at frequencies higher than their resonance frequency, resulting in forced sound transmission. The vibration of the panel is dominated by resonant vibration which radiates sound inefficiently.

The normal functions associated with bending vibrations within the panel satisfy Equation 2.32, and the appropriate boundary conditions.

$$\nabla_2^4 w_n = g_n^4 w_n \qquad \textbf{2.32}$$

Where w_n is the surface velocity of the panel and g_n is the greens function associated with the panels response.

Further conditions are imposed in order to derive the equation for the acoustic pressure. The normal velocity of the fluid particle is assumed to be equal to that of the panel at the surface, and

equal to zero at the surface of the baffle. Furthermore the pressure in the fluid (p) is required to satisfy Equation 2.33.

$$\nabla^2 p + k^2 p = 0 \qquad \textbf{2.33}$$

This allows the pressure distribution to be described by Equation 2.34 .

$$p(x,y,z) = \begin{cases} 2\mathrm{e}^{(ik_x x + ik_z z)} \cosh k_x x - p^+(-x,y,z) & \text{for } x < 0 \\ p^+(x,y,z) & \text{for x} > 0 \end{cases} \qquad \textbf{2.34}$$

This equation can be utilised to derive the exact sound transmission coefficient. Equation 2.35 gives the exact transmission coefficient of a finite panel in an rigid infinite baffle.

$$\tau_f = \{4\pi/(Ak^2)\}\mathrm{Tr}\left(\boldsymbol{Z^{-1}RZ^{*-1}R}\right) \qquad \textbf{2.35}$$

where A is the area of the panel, $\boldsymbol{Z}$ the impedance matrix of the panel and $\boldsymbol{R}$ is a matrix of coefficients. This calculation can be simplified by ignoring the non-diagonal elements of $\boldsymbol{Z}$ dramatically simplifying the inverse problem. Only considering the forced vibration through the partition yields a further expression for the transmission coefficient (Equation 2.36).

$$\tau_f = \Omega^2\left[\ln\left(k\sqrt{A}\right) + 0.160 - U(\Lambda) + 1/(4\pi k^2 A)\right] \qquad \textbf{2.36}$$

where Ω is given by Equation 2.37, $U(\Lambda)$ is given by Equation 2.38, and Λ is the ratio between the two edge lengths l_x/l_y.

$$\Omega = \left[\frac{2\pi f \omega}{2\rho_0 c_0}\right]\left[1 - \frac{f^2}{f_c^2}\right] \qquad \textbf{2.37}$$

$$U(\Lambda) = U(1/\Lambda) = \frac{1}{2\pi}\left(\Lambda + \frac{1}{\Lambda}\right)\ln(1+\Lambda^2) - \left(\frac{1}{2} + \frac{\Lambda}{\pi}\right)\ln\Lambda - \frac{1}{\pi} \qquad \textbf{2.38}$$

Equation 2.36 can be approximated by Equation 2.39.

$$\tau_f = \Omega^2 \ln(\sec^2\theta_L) \qquad \textbf{2.39}$$

where,

$$\sec^2\theta_L = k\sqrt{A} \qquad \textbf{2.40}$$

Equation 2.36 was shown to yield transmission loss measurements that achieved reasonably good agreement with experimental results. This agreement was only seen in the region below the coincidence frequency. This is due to the fact that the model presented only accounts for forced vibrations within the panel. The inclusion of the resonant contribution was shown to improve the performance at higher frequencies.

2.2.4. Sharp's Model

Sharp published two articles that developed a sound loss prediction method that expands on the model presented in Section 2.2.2 [22, 72]. The original analytical model was found to suffer poor agreement with measured results. A limiting angle of incidence was applied to the integration of the transmission coefficient to force the predictions to achieve better correlation with the measured results. At the time of the initial publication the limiting angle was set to a value between 75° and 85°. This limit was justified by assuming that the sound incident on the source side was not equal across all angles of angles of incidence and that little energy comes from grazing angles of incidence. At the time of publication there was little experimental evidence to support this theory.

Sharp develops a pair of equations that can be used to predict the sound transmission loss of double leaf partitions. The frequency range below the one half of the critical frequency is calculated using Equation 2.41, from [73].

$$TL = 20\log(mf) - 48 \qquad \textbf{2.41}$$

Above the critical frequency Equation 2.42 is used, which was initially presented by Cremer [17]. This formula introduces the damping loss factor (η) as this has a significant influence on the sound transmission loss above the critical frequency.

$$TL = 20\log\left(\frac{2\pi fm}{2\rho_0 c_0}\right) - 20\log\left(\frac{2\eta 2\pi f}{\pi 2\pi f_c}\right) \qquad \textbf{2.42}$$

Equation 2.41 and Equation 2.42 are combined using a piecewise approach. The intermediate frequency range, between one half of the critical frequency and the critical frequency, is approximated using a straight line between the two calculated values. The formulation provides a relatively simple expression for the sound transmission loss that has been shown to give reasonable comparisons with experimental data. The correlation near the coincidence frequency is often poor due to the straight line approximation.

Sharp also presented a method for predicting the sound transmission loss of a double leaf partition in his 1973 publication [72]. The frequency range was separated into three sections using

the mass-air-mass resonance frequency (f_0) and the limiting frequency (f_l). The simplified model is presented in Equation 2.43.

$$TL = \begin{cases} TL_M & f < f_0 \\ TL_{m_1} + TL_{m_2} + 20\log(fd) - 29 & f_0 < f < f_l \\ TL_{m_1} + TL_{m_2} + 6 & f > f_l \end{cases} \quad \textbf{2.43}$$

where TL_M is the transmission loss for a panel of mass, $M = m_1 + m_2$, and m_1, m_2 are the individual panel surface masses. Correspondingly TL_{m_1} and TL_{m_2} are the predicted transmission losses for the individual panels. The mass-air-mass and limiting frequency were defined in Equations 2.6 and 2.8. This method was shown to give reasonable agreement with measured results when the cavity is filled with absorbing material. A major limitation in this model is that it does not account for structural coupling between the panels. Sharp also provided a formula for the sound transmission via point and line connections. These formulas provided reasonable agreement with measured results for double leaf wall systems.

2.2.5. Davy's Model

A comprehensive sound transmission loss model was developed by Davy via adaptation of Cremer's model. The initial development of Davy's model was presented in 1990 [49], in the following eight years several papers [60, 74-78] developed a theoretical model for the prediction of sound transmission loss of partitions. These models were focused on the prediction of the sound transmission loss of double leaf partitions but several also considered single leaf partitions.

As described in Section 2.2.4 the inclusion of a limiting angle of incidence on the integration of the sound transmission coefficient yields significantly better agreement between predicted and experimental results. Davy refined the justification for the implementation of this limiting angle; this was achieved by assessing the behaviour of a finite plate. This only applies to the resonant vibration. The forced sound waves are efficient radiators, but their radiation efficiency depends on the size of the panel in terms of the wavelength.

An expression for the limiting angle is derived from Sewell's work on finite plates (see Section 2.2.3). The expression for the limiting angle is given by Equation 2.44; this is applied to the transmission coefficient across the frequency range of interest.

$$\cos^2\theta_l = \begin{cases} 0.9 & \text{if } \dfrac{1}{k\sqrt{A}} > 0.9 \\ \dfrac{1}{k\sqrt{A}} & \text{if } 0.9 \geq \dfrac{1}{k\sqrt{A}} \end{cases} \quad \textbf{2.44}$$

where A is the area of the panel and k is the wavenumber of the incident wave.

The application of this variable limiting angle improved the correlation between predicted and measured results. A further publication by Davy [77] provided a more detailed development of a model for predicting the sound transmission of a single leaf partition via the application of a single sided radiation efficiency approach. This prediction also allowed for the inclusion of a shear wave correction for the prediction of thicker walls. The dependence on the limiting angle of incidence was removed as it was accounted for via the application of the single sided radiation efficiency. The single sided radiation efficiency was incorporated into the transmission coefficient using Equation 2.45.

$$\tau_d = 2\int_0^{\pi/2} \frac{\tau(\theta)}{\sigma(\theta)} \sin\theta \, d\theta \qquad \textbf{2.45}$$

where $\tau(\theta)$ is given by Equation 2.46 and $\sigma(\theta)$ is the single sided radiation efficiency of the partition.

$$\tau(\theta) = \left| 1 + \frac{Z_\omega(\theta)}{2\rho_0 c_0 \sigma(\theta)} \right|^{-2} \qquad \textbf{2.46}$$

The bending wave impedance utilised in this prediction method is given by Equation 2.47, and was presented by Cremer [17].

$$Z_\omega(\theta) = m\omega \left[j\left(1 - \left(\frac{\omega}{\omega_c}\right)^2 \sin^4\theta \right) + \eta \left(\frac{\omega}{\omega_c}\right)^2 \sin^4\theta \right] \qquad \textbf{2.47}$$

Following the derivation presented in the paper yields an expression for the diffuse field transmission coefficient, as given by Equation 2.48.

$$\tau_d = \frac{\sigma^2(\theta_c)}{2\left(\frac{\omega m}{2\rho_0 c_0}\right)\left(\frac{\omega}{\omega_c}\right)\left(\sigma(\theta_c) + \left(\frac{\omega m}{2\rho_0 c_0}\right)\eta\right)} \left\{ \arctan\left[\frac{2\left(\frac{\omega m}{2\rho_0 c_0}\right)}{\left(\sigma(\theta_c) + \left(\frac{\omega m}{2\rho_0 c_0}\right)\eta\right)} \right] - \arctan\left[\frac{2\left(\frac{\omega m}{2\rho_0 c_0}\right)\left(1 - \left(\frac{\omega}{\omega_c}\right)\right)}{\left(\sigma(\theta_c) + \left(\frac{\omega m}{2\rho_0 c_0}\right)\eta\right)} \right] \right\} \qquad \textbf{2.48}$$

where η is the damping loss factor of the partition.

Below the critical frequency some modifications are made to the prediction of the transmission coefficient. The bending wave impedance is modified to be purely a mass reactance (Equation 2.16). The diffuse field transmission coefficient can be solved with this bending wave impedance, yielding Equation 2.49.

$$\tau_d = \frac{2\langle\sigma\rangle}{\left(\frac{\omega m}{2\rho_0 c_0}\right)^2} \tag{2.49}$$

where $\langle\sigma\rangle$is the single sided radiation efficiency integrated across all angles of incidence; as given by Equation 2.50.

$$\langle\sigma\rangle = \int_0^{\pi/2} \sigma(\theta)\sin\theta\, d\theta$$
$$= \ln\left(\frac{1+\sqrt{1+q^2}}{p+\sqrt{p+q^2}}\right) + \frac{1}{a}\ln\left(\frac{k+\sqrt{k+q^2}}{p+\sqrt{p^2+q^2}}\right) \tag{2.50}$$

where p, q, k and a are calculated using the Equations 2.51 – 2.54. The values of the constants, $\mathcal{W}$ and $\mathcal{B}$ in the equations are set to achieve the best possible agreement with the numerical calculations undertaken by Sato [79]. The values used by Davy are: $\mathcal{W} = 1.3$ and $\mathcal{B} = 0.124$.

$$p = \begin{cases} \mathcal{W}\sqrt{\dfrac{\pi}{2k\left(\frac{\omega m}{2\rho_0 c_0}\right)}} & \text{if } \mathcal{W}\sqrt{\dfrac{\pi}{2k\left(\frac{\omega m}{2\rho_0 c_0}\right)}} \le 1 \\ 1 & \text{if } \mathcal{W}\sqrt{\dfrac{\pi}{2k\left(\frac{\omega m}{2\rho_0 c_0}\right)}} \ge 1 \end{cases} \tag{2.51}$$

$$k = \frac{1}{\frac{2}{3}\sqrt{\frac{2k\left(\frac{\omega m}{2\rho_0 c_0}\right)}{\pi}} - \mathcal{B}} \tag{2.52}$$

$$a = \frac{k}{p} - 1 \tag{2.53}$$

$$q = \frac{2\pi}{k^2 S} \tag{2.54}$$

Shear wave effects can be included using Heckl and Donner's correction [80]. This can be applied by calculating a "corrected" wavenumber for the free bending wave. The derivation of this correction is not shown here as it is intended for very thick single leaf partitions.

The model developed by Davy achieves good agreement with the experimental results presented. Removing the reliance on a fixed limiting angle of integration removes an empirical correction from the original model.

Davy's double leaf partition model was developed alongside the single panel model described in Section 2.2.5. The model presented in this section is the result of several years of development presented in a number of publications. The initial publication presented a method for predicting the sound transmission loss of double leaf partitions lined with thin lightweight panels [49]. Research presented in several subsequent publications [60, 74-76, 78] attempted to rectify some of the issues with the original models. The aim of these publications was to achieve better agreement with experimentally measured values.

Initially a method was presented for predicting the air-borne transmission across the cavity, with no considerations for the stud-borne transmission. The stud-borne transmission was treated separately. The method derived by Mulholland [81] is utilised, and following some algebra an expression for the airborne sound transmission loss can be derived. The prediction method is a piecewise function that uses Equation 2.55 for the frequency between the mass-air-mass and the lowest critical frequency of the two leaves.

$$\tau = \frac{1 - \cos^2 \theta_l}{(q_D + p_D \cos^2 \theta_l)(q_D + p_D)} \qquad \textbf{2.55}$$

where p and q are variables utilised for convenience and are given by Equations 2.56 and 2.57. The limiting angle of incidence (θ_l) was set to 61.4 in Davy's 2009 paper [77].

$$q_D = \frac{1}{2}\left(\frac{m_2}{m_1} + \frac{m_1}{m_2}\right) \qquad \textbf{2.56}$$

$$p_D = \left(\frac{2\pi f m_1}{2\rho_0 c_0}\right)\left(\frac{2\pi f m_2}{2\rho_0 c_0}\right)\alpha \qquad \textbf{2.57}$$

Above the lower of the two critical frequencies a separate equation is used, as given by Equation 2.58.

$$\tau = \frac{\pi(\xi_1 + \xi_2)\mathrm{n}}{4\mathrm{B}_1^2\mathrm{B}_2^2\eta_1\eta_2\xi_1\xi_2(\mathrm{n}^2 + \mathrm{v}^2)\alpha^2} \qquad \textbf{2.58}$$

where B_i, ξ_i, n, and v are also variables used for convenience and are given by Equations 2.59 – 2.62. The sound absorption coefficient of the cavity is α.

$$B_i = \frac{\omega m_i}{2\rho_0 c_0} \quad \textbf{2.59}$$

$$\xi_{\mathrm{i}} = \sqrt{\frac{\omega}{\omega_c}} \quad \textbf{2.60}$$

$$\mathrm{n} = \eta_1 \xi_1 + \eta_2 \xi_2 \quad \textbf{2.61}$$

$$\mathrm{v} = 4(\xi_1 - \xi_2) \quad \textbf{2.62}$$

These equations are combined with a prediction method for the stud-borne transmission, given by Equation 2.63.

$$\tau = \frac{64\rho_0 c_0 D}{[\mathrm{g}^2 + (4\omega^{3/2} m_1 m_2 c \mathrm{C}_M - \mathrm{g})^2]\mathrm{h}\omega^2} \quad \textbf{2.63}$$

where b is the stud spacing, g and h are given by Equations 2.64 and 2.65.

$$\mathrm{g} = m_1 \omega_{c2}^{1/2} + + m_2 \omega_{c1}^{1/2} \quad \textbf{2.64}$$

$$\mathrm{h} = \left[1 - \left({}^{\omega}/_{\omega_{c1}}\right)^2\right]\left[1 - \left({}^{\omega}/_{\omega_{c2}}\right)^2\right] \quad \textbf{2.65}$$

This theory achieves reasonable agreement with the experimental results presented. Although it is noted that significant modifications are required to improve the model's agreement in a wider variety of partitions.

The later articles [75, 77] presented a number of changes to this prediction method. Above the critical frequency the integral format of the transmission coefficient is approximated by extending the range of integration from $-\infty$ to ∞. The presented high frequency model is also utilised as a correction below the critical frequency.

The changes made to the prediction method dramatically improve the agreement with experimentally measured results. An approximation was developed which allows the effective absorption of the empty cavity to be calculated. The approximations were different for the materials tested, with Equation 2.66 representing the absorption of the cavity of a double glazed glass system and Equation 2.67 representing the absorption coefficient of an unfilled gypsum plasterboard partition cavity.

$$\alpha = 0.027 + 2.4d \quad \textbf{2.66}$$

$$\alpha = 0.043 + 0.73d \quad \textbf{2.67}$$

There are no tabulated results providing a similar result for plywood partitions, but it is assumed that they will behave in a similar manner to the gypsum plasterboard partitions.

2.2.6. Other Relevant Work

Several other authors have also presented research focused on the prediction of sound transmission loss behaviour. Some of the findings from this literature review are discussed and the theories behind some of the other prediction methods are presented.

Recent publications by Tadeu *et al.* [53, 54, 82, 83] explored the accuracy of various prediction models when predicting the sound insulation of glass, ceramic and concrete partitions with various constructions. Initially a simple analytical equation was applied to predict the sound transmission loss of single, double and triple glazed windows [54]. In this research it was found that the analytical models did not accurately model the behaviour of many of these systems. A later article [82] explored the effectiveness of an alternative analytical model and compared it with the mass law. The model developed was used to evaluate a partition excited by plane waves; this yielded significant variations from the experimental data. Better agreement was seen between the experimental and theoretical results in a further analytical model [83].

Bradley and Birta [84] presented a model for predicting the sound insulation of gypsum plasterboard panels mounted on resilient supports. The model was limited to the prediction of sound transmission in the lower frequency range. This model was empirically tuned to fit the measured data; once this tuning was completed the model was able to predict incremental effects of the addition of resilient channels. This model is very specific to the partition being tested but could be altered to fit other experimentally tested systems. The model shows the significant influence of the stiffness of the studs when the partition has a large cavity depth. This is because the cavity is the dominant transmission path when the cavity is shallow.

A progressive impedance method was developed by Fringuellino and Guglielmone [85]. This was based on the methods presented by Beranek and Work [51], and Mangiarotty [86]. Beranek and Work presented a method for predicting the sound insulation of multi-layer structures lined with flexible blankets. This was modelled using a set of impedances describing the air-panel impedances. Mangiarotty used a similar method to optimise a multi-layered panel system, but did not compare the calculated results with experimental measurements. The more recent work by Fringuellino and

Guglielmone built a system by combining two types of layers; propagative layers and non-propagative layers. In the case of propagative layers the solution to the wave equation is a stationary plane acoustical pressure wave, whereas in the non-propagative layers a continuity of the normal component of the particle velocity is required. The impedance for each of these layers allows the ratio between the incident and transmitted pressures to be evaluated using Equation 2.68.

$$\frac{p_{in}}{p_t} = \frac{p_{in}}{p_N} \cdot \frac{p_N}{p_{N-1}} \cdots \frac{p_1}{p_t} \qquad \textbf{2.68}$$

where p_{in} is the incident pressure, p_t is the transmitted pressure and $p_{n=1:N}$ is the pressure within each layer modelled. The ratios between the adjacent pressures can be evaluated using the ratio of adjacent impedances. This allows an equation to be built which represents the incident to transmitted powers, which can be used to calculate the sound transmission loss. The expression derived via this method is dependent on the angle of incidence and is thus integrated across the possible angles of incidence to calculate the field incidence transmission coefficient. Fringuellino and Guglielmone [85] showed that this prediction scheme overestimated the sound transmission loss from experimental data by approximately seven decibels across much of the frequency range evaluated. This was concluded to be due to the limitations of the model, such as the infinite baffle and the infinite edge constraints.

Mulholand *et al.* presented a number of articles which developed prediction methods for infinite and finite multi-leaf partitions. Two articles present the development of a model for double leaf partitions of infinite [81] and finite extent [87]. The infinite model achieved reasonably good agreement when the correct reflection coefficient within the cavity was selected. The use of a reflection coefficient replaces London's [55] "R" term which lacked a clear physical explanation. The finite extent of the double leaf partition is accounted for by adding a sound absorbing boundary to the internal surface of the panel. This causes the internally reflected waves to be "damped" out as they are reflected back and forth within the cavity. This method also requires a value for the surface absorption coefficient to be chosen in order to make the prediction match the measured data.

Two further articles by Mulholand *et al.* explored the application of similar techniques for other multi-layered systems. The transmission loss of a partitions at oblique incidence [88] was derived based on the work of Beranek and Work [51]. The model developed was applied to single leaf partitions, and then to double sandwich panels with impervious septa on the surfaces of the material layers. This publication did not provide a comparison with experimental results as the solution derived required numerical evaluation. Another publication investigated the optimal cavity depth for double and triple leaf partitions [89]. A number of experimental tests were utilised to

evaluate the effects of cavity depth on double and triple leaf partitions. It was found that in general increasing the cavity depth increases the sound transmission loss but some variations can occur. The addition of a third leaf was found to increase the sound transmission loss of the partition at high frequencies.

Several authors have developed methods that use a statistical energy analysis to predict the sound transmission loss behaviour of a range of building elements. Statistical energy analysis represents the transmission loss system as a collection of coupled systems; for example the source room can be represented as system one, the wall can be system two, and the receiving room can be system three [90]. The coupling between these systems is derived based on the radiation efficiency of the elements. This system can then be solved to predict the sound transmission loss of the wall. This representation can be further expanded to incorporate more rooms or walls, and the flanking behaviour between building elements [91, 92].

It has been found that there are four main approaches for predicting the sound transmission loss of systems. These are analytical methods, transfer matrix methods, statistical energy analysis methods (which are related to analytical methods), and finite element modelling. Research presented by Hongisto [93] evaluated the effectiveness of 17 commonly used prediction methods. Hongisto took these prediction models from several different authors. The aim of the investigation was to assess if the models performed as well as claimed on a number of different systems. It was found that all of the models investigated did not perform as well as claimed in the original papers. This research also noted that Davy's model was the only one that could predict the sound transmission loss of the four different systems evaluated. This evaluation indicated that the understanding of the sound transmission loss behaviour of double leaf partitions is still incomplete and an improved generalised model is required.

2.3. Transfer Matrix Methods

Transfer function methods were initially developed for modelling the transmission of elastic waves through a medium. Thomson [23] presented the development of a method for modelling the transmission of an elastic plane wave within a stratified solid medium. A set of transfer matrices were utilised to simplify the calculations required. This method was readily applied to the propagation of seismic waves in the earth's crust [94, 95] and other theoretical applications [96]; the models were expanded for use with explosive sound [97] and ultrasonic applications [25, 26, 98].

The use of transfer matrices for the prediction of airborne sound transmission loss was presented by Lee and Xu [27], which was developed from the work presented by Sastry and Munjal

[99]. Sastry and Munjal's work presented a method for applying transfer matrix methods to evaluate the response of an infinite plate by two dimensional plane wave excitation. This technique was utilised to predict the transmission coefficient and reflection coefficient of infinite multilayer panels; for the ultrasonic excitation of materials in sea water. Lee and Xu calculated the transfer function using a standing wave tube as outlined in an earlier paper by Lee and Wang [100]. The transfer function calculated from the standing wave tube measurements require modification in order to account for the lateral extent of the test sample. This was specifically applied to the sound transmission loss of multilayer panels by multiplying the transfer matrices of each material layer to calculate the total transmission coefficient of the system.

Recent work presented by Vigran studied the inclusion of finite structural connections into a transfer matrix prediction scheme [101, 102]; based on the research outlined by Munjal [103]. The method models the finite connections using the approach given by Sharp [22]. The sound transmitted is modelled by modifying the original transfer function and including the input impedances for a point connection (Equation 2.69) and a line connection (Equation 2.70).

$$Z_{B,point} = 8\sqrt{mB} \qquad \textbf{2.69}$$

where m is the surface mass of the panel and B is the bending stiffness of the panel.

$$Z_{B,line} = \frac{2(1-i)m\omega}{k_p} \qquad \textbf{2.70}$$

where k_p is the free surface wavenumber and ω is the frequency of excitation. The finite size of the partitions was accounted for via the method described by Villot [104, 105]. Reasonably good agreement was achieved between the predicted and measured results using this prediction scheme.

Transfer function methods are very well suited to predicting the transmission of sound through multi-layered materials with layers of porous material. A detailed literature review focused on the prediction of such systems will be presented in Section 8.2. The transfer matrix method is a developing field of research, and is expected to be of significant use for the prediction of sound transmission loss.

2.4. Finite Element Analysis (FEA)

Finite element modelling is utilised in a wide range of engineering applications [106, 107]. It involves breaking a physical system into many small elements and solving the relevant characteristic equations for each of these elements. This results in a large set of simultaneous equations that need to be solved to predict the behaviour of the system. These simultaneous equations can either be solved directly or approximated using any of a wide range of approximation schemes. The characteristic equations for each element depend on the problem being solved; for example the Navier-stokes equations for fluid modelling.

Finite element modelling can be applied to a range of acoustics problems including fluid-structure interaction [108-110], impact noise [111], acoustic scattering [112, 113], and sound propagation [114, 115]. There has been a significant amount of research dedicated to applying finite element methods to the evaluation of sound transmission loss problems [29-38]; which have achieved varying levels of accuracy.

Three dimensional models of the sound transmission loss measurement facility allow the full behaviour of a test partition and test rooms to be evaluated using an FEA model [29, 30]. The major limitation of these models is the number of elements required to model a full sized facility across the required frequency range. Due to the wide range of frequencies that need to be evaluated the element size becomes relatively small, and the corresponding number of mesh elements becomes very large. The sound transmission loss model presented by Papadopoulos [29] is valid between 100 Hz and 700 Hz, which is only a small component of the range of interest. Despite these limitations full three dimensional finite element models are useful, especially for investigating the poorly understood low frequency behaviour of partitions. Maluski and Gibbs [35, 36] used finite element methods to predict the sound transmission loss of walls in buildings for frequencies below 100 Hz, which is difficult to measure in practice.

Diaz *et al.* applied FEA methods to a two dimensional model of a lightweight concrete brick wall [32, 33]. In this model it was assumed that variations in the density are small and convection and viscous effects can be ignored. This simplified model allowed the sound pressure in the modelled volumes to be calculated with reasonable efficiency. The reduction from a three-dimensional to a two-dimensional model allowed the sound transmission loss to be calculated across a wide frequency range (100 – 5000 Hz). Reasonably good agreement with experimentally measured data was seen across the frequency range for this model.

FEA models have the potential to greatly expand our understanding of the sound transmission loss behaviour of partitions. The problems associated with FEA are gradually being solved by further

research and the increasing processing capacity of personal computers. Combining the knowledge developed in analytical models, such as the influence of incidence angle and niche effects, with new finite element models shows promise for developing a “complete” sound transmission loss model.

2.5. Analytical Modelling of Orthotropic Material Behaviour

All the prediction methods presented previously only consider panels with isotropic material properties. This assumption is valid for a large number of building materials such as gypsum plasterboard and lightweight concrete blocks, but there are some common building materials that have significantly orthotropic material properties; such as corrugated or plywood panels. These materials have significantly different material properties in orthogonal directions (x and y), as shown in Figure 2.9.

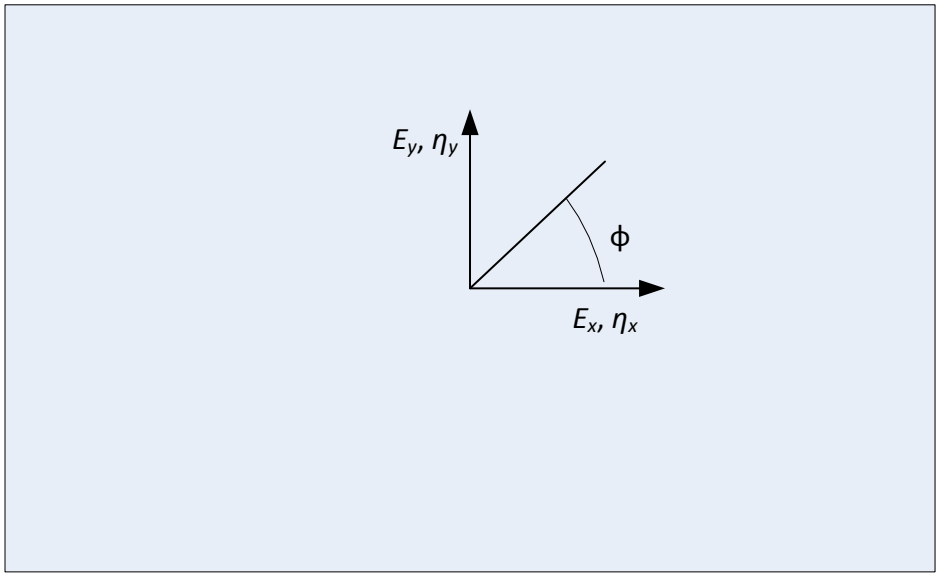

Figure 2.9: Definition of orthotropic panel and relevant material properties

The variation between the two stiffness values,E_x and E_y, in the case of an orthotropic panel results in a large difference in the sound transmission loss when compared to that of a similar isotropic panel. The typical behaviour of an orthotropic panel is shown in Figure 2.10.

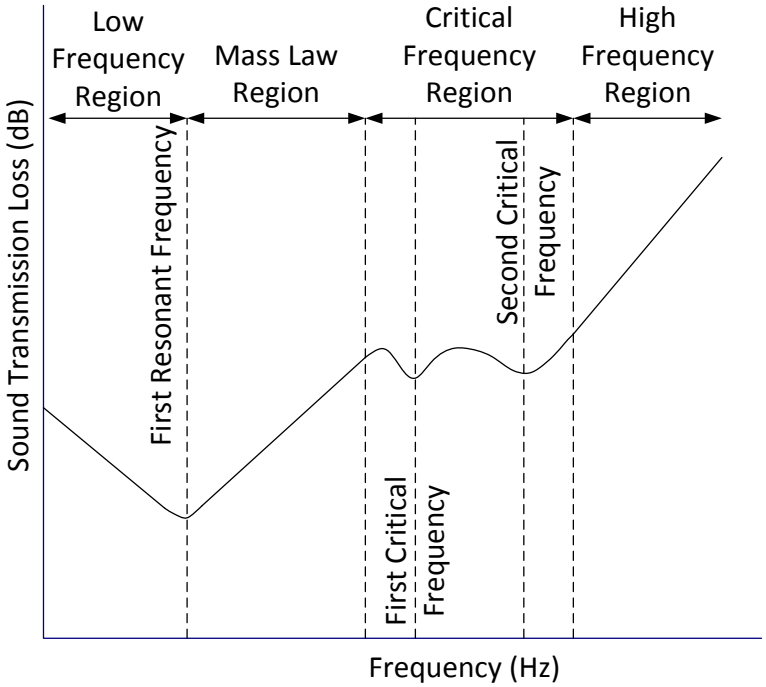

Figure 2.10: Typical sound transmission loss behaviour of orthotropic single leaf partitions.

The orthotropic stiffness causes a widening of the coincidence region, relative to a similar partition material with an isotropic stiffness. The coincidence condition identified in Equation 2.11 is no longer a single frequency, but a range of frequencies given by Equation 2.71.

$$f_{c1} = \frac{{c_0}^2}{2\pi}\sqrt{\frac{m}{B_{high}}} \leq \text{Coincidence Region} \leq f_{c2} = \frac{{c_0}^2}{2\pi}\sqrt{\frac{m}{B_{low}}} \qquad \textbf{2.71}$$

Between these two bounding frequencies the coincidence condition is met by plane waves incidence at different azimuthal angles. In general predicting the sound transmission loss of a system within the coincidence region is difficult. Thus the increased size of the coincidence region increases the difficulty in producing accurate predictions of the sound transmission loss for these orthotropic materials.

A limited number of models exist for the prediction of orthotropic transmission loss [21, 116-119], but these are generally focussed on very orthotropic materials. In the case where the ratio between the stiffness's is moderate, $2 < E_x/E_y < 5$, the current models tend to encounter problems. The prediction between f_{c1} and f_{c2} is where current methods tend to do poorly for moderately orthotropic materials. Plywood is orthotropic with a hard stiffness which is 2 – 5 times higher than the soft stiffness. The prediction of the sound transmission loss of plywood requires a different approach to that used in existing methods.

Guyader and Lesueur presented two papers [117, 118] focused on the prediction of the sound transmission loss of orthotropic multi-layered plates. This was primarily focused on the sound transmission loss of sandwich plates with a low rigidity material between the outer layers. The first of the two papers [118] explored the vibrational behaviour of the sandwich panels. The general equations for the behaviour of the plates were derived and a numerical study was performed to evaluate the dependency of the Eigen-frequencies and modes on the material properties. The information from this study was utilised in the second publication [117] to derive the sound transmission loss behaviour of orthotropic sandwich panels. Combinations of statistical and deterministic methods are used to develop a model that could be compared to experimentally measured results. The response of a multi-layered plate to an excitation force is combined with the radiation impedance of a panel in order to calculate the sound transmission loss. These models achieved reasonably good agreement with narrow-band measurements of the sound transmission loss.

Hansen presented a simplified model for the sound transmission loss of corrugated panels [120, 121]. These panels are generally very orthotropic due to the large difference in second moment of area caused by the corrugations. Hansen used a statistical energy analysis to derive an equation for the transmission loss of the orthotropic panel. The statistical energy analysis formulation for the transmission loss of a single isotropic panel is modified to accommodate the orthotropic panel behaviour (Equation 2.72 [90]).

$$\tau = 10\log_{10}\left[\zeta_{13} + \zeta_{rad}^2 \left(\mathrm{n}_2/\mathrm{n}_1\right)\Big/\left(\zeta_{int} + \zeta_{rad}\right)\right] - 10\log_{10}[\zeta_3 + \zeta_{13}(\mathrm{n}_1/\mathrm{n}_3) + \zeta_{rad}(\mathrm{n}_1/\mathrm{n}_3)] + 10\log_{10}\left[\frac{A}{\alpha_3 S_3}\right] \quad \textbf{2.72}$$

where ζ_i represents the various coupling loss factors between the rooms (1 and 3) and partitions (2), ζ_{rad} is the radiation coupling factor, ζ_{int} is the internal coupling factor, S_3 is the surface area of receiving room, α_3 is the Sabine absorption coefficient of the receiving room, A is the area of the partition, and n_i is the modal density of each component. To account for the orthotropic nature of the panels alternative versions of the factors n_i and ζ_i are utilised.

Krajci *et al.* [116] presented an assessment of the sound transmission loss of cross-laminated timber panels. The sound transmission loss of the panels and a range of other parameters were measured, including: the bending stiffness, the longitudinal wave speed, the point mobility, and the critical frequency. The transmission loss was predicted using both an isotropic and an orthotropic model. The isotropic model included an expression for the radiation efficiency that was derived from the

measured results. Some agreement between the observed trends from equivalent isotropic model and the measured results were achieved, but overall the agreement between both models was poor.

2.5.1. Ordubadi and Lyon's Model

The model presented by Ordubadi and Lyon [122] is an analytical model for the sound transmission loss of single infinite panels made from plywood. The model presented incorporates a model for the bending wave impedance of an orthotropic plate; this is combined with the radiation efficiency of an infinite panel to give an expression for the transmission loss of plywood. Ordubadi and Lyon derive the transmission loss using the previously defined formula for the transmission coefficient (Equation 2.15). The corresponding diffuse field transmission coefficient can be written as Equation 2.73.

$$\langle \tau \rangle_{\Omega} = \Gamma \int_0^{\phi_l} \int_0^{\theta_l} \left| 1 + {Z_{\omega} \cos\theta}/{2\rho_0 c_0} \right|^{-2} \sin\theta \cos\theta \, d\theta d\phi \qquad \textbf{2.73}$$

where Γ is an integral constant (Equation 2.74).

$$\Gamma = \int_0^{\phi_l} \int_0^{\theta_l} \sin\theta \cos\theta \, d\theta d\phi = \frac{\phi_l}{2}(1 - \cos^2\theta_l) \qquad \textbf{2.74}$$

This model utilises Leissa's [123] derivation for the equation of motion of an orthotropic plate subjected to an applied force. The plate impedance can be calculated from the equation of motion when the plate is excited by a plane wave force; this equation of motion is given by Equation 2.75.

$$B_x \frac{\partial^4 u}{\partial x^4} + B_y \frac{\partial^4 u}{\partial y^4} + 2H \frac{\partial^4 u}{\partial x^2 \partial y^2} + m \frac{\partial^2 \omega}{\partial t^2} = q(x, y) \qquad \textbf{2.75}$$

where q is a periodic forcing function (in this case a plane wave) that is defined by Equation 2.76. B_x and B_y are the orthotropic bending stiffness values, calculated by inserting E_x and E_y into Equation 2.10.

$$q = p_0 e^{i[\omega t - k_p(x\cos\phi + y\sin\phi)]} \qquad \textbf{2.76}$$

This yields Equation 2.77 as the plate impedance. It should be noted that there is an error in Ordubadi and Lyon's original manuscript; the plate impedance presented in the original should be divided by $i\omega$. This error was carried through the subsequent derivation in Ordubadi and Lyon's manuscript, although the final expression derived for the transmission loss is correct.

$$Z_\omega = \frac{[k_0^4 \sin^4\theta B'(\phi) - \rho_s \omega^2]}{i\omega} \quad \textbf{2.77}$$

where $B'(\phi)$ is the complex, orthotropic bending stiffness. The bending stiffness can be evaluated via Equation 2.78.

$$B'(\phi) = \left(B_x \cos^4\phi + B_y \sin^4\phi + 2H \sin^2\phi \cos^2\phi\right)(1 + i\eta) \quad \textbf{2.78}$$

This allows an expression for the sound transmission loss to be derived, as shown in Equation 2.79.

$$TL = 10\log\left[\Gamma^{-1}\int_0^{\phi_{lim}}\int_0^{\theta_{lim}}\left\{\left[1 + \Lambda\eta\left(\frac{f}{f_{cs}}\right)^2 M(\theta)S(\phi)\right]^2 + \Lambda\left[\Lambda^2\left(\frac{f}{f_{cs}}\right)^2 M(\theta)S(\phi) - \cos\theta\right]^2\right\}^{-1}\cos\theta\sin\theta\, d\theta d\phi\right] \quad \textbf{2.79}$$

where $M(\theta)$, $S(\phi)$ and Λ are coefficients of convenience given by Equations 2.80, 2.81, and 2.82 respectively.

$$M(\theta) = \sin^4\theta\cos\theta \quad \textbf{2.80}$$

$$S(\phi) = \cos^4\phi + \left(\frac{B_y}{B_x}\right)\sin^4\phi + 2\left(\frac{H}{B_x}\right)\sin^2\phi\cos^2\phi \quad \textbf{2.81}$$

$$\Lambda = k_o\rho_s/2\rho \quad \textbf{2.82}$$

This formula for the transmission loss lacks an analytical integral solution; therefore the sound transmission loss was calculated using numerical integration methods. Ordubadi and Lyon showed reasonable agreement between the predicted sound transmission loss results and two measured plywood samples, but this equation does not account for the influence of the sample size on the sound transmission loss. This model is compared to a range of measured sound transmission loss results in Section 9 of this thesis. The presented prediction method is used as the basis for developing the model developed in this thesis.

2.6. Single Number Ratings

In order to compare the sound transmission loss properties of partitions easily and efficiently numerous single number ratings have been proposed. Different ratings emphasise different aspects of the measured sound transmission loss. At the time of writing (2014) the standard single number ratings do not utilise frequencies outside the 100 Hz – 5000 Hz range measured in this testing, but spectral adaption terms allow this range to be expanded to 50 Hz – 5000 Hz. Currently (2014 when this thesis was written) significant discussion is being undertaken focused on the possibilities of expanding all ratings to 50 Hz – 5000 Hz. The single number ratings presented in this work are only measured and assessed within the 100 Hz – 5000 Hz frequency range. Two single number ratings were calculated for all the measured samples; the STC value and the R_w value. A description of each of these ratings is presented in the following two sections.

A range of alternative single number ratings are used around the world with varying levels of accuracy. Recent studies by Rasmussen *et al.* have evaluated the differences between a range of different single number metrics commonly used in Europe [124, 125]. It was found there was a very large variation in how single number ratings were applied between countries. This variation becomes even more significant when countries outside of Europe are included. This has a significant impact on the acoustic performance of buildings, and the variation causes issues when comparing different measurements and performance criteria.

2.6.1. STC

The STC rating is defined in ASTM E413-04 [126]. The reference curve is given in Figure 2.11. This curve is compared to the measured sound transmission loss curve, rounded to 1 decibel. The STC value is the value of the STC curve at 500 Hz when the following criteria are achieved:

1. The STC curve is less than or equal to 8 decibels above the measured sound transmission loss curve in all one third octave frequency bands.
2. The total of the differences in the one-third octave band where the measured transmission loss is below the STC curve in all the one-third octave bands is less than or equal to 32 decibels.

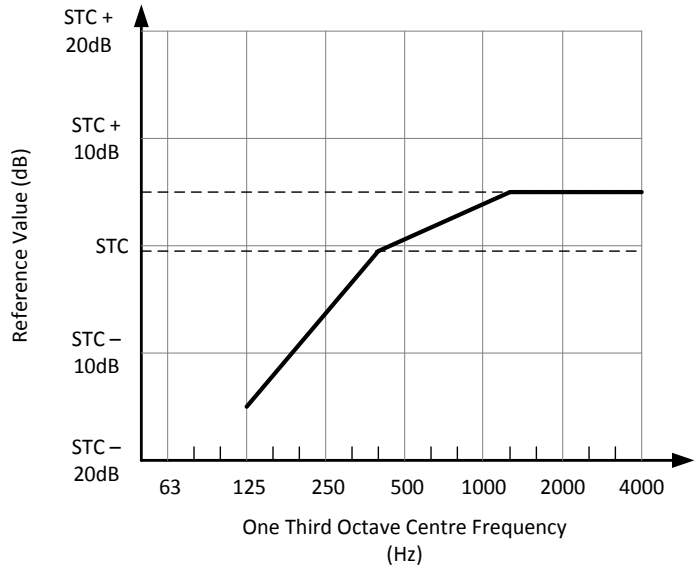

Figure 2.11: STC standard curve

2.6.2. R_w

The calculation of an R_w rating is described in ISO 717-1:2000 [44]. The reference curve is given in Figure 2.12. The single number is given by the curve value at 500 Hz when the following conditions are met. The sound transmission loss, rounded to 0.1 decibel, is compared to the reference curve. The reference curve is shifted up until the sum of the positive difference between the reference curve and the measured data is as large as possible, but not larger than 32.0 decibels.

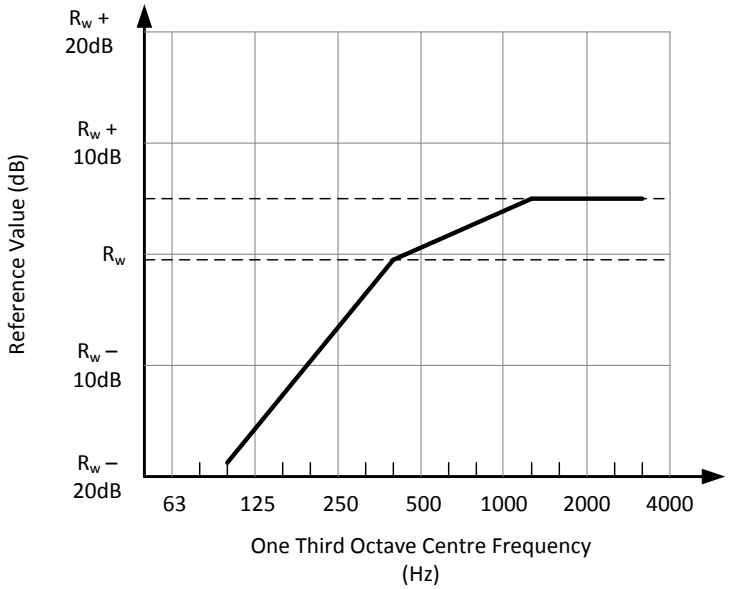

Figure 2.12: Rw standard curve

2.7. Radiation Efficiency

A vibrating surface will radiate sound into the surrounding space. The effectiveness of this radiation is governed by the radiation efficiency of the surface [20], which is defined by Equation 2.83.

$$\sigma = \frac{\bar{P}}{\rho_0 c_0 S \langle \overline{v_n^2} \rangle} \quad \textbf{2.83}$$

where $\bar{P}$ is the time averaged sound power radiating from the source (defined by Equation 2.84), $\langle \overline{v_n^2} \rangle$ is the space and time averaged squared vibration velocity of the surface (defined by Equation 2.85), S is the area of the panel and σ is the radiation efficiency.

$$\bar{P} = \int_S \bar{I}(\theta, \phi, \omega) dS \quad \textbf{2.84}$$

$$\langle \overline{v_n^2} \rangle = \frac{1}{S} \int_S \left[\frac{1}{T} \int_0^T v_n^2(x, z) dt \right] dS \quad \textbf{2.85}$$

This radiation efficiency is not restricted to values below unity, making the term radiation efficiency somewhat misleading, although in most situations the radiation efficiency is below or near unity. The radiation efficiency is equal to the real part of the normalized wave impedance.

Wallace [127] presented a theoretical derivation of the radiation efficiency of the natural modes of a finite rectangular panel. The panel was assumed to be simply supported and vibrating in it's natural modes. This derivation provides the typical radiation efficiency behaviour for low (Figure 2.13) and high (Figure 2.14) numbered modes.

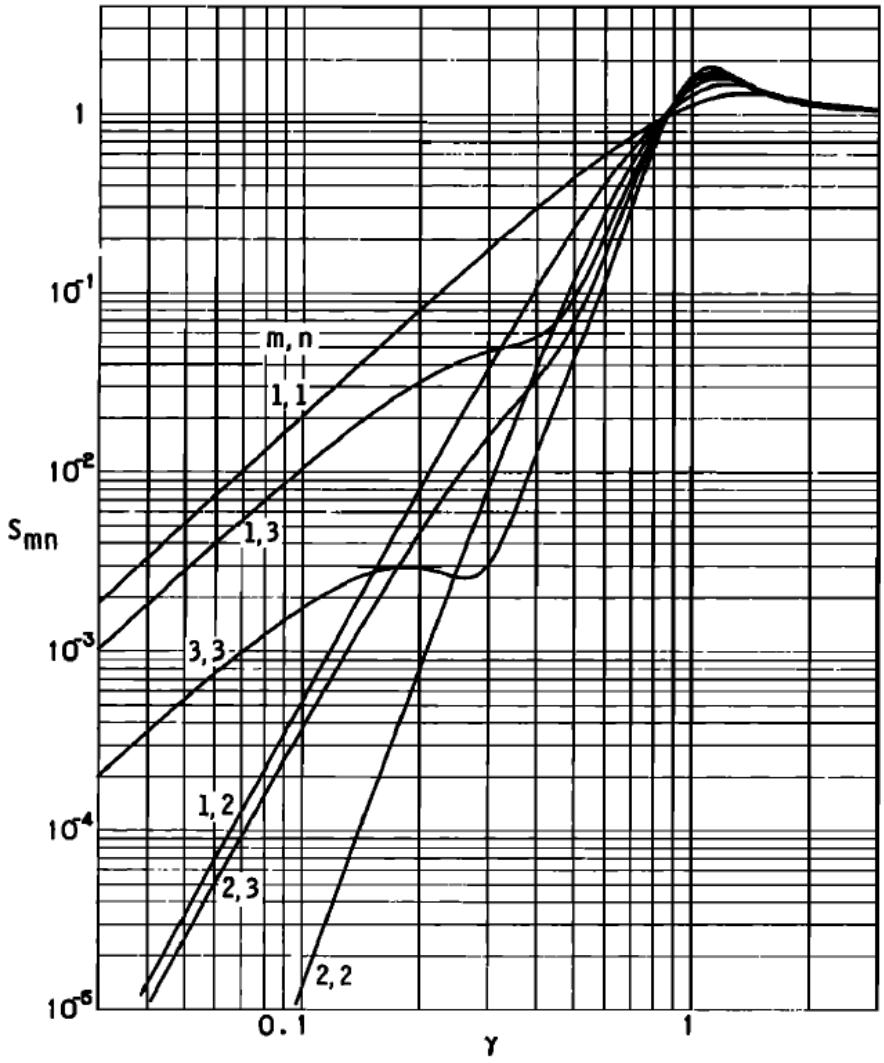

Figure 2.13: Radiation efficiency for the low-numbered modes of a square panel (Reproduced from [127])

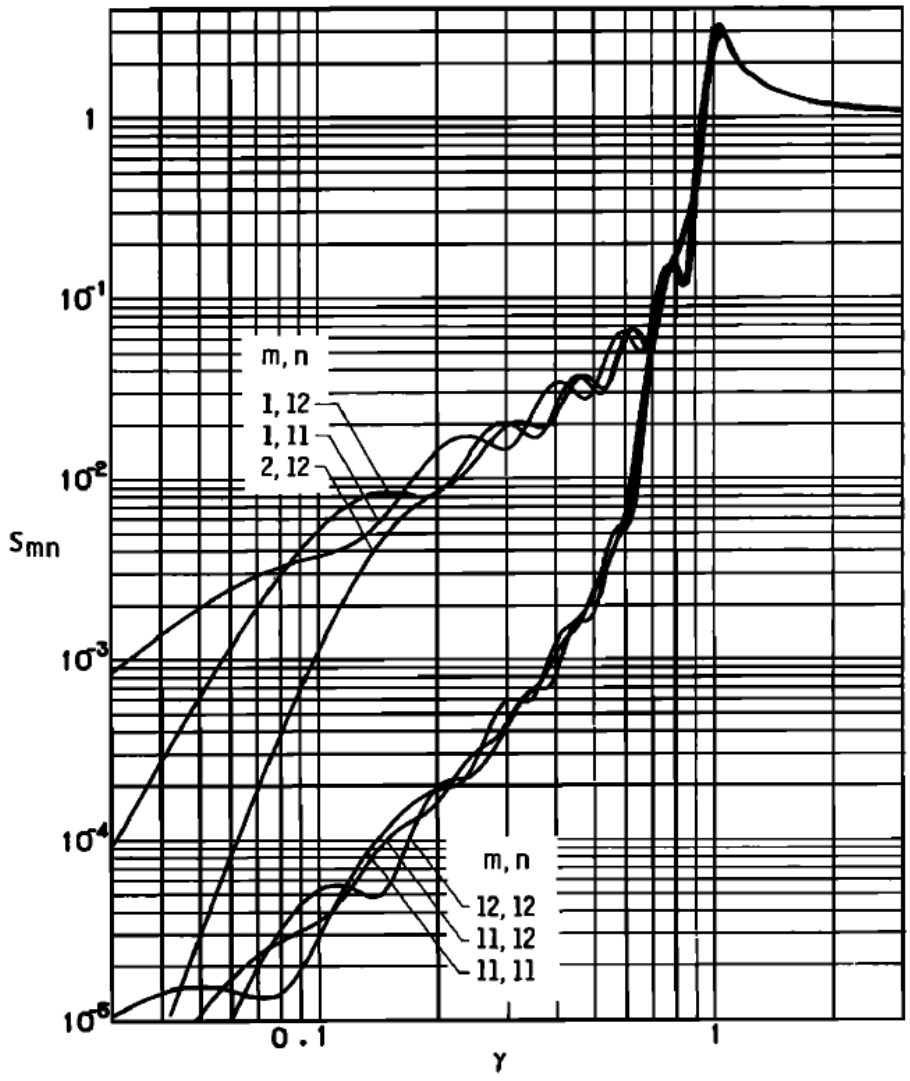

Figure 2.14: Radiation efficiency for the high-numbered modes of a square panel (Reproduced from [127])

Note: In Figure 2.13 and Figure 2.14 $\gamma = k/k_p$*, where* k *is the acoustic wavenumber and* k_p *is the plate wavenumber. The condition of* $\gamma = 1$ *is analogous to the coincidence criteria utilised in sound transmission loss calculations.*

It can be seen in these figures that the radiation efficiency generally increases from a low value at frequencies $\gamma < 1$ to a peak at or slightly above $\gamma = 1$. Above this peak the radiation efficiency decays asymptotically towards a value of 1. The behaviour of the radiation efficiency was shown to be dependent on the shape of the panel, but the general trends remain constant.

Thomasson presented work based on applying the normalized radiation impedance to the prediction of absorption coefficients [128, 129]. The normalized radiation impedance was calculated using numerical approaches, and presented in a tabulated format including the influence of changing angles of incidence. In a recent publication by Davy *et al.* [1, 6, 7] the derivation from Thomasson's

work is combined with the work of Li and Gibeling [130] and Allard and Atalla [131] to derive an approximation to the radiation impedance. A more detailed treatment of this work will be presented in Section 9 where it is utilised to introduce radiation impedance of a finite panel into the predictions of the sound transmission coefficient.

The influence of boundary conditions on the sound radiated from rectangular panels was evaluated by Berry *et al.* [132]. The method used was found to agree well with existing numerical results. The deflection stiffness was found to sigificantly influence the radiation efficiency, with a low deflection stiffness resulting in lower radiation efficiency. Variations in the rotational stiffness were found to have a negligible influence on the radiation efficiency.

A publication by Novak [133] investigated the influence of panel size on the overall radiation efficiency. The radiation efficiency was found to be dependent on the size of the panel. The forced vibration radiation efficiency was seen to increase as the sample size was increased. In the case of free vibrations the larger panel size caused an increase near the critical frequency, but the variations were less consistent at lower frequencies. The model presented was seen to agree reasonably well with both Sato's [79] and Ljunggren's [134] calculated values.

Davy [135] presented a simple analytical model that was found to agree reasonably well with the numerical calculations performed by Sato [79]. This paper utilised a two dimensional strip model that was able to be integrated across all angles of incidence. An analytical equation was derived for the finite panel radiation efficiency which was found to agree reasonably well with the numerical calculations.

The influence of radiation efficiency on the sound transmission loss is significant. Whilst the finite panel radiation efficiency has been incorporated into SEA and FEA models, it has not been incorporated into existing analytical models. The inclusion of the radiation efficiency allows the size of the sample and the influence of various construction parameters to be incorporated in a natural manner. The major issue associated with incorporating the radiation efficiency is that it usually results in an expression for the transmission coefficient that cannot be integrated analytically.

2.8. Conclusions

The current state of research in the prediction of sound transmission loss, and the associated fields of single number ratings and radiation efficiency has been considered. An extensive body of work has been presented on the prediction of the sound transmission loss of a wide variety of different systems. The literature review presented in this section is by no means exhaustive; but is intended to provide a suitable foundation for the development of this thesis.

The topic of single number ratings remains a hotly contested subject to this day. In this thesis only the STC and R_w values are considered as these are commonly used in New Zealand. The sound transmission loss was evaluated between 100 Hz and 5000 Hz in this thesis, and the STC and R_w values were calculated within their normal range.

Finally a brief overview of research into the radiation efficiency of vibrating panels was undertaken. Whilst this topic has been the subject of research for many years the field appears to remain very active with many new research publications being presented. A more detailed review of the theories of radiation efficiency is presented in Section 9 where the radiation efficiency is heavily used.

This review has shown that the field of sound transmission loss is well developed and has been the subject of extensive research. Despite this fact there are still significant gaps in the understanding of sound transmission loss behaviour. The large range of prediction methods that have been developed have been shown to be relatively limited in their applications outside of the small range of systems they were initially designed for. The following sections attempt to develop a prediction method that allows for several more variables to be accounted for; the orthotropic stiffness, the frequency dependent stiffness and a variable sample size.

3. Materials Testing Methodology and Results

The procedures used for measuring the material properties of the plywood samples are presented in this section. A comparison of stiffness values and damping loss factors measured using dynamic and static test methods are presented. A set of approximations for the dynamic properties of the samples was developed. The influence of a layer of viscoelastic damping material incorporated into the samples was evaluated using a reverberation time technique. Finally the method used for measuring the material properties of an open cell decoupling foam is described and the results presented.

3.1. Plywood Material Properties: Beam Test Methodology

Three important material properties are required to predict the sound transmission loss of a partition. These properties are the density (or surface mass), the bending stiffness, and the damping loss factor. The bending stiffness can be evaluated using static methods such as a three point bending test, or dynamic methods such as the measurement of the modal response of a cantilevered beam. The damping loss factor requires a dynamic measurement method as it cannot be obtained from static tests. The density of the samples can be obtained from the weight and dimensions of each sample.

Dynamic test methods allow both the stiffness and the damping loss factor to be calculated simultaneously. Two dynamic test methods are presented in this section, a clamped-free cantilever beam method and a free-free beam method. The stiffness results from the dynamic test methodologies were compared with the results from static three point bending tests. The three point bending tests were undertaken using the University of Canterbury's material test facility (MTS).

3.1.1. Clamped-Free Beam Method

The clamped-free beam method that was used in this research is similar to the method described in ASTM E756 [136]. The dynamic method was used in this work to measure the stiffness and damping loss factor of the base material; whereas ASTM E756 is designed for measuring the damping loss factor of a layer on a beam. The method consists of; clamping a beam to a mount, applying an excitation force and measuring the beam's response. Magnetic exciters were unable to produce an adequate excitation force, due to the size and mass of the samples. An impact excitation was used instead to provide a sufficient vibration response of the plywood samples.

A heavy steel test rig was developed to clamp the samples into place as shown in Figure 3.1. An accelerometer (PCB 352A60 high sensitivity – Figure 3.2) was attached to the beam using superglue. Superglue was superior to wax as this did not adhere well to the plywood. The impact excitation was applied to the beam using a PCB T086C01 impact hammer. The schematic of the test arrangement is shown in Figure 3.3. The accelerometer was placed approximately one fifth of the beam length from the end of the beam. This location was chosen as it maximised the number of modes that could be evaluated with one accelerometer position.

Figure 3.1: Plywood sample in clamped-free test rig

Figure 3.2: PCB 352A60 high sensitivity accelerometer

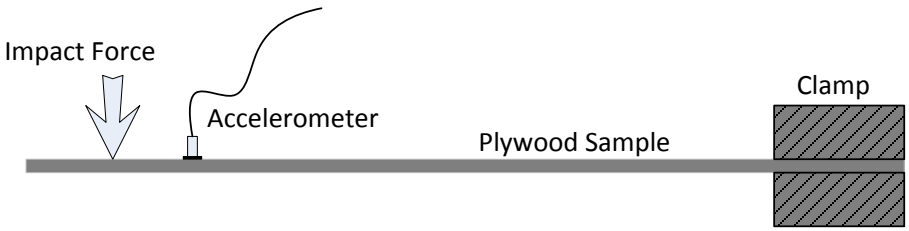

Figure 3.3: Layout of clamped-free dynamic material properties test rig

The acceleration response was collected using a Brüel & Kjær Pulse system (Figure 3.4). The frequency response of the signal from the accelerometer response was evaluated by the Pulse system. The frequency span of the measurement was varied depending on the sample to ensure the

first five resonant modes were captured. This variation allowed for the smallest possible frequency steps to be recorded, increasing the resolution of the frequency response and accuracy of the measured properties. For each measurement five impact excitations were applied and averaged, this was repeated three times for each beam.

Figure 3.4: Brüel & Kjær Pulse System

The FFT data was transferred into Matlab for processing. The frequency of each resonant frequency was identified using a Matlab peak location function. The values of the three decibel down points at each of the resonance frequency were also evaluated. A typical frequency response with the peaks and the three decibel down points located is shown in Figure 3.5.

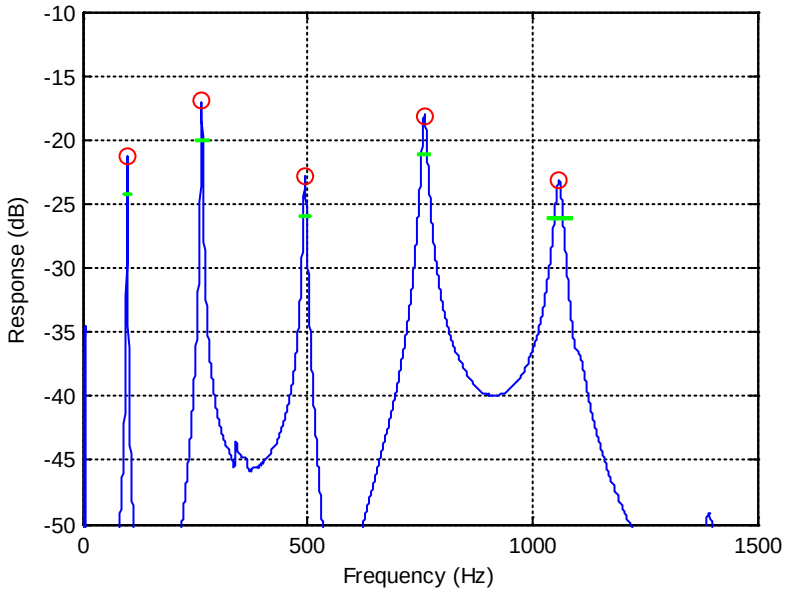

Figure 3.5: Typical frequency response of cantilevered beam with peaks and 3dB down points located

The location of the resonance frequency and the corresponding three decibel down points can be used to calculate the stiffness and damping loss factor of each beam. An expression for the i^{th} resonant frequency of a fixed-free beam was taken from Pilkey [10] (Equation 3.1). This equation assumes that the beam is vibrating in purely bending modes with no torsional behaviour. This assumption is valid in beams where the length is large in comparison with the width and thickness. The samples tested meet this criterion.

$$f_{bi} = \frac{{\chi_i}^2}{2\pi {L_b}^2}\left(\frac{E_{bi} I_b}{\rho_b}\right)^{1/2} \quad \textbf{3.1}$$

where L_b is the unsupported length of the beam, ρ_b is the mass per unit length, E_{bi} is the Young's modulus of the beam in the longitudinal direction at the i^{th} resonant frequency, I_b is the second moment of area of the test sample (Equation 3.2) and χ_i is a frequency factor taken from Pilkey's tables (Equation 3.3) for the appropriate value of i.

$$I_b = \frac{w_b {t_b}^3}{12} \quad \textbf{3.2}$$

where w_b is the width of the beam and t_b is the thickness of the beam.

$$\chi_i = \begin{cases} i = 1 \rightarrow 1.87510407 \\ i = 2 \rightarrow 4.69409113 \\ i = 3 \rightarrow 7.8575744 \\ i = 4 \rightarrow 10.99554073 \\ i = 5 \rightarrow 14.13716839 \\ i > 5 \rightarrow (2i - 1)\pi/2 \end{cases} \quad \textbf{3.3}$$

Equation 3.1 can be rearranged to yield an expression for the Young's modulus, as shown in Equation 3.4. Combining this equation with the known variables and the measured resonance frequency allows the Young's modulus to be calculated. The mass per unit length was calculated from the sample density.

$$E_{bi} = \frac{\rho_b}{I_b}\left(\frac{2\pi f_{bi} {L_b}^2}{{\chi_i}^2}\right)^2 \quad \textbf{3.4}$$

The damping loss factor was calculated using the half power bandwidth method. The bandwidth between the upper and lower half power points were calculated from the measured FFT data. This bandwidth allowed Equation 3.5 to be evaluated.

$$\eta_{bi} = \frac{\Delta BW_{3dB}}{f_i} \quad \textbf{3.5}$$

Where η_i is the damping loss factor at the i^{th} resonance, ΔBW_{3dB} is the bandwidth between the high and low frequency half power points, and f_i is the centre frequency at the i^{th} resonant frequency.

3.1.2. Free-Free Beam Method

The material properties were also measured using a free-free beam to check the reliability of dynamic stiffness measurements. The free-free condition was achieved by hanging the beam vertically from a light piece of cotton as shown in Figure 3.6. The beam's response to an impact excitation is measured using the same equipment described in Section 3.1.1. The test layout is shown in Figure 3.7.

Figure 3.6: Plywood sample mounted in free – free test rig

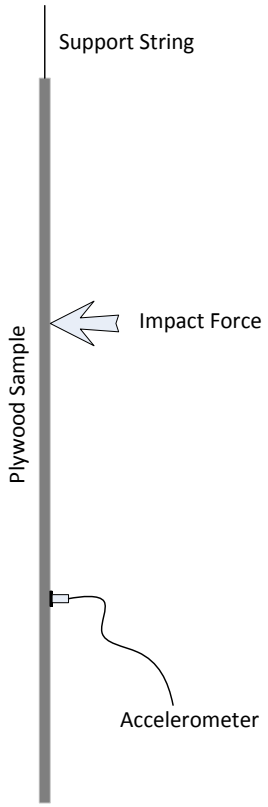

Figure 3.7: Schematic of fixed-free dynamic material properties test rig

The vibration acceleration frequency response was measured and evaluated in the same manner as the clamped-free system. The Young's modulus was calculated using Equation 3.4; but the value of χ_i was altered to account for the new boundary conditions. The new values of χ_i are given by Equation 3.6. The damping loss factor was calculated in the same manner as for the clamped-free beam with no modifications.

$$\chi_i = \begin{cases} i = 1 \rightarrow 4.73004074 \\ i = 2 \rightarrow 7.85320462 \\ i = 3 \rightarrow 10.99560790 \\ i = 4 \rightarrow 14.13716550 \\ i = 5 \rightarrow 17.27875970 \\ i > 5 \rightarrow {}^{(2i+1)\pi}/_{2} \end{cases} \quad \textbf{3.6}$$

3.1.3. Evaluation of Beam Tests

The two methods described above are evaluated in this section. The effect of the torque on the clamping bolts and the unsupported beam length were found to influence the results. The dynamic results are compared to the results of several static three point bending tests.

The effect of altering the clamping force on the measured stiffness and damping loss factor was assessed by applying different torques to the bolts that clamped the sample in place. The stiffness

and damping loss factor was determined for six torques: 2 Nm, 4 Nm, 6 Nm, 8 Nm, 10 Nm and 12 Nm.

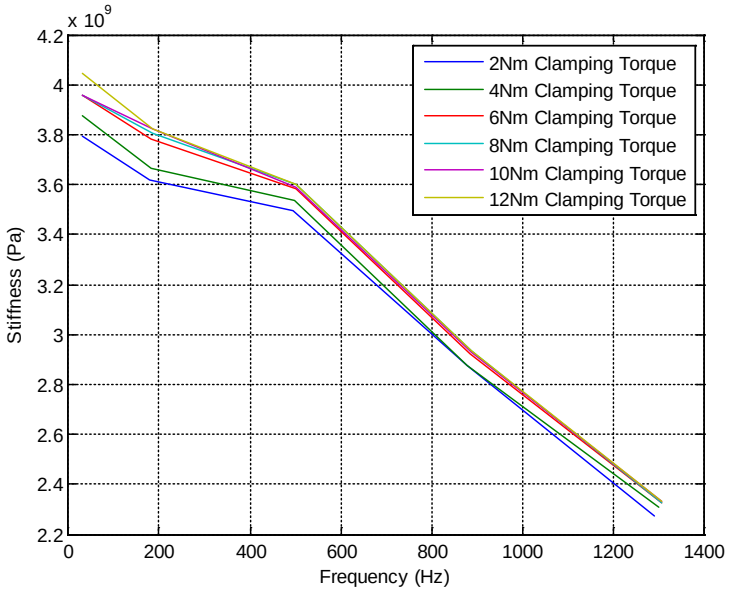

Figure 3.8: Variation in measured stiffness with varying clamping torques

Figure 3.8 show the variation of the calculated stiffness of a plywood beam as the clamping force is increased. There is an increase in the dynamic stiffness with increasing clamping torque. This increase is probably caused by the low clamping force resulting in a poor clamping condition which increases the effective beam length, and therefore lowers the frequency of the measured resonances. This reduction in the locations of the resonance frequencies results in a decrease in the calculated stiffness if all the other variables are held constant. The stiffness was seen to converge with a clamping torque of 6 – 8 Nm.

The effect of the clamping torque on the damping loss factor was also evaluated. The results of these tests are shown in Figure 3.9. The damping loss factor does not converge as clearly as the stiffness, but some level of convergence is seen at 10 – 12 Nm. The convergence is attributed to the increasing clamping force reducing excess damping caused by the vibration of the beam in the clamp.

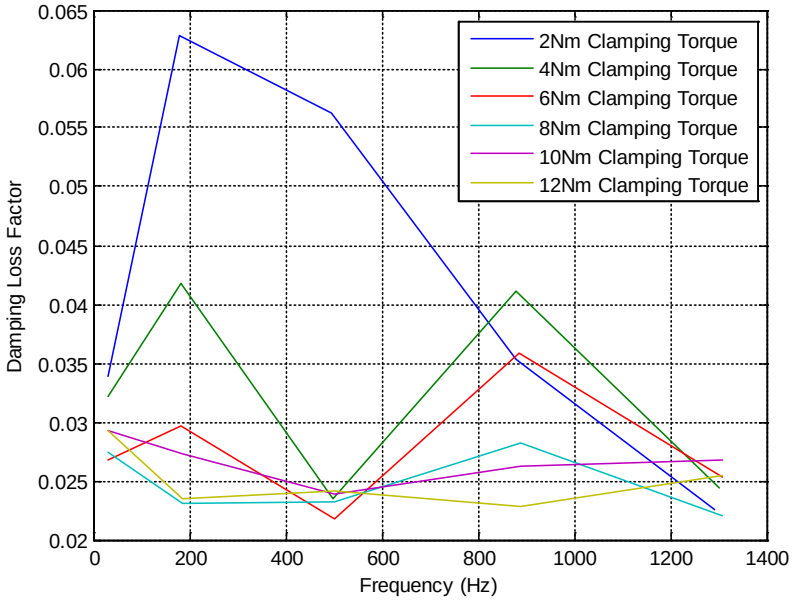

Figure 3.9: Variation in measured damping loss factor with varying clamping torques

The effect of altering the length of the sample was also assessed by moving the sample through the clamping unit. This changes the effective beam length, as shown in Figure 3.10. The stiffness of each sample was calculated for each beam length. It should be noted that the resonance frequency shift as the beam length is altered, changing the frequency location of each stiffness.

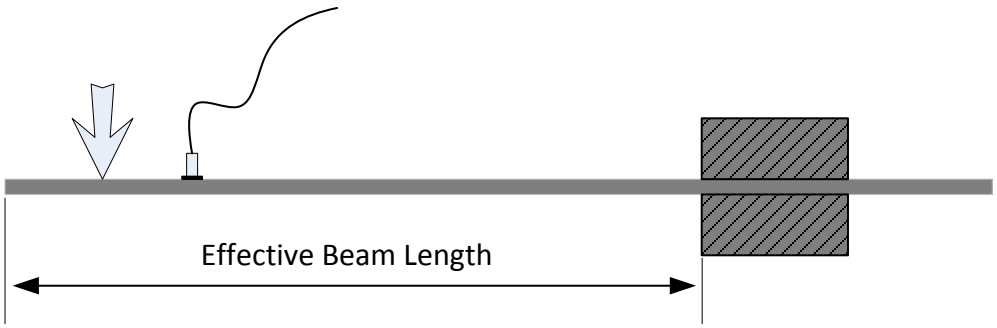

Figure 3.10: Method used to alter the effective length of the beam for validation tests

The measured stiffness values of a 17 mm thick plywood sample of various lengths is presented in Figure 3.11.

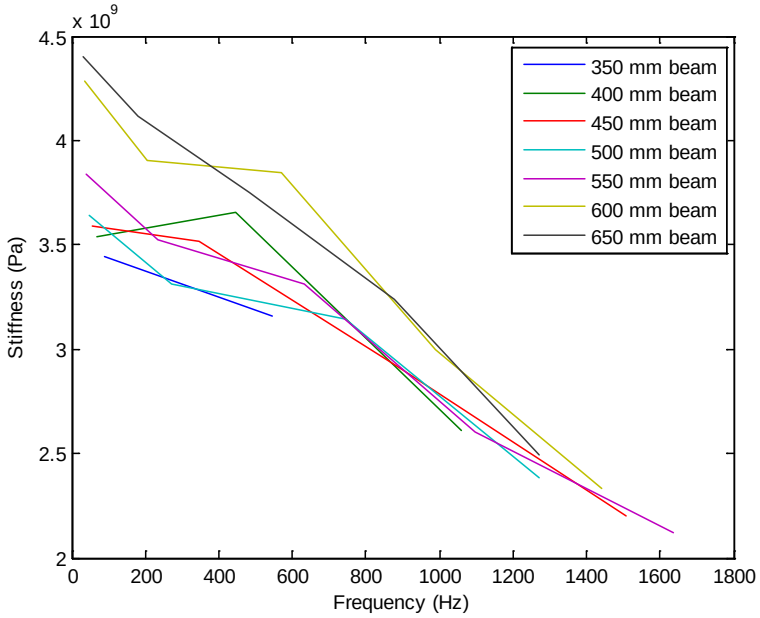

Figure 3.11: Variation in stiffness as the effective beam length is altered

Alterations to the effective beam length cause a significant variation in the measured stiffness. It was difficult to obtain clear resonance frequency as the beam length was decreased. The decreasing length to width ratio introduces other modes (such as torsional) into the system. It was also noted that there is a significant variation in the measured stiffness with frequency.

The static stiffness was measured with the MTS machine (Figure 3.12). The variation between the static and dynamic values of the stiffness and damping loss factor was evaluated. The variation between the two dynamic measurement techniques was also evaluated. The stiffness and damping loss factors were averaged across the different resonance frequency in order to produce an equivalent static stiffness. The average was chosen as extrapolating the dynamic value to 0 Hz resulted in a large over estimation in the bending stiffness. In order to evaluate the accuracy of the two dynamic stiffness measurements the stiffness of a steel beam was measured, the results are presented in Figure 3.13. The sample tested was a 10 mm × 20 mm × 700 mm steel beam.

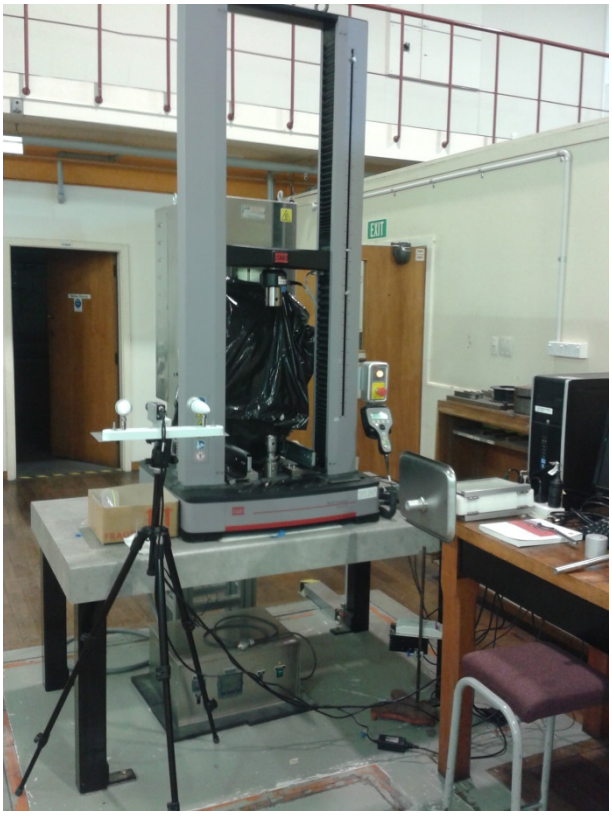

Figure 3.12: University of Canterbury MTS material test facility.

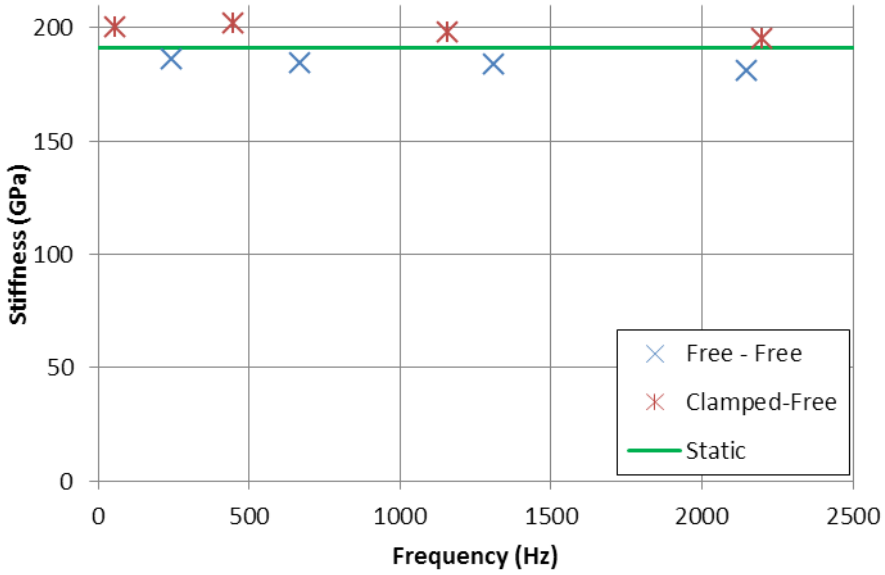

Figure 3.13: Measured stiffness properties of steel sample using multiple different measurement techniques

There is a slight difference between the two dynamic testing methods probably due to the interaction between the sample and the clamp. Achieving a perfect clamping condition is difficult; especially in the case of a steel beam where the beam had similar surface properties to the clamps themselves. Any misalignment in the clamp or loose clamping will alter the vibration response;

which will alter the measured stiffness. The stiffness of the steel sample is seen to be constant across the frequency range tested, which is expected due to the nature of the sample.

The stiffness of a 21 mm plywood beam was tested using both techniques to compare their effectiveness. Figure 3.14 shows the measured dynamic stiffness measured using the two dynamic stiffness tests; the equivalent static stiffness of the same beam is 2.5 GPa.

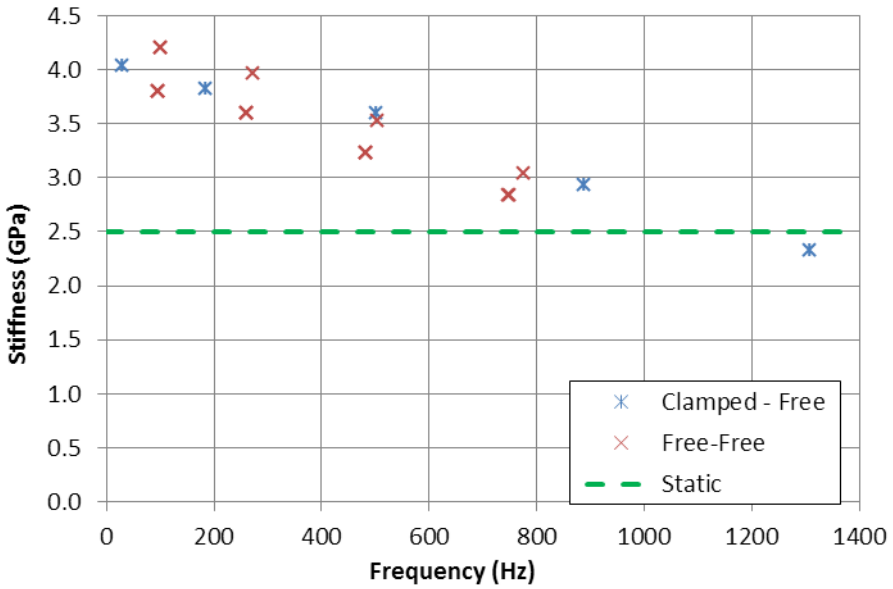

Figure 3.14: Measured frequency dependent stiffness of a 21 mm plywood beam using two dynamic measurement techniques

There is a small variation between the clamped-free and free-free beams probably due to non-ideal clamping conditions. A significant variation in the bending stiffness with frequency was observed in the plywood beams. This variation was not seen in the steel sample, indicating that it is probably due to the plywood's behaviour under vibration excitation. To further test this frequency dependency a beam of 10 mm gypsum plasterboard was tested. The dynamic and static stiffness values of this sample is presented in Figure 3.15.

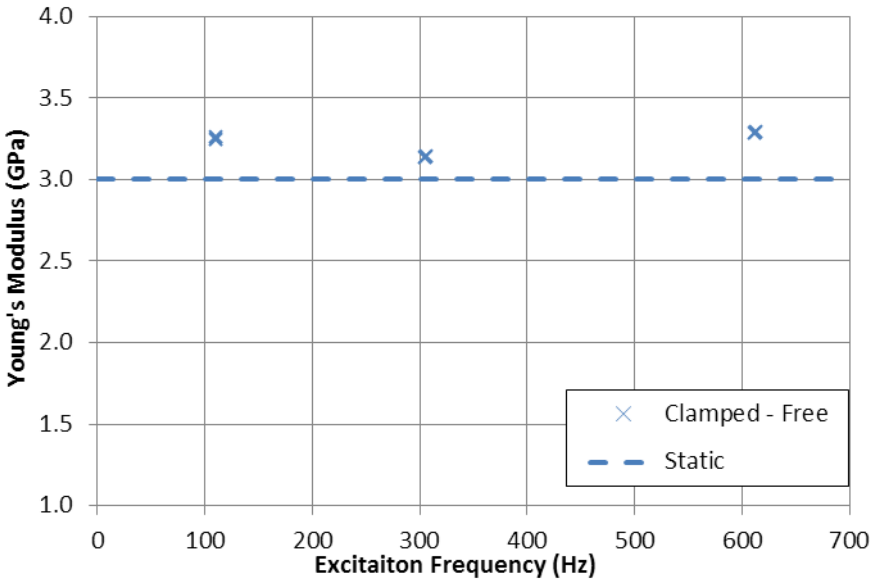

Figure 3.15: Measured frequency dependent stiffness of a 10 mm gypsum plasterboard

The gypsum plasterboard does not show the same variation in stiffness with increased frequency. This indicates that the frequency dependence is due to the plywood's internal construction. Formulas for approximation of the dynamic plywood stiffness are presented in the following section. The effects of this variable stiffness on the sound transmission loss will be assessed in Section 9.4.

3.1.4. Results

All the plywood beam samples were tested using the free-free technique. The clamped-free method was found to be less repeatable as the clamped beam had unclear resonant peaks and it was difficult to achieve reliable clamping conditions. The free-free tests were also significantly faster. Many of the prediction methods used to calculate the sound transmission loss generally utilise a single frequency independent stiffness; in this case an average stiffness value was calculated for each sample. This average stiffness was averaged across the frequency range and the results for all the plywood beam samples are presented in Table 3.2, along with the damping loss factor and surface density. The stiffness variation factor (H) was assumed to be the geometric mean of the two stiffness values. This factor alters the rate at which the stiffness varies between the two orthogonal stiffness values.

The plywood panels were cut into beams, the dimensions of which were adjusted to maintain a relatively constant length to cross section area ratio. An example of some test beams are shown in Figure 3.16, and the dimensions of each thickness are presented in Table 3.1. Several beams were

cut from each panel in a cross-ply and a with-ply direction, allowing the maximum and minimum stiffness to be calculated.

Figure 3.16: Plywood samples for stiffness testing

Table 3.1: Plywood test beam dimensions

Plywood Thickness	Average Length (m)	Average Width (m)	Average Mass (m)	Density ($^{kg}/_{m^3}$)
7 mm	0.70	0.05	0.13	520
9 mm	0.70	0.05	0.15	480
12 mm	0.70	0.05	0.20	480
15 mm	0.70	0.05	0.27	510
17 mm	0.70	0.05	0.27	450
19 mm	0.70	0.05	0.32	480
21 mm	0.78	0.06	0.50	510

Eight samples of each thickness of plywood were tested. Four samples had the surface grains running parallel to the beam length, and four had the surface grains running perpendicular to the beam length. The average material properties are presented in Table 3.1.

Table 3.2: Average material properties calculated from free-free beam tests

Thickness (h)	Parallel Ply Damping Loss Factor (η_{cp})	Cross Ply Damping Loss Factor (η_{pp})	Parallel Ply Young's modulus (E_{cp})	Cross Ply Young's modulus (E_{pp})
7 mm	0.012	0.032	12.2 GPa	8.1 GPa
9 mm	0.016	0.028	9.6 GPa	2.3 GPa
12 mm	0.015	0.018	5.9 GPa	2.3 GPa
15 mm	0.014	0.014	6.5 GPa	2.5 GPa
17 mm	0.015	0.015	4.5 GPa	3.0 GPa
19 mm	0.014	0.017	6.6 GPa	2.5 GPa
21 mm	0.014	0.014	7.1 GPa	3.4 GPa

Table 3.3: Orthotropic ratios of stiffness and damping loss factor

Thickness (h)	Damping Loss Factor Orthotropic Ratio	Young's Modulus Orthotropic Ratio
7 mm	2.67	1.51
9 mm	1.75	4.17
12 mm	1.20	2.57
15 mm	1.00	2.60
17 mm	1.00	1.50
19 mm	1.21	2.64
21 mm	1.00	2.09

The dynamic measurement technique used allowed the values listed in Table 3.2 to be calculated for each modal frequency. In all cases there is a significant variation in the measured stiffness as the frequency of excitation is increased. This yields the frequency dependent stiffness and damping loss factor. The results of all the frequency dependent measurements are presented in Appendix 0. The damping loss factor shows some variation with frequency but this follows no obvious trend. The variation in the dynamic stiffness with frequency was found to be modelled reasonably well by an exponential decay. An exponential decay curve was fitted to all of the measured stiffness data; the results of which are presented in Appendix 0. The goodness of fit data is also presented for all of the measured results. An example of the fitted data is presented in Figure 3.17.

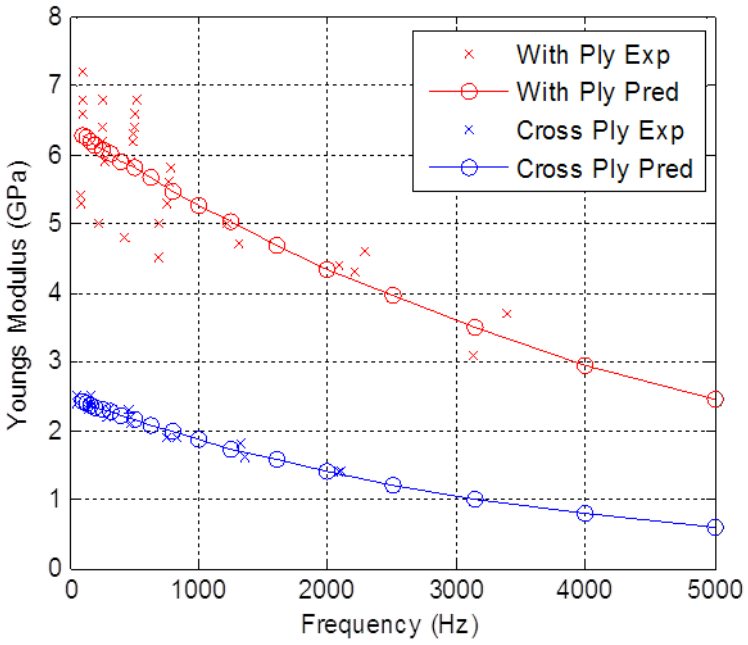

Figure 3.17: Frequency dependent stiffness values of 12 mm plywood sample

This fitted curve allowed for the stiffness values to be evaluated at each one-third octave band centre frequency. These values could then be incorporated into the formulation for the prediction of the sound transmission loss. A similar method of curve fitting was applied to the damping loss factor, but this was unsuccessful. The damping loss factor was observed to vary significantly with frequency but did not follow a particular trend.

3.2. Plywood Material Properties: Panel Test Methodology

A number of the plywood panels were also tested using dynamic methods applied to the whole panels. The damping loss factor and vibration variation across a whole panel was measured. The two tests performed and the results of these measurements are presented below. The panels were evaluated to assess the level of inhomogeneity in the plywood, and it's probable influence on the sound transmission loss of the measured partitions.

3.2.1. Vibration Variation

A point scan was made of the panel when excited via a point source. This test was designed to assess the effect of inhomogeneity in the plywood had on the vibration response. The panel was hung by two thin cables attached at the corners and 10 of the same PCB accelerometers as used previously were attached in a grid to the surface of the plywood panel. The vibration excitation was applied via the same Brüel & Kjær 10 N Shaker Type 4810. The grid of measurements and the test arrangement are presented in Figure 3.18.

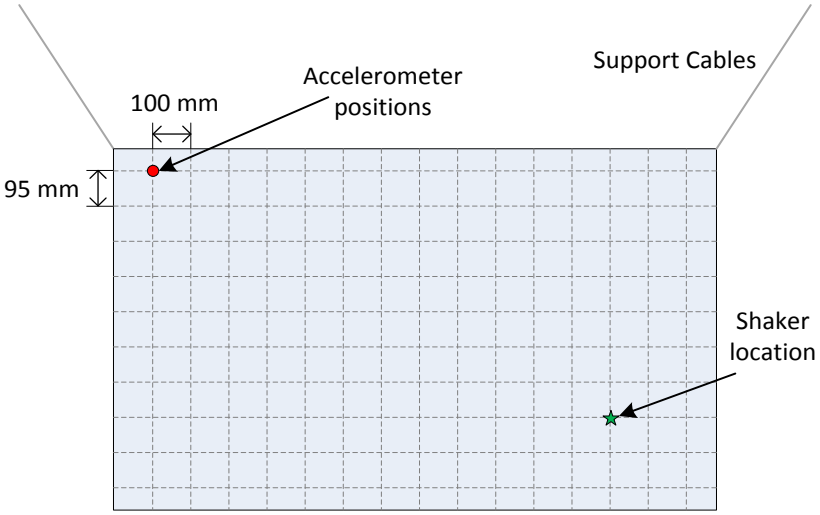

Figure 3.18: Schematic of system used to measure vibration response of a panel in order to identify the effect of material variations

Figure 3.19 shows the panel with a grid drawn on for locating the accelerometers, ten of which were attached for each of the measurements. A 30 second measurement of the panel's response to a white noise excitation was performed at each location.

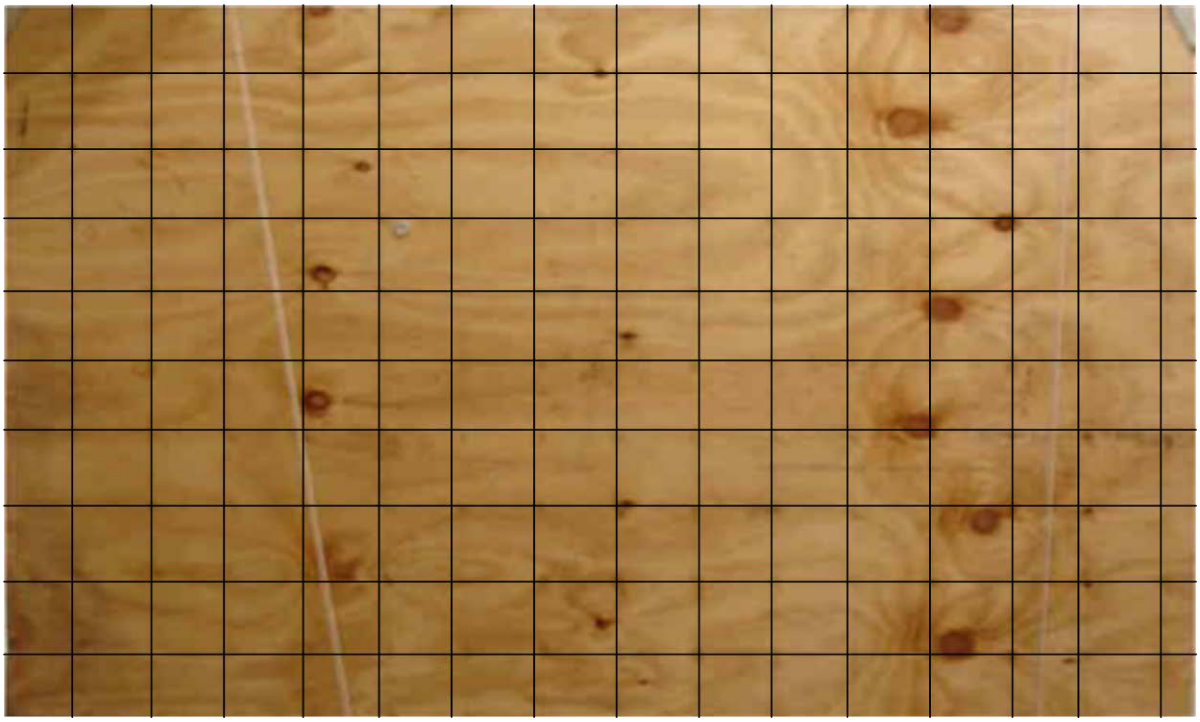

Figure 3.19: Image of panel with grid for modal analysis

The measured frequency response was recorded and processed in Matlab. The frequency response at each point was used to develop a contour plot of the panel response. This response was combined with an image of the panel in order to allow possible variations in the acceleration response due to the panel structure to be identified. Typical low frequency response of the panel (100 Hz) is shown in Figure 3.20, and a typical high frequency response (3000 Hz) is presented in Figure 3.21.

Figure 3.20: Vibration response of plywood panel at 100 Hz

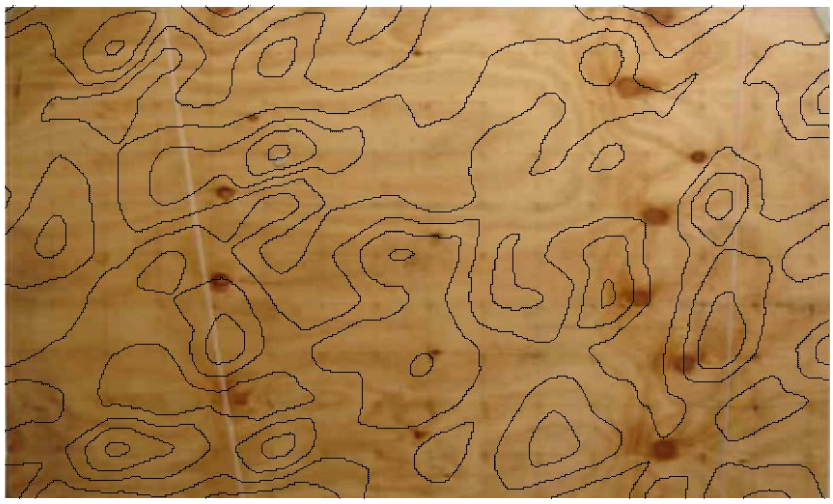

Figure 3.21: Vibration response of plywood panel at 3000 Hz

No clear variations in the vibration response were seen on the panel despite the presence of significant variations in the visual appearance material. It was expected that there would be large variations near obvious variations such as knots. This was not evident from the measurements made and was taken as justification for assuming that the material properties of the plywood were homogenous for the purposes of the prediction of the sound transmission loss models. It is possible that the grid of accelerometers used was insufficiently fine to accurately visualise variations in the material properties. At 5000 Hz the bending wavelength within the panel is approximately 100 mm. Despite this the measurements presented in this section are still valid. This assumption is useful as accounting for heterogeneity in the samples, whilst possible [137, 138], significantly increases the complexity of the model.

3.3. Material properties of the decoupling layer treatments

A layer of open-celled foam that is commonly used as an absorption material was utilised in the construction of an acoustic treatment. This treatment consisted of a layer of this foam with a layer of limp mass loaded barrier attached to one side. The evaluation of this treatment is presented in Section 8.2, where a prediction method for the sound transmission loss of the treated systems is also presented. In order to predict the sound transmission loss of these systems the material properties of the acoustic foam were required. This section presents the technique used for evaluating these properties.

A number of methods were used to evaluate the material properties of a decoupled layer treatment that is utilised in Section 8.2. The material construction complicated the measurement procedure. Dynamic methods were not able to be used to evaluate the properties of the mass loaded barrier or the combined system. The dynamic measurement of both stiffness and damping

loss factor require that waves propagating in the material can be accurately measured, this is not the case in very heavily damped systems.

The compressional stiffness of the foam was tested using the MTS. A 30 mm × 30 mm square of the foam layer was tested in a compression test apparatus; this was found to be poorly repeatable. The procedure described in ASTM D1621-10 [139] was then followed using circular samples. Typical samples are shown in Figure 3.22 and a sample in the test rig is shown in Figure 3.23.

Figure 3.22: Samples of decoupling foam ready for compression tests

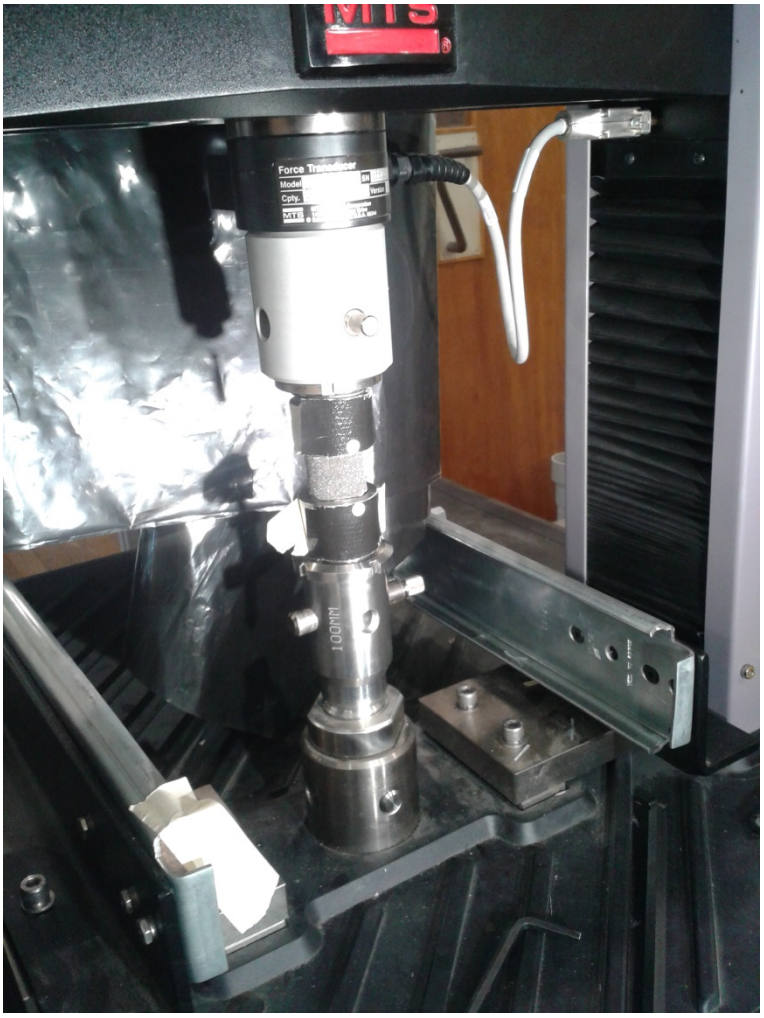

Figure 3.23: Decoupling foam in compression test rig

The MTS test rig applies a force to the sample and measures the displacement. This displacement can be plotted against the compression force, as shown in Figure 3.24. The compressional stiffness is measured from the highlighted section of the curve. Five foam samples were tested resulting in a compressional stiffness of 0.025 MPa, with a standard deviation of 0.003 MPa.

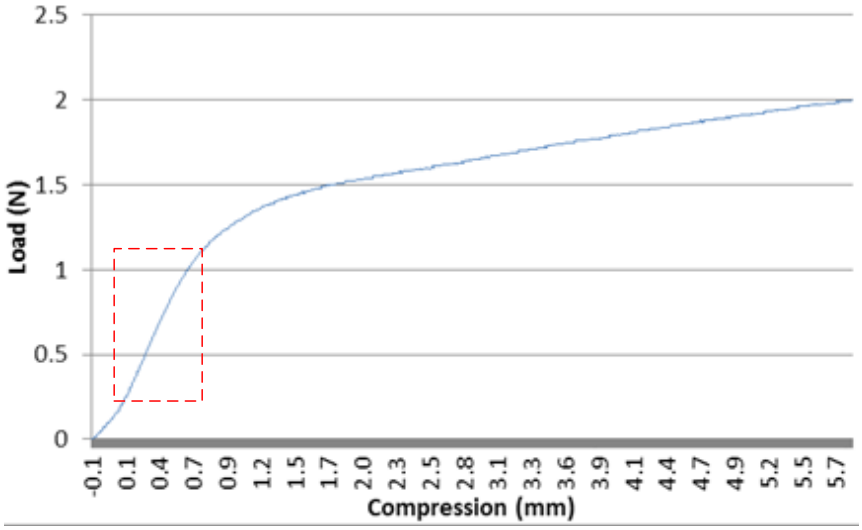

Figure 3.24: Results of a compressional stiffness test of decoupling foam

The approximate bending stiffness of the mass loaded barrier and foam layer were tested using a basic three point bending stiffness test. This test could not be carried out effectively in the material test machine used for the foam stiffness, due to the construction of the foam and barrier system. As the barrier was on one side it meant that standard three point bending tests would not work, as the foam absorbed a large amount of the displacement which resulted in an inaccurate measurement of the stiffness. Instead pins were inserted through the system so that force could be applied to the mass loaded barrier as shown by the schematic given in Figure 3.25. The central rod was loaded with a small mass and the deflection due to this load was measured, allowing the stiffness of the system to be estimated.

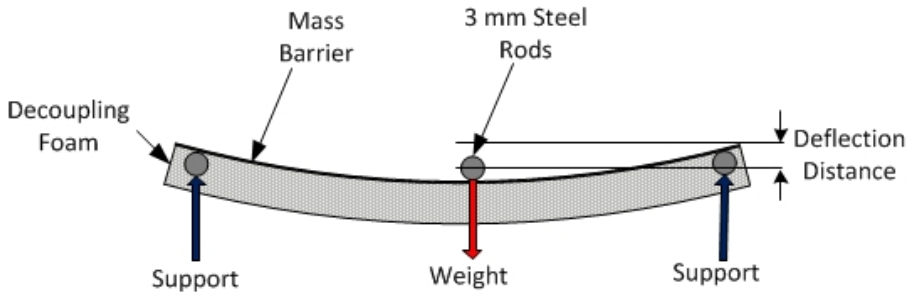

Figure 3.25: Schematic of testing method used for bending stiffness testing of decoupled layer treatment

The measured bending stiffness of the mass loaded barrier and decoupling foam was measured to be approximately 0.05 MPa. This measurement technique was sufficient to provide an order of magnitude indication of the bending stiffness, which was required for the sound transmission loss predictions.

4. Sound Transmission Loss Measurement

This section presents the method used for measuring the sound transmission loss of various partitions. Two sound transmission loss facilities are described and the application of sound intensity for sound transmission loss measurements is explained. Finally the use of a point grid scan to evaluate the intensity and radiation efficiency across the surface of the panel is evaluated.

4.1. Introduction

The sound transmission loss of each partition was measured using sound intensity methods in the University of Canterbury's sound transmission loss suites. Two sample sizes were utilised; a small (950 mm × 1550 mm) partitions, and full sized (4800 mm × 2400 mm) partitions. Both facilities utilised the same reverberation room, with different test apertures (Figure 4.1). Each facility is described and the effectiveness of each is discussed.

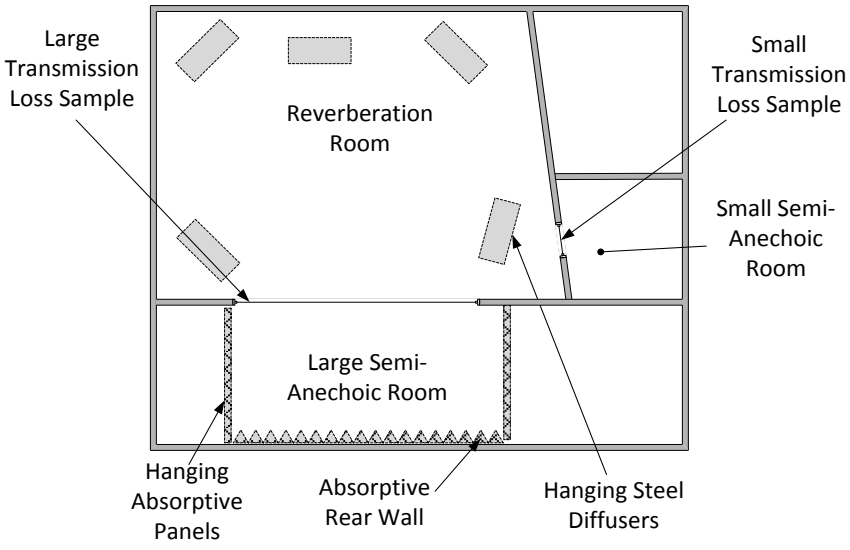

Figure 4.1: Transmission loss facilities at the University of Canterbury

The repeatability of the measurements was important for the transmission loss measurements. The speaker position, microphone positions, reverberation room arrangement and receiving room arrangement can all affect the measured transmission loss. To overcome these factors the tests were performed using ISO 15189-1 [140] as a guideline and the facility was assessed using ISO10140-5 [141].The use of these standards helped ensure reliable and repeatable results.

Additional tests were also performed on the samples to assess the vibration and radiation efficiency of the partitions. These tests are discussed at the end of this section.

4.2. Sound Intensity

Sound intensity is a measure of the sound power per unit area (measured in W/m^2). For sound transmission loss measurements the time and space averaged sound intensity radiated from the receiving side of the sample is measured. This allows the calculation of the radiated sound power. The intensity was measured using two systems, a 2260 Brüel & Kjær sound intensity system, and a Brüel and Kjær Pulse system equipped with sound intensity hardware. A brief overview of sound intensity measurement is presented in this section.

A detailed study of the theory and application of sound intensity in a wide range of acoustic applications is presented by Fahy [142, 143]. The theoretical derivations in this section are taken from these references and were used as a guide for intensity measurements. The details of how the sound intensity measurements were implemented for the assessment of sound transmission loss is described in Sections 4.3 and 4.4.

The method used to measure the intensity on the receiving side of the transmission loss samples was the pressure-pressure method. This method requires two "identical" microphones mounted a known distance apart in a sensor array. The system used was a pair of phase matched Brüel & Kjær 4189 ½ inch microphones that are mounted 12 mm apart in a portable handset. The sound pressure halfway between the two microphones ($p_I(t)$) is approximated using Equation 4.1.

$$p_I(t) \approx \frac{1}{2}\left[p_{I_1}(t) + p_{I_2}(t)\right] \quad \textbf{4.1}$$

Where $p_{I_1}(t)$ and $p_{I_2}(t)$ are the sound pressures at each microphone.

A finite difference approximation was applied to the two sound pressure measurements to evaluate the sound pressure gradient ($\frac{\partial p_I}{\partial r}$) between the two microphones (Equation 4.2), which allows the particle velocity half way between the two microphones (u_I) to be evaluated using Equation 4.3.

$$\frac{\partial p_I}{\partial r} \cong \frac{\left(p_{I_2} - p_{I_1}\right)}{\Delta r} \quad \textbf{4.2}$$

where Δr is the spacing between the two microphones.

$$u_I \cong -\frac{1}{\rho_0}\int \frac{\left(p_{I_2} - p_{I_1}\right)}{\Delta r}\,\mathrm{d}t \quad \textbf{4.3}$$

These approximations can be combined to give the instantaneous intensity component (I_n) via Equation 4.4.

$$I_n(t) \approx \frac{1}{2\rho_0 \Delta r}\left[p_{I_1}(t) + p_{I_2}(t)\right] \int_{-\infty}^{t} \left[p_{I_1}(t) + p_{I_2}(t)\right] d\tau \qquad \textbf{4.4}$$

In the case of a time-stationary signal, such as the sound radiated from a panel, the intensity can be expressed as the product of one microphone signal and the integral of the other signal (Equation 4.5).

$$I_n = -\frac{1}{\rho_0 \Delta r} \lim_{T\to\infty} \left({}^{1}/_{T}\right) \int_{0}^{T} p_{I_1}(\tau) \int_{-\infty}^{t} p_{I_2}(\tau) d\tau \qquad \textbf{4.5}$$

In the pressure-pressure technique there are inherent systematic errors [144], associated with the assumptions inherent the derivation of Equation 4.5. These errors are related to the finite difference approximations [145] of the pressure (Equation 4.1) and the particle velocity (Equation 4.3).

The total error in an intensity measurement is dependent on the sound field being measured, the microphones, the microphone phase mismatch and the microphone spacing [146-148]. The microphone spacing has a large effect on the accuracy of the intensity measurements and also alters the influence of other factors on the intensity measurements. In the investigation performed by Pavić [149] it was shown that the accuracy of the finite difference approximation improves inversely to the square of the microphone spacing. The effects of unwanted noise, unequal phase shifting and the finite duration of averaging were shown to decrease proportionally to the microphone spacing. These sources of error result fortuitously cancel each other out to a large extent and result in a microphone spacing that is optimal for a particular frequency. To perform the measurements between 100 Hz and 5000 Hz simultaneously a compromise was made that balances the performance across this frequency range. Brüel & Kjær suggest using the 12 mm spacing between 125 Hz and 5000 Hz, although Jacobsen *et al.* [150] showed that the upper range can be extended significantly. The research presented by Jacobsen et al [151] investigated the influence of the spacing on the frequency range that can be accurately evaluated. It was shown that a 12 mm spacer and ¼ inch microphone can be used with reasonable accuracy between 63 – 10k Hz. This is due to the interaction between the diffraction effect and the finite difference, which combine to effectively cancel the two sources of error.

4.3. Small Transmission Loss Rig

The University of Canterbury's small transmission loss rig is typically used to quickly and easily perform indicative transmission loss measurements. The rig does not conform to ISO15186-1 due to the sample size, sample location and receiving room conditions.

The transmission loss sample is clamped into a 1550 mm × 950 mm frame (Figure 4.2), separating a reverberation room and a semi anechoic receiving room. Noise was generated within the reverberation room and was played using a Brüel & Kjær 4296 omnidirectional speaker. The transmitted sound intensity was measured using either a Brüel & Kjær 2260 system or a Brüel and Kjær Pulse system.

Figure 4.2: Small transmission loss facility viewed from receiving room side

The reverberation room has a volume of 216 m^3. Six stationary diffusing panels ensure the sound field is sufficiently diffuse. The total two-sided area of the diffusing elements is 13% of the total boundary surface area of the room. The total surface area of the reverberation room boundaries and diffusing elements is 305 m^2. The layout and dimensions of the reverberation room are shown in Figure 4.3.

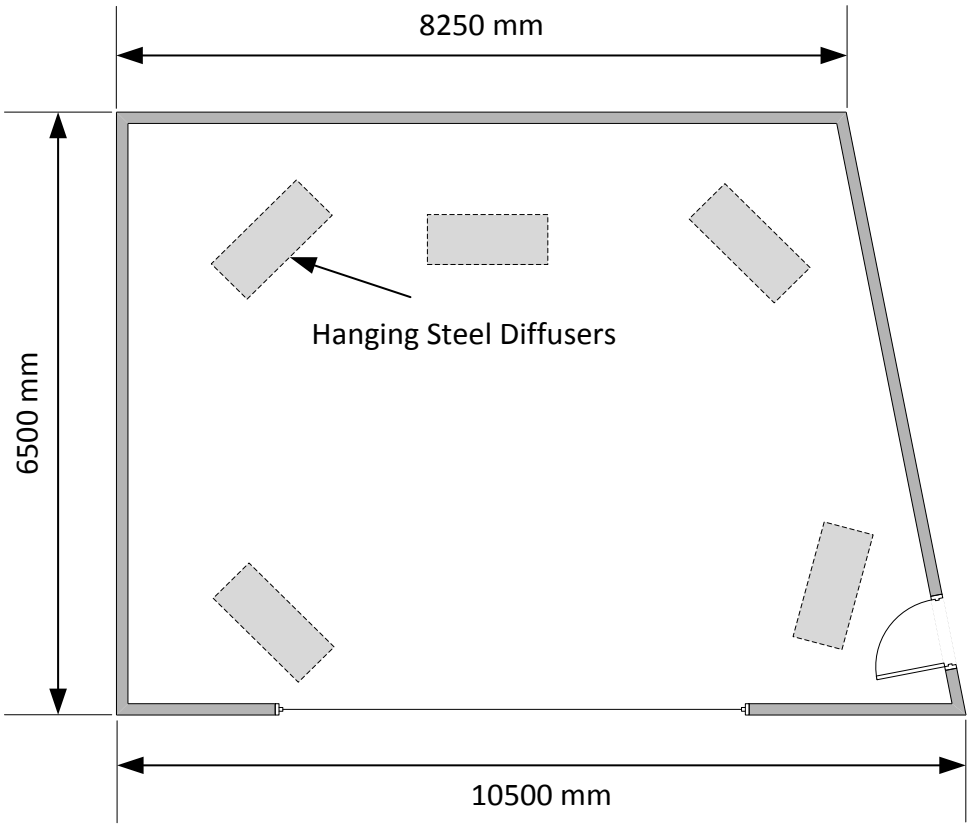

Figure 4.3: Reverberation room dimensions and locations of diffusers

The receiving room was a small semi-anechoic room with dimensions as shown in Figure 4.4. The receiving room had a volume of 9 m^3 and a surface area of 26.4 m^2. This room is lined with sound absorption on all the surfaces except the floor, which is covered in deep pile carpet.

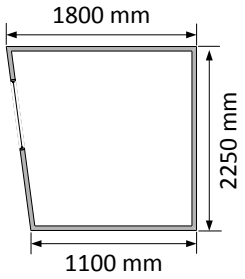

Figure 4.4: Small semi anechoic receiving room

The reverberation time of the source room was measured and the results are presented in Figure 4.5.

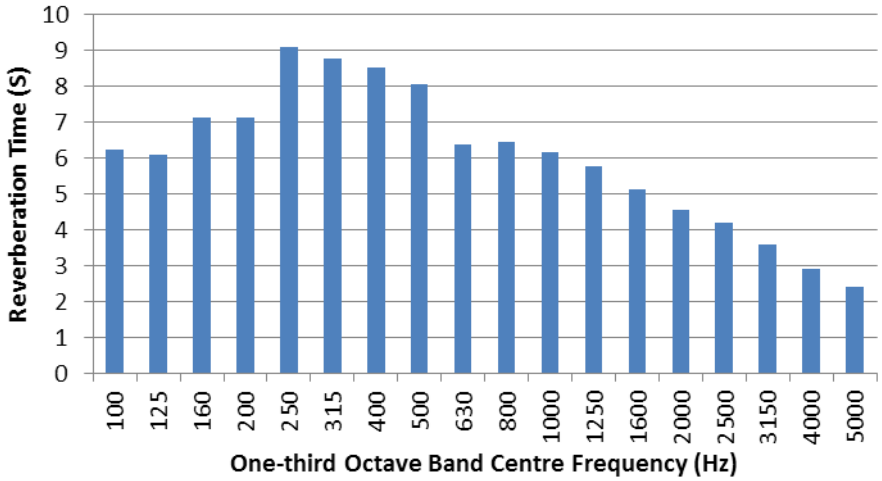

Figure 4.5: Measured reverberation time of the source room (reverberation room)

The measurement follows the process described in ISO 15186-1. However, the standard provides a reliable, repeatable method to base the test procedures on. The process followed is summarised below:

1. Five Brüel and Kjær 4189 free field microphones were arranged within the reverberation room (the measured sound pressure was post processed to account for the diffuse field conditions within the reverberation room). A Brüel and Kjær 4292-L dodecahedron sound source was also placed within the reverberation room.
2. The source room microphones were calibrated using a Brüel and Kjær Type 4231 sound level calibrator.
3. The sound intensity probe was calibrated using the Brüel and Kjær Type 4231 sound level calibrator and the associated coupler, as shown in Figure 4.6.

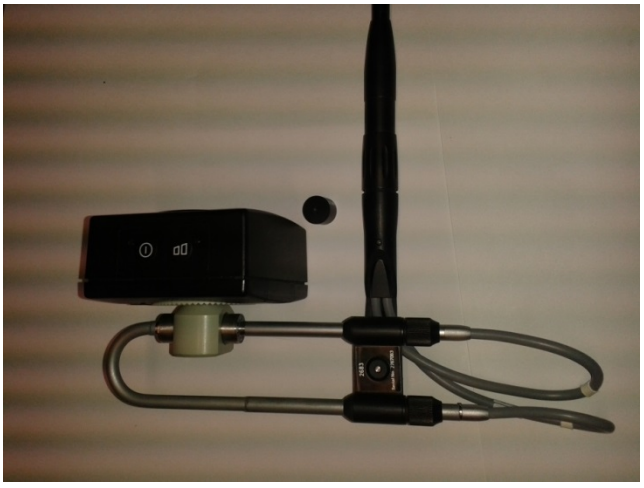

Figure 4.6: Calibration of the sound intensity probe

4. The sample was installed into the test aperture as shown in Figure 4.7. The installation is achieved via 14 M8 bolts which are tightened onto a section of steel box section (Figure 4.8); these bolts are torqued to 2 Nm.

Figure 4.7: Test aperture for small transmission loss samples

Figure 4.8: Mounting conditions for small transmission loss rig

5. The background sound pressure in the reverberation room level was measured.
6. The sound pressure level in the reverberation room with the sound source operating was measured.
7. The background pressure and intensity level was measured by placing the intensity probe 150 mm from the receiving room side of the sample and recording a 30 second measurement.
8. The sound source was switched on and the intensity level was measured on the receiving side. A vertical and a horizontal scan was performed across the surface of the panel as shown in Figure 4.9.

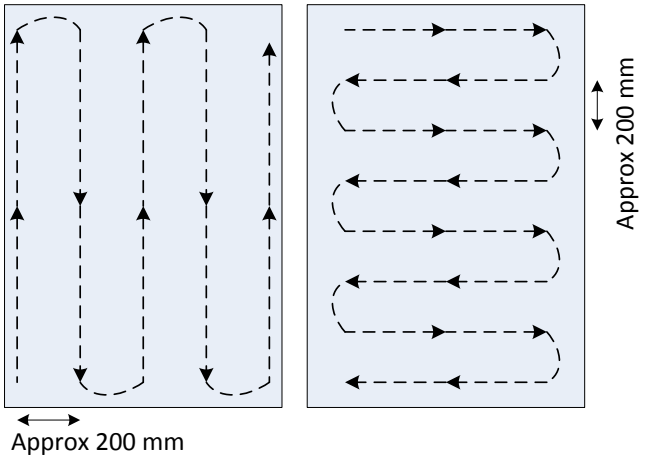

Figure 4.9: Scans used for small sound transmisison loss tests

9. The pressure-intensity index for each of these scans was calculated and the repeatability index was evaluated. If the pressure-intensity index was greater than 10 decibels and/or the repeatability index was greater than one decibel in any of the one-third octave frequency bands measured the measurement was repeated.
10. Steps 8 and 9 were repeated three times for each sample.

ISO 15186-1 provides Equation 4.6, which allows for the sound transmission loss to be calculated from source room pressure measurements and receiving room intensity measurements.

$$STL = L_{P_{(source\ room)}} - L_{I_{(receiving\ room)}} - 6 \qquad 4.6$$

where, $L_{P_{(source\ room)}}$ is the average sound pressure measured within the reverberation room and $L_{I_{(receiving\ room)}}$ is the sound intensity averaged over the surface of the sample.

Two primary checks were performed during measurements to assess whether the data was reliable. The pressure-intensity index (PI index, PI_{index}) and the repeatability index (R_{index}) was evaluated. The PI index is the difference between the mean pressure level and the measured intensity level at the location of the intensity probe, as given in Equation 4.7.

$$PI_{index} = L_{P_i} - L_I \qquad 4.7$$

where L_{P_i} is the mean pressure level measured by the intensity probe and L_I is the measured intensity level.

The repeatability index is the difference between the horizontal and vertical intensity scans and was calculated for each one third octave band (Equation 4.8).

$$R_{index} = L_h - L_v \quad 4.8$$

where L_h is the average intensity level measured during the horizontal scan and L_v is the average intensity level measured during the vertical scan.

The final sound transmission loss was calculated using the logarithmic average of the three intensity measurements (Equation 4.9). The repeatability of the measurements can be further evaluated by calculating the variation between these measurements. This can be represented as the standard deviation or variance of the measured transmission loss values.

$$L_{I_{tot}} = 10\log_{10}\left\{\frac{10^{\left(L_{I1}/10\right)} + 10^{\left(L_{I2}/10\right)} + 10^{\left(L_{I3}/10\right)}}{3}\right\} \quad 4.9$$

The results from the small transmission loss tests are evaluated in Section 5 and the full set of measurements with all the accuracy parameters are presented in Appendix A. As the sample size and location were not standard the measurements presented do not fully comply with ISO 151867-1 and ISO 10140; these measurements are still useful for comparative testing and initial evaluations of performance. The small transmission loss measurements are used extensively in Section 7 which evaluates the effects of sample size on the measured sound transmission loss.

4.4. Large Transmission Loss Rig

The University of Canterbury also has a large transmission loss facility. This facility is a 4200 mm × 2400 mm frame that separates a reverberation room from a semi-anechoic receiving room. The reverberation room is the same room as used in the small transmission loss tests (described in Section 4.3). The semi-anechoic receiving room has a volume of 200 m^3 and a surface area of 236 m^2. The receiving room is lined with absorptive materials on the walls and roof. The absorption in this room is increased by the addition of numerous hanging absorbers resulting in an absorptive "tunnel". This is projected out from the transmission loss sample to increase absorption of emitted sound. The floor directly behind the sample is also treated with a large number of absorptive panels that are laid down to reduce unwanted reflections.

To ensure accuracy and repeatability the large transmission loss test facility was evaluated following ISO 10140-5 [152] and ISO 10140-4 [153]. This evaluation required that a low performance partition were constructed in the test aperture. This test partition had to have a sound transmission loss that was below a maximum required level in the one third octave bands between 100 Hz and

315 Hz. The test sample selected was a single leaf 10 mm gypsum plasterboard wall, which had a transmission loss below the specified limit across the frequency range of importance (Figure 4.10).

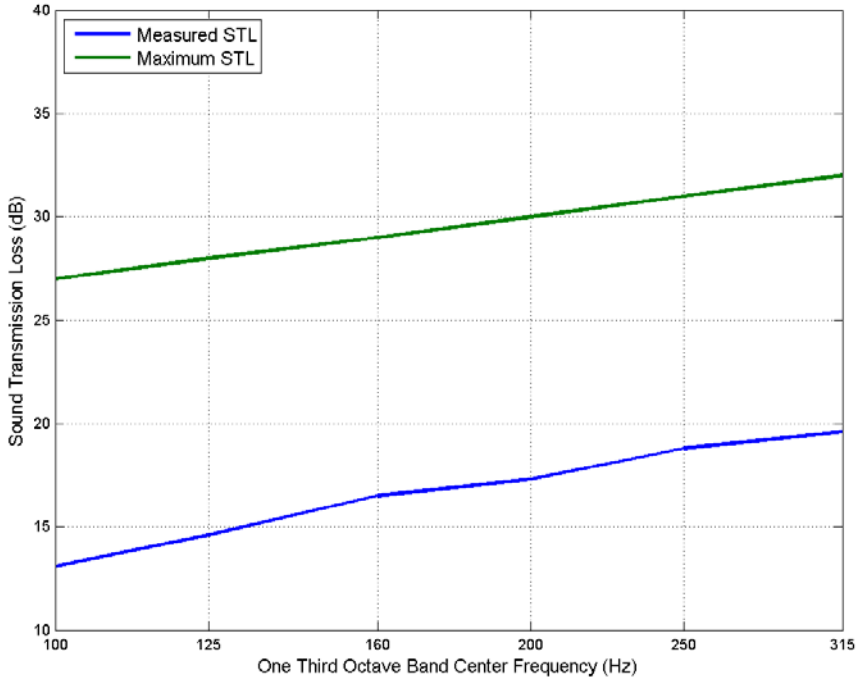

Figure 4.10: Sound transmission loss of validation partition

The effect of the speaker position on the measured transmission loss was evaluated. Six speaker positions were selected (Figure 4.11 and Table 4.1) based on the criteria given in Annex-D of ISO10140-5. It was assumed that the sound transmission loss calculated using the intensity method was equivalent to that of the pressure difference method.

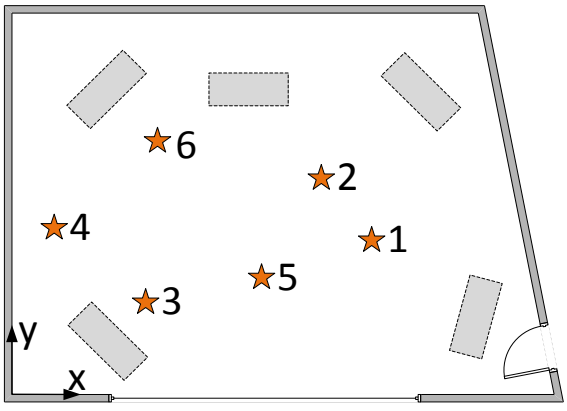

Figure 4.11: Speaker positions used to evaluate the large transmission loss facility's performance

Table 4.1: Positions of sound source for sound transmission loss tests

Location	X [m]	Y [m]	Z [m]
1	6.3	2.1	1.4
2	5.6	3.5	1.4
3	2.8	1.4	1.4
4	1.4	3.5	1.4
5	4.2	2.1	1.4
6	2.8	4.5	1.4

The variation between the transmission loss measured at each speaker position was evaluated (Figure 4.12). The mean sound transmission loss and the associated standard deviations were

calculated from all the speaker positions. The maximum variation must be below a set of values specified in Table D.1 of the standard. This condition was satisfied, as shown in Table 4.2.

Table 4.2: Allowable standard deviations due to speaker location

One Third Octave Frequency Band	Maximum Allowable Standard Deviation [dB]	Measured Standard Deviation [dB]
100	1.4	0.7
125	1.2	0.5
160	1.0	0.5
200	0.8	0.3
250	0.8	0.5
315	0.8	0.5

The number of speaker locations was specified by three conditions, given in Equations 4.10 through 4.12.

$$N_{speaker\_1} \geq 2 \tag{4.10}$$

$$N_{speaker\_2} \geq \left[\frac{\text{Measured Standard Deviation}}{\text{Maximum Allowable Standard Deviation}}\right]^2 \tag{4.11}$$

$$N_{speaker\_3} \geq \left[\sum_{\text{\# of Test Locations}} \left\{\frac{\text{Measured Standard Deviation}}{4.8\ \text{dB}}\right\}\right]^2 \tag{4.12}$$

The sum of the squared difference between the average transmission loss and the different speaker locations was used to select the speaker locations (Equation 4.13).

$$Diff\_1 = \sum_{i=1}^{6} \{\text{Difference between Mean STLand } i^{th} \text{ STL Measurement}\} \tag{4.13}$$

The results of Equations 4.11 – 4.14 are summarised in Table 4.3

Table 4.3: Results of speaker location selection calculations

One Third Octave Frequency Band	$N_{speaker\_2}$ [dB]	$N_{speaker\_6}$ [dB]	Smallest Squared Difference ($Diff\_1$)
100	0.23	0.14	1619
125	0.14	0.09	1538
160	0.24	0.10	1532
200	0.15	0.06	1568
250	0.35	0.10	1624
315	0.34	0.10	1583

The location that had the smallest squared difference was selected as the primary location. A secondary position was also selected for performing two speaker measurements; this position was selected to have the second lowest squared difference. The final speaker positions are given in Figure 4.13 and Table 4.4.

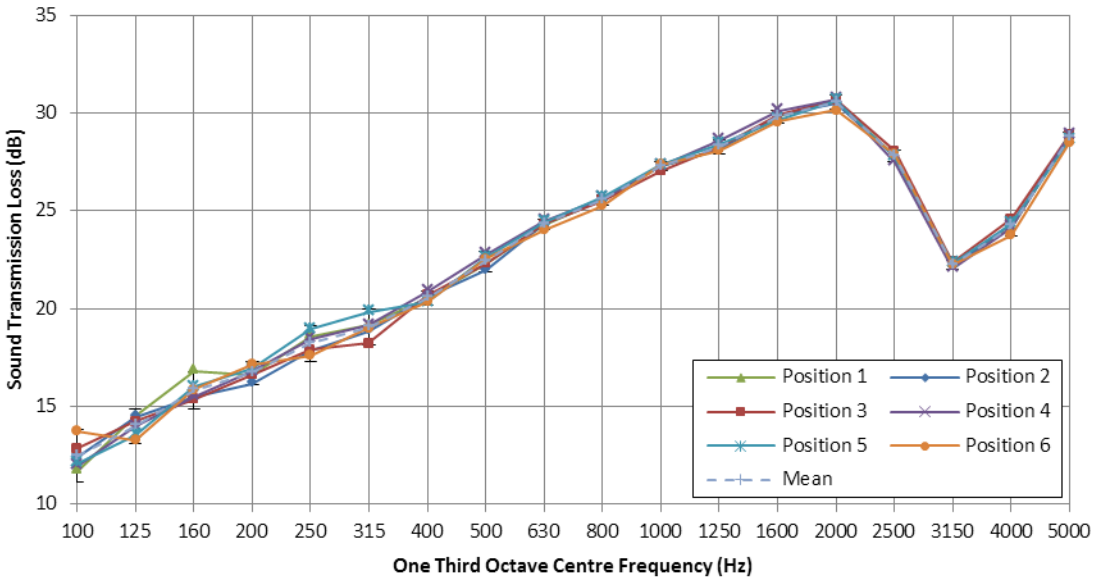

Figure 4.12: Sound transmission loss results for six speaker position tests performed

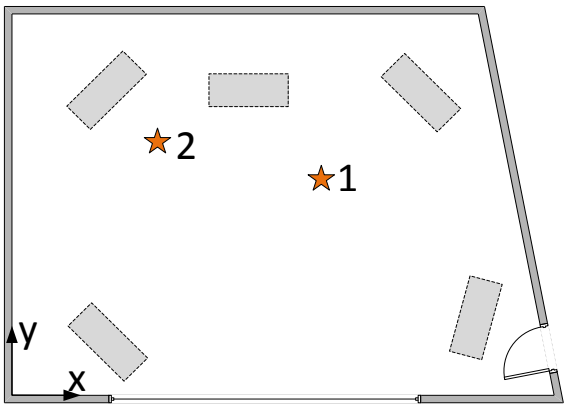

Figure 4.13: Final speaker positions used for all sound transmission loss measurements

Table 4.4: Final speaker locations for transmission loss measurements

Location	X	Y	Z
1	5.6	3.5	1.4
2	2.8	4.5	1.4

The use of two speaker positions improves the reproducibility of the measurements. The two speaker locations allowed the variation between these two positions to be evaluated. The difference between the two speaker positions was utilised to evaluate the transmission loss dependence on location. If the location dependence was larger than a 95% confidence interval of the measured sound transmission loss it was assumed that the system had become location dependent. This 95% confidence interval was calculated from the repeated sound transmission loss scans performed for all the speaker locations.

The optimal microphone positions were selected by performing 30 sound pressure level measurements within the reverberation room. The positions were selected according to the requirements set out in ISO10140 and ISO15186-1. These test positions are presented in Figure 4.14 and Table 4.5.

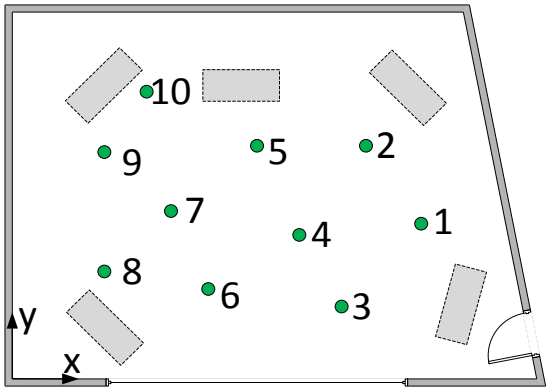

Figure 4.14: Approximate microphone positions for room evaluation

Table 4.5: Microphone locations tested for ISO 10140-4

Location	X [m]	Y [m]	Z [m]
1	7.7	2.8	0.7, 1.4, 2.1
2	7	3.9	0.7, 1.4, 2.1
3	6.6	1.8	0.7, 1.4, 2.1
4	5.6	2.8	0.7, 1.4, 2.1
5	4.9	3.9	0.7, 1.4, 2.1
6	3.9	2.1	0.7, 1.4, 2.1
7	3.2	3.2	0.7, 1.4, 2.1
8	1.8	2.9	0.7, 1.4, 2.1
9	1.8	3.9	0.7, 1.4, 2.1
10	2.1	4.9	0.7, 1.4, 2.1

At each of these locations the sound pressure level was measured. From this set six final locations were selected that are close to the average pressure level and result in a reasonable spatial sample of the reverberation room. The measured sound pressure levels of these selected microphone positions are presented in Figure 4.15.

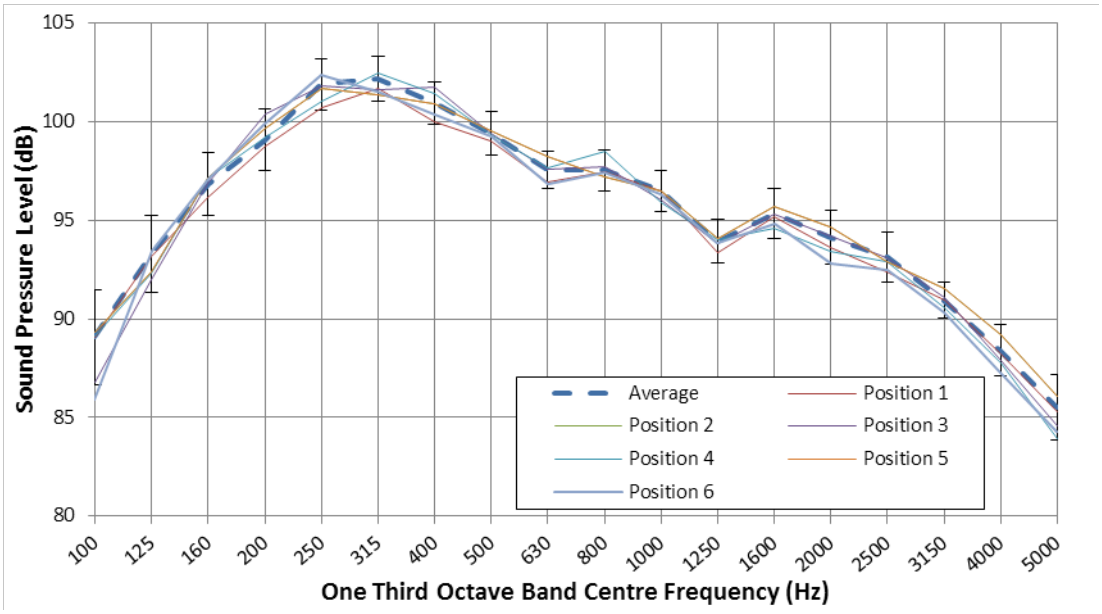

Figure 4.15: Sound pressure levels of selected microphones

Standardising the microphone locations also allowed for greater repeatability between tests; as the microphones were often removed from the reverberation room for other tests. The final locations used are given in Figure 4.16 and Table 4.6.

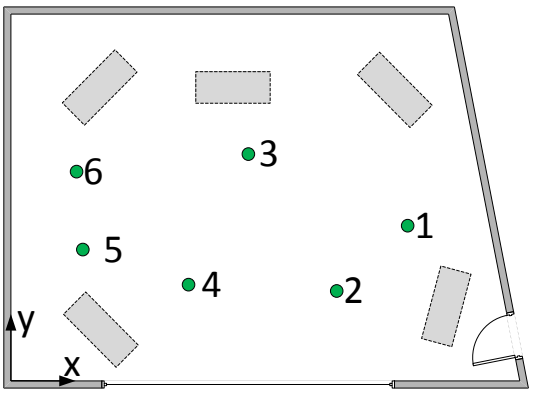

Figure 4.16: Positions of microphones for sound transmission loss tests

Table 4.6: Positions of microphones for sound transmission loss tests

Location	X [m]	Y [m]	Z [m]
1	7.7	2.8	1.4
2	6.6	1.8	0.7
3	4.9	3.9	1.4
4	3.9	2.1	1.4
5	1.8	2.9	1.4
6	1.8	3.9	1.4

The 30 measurements of the sound pressure levels were also used to evaluate the variation in the pressure level within the room. The variance and standard deviation of the sound pressure level was evaluated from the 30 measurements (Figure 4.17). The standard deviation was less than 2 decibels throughout the room, except in the 100 Hz band which is expected due to the large wavelengths of the sound in this band.

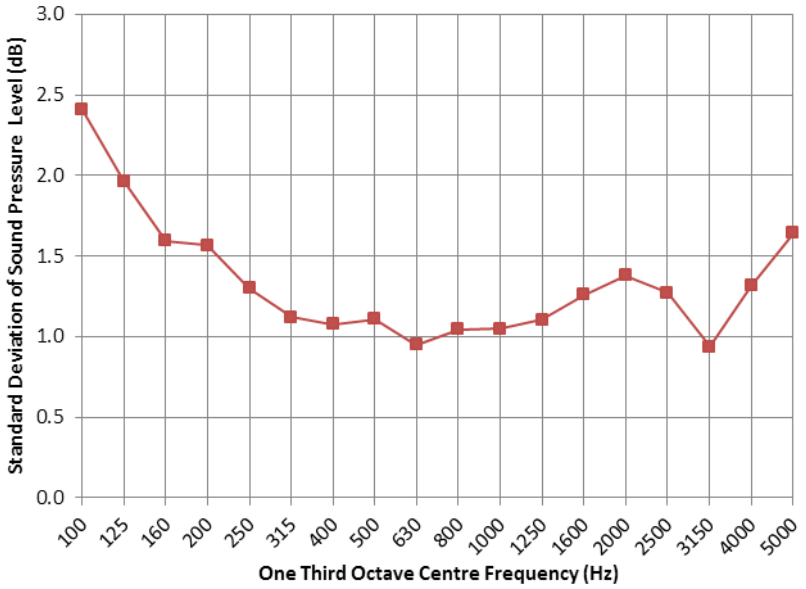

Figure 4.17: Standard deviation of sound pressure levels within the reverberation room

The sound transmission of the large partitions was measured using a Brüel & Kjær Pulse System unit running Brüel & Kjær Pulse software. This system was evaluated against a Brüel & Kjær 2260 system that was traditionally used in sound transmission loss tests at the University of Canterbury. The sound transmission loss measured using both the Brüel & Kjær 2260 and the Brüel & Kjær Pulse

system is presented in Figure 4.18. There is very little variation between the two methods with the absolute variation less than one decibel in all one third octave bands of interest.

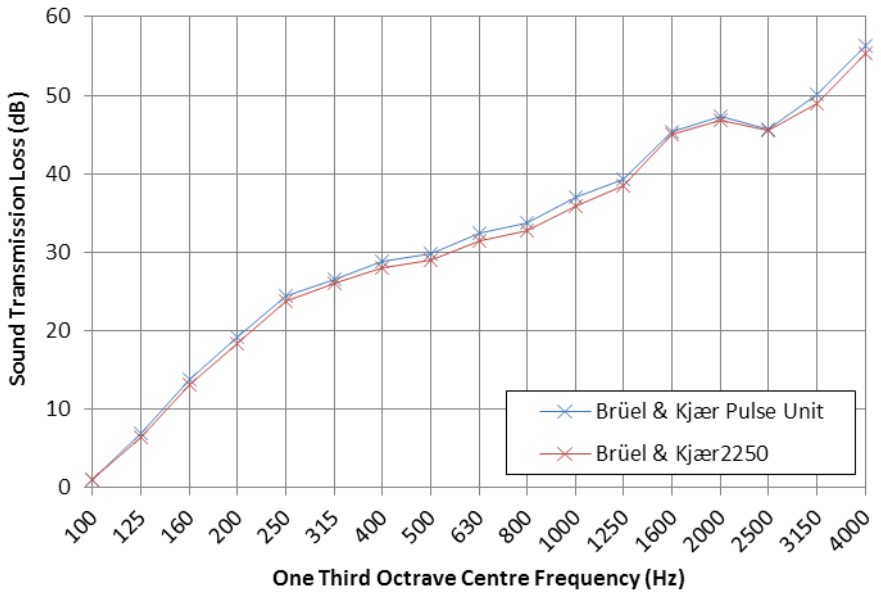

Figure 4.18: Sound intensity of a sample partition using two measurement systems

The 2260 was used for some of the transmission loss measurements when the Pulse System was unavailable, but the majority of measurements were made using the Pulse system as it allowed the intensity variations to be assessed immediately.

The process used for the testing was similar to the method described for the small test rig. The test steps are highlighted below.

1. The test partition was constructed in the aperture.
2. The five microphones were placed in the positions outlined in Table 4.6, and the sound source was placed in the first location given in Table 4.4.
3. The microphones were calibrated using the Brüel and Kjær Type 4231 sound pressure level calibrator.
4. The intensity probe was calibrated as described in the small sample methodology.
5. A 30 second measurement was made of the background sound pressure level and the sound pressure level when the sound generator was activated.
6. The background intensity and pressure levels were measured on the receiving room side at 150 mm from the surface of the panel.
7. The intensity was measured using the scan pattern shown in Figure 4.19.

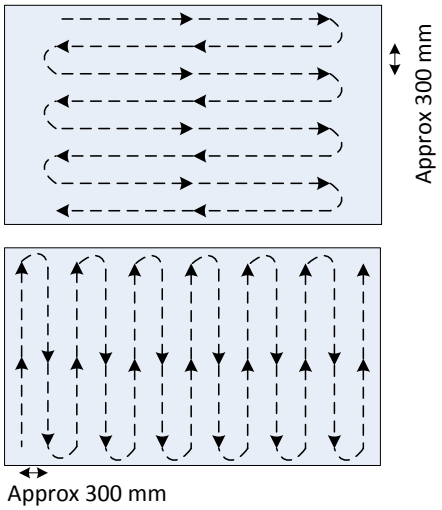

Figure 4.19: Intensity scan pattern for large transmisison loss rig

8. As with the small transmission loss facility the pressure-intensity and repeatability indexes were calculated. If the pressure-intensity index was greater than 10 decibels or the repeatability index was greater than one decibel in any one-third octave band the measurement was repeated.
9. Five pairs of scans were performed for each of the two speaker locations, yielding a total of ten scans for each total measurement.

The average transmission loss for each speaker location was calculated using the logarithmic averaged intensity measurements given by Equation 4.14. The two transmission loss measurements from each position were calculated, these logarithmically averaged to provide the final sound transmission loss.

$$L_{I_{tot}} = 10\log_{10}\left\{\frac{10^{\left(L_{I1}/10\right)} + 10^{\left(L_{I2}/10\right)} + 10^{\left(L_{I3}/10\right)} + 10^{\left(L_{I4}/10\right)} + 10^{\left(L_{I5}/10\right)}}{5}\right\} \qquad 4.14$$

4.5. Radiation Efficiency Tests

The radiation efficiency of the large partitions was evaluated experimentally. The radiation efficiency is defined in Section 2.7. Equation 4.14 can be rewritten in terms of the measured sound intensity, by expressing the sound intensity as the sound power per unit area radiated from the surface of the panel. This yields Equation 4.15 for the radiation efficiency of a surface (σ) which is a function of the intensity and surface velocity.

$$\sigma = \frac{I}{\rho_0 c_0 \langle \dot{x}^2 \rangle_{t,s}} \qquad \textbf{4.15}$$

where $\dot{x}$ is the normal surface velocity.

The surface velocity of the receiving room leaf was measured using two PCB 352C42 accelerometers. These accelerometers were placed at 14 randomised locations across the surface of the panel, the approximate location of the measurements is shown by Figure 4.20.

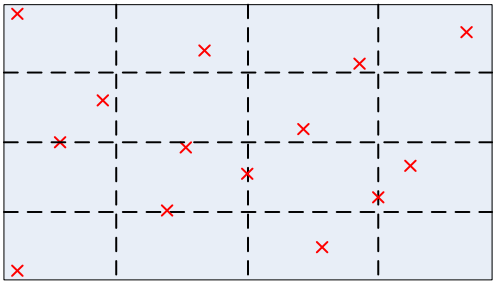

Figure 4.20: Location of accelerometer measurement positions for radiation efficiency tests

An effort was made to ensure measurements were performed on both the unsupported areas as well as the areas with studs or dwangs behind them. The acceleration and velocity spectra at each of these points were measured in one third octave bands. The accelerometer measurements were averaged over 30 seconds to give a time averaged velocity value. The velocity response of the partition was combined with the radiated sound intensity measured during the sound transmission loss measurements. This yields the average normalised radiation efficiency of the panel.

4.6. Point Intensity, Vibration and Radiation Scans

Two point scans were performed on the full sized transmission loss samples. These point scans were undertaken to assess the effect of the studs and edges on both the sound transmission loss and the radiation efficiency of the panel. The measurements were performed on a 12 mm single leaf partition. The point scan was performed using the same Brüel and Kjær intensity equipment as used for the sound transmission loss measurements. This was combined with a series of point vibration measurements of the partition that were undertaken using PCB 352C03 accelerometers.

The intensity was measured using the intensity probe mounted to a tripod, with a small piece of plastic designed to ensure the probe was 150 mm from the surface. The arrangement used is shown in Figure 4.21.

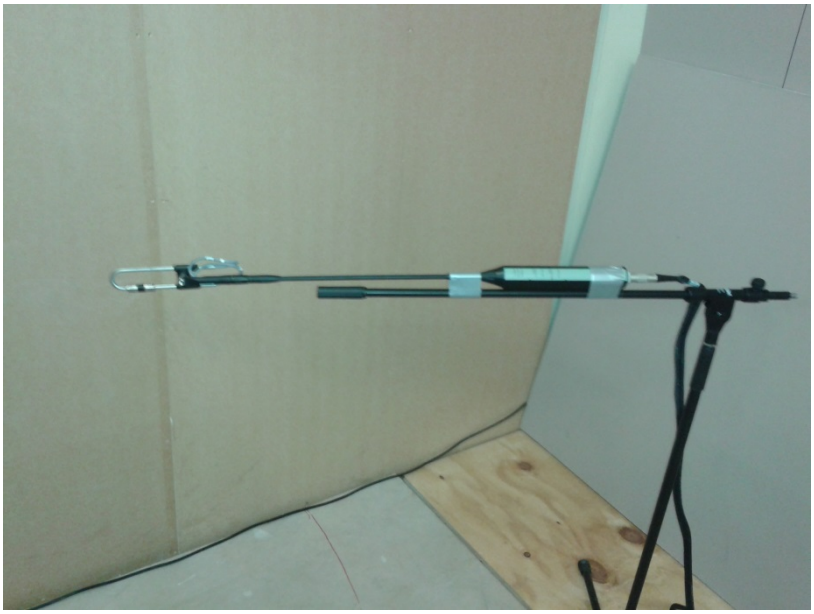

Figure 4.21: Intensity probe mounted on tripod to perform point scan of plywood partition

The sound source was the same as used in the sound transmission loss measurements. A 30 second measurement of the sound intensity on the receiving room side was performed for each point in an offset measurement grid, as shown in Figure 4.22. The surface velocity and the surface acceleration was measured at the same points.

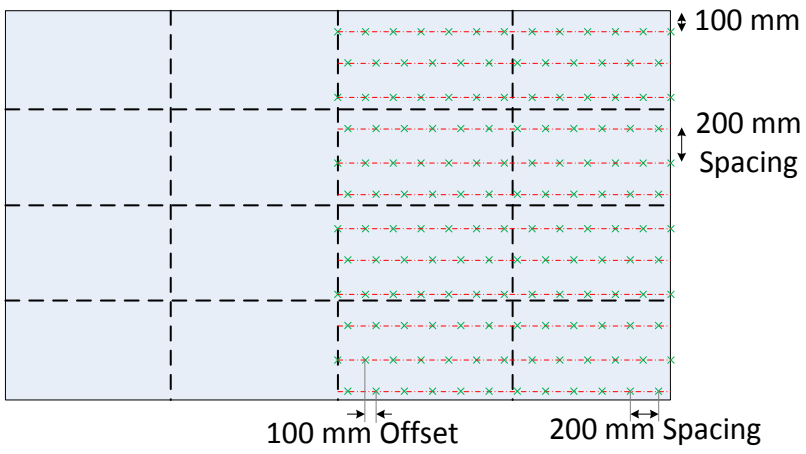

Figure 4.22: Measurement grid used to perform point scan on surface of large transmisison loss rig

These measurements were processed to calculate the vibration, intensity and radiation efficiency across the surface of the partition. This allows surface contours of the partition vibration, intensity, and radiation efficiency to be produced. These results are presented in Section 6.3.

5. Sound Transmission Loss Results from Small Test Rig

This section presents the sound transmission loss results from the plywood samples in the small transmission loss facility. A brief discussion of the results and the trends observed is presented.

5.1. Description of Tests

The sound transmission loss of seven small single leaf plywood samples was evaluated using the small transmission loss facility described in Section 4.3. A double leaf plywood partition and a single leaf partition of gypsum plasterboard were also evaluated. This small facility allows numerous samples to be tested quickly and efficiently. Section 7 discusses the effect of the smaller transmission loss rig on the measured transmission loss on a range of different samples.

Table 5.1: Samples tested in the small sound transmission loss facility

Sample Number	Number of Leaves	Details of Leaves
1	1	7 mm plywood (without studs)
2	1	9 mm plywood (without studs)
3	1	12 mm plywood (without studs)
4	1	12 mm plywood (with studs)
5	1	15 mm plywood (without studs)
6	1	17 mm plywood (without studs)
7	1	18 mm plywood (without studs)
8	1	19 mm plywood (without studs)
9	1	21 mm plywood (without studs)
10	2	12 mm plywood (double leaf with studs
11	1	10 mm gypsum plasterboard (without studs)

The measured sound transmission loss, and the associated pressure-intensity and repeatability indexes, of each sample are presented in Appendix A. The corresponding calculated STC and R_w values are also presented for each sample.

5.1.1. Installation Details

A sample mounted in the small transmission loss test rig is shown in Figure 5.1. These panels are clamped in place using the bolts that can be seen around the outside edges of the sample. These bolts press on a steel box section that provides an even clamping force around the edges of the panel

Figure 5.1: Small transmission loss sample installed in small test rig

The double leaf partitions were tested in the same manner, the mounting frame is 550 mm deep, allowing double leaf studded partition systems to be installed.

The frame is mounted to a heavy concrete wall; which is also the reverberation room wall. The samples are then clamped in place using a frame of RHS steel around the perimeter. The location of the sample within the frame yields two niches; a source room niche and a receiving room niche; as shown in Figure 5.2 and Figure 5.3. The effective niche depths are summarised in Table 5.2.

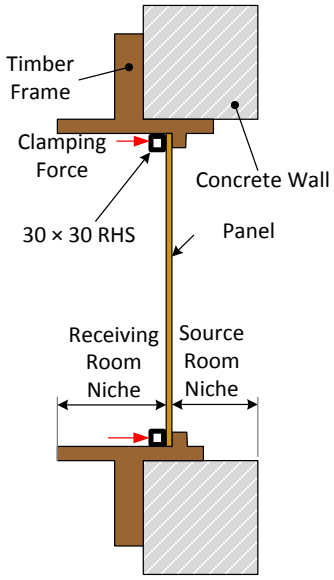

Figure 5.2: Location of single leaf test sample within small transmission loss rig

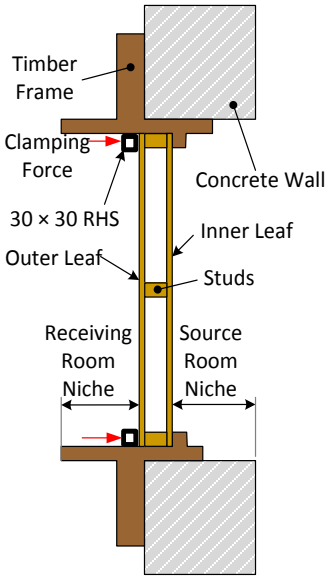

Figure 5.3: Location of double leaf test sample within small transmission loss rig

Table 5.2: Niche details of small transmission loss rig

Sample	Source Room Niche Depth	Receiving Room Niche Depth
Small Single Leaf Samples	350 mm	200 mm (less the panel thickness)
Small Double Leaf Samples	350 mm	200 mm (less the partition thickness)

5.2. *Results and Discussion*

Figure 5.4 shows the measured sound transmission loss of seven single leaf plywood panels tested using the small transmission loss facility. The plywood exhibits typical single leaf sound transmission loss behaviour. In all cases a coincidence dip is seen at the higher frequencies (2000 to 4000 Hz) the location of which was dependent on the stiffness and the mass of the panel. As the thickness of the plywood is increased the low frequency transmission loss increases as is predicted by the mass law. Above the mass controlled region all the plywood samples enter a coincidence region as discussed in Section 2. Above the coincidence dip the sound transmission loss behaviour enters a region of relatively consistent sound transmission loss increase.

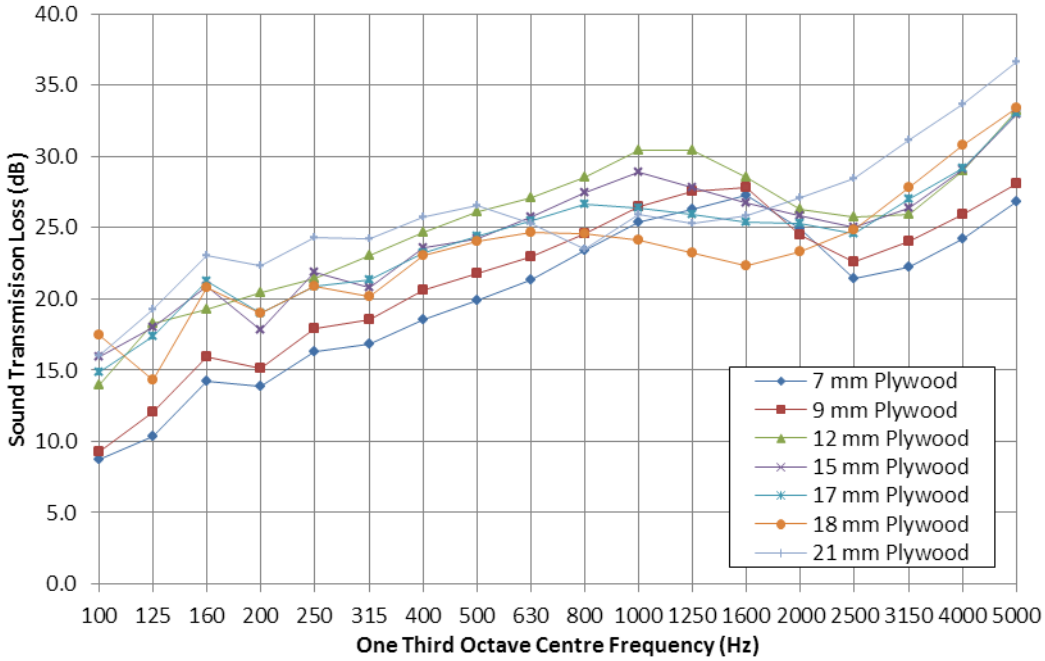

Figure 5.4: Sound transmission loss of various thicknesses of plywood panels

The coincidence region is heavily influenced by the orthotropic properties of the plywood. This orthotropic stiffness causes the coincidence region to be extended over a much larger frequency range that would be expected in an isotropic material. The plywood thickness strongly affects the location, depth and extent of this coincidence region. This dependence on thickness is due to the orthotropic bending stiffness being heavily dependent on the total thickness of the panel.

As the thickness of the panels increases, the ratio between the two bending stiffness's decreases. The results presented in Section 3 show the variation in material stiffness with thickness. The two bending stiffness allow two coincidence frequencies to be calculated for a single panel. This causes the orthotropic stiffness to stretch the coincidence dip of the panel over a wider frequency range.

A narrower and deeper reduction in the measured sound transmission loss around the coincidence frequencies as the orthotropic stiffness ratio is decreased is expected from current theories. This is not evident in Figure 5.4. Despite the fact the thinner plywood has a larger orthotropic stiffness ratio than the 21 mm plywood, the thinner 7mm plywood has a much deeper coincidence dip. This is due to the significantly lower surface density causing the plywood to be more susceptible to the rapid decrease in sound transmission loss that occurs at the critical frequency.

The transmission loss of a single leaf partition without studs is compared to a single leaf partition with studs in Figure 5.5. It is evident that the studs cause a significant difference in the measured sound transmission loss. This is especially evident around the critical frequency, where the studs appear to shift the coincidence dip approximately two thirds of an octave below the sample without studs. This is probably due to the large increase in bending stiffness caused by the studs; the critical frequency is proportional to the square root of the bending stiffness and as such the studs lower the critical frequency. It is interesting to note that the increased mass due to the studs should increase the critical frequency, but this effect is less significant than the influence of the increased stiffness.

Outside of the critical region there is less variation between the two sets of measurements. The low frequency behaviour is very similar; with some variations at the very low frequencies that could be due to resonant behaviour. Above the coincidence regions of both samples the transmission loss behaviour appears to move towards convergence.

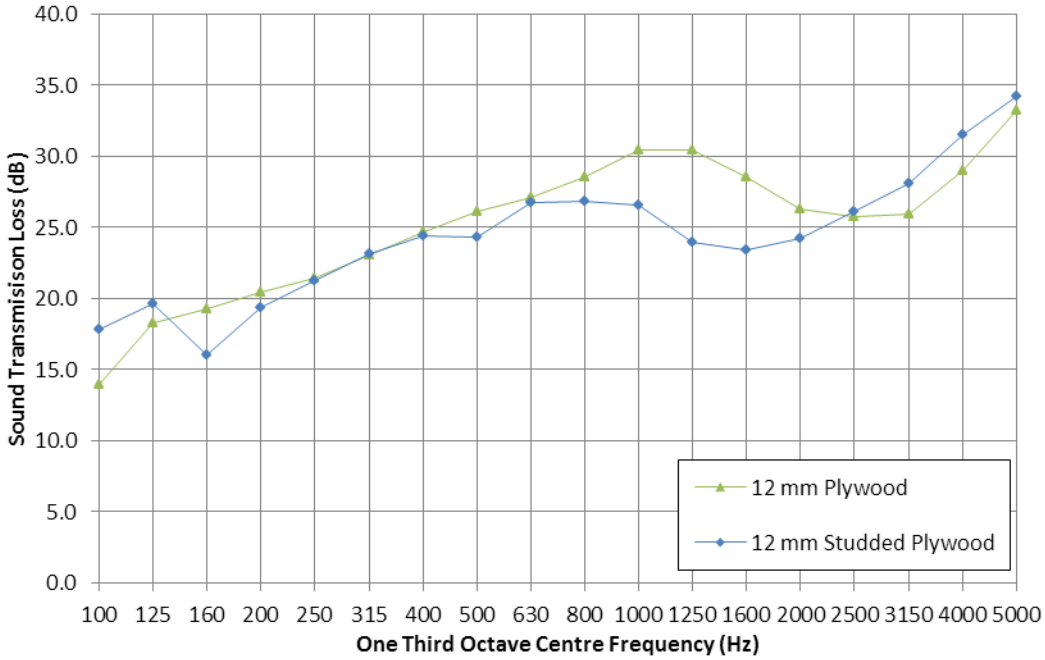

Figure 5.5: Effect of the inclusion of studs on the sound transmission loss of a small single leaf 12 mm plywood partitions

Figure 5.6 shows the difference between a single and double leaf 12 mm plywood partitions measured using the small transmission loss rig. As expected the double leaf sample has a significantly higher sound transmission loss curve over the entire frequency range. There is some convergence in the 160 Hz one-third octave frequency band, which is likely due to the mass-air-mass resonance of the double leaf which can be calculated using Equation 2.6. For a 12 mm plywood panel with a surface mass of approximately 6 kg/m^2 and a separation of approximately 100 mm, the mass-air-mass resonance is between 110 Hz and 145 Hz (depending whether the 1.8 factor proposed by Fahy is utilised [20]). This resonance causes a decrease in the transmission loss of the double leaf system resulting in convergence between the single and double leaf partitions. Above this frequency the sound transmission loss curves diverge, with the double leaf partition having a significantly higher sound transmission loss across the rest of the frequency range. The coincidence region is also less significant in the double leaf partition whereas a very wide and shallow coincidence dip is seen in the behaviour of the single leaf plywood panel.

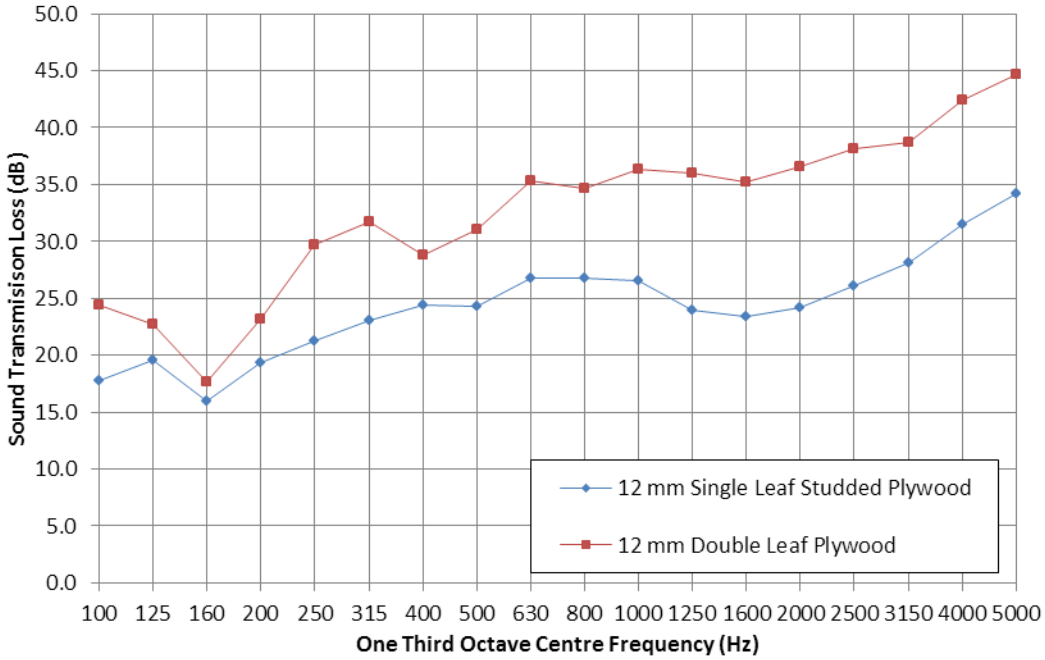

Figure 5.6: Difference between a single and a double leaf 12 mm plywood partitions

To investigate the influence of the orthotropic stiffness on the measured sound transmission loss a 10 mm gypsum plasterboard panel was tested. The plasterboard can be assumed to be relatively orthotropic in comparison to the plywood panels. Figure 5.7 compares the transmission loss of several plywood samples with the transmission loss of the 10 mm plasterboard sample. The coincidence dip of the plasterboard is much narrower and deeper than that of an equivalent plywood panel. This behaviour is expected as the orthotropic stiffness spreads the coincidence behaviour over a wider range of frequencies.

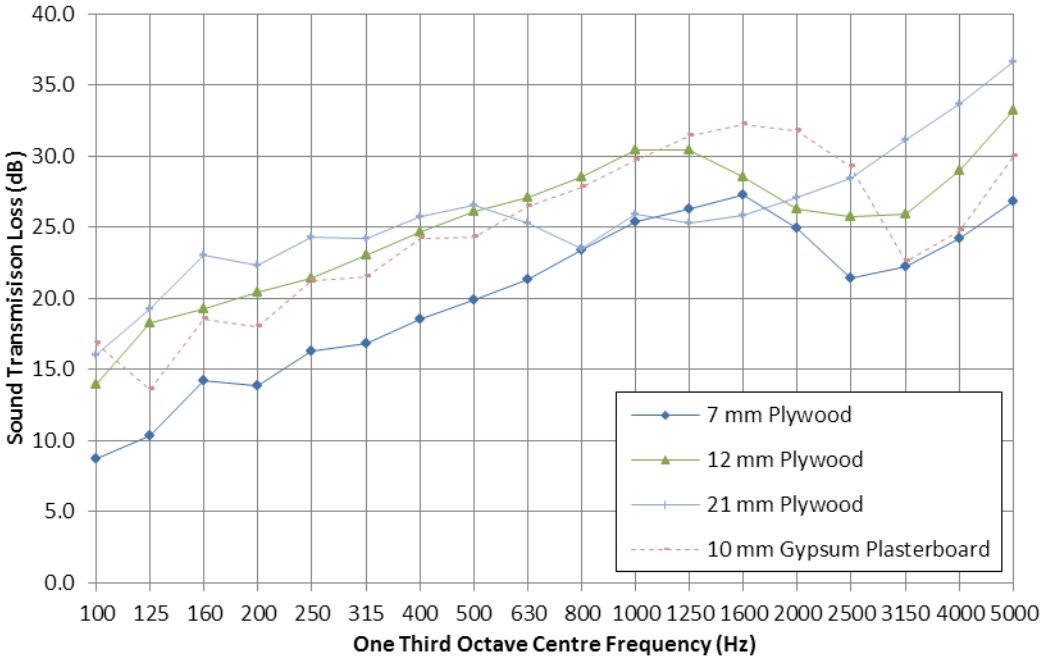

Figure 5.7: Difference between a several plywood and a plasterboard single leaf partitions

The above qualitatively correspond to current theories of the behaviour of both isotropic and orthotropic materials. These results will be compared to the results from the large transmission loss samples in Section 7. The results presented here are utilised along with the results from the large facility presented in Section 6 to investigate the performance of the transmission loss models presented (see Section 9).

6. Sound Transmission Loss Results from Large Test Facility

The results of sound transmission loss tests performed in the large (2.4 m × 4.8 m) transmission loss facility are presented and discussed. The discussion explores the effects of the construction (studs) on the vibration and radiation efficiency.

6.1. Description of Tests

The sound transmission loss of fourteen partitions (see Table 6.1) were measured in the large test facility. The samples were constructed on a 90 mm timber stud frame mounted in the test aperture between the reverberation room and the semi anechoic space.

The cavity in the double leaf partition was empty (i.e. no absorbing material was present). This maximised the influence of the airborne transmission path which was appropriate in view of the prediction work presented later in this thesis.

A number of the samples consisted of mismatched double leaf partitions. The interaction between the leaves of these mismatched samples was of considerable interest when combined with the effects of orthotropic stiffness and frequency dependent material properties. This mismatch causes the partition to have two different critical frequencies resulting in a less significant coincidence dip. Furthermore these mismatched leaves result in altered mass-stiffness-mass behaviours.

Table 6.1: Samples tested in the large sound transmission loss facility

Sample Number	Number of Leaves	Leaf One	Leaf Two
1	1	7 mm plywood	N/A
2	1	9 mm plywood	N/A
3	1	12 mm plywood	N/A
4	1	21 mm plywood	N/A
5	2	9 mm plywood	9 mm plywood
6	2	12 mm plywood	12 mm plywood
7	2	21 mm plywood	21 mm plywood
8	2	10 mm gypsum plasterboard	10 mm gypsum plasterboard
9	2	7 mm plywood	9 mm plywood
10	2	7 mm plywood	10 mm gypsum plasterboard
11	2	9 mm plywood	12 mm plywood
12	2	21 mm plywood	12 mm plywood
13	1	12 mm damped plywood	N/A
14	2	12 mm damped plywood	12 mm damped plywood

6.1.1. Installation Details

The test partitions were installed in the test aperture on a timber stud frame. The frame is shown in Figure 6.1 without one of the leaves removed.

Figure 6.1: Timber frame with one leaf removed

The frame was constructed from 90 mm × 45 mm timber. The frame had studs placed at 600 mm centres and dwangs at 800 mm centres; as shown in Figure 6.2. The edges of the timber frame were bolted to the surrounding concrete wall system. The leaves were installed on either side of this frame, resulting in a single stud arrangement.

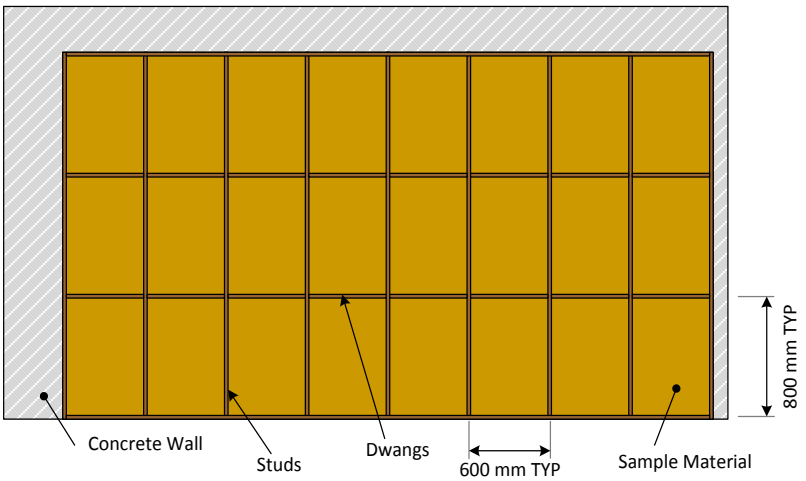

Figure 6.2: Schematic of timber frame for large tests

Bolts ensured the frame was mounted in the same location in the concrete aperture for all the samples, resulting in a constant niche depth on the source and receiving room sides. The

arrangement of a single leaf partition in the large transmission loss rig is shown in Figure 6.3; and a double leaf partition is shown in Figure 6.4.

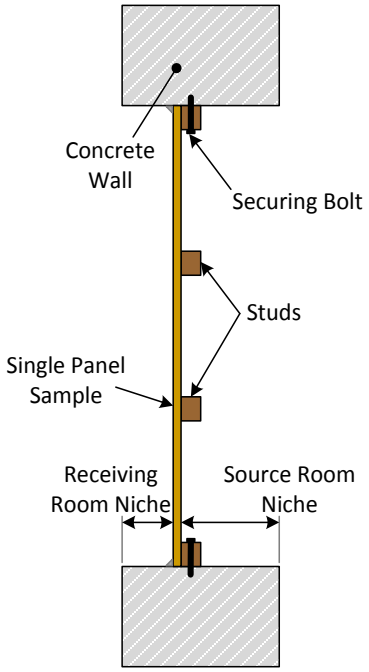

Figure 6.3: Arrangement of single leaf studded partition within the large transmission loss facility

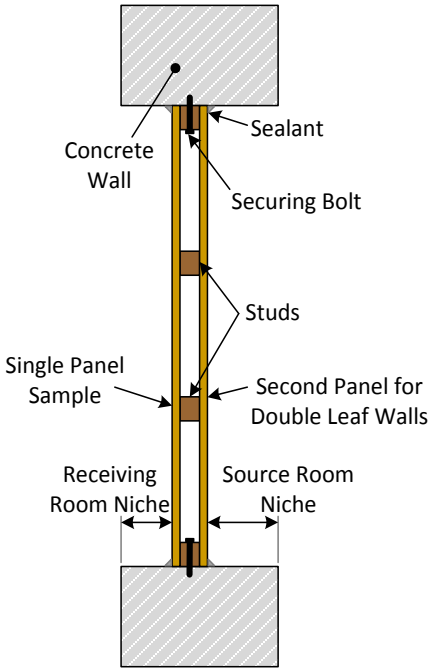

Figure 6.4: Arrangement of double leaf studded partition within the large transmission loss facility

The niche depth associated with the arrangements depended on the thickness of the facing sheets. The overall niche depths are presented in Table 6.2.

Table 6.2: Niche details of large transmission loss rig

Sample	Receiving Room Niche Depth	Source Room Niche Depth
Large Single Leaf	210 mm (less the panel thickness)	160 mm
Large Double Leaf	210 mm (less the panel thickness)	70 mm (less the panel thickness)

The samples were attached to the frame using screws at 150 mm centres. The screwing and subsequent re-screwing of panels onto the frame resulted in damage to the timber frame. Once the frame had become significantly damaged (usually after the construction of 3 to 4 partitions) the frame was replaced.

Once attached the plywood panels were sealed using a jointing compound around the edges, as shown in Figure 6.5. The joints between individual panels were sealed with a jointing compound and covered with tape. This ensured the walls were well sealed and direct airborne paths were minimised.

Figure 6.5: Screwed and sealed partition

6.2. Results and Discussion

The sound transmission loss results are compared in this section and are presented in detail in Appendix B. This appendix also presents the measured pressure-intensity and repeatability indexes.

Figure 6.6 shows the variation in the sound transmission loss of large, studded single leaf plywood partitions. The plywood results are also compared to a single leaf 10 mm gypsum plasterboard partition of the same area. The general trends present in the small sample size (Section 5) are seen in the large sample size. As the thickness of the plywood increases the low frequency transmission loss increases. This is due to the increased mass of the thicker plywood panels; as predicted by existing theories. An increased surface mass wasalso expected to result in a higher sound transmission loss at higher frequencies.

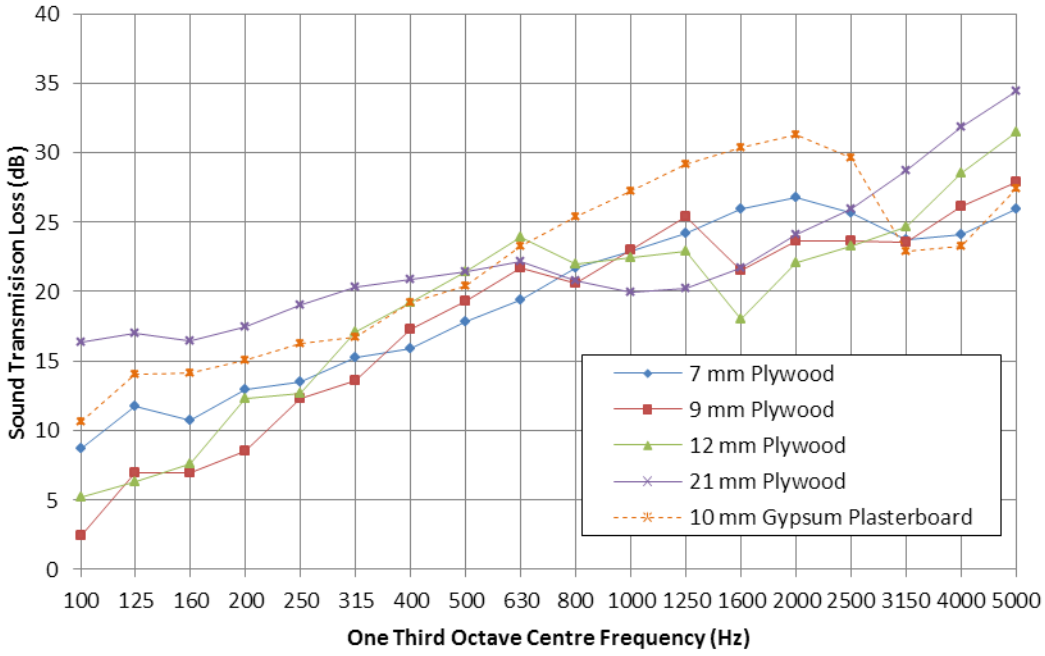

Figure 6.6: Transmisson loss of single leaf plywood partitions measured in the large transmission loss facility

The single leaf plywood partitions all have a relatively wide coincidence region, due to their orthotropic stiffness. The gypsum has similar low frequency behaviour to the plywood, but the coincidence region of the gypsum is markedly narrower and deeper than the plywood partitions.

Above the coincidence region the sound transmission loss of the plywood increases at a relatively consistent rate about of eight decibels per octave. This is the damping controlled region predicted by classical transmission loss models. The onset of the stiffness controlled region is delayed by the wider coincidence region.

The double leaf partitions exhibit some of the orthotropic behaviour seen in the single leaf samples; see Figure 6.7. There is a very wide and shallow coincidence region at a similar frequency. There is no clear coincidence dip, rather the region is a slight but wide reduction in the gradient of the transmission loss curve.

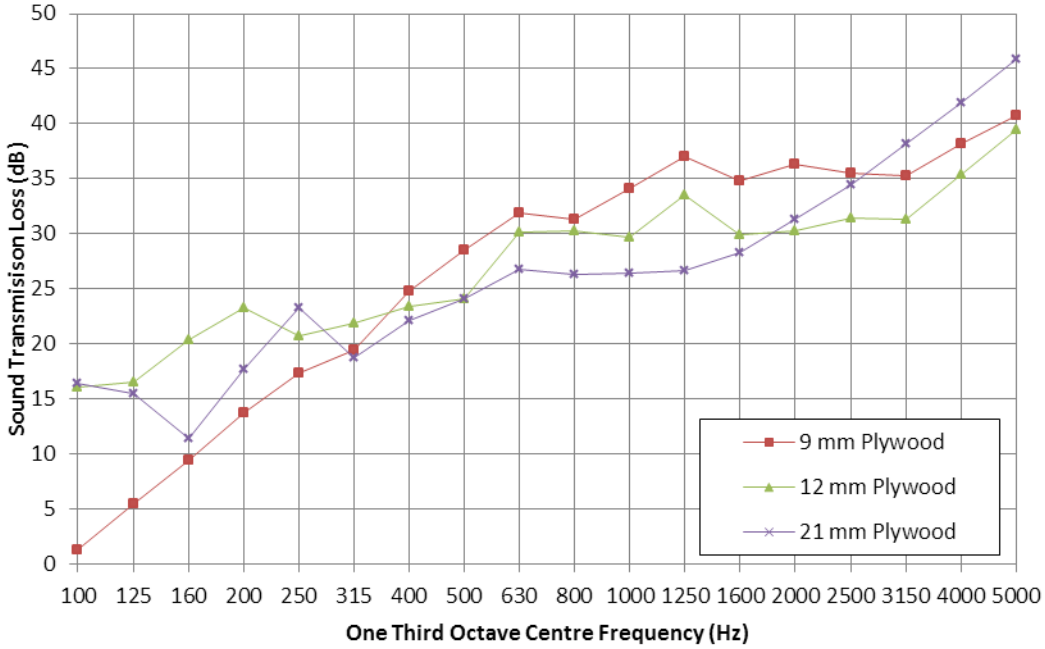

Figure 6.7: Transmission loss of double leaf plywood panels measured in the large transmission loss facility

Figure 6.8 shows the measured sound transmission loss of three mismatched double leaf partitions. These systems exhibit a clear combination of the sound transmission loss behaviour of each of the leaves. The lighter panel generally dominates the overall sound transmission loss behaviour. The two samples that have a 7 mm plywood panel show the influence of the lightweight plywood panel (see Figure 6.6). These effects are compounded by a mass-air-mass resonance that occurred within the 100 Hz one third octave centre frequency which results in a significant decrease in the sound transmission loss.

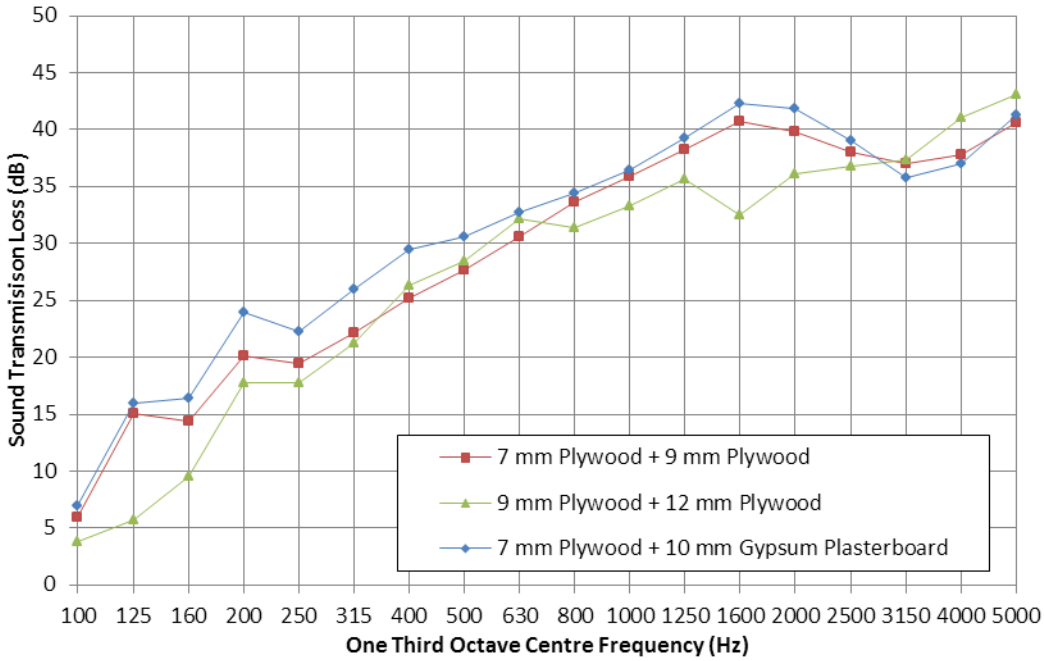

Figure 6.8: Sound transmission loss of mismatched double leaf partitions measured in the large transmission loss facility

The transmission loss measurements that have been presented above provide a basis for the development of analytical models of the sound transmission loss (presented in Section 9). The influence of the orthotropic properties on the measured behaviour of the partitions justifies the development of a model that accounts for this behaviour.

6.3. Point Intensity and Vibration Measurement

As described in Section 4.6 a point scan of a single leaf partition was performed. This allowed the intensity, velocity and radiation efficiency to be evaluated across the surface of the partition, as presented in Figure 6.9 – Figure 6.17. The intensity scans (Figure 6.9, Figure 6.10 and Figure 6.11) show a relatively small variation in intensity levels. The variation in the intensity is approximately seven decibels across the surface of the panels.. This relatively uniform sound intensity distribution indicates that the free scan method used in the sound transmission loss measurements is appropriate. The uniformity of the sound intensity also explains why the repeatability index requirements were easily met. The scan was performed over one half of the partition as it was assumed this would sufficiently sample the behaviour.

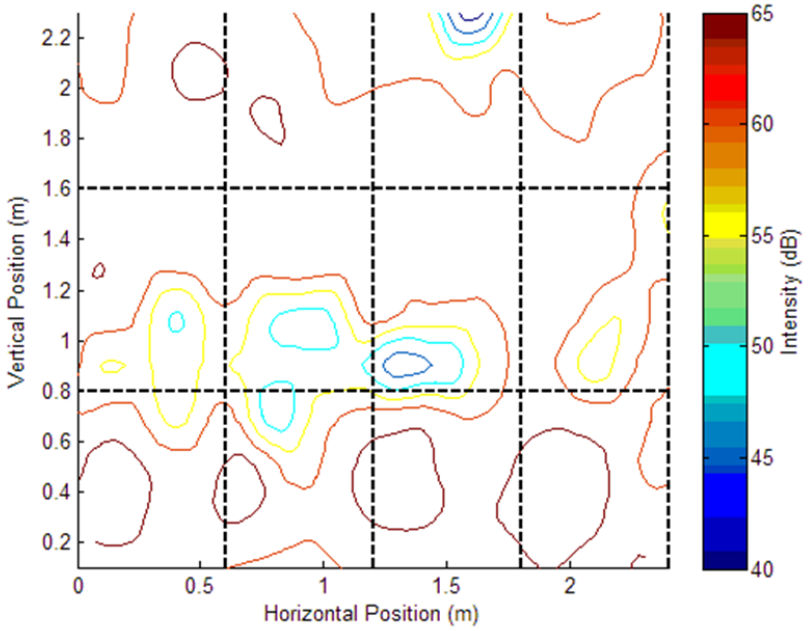

Figure 6.9: Point intensity scan of large 12 mm single leaf plywood partition at 100 Hz

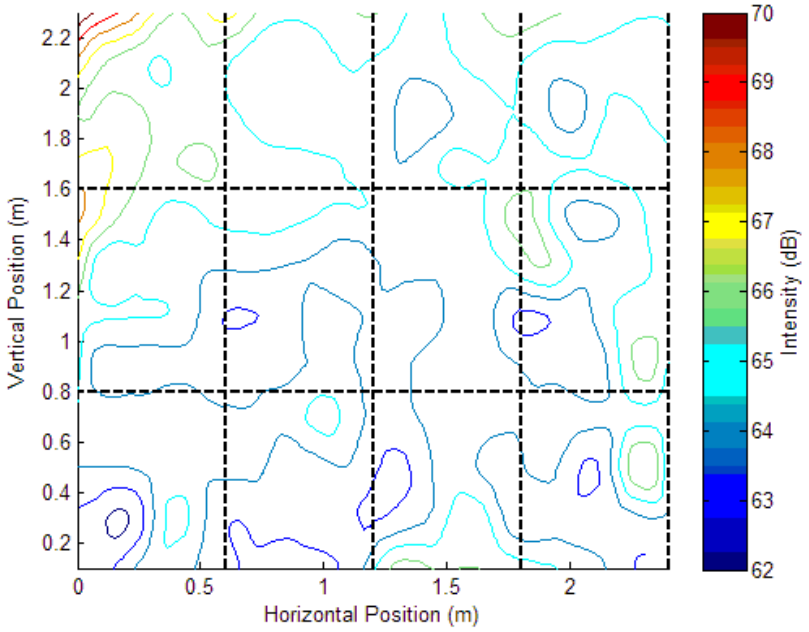

Figure 6.10: Point intensity scan of large 12 mm single leaf plywood partition at 1000 Hz

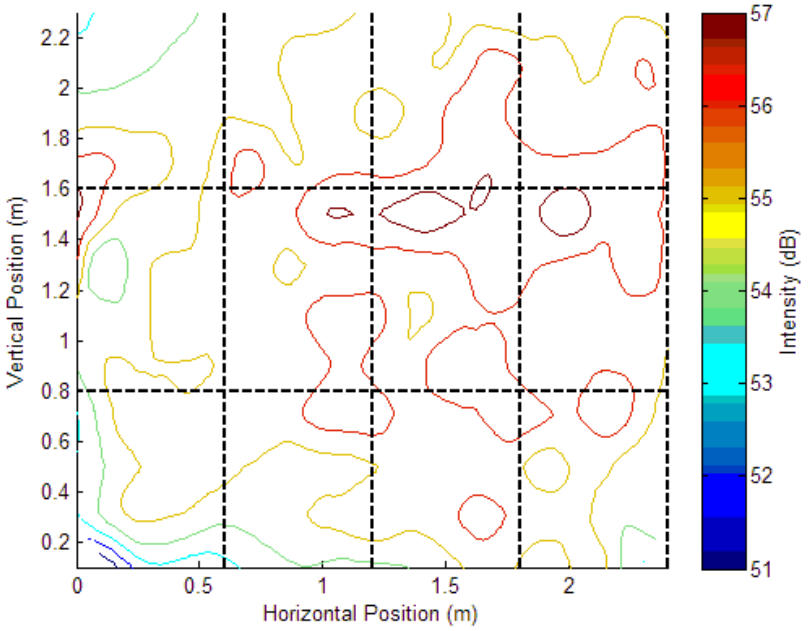

Figure 6.11: Point intensity scan of large 12 mm single leaf plywood partition at 5000 Hz

The vibration behaviour of the panels was relatively varied, depending on the frequency of excitation. The 100 Hz measurements (Figure 6.12) show clear modal behaviour, with significantly higher vibration at the centre of the unsupported components than at the studs and dwangs. This low frequency behaviour was expected as the partition acts as an array of individual panels. As the frequency was increased the vibration levels become more uniformly distributed across the surface of the panel.

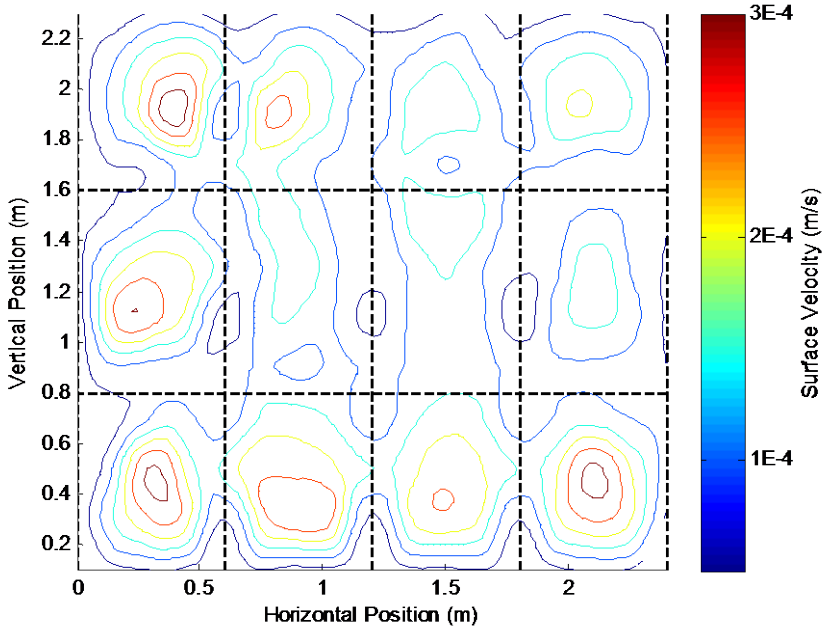

Figure 6.12: Point vibration scan of large 12 mm single leaf plywood partition at 100 Hz

Figure 6.13 and Figure 6.14 present the vibration levels at 1000 Hz and 5000 Hz respectively. The 1000 Hz response shows areas of low surface velocity on the vertical studs. The 5000 Hz response shows areas of low surface velocity at the vertical studs, although this was primarily focused on the central vertical stud. This increasing uniformity in the surface velocity was expected as the frequency of excitation increased.

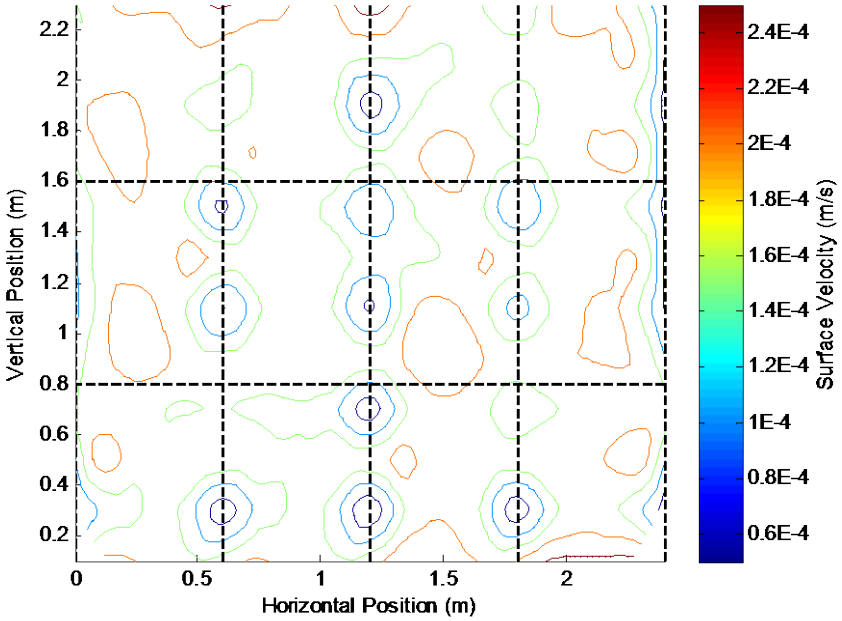

Figure 6.13: Point vibration scan of large 12 mm single leaf plywood partition at 1000 Hz

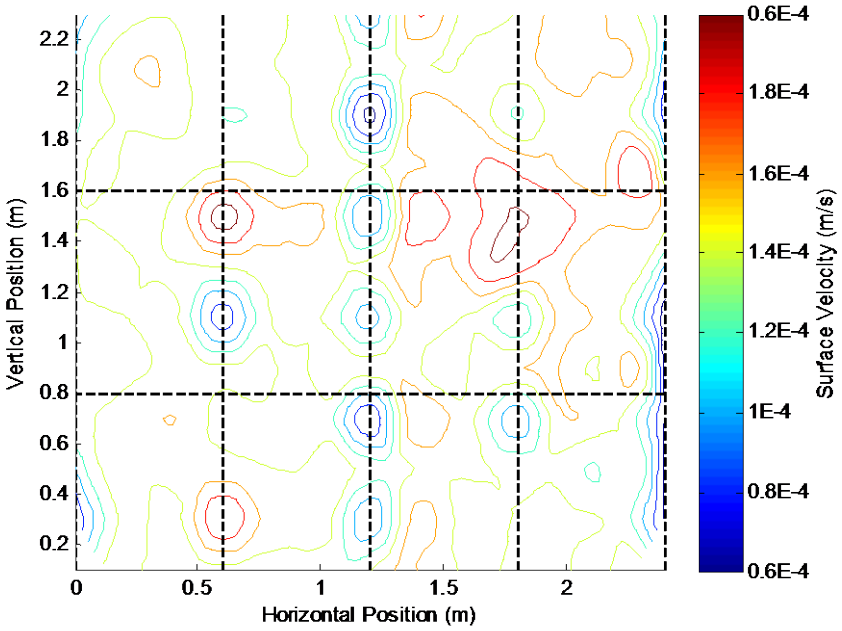

Figure 6.14: Point vibration scan of large 12 mm single leaf plywood partition at 5000 Hz

The point scan of the radiation efficiency of the partition is presented in Figure 6.15 – Figure 6.17. The radiation efficiency of the partition is significantly higher near the studs. This is expected based on the scattering of free waves near the panels. The fact that the vibration levels are much lower near the studs means that the measurement procedure may somewhat overestimate the radiation efficiency near the studs. The low vibration levels at the studs and the fact that the intensity measurement will average a finite area of the panel will cause the calculated radiation efficiency to be high. This agrees with the discussions presented in Section 2.7 in relation to the resonant sound radiation.

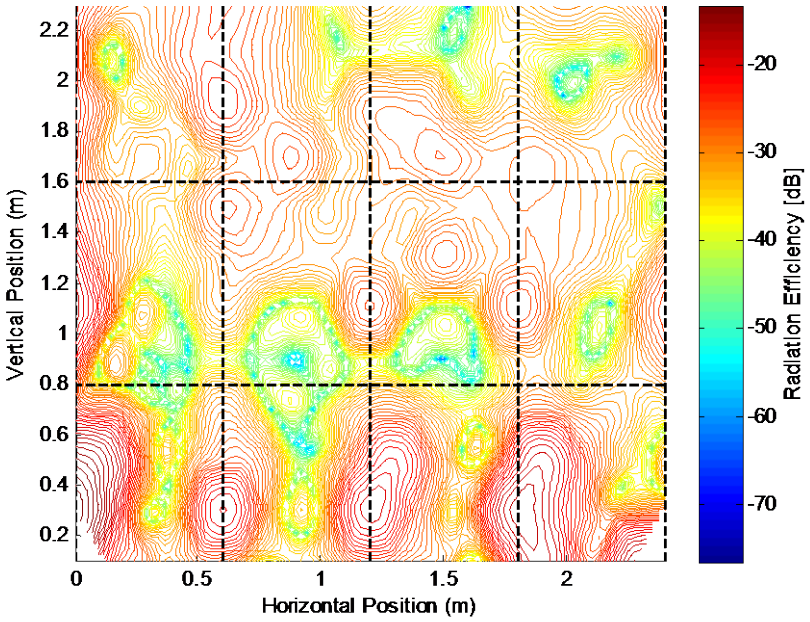

Figure 6.15: Point scan of radiation efficiency of large 12 mm single leaf plywood partition at 100 Hz

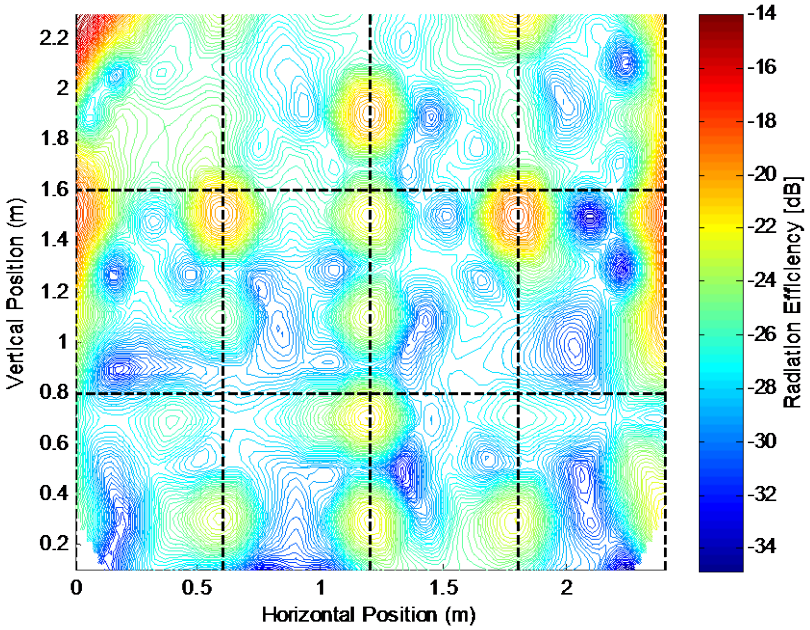

Figure 6.16: Point scan of radiation efficiency of large 12 mm single leaf plywood partition at 1000 Hz

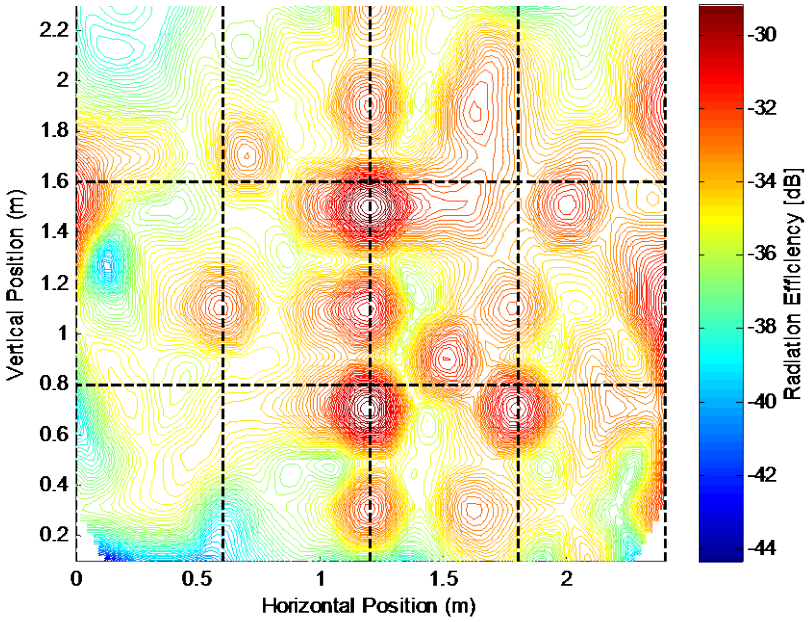

Figure 6.17: Point scan of radiation efficiency of large 12 mm single leaf plywood partition at 5000 Hz

The point scans performed on the panel assessed the general behaviour of a panel when excited by a diffuse sound field. There were no significant variations in the panel behaviour that were not caused by the underlying timber frame. The construction of the partition had a significant effect on the radiation efficiency, as expected. The limited influence of variations with the unsupported sections suggested that the assumption that the material properties were homogeneous throughout the panel is valid.

7. Variations between Small and Large Transmission Loss Facilities

The observed variations between results obtained using the small and large transmission loss facilities are considered. Several additional transmission loss samples were tested to evaluate the influence of various parameters. A qualitative assessment of the various parameters and their theoretical influence on the measured sound transmission loss is made. The combined interaction of these factors on the measured sound transmission loss is evaluated.

7.1. Introduction

Comparison of the results presented in Sections 5 and 6 show a significant variation in the transmission loss measured using the small and large facilities. The reasons for these variations were investigated experimentally. A qualitative analysis of the results was performed and compared with the results expected from the theories that assess the effects of sample size [3, 5]

ISO 15186-1 [140] requires a sample size between 10 m^2 and 12 m^2, with provisions to test smaller elements such as windows using a smaller 1250 mm × 1500 mm sample. Whilst the University of Canterbury does have a facility for testing large 11.5 m^2 samples, preparation and testing of these samples can be prohibitively expensive and time consuming. In large scale product development projects testing to an exact standard is of minor importance, but reducing the cost and time required to perform each measurement is a major factor. To allow a large number of comparative tests to be performed a smaller transmission loss facility has been developed in the University of Canterbury's acoustic testing facility.

The smaller test facility is a frame that is bolted into a large doorway between the reverberation room and a small semi anechoic space (as described in Section 4.3). This facility does not conform to ISO15186-1 due to the sample size. During the testing presented in this thesis it was noted that there was a significant variation between the sound transmission loss results from the small and large transmission loss facilities.

Previous research undertaken by various authors on the effect of sample size is based on measurements which were performed using the pressure-pressure method. This research is still relevant although different laboratory parameters can affect the results from different measurement techniques. A more detailed examination of some of the articles presented here will be discussed in greater detail throughout this section. Important aspects of a sound transmission loss facility were found to be; the presence and depth of a sample niche [154-158], the sample size

[159, 160], the size of receiving and source room [90, 161], the sample mounting conditions [132, 154, 162-164], source and receiving room conditions [162, 165], and the construction of the sample [90, 166].

Research presented by Kihlman and Nilsson [154], and Guy *et al.* [163] identified that the sound transmission loss is influenced by a number of interrelated parameters. Kihlman and Nilsson found that above the coincidence region, the behaviour was independent of laboratory design and mounting conditions. Below the critical frequency the sound transmission loss was found to depend on a range of different parameters. Guy *et al*. showed that the largest effects were due to the sample size and mounting conditions. It was also noted that changes to the sample size and mounting conditions could result in changes to the measured critical frequency.

The measurement procedure can also influence the measured sound transmission loss. The sound transmission loss values presented here were measured using the pressure-intensity method as described in ISO 15186-1:2000 [140]. ISO 15186-1:2000 allows these measurements to be compared to measurements made using the pressure-pressure method (described in ISO 10140-2 [167] and ISO 10140-4 [152]). The sound transmission loss measured using the pressure-pressure and intensity methods have been compared experimentally [168]. It has been found that there are some variations between the measured results, especially at low frequencies [169, 170]. A major variation is due to the fact that the pressure-pressure method measures the transmission loss of the entire wall system, including any baffles and mountings. The intensity method only measures the transmission loss of the sample scanned by the intensity probe. Despite the different method used, the observed trends and behaviours reported here are considered to be compatible with the results presented by other authors who utilised the pressure-pressure method.

Theories for the prediction of sound transmission loss use different methods to account for the finite size of a real transmission loss sample. The original theories of sound transmission loss were based on an infinite panel system [17]. The transmission loss of an infinite panel is inherently easier to predict than that of a finite panel as the interaction at the edges and baffles adds significant complexity. These infinite panel models are adjusted and modified to accommodate finite sized panels [47, 77, 171]. It is known that altering the size of the sample will alter the natural frequencies of the sample and modify the effective panel impedance. The transmission loss of a sample will increase below the critical frequency as the sample size is decreased [163].

7.2. Sound Transmission Loss Tests and Results

The influence of the smaller sample size on the measured transmission loss was evaluated via several tests. The additional samples were tested in addition to the results presented in Sections 5 and 6. The samples utilised in this section of research are described in Table 7.1.

Table 7.1: Samples tested in small and large transmission loss facilities

Inner Leaf	Outer Leaf	Notes
7 mm plywood	None	Small – without studs Large – with studs
9 mm plywood	None	Small – without studs Large – with studs
12 mm plywood	None	Small – without studs Large – with studs
12 mm plywood	None	Small – without studs Large – with studs
21 mm plywood	None	Small – without studs Large – with + without studs
10 mm gypsum plasterboard	None	Small – without studs Large – with studs
2 kg mass loaded barrier	None	Small – without studs Large – without studs
10 mm gypsum plasterboard	10 mm gypsum plasterboard	Small – with studs + cavity absorption Large – with studs + cavity absorption
12 mm plywood	12 mm plywood	Small – with studs Large – with studs

In all the cases the pressure-intensity and repeatability indexes were checked as described in Section 4. The sound transmission loss of four thicknesses of plywood partitions were tested (7 mm, 9 mm, 12 mm, and 21 mm). Figure 7.1 shows the influence of the sample size on the sound transmission loss of 7 mm and 9 mm single leaf plywood partitions.

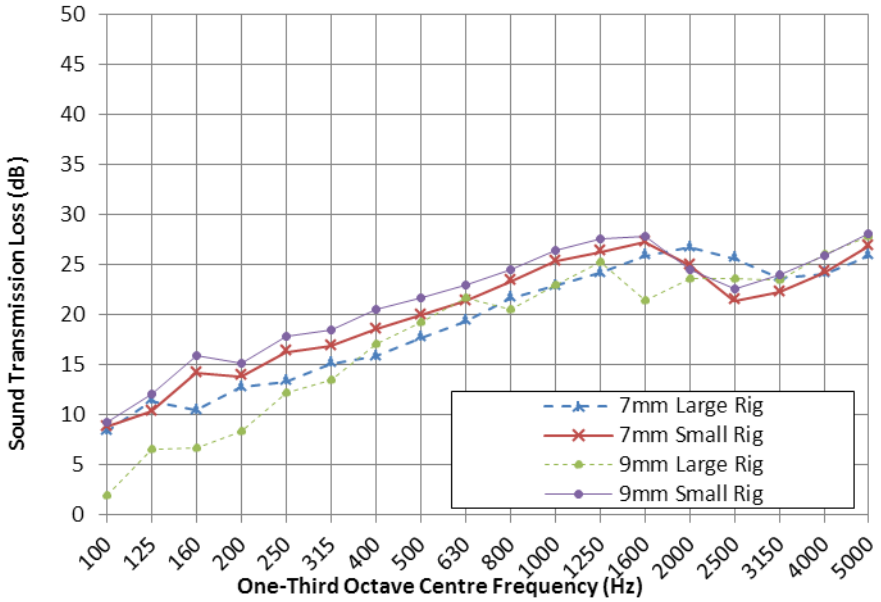

Figure 7.1: Comparison between small and large transmission loss facilities when measuring 7 mm and 9 mm plywood partitions. The large partitions has studs and the small partition does not

The small sample size exhibits a consistently higher sound transmission loss across most of the frequency range; as shown in Figure 7.1. The variation is approximately three to four decibels below the critical frequency. This difference was reduced at and above the critical frequency. The large sample size had a shallower coincidence dip than the small sample; resulting in the convergence of the transmission loss curves near the critical frequency. The large sample displays some unusual behaviour in the lower frequency regions. The 7 mm plywood has a higher sound transmission loss than the 9 mm plywood despite the 9 mm plywood panel being 0.6 kg/m^2 heavier with a similar bending stiffness. This increased mass should result in a higher sound transmission loss especially in the frequency range below coincidence. The higher sound transmission loss seen in the 7 mm large sample near 1600 Hz is due to the thinner sample having a higher coincidence frequency, although the difference is larger than expected.

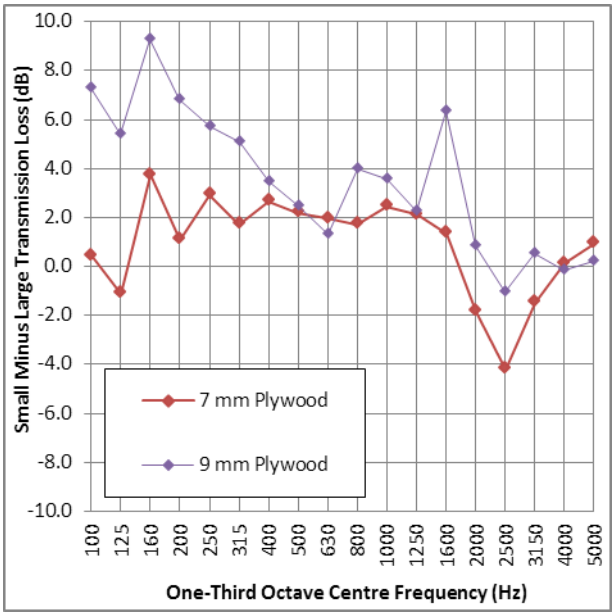

Figure 7.2: Variation in decibels between small transmission loss facility and large transmission loss facility. Calculated for 7 mm, 9 mm

The behaviour of the small test samples is closer to what would be expected due to the increased mass of the 9 mm samples over the 7 mm samples. The convergence at the coincidence region is due to the similar bending stiffness and damping loss factor of both sample sizes.

In Figure 7.1 the small sample did not have any form of stud system installed. The effect of introducing studs into the small sample was explored by constructing a partition with studs that could be clamped into the small transmission loss facility, see Figure 7.3. The construction of the small test facility meant the stud spacing in the small facility did not match that of the large test facility. The small rig's stud spacing was 450 mm and the large facility's stud spacing was 600 mm.

Figure 7.3: Small timber frame used to test small partitions with studs

Figure 7.4 shows the measured variations in single leaf partitions constructed from 12 mm plywood. These samples were tested in both the small and the large sound transmission loss facilities. The small samples generally have a higher sound transmission loss than the large samples. The variation in measured sound transmission loss is less consistent when the studs are present than seen in the case of the samples without studs. The introduction of the studs from the small single leaf samples causes a significant reduction in the coincidence frequency, as described in Section 5.

The small sample was tested with the panel on the inside and the outside of the frame. The niche depth present when the panel was on the inside was unchanged from all the other small single leaf samples. The source room niche depth with the panel on the outside of the frame was 445 mm and the receiving room niche depth was approximately 250 mm. The two samples have a similar transmission loss across most of the frequency; but some variation occurs between 400 Hz and 1200 Hz. In this frequency range the sample with the larger source niche has a lower sound transmission loss.

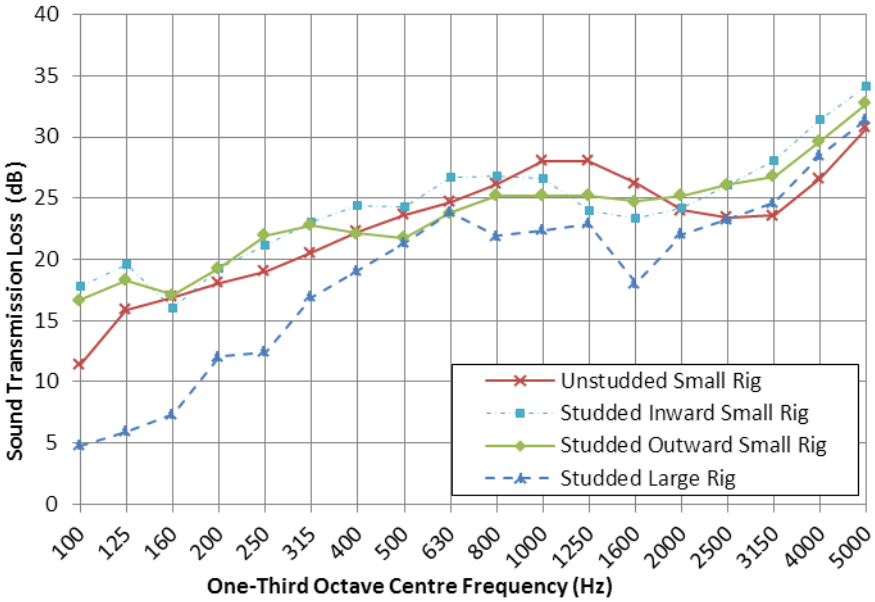

Figure 7.4: Sound transmission loss single leaf 12 mm partitions; with and without studs in the small sample

A second leaf was then attached to this frame; creating a double leaf partition with studs. The measured transmission losses of the two studded 12 mm partitions are presented in Figure 7.5. The small double leaf partition has a consistently higher sound transmission loss across most of the frequency range. The small sample exhibits a significant “dip” in the sound transmission loss in the 160 Hz one third octave band, causing the small sample to have a lower sound transmission loss than the large sample in the 160 Hz and 200 Hz one third octave bands. This is probably due to resonances that occur in the length direction of the studded partition; the first lengthwise resonance of the small partition occurs at approximately 130 Hz. This hypothesis is further supported by the fact that the first axial mode in the cross stud direction occurs in the small test facility at approximately 360 Hz; where another “dip” occurs in the transmission loss results.

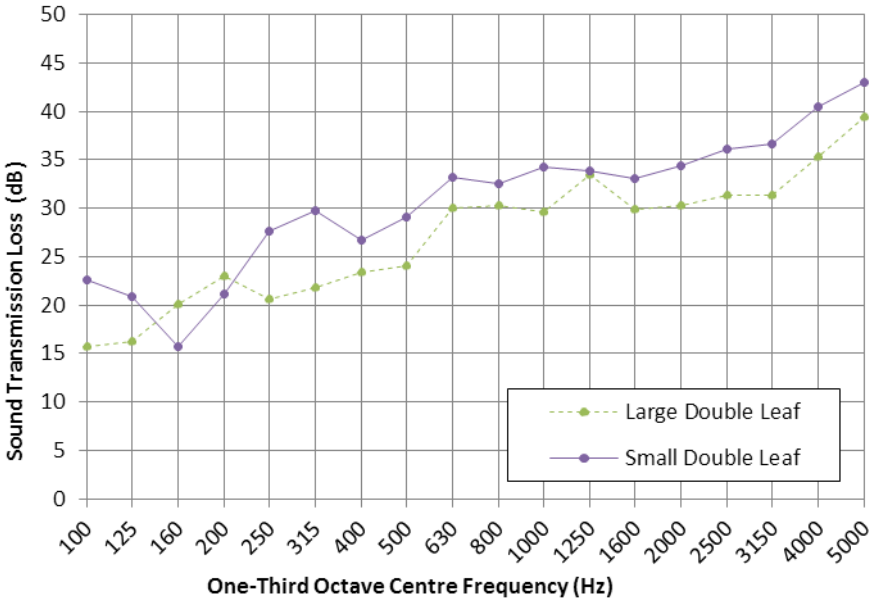

Figure 7.5: Sound transmission loss double leaf 12 mm partitions

A large partition without studs was constructed by removing the studs and dwangs from the timber frame, leaving an outer frame. The 21 mm plywood was screwed at 150 mm centres around the edge of the test rig. The sample was taped and glued along the joints between the plywood panels and acoustic sealant was used around the edge to effectively seal the sample. The construction of the un-studded partition is depicted in Figure 7.6.

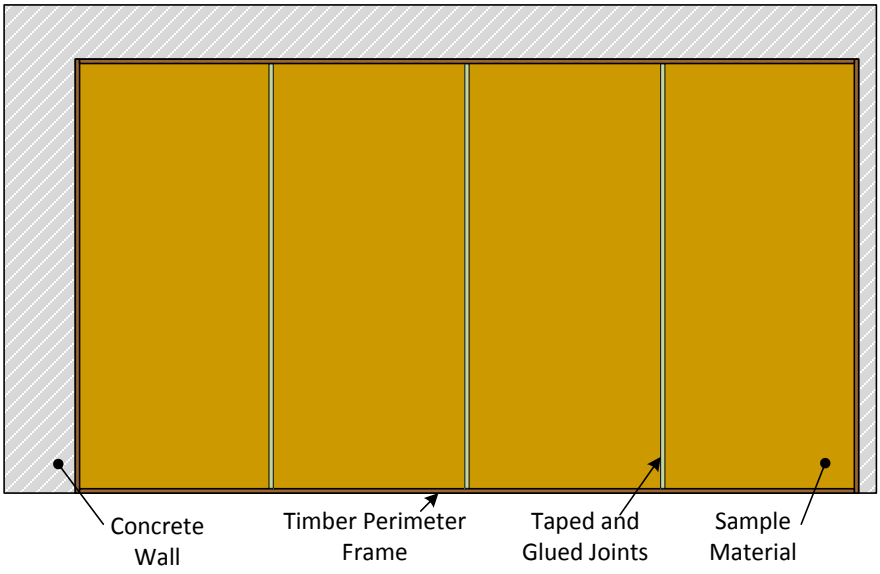

Figure 7.6: Arrangement of large sound transmission rig construction without studs

The 21 mm plywood was tested in a range of different arrangements including the partitions without studs. The results of these measurements are presented in Figure 7.7. These results compare the behaviour of small and large 21 mm plywood partitions. The removal of the studs

reduces the coincidence frequency; the large partition with studs present exhibited a coincidence dip at approximately 1600 Hz whereas the partition without studs has a coincidence region two thirds of an octave below (at approximately 1000 Hz). This variation is due to the changes in mass and stiffness that occurs when the studs are removed.

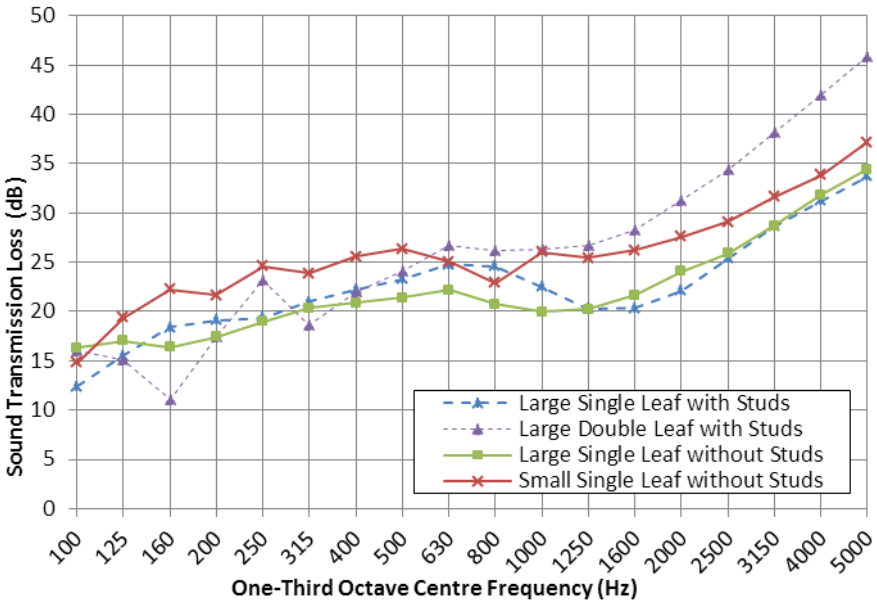

Figure 7.7: Comparison between small and large transmission loss facilities when measuring 21 mm plywood samples. The large partition without studs was taped and glued at the joints. The samples with studs were built on the original timber frame

In order to assess the influence of these parameters on other materials a set of measurements were performed on single and double leaf gypsum plasterboard partitions. The results of these measurements are presented in Figure 7.8. Further tests were performed on a 2 kg/m^2 mass loaded barrier; the results of which are presented in Figure 7.9. The mass loaded barriers were constructed without studs; these samples were stapled and glued around the edges of the samples. The joints between the mass loaded barriers were overlapped, glued and taped to ensure an adequate seal.

The plasterboard partitions are not influenced by the sample size to the same extent as the plywood partitions (Figure 7.8). In the case of single leaf panels the small samples have a higher sound transmission loss below the coincidence region of the order of two to three decibels. A complete convergence occurs near the coincidence region. It appears that the sound transmission loss of the smaller sample may be slightly higher above the coincidence region. The double leaf partitions showed no obvious trends, with both the sample sizes having a similar transmission loss across much of the frequency range.

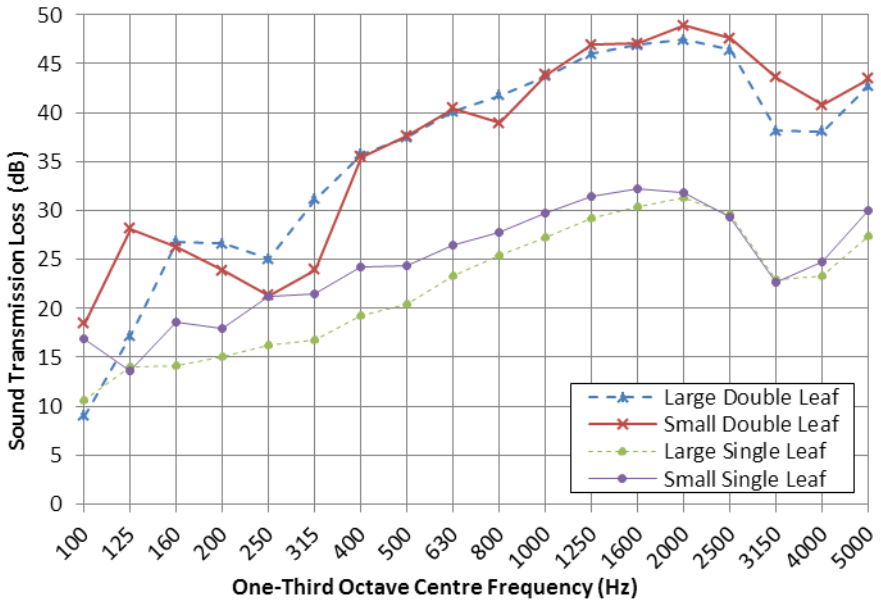

Figure 7.8: Sound transmission loss of 10mm gypsum plasterboard samples measured in small and large test rigs. The large sample is a single leaf supported by a timber stud frame. The small sample is a clamped, unsupported panel

The mass loaded barrier showed the same trends as all the other single leaf samples. The transmission loss of the smaller sample was significantly higher below the critical frequency. The measured transmission losses were seen to converge somewhat near the critical frequency. Above the critical frequency the small sample exhibits a higher transmission loss than the large sample. The convergence of the two mass loaded barriers was less significant than that seen in the plasterboard samples, this is due to the very high internal damping present in the mass loaded barrier sample. This high damping reduces the influence of the coincidence effect. Above the critical region the difference between the small and large rigs is relatively constant.

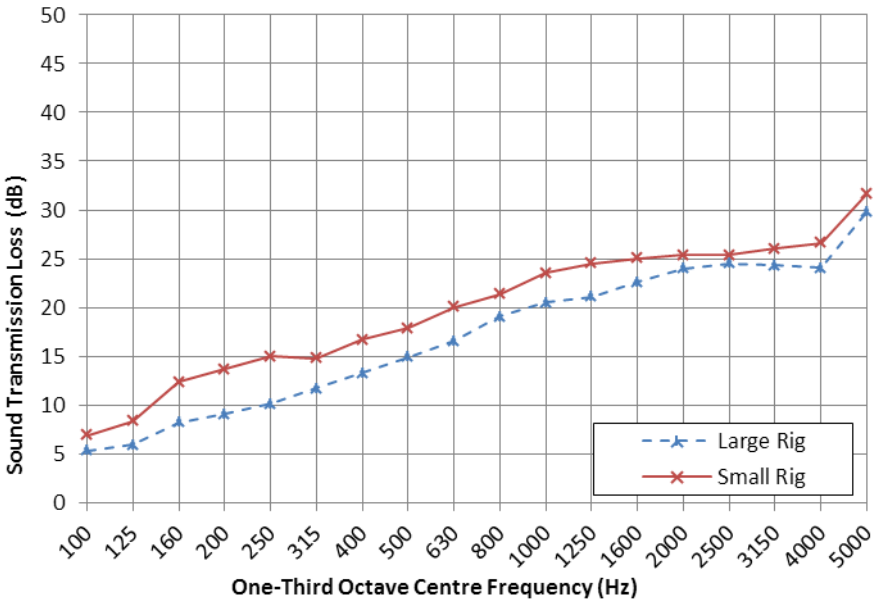

Figure 7.9: Sound transmission loss of 2kgm^{-2} mass loaded barrier samples in small and large test rigs. Both the samples were glued and stapled around the edges

The double leaf partitions were also influenced by size of the test sample, but this influence was less pronounced. In all double leaf cases the transmission loss curve was significantly more complex than that of the single leaf partitions; with a large number of small troughs and peaks. This added complexity was due to the existence of the additional resonant behaviours in double leaf partitions. The resonances can influence the measured sound transmission loss significantly.

In all the single leaf samples the small sample size was found to result in a consistently higher sound transmission loss across the entire frequency range. The variation is between three and five decibels below the critical frequency. The difference is reduced at and above the critical frequency. The larger sample size had a less severe coincidence dip than the small sample; resulting in convergence of the transmission loss curves near the critical frequency.

The pressure-intensity index was calculated for each of the samples. In all the measured samples the pressure-intensity index was higher for the large sample between 100 Hz and 200 Hz. Above this frequency range the pressure-intensity index was very similar for both the sample sizes; a typical pressure-intensity index is presented in Figure 7.10. This variation in the pressure-intensity index is due to the higher low-frequency background noise levels in the receiving room for the large transmission loss facility. The higher pressure-intensity index may also indicate slightly higher levels of flanking noise at low-frequencies for the large transmission loss facility.

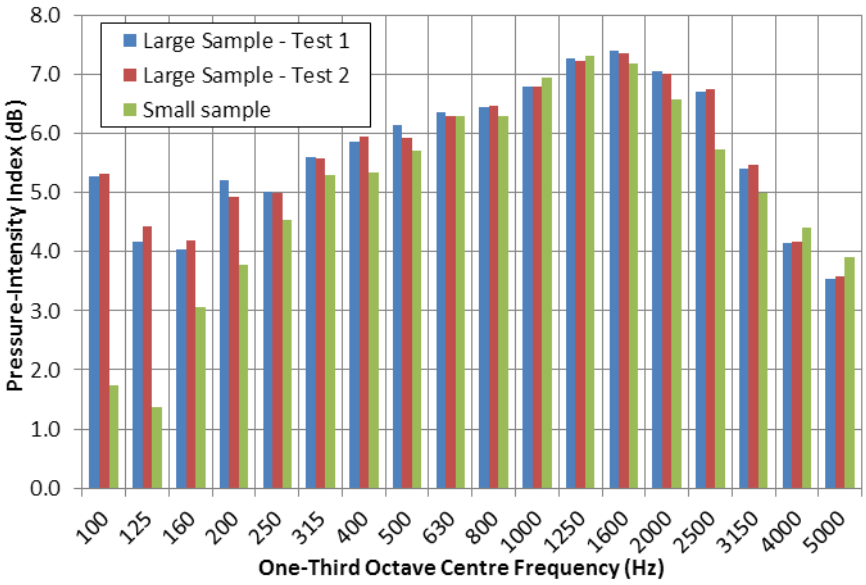

Figure 7.10: Pressure-intensity index of single leaf 12 mm plywood measured using small and large partitions

The variation in the measured sound intensity for the single leaf 12 mm plywood sample is presented in Figure 7.11. The large samples have a greater variation in the measured intensity levels across most of the measured frequency range. These trends were typical of all the sound transmission loss samples.

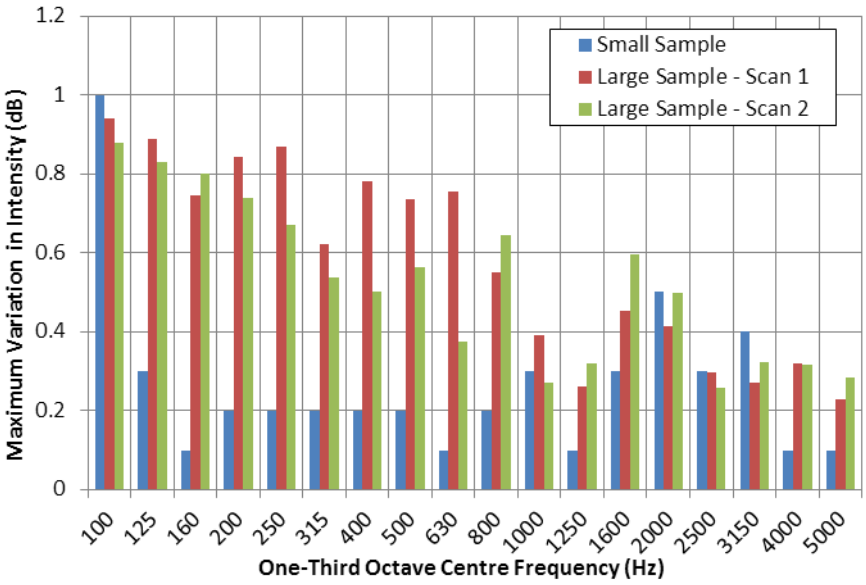

Figure 7.11: Maximum variation in intensity measurements for single leaf of 12 mm plyood partitions

The higher variation and higher pressure-intensity index in the large sample is probably due to a higher background noise level. Different semi-anechoic rooms are used for each of the transmission loss samples; this causes different measurement conditions for each of the samples. In all cases the repeatability index and pressure-intensity indexes were measured and checked against the

requirements in ISO 15186-1. The different background pressure levels for two typical sound transmission loss measurements are shown in Figure 7.12.

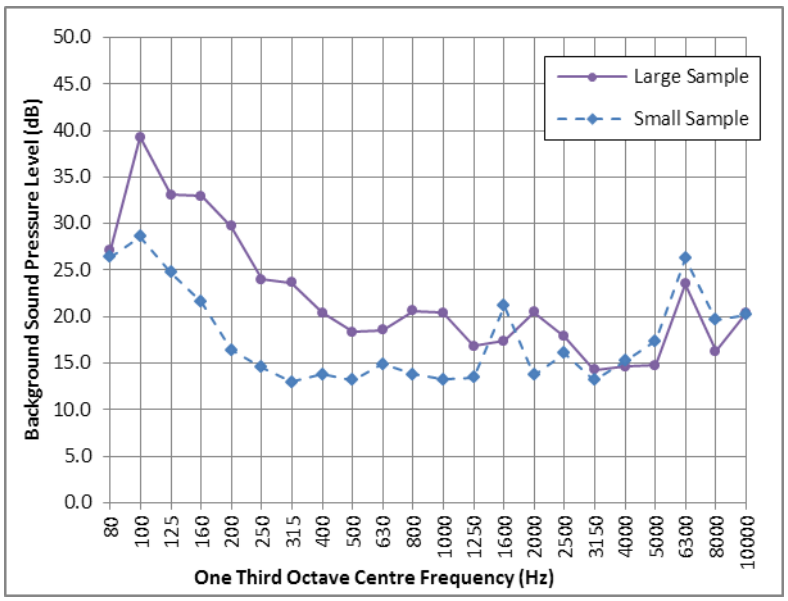

Figure 7.12: Background sound pressure level in both semi-anechoic rooms used for the transmission loss tests

The background sound pressure level was measured using the intensity probe placed 200 mm from the receiving side of the transmission loss sample. The large sample has significantly higher background sound pressure below 1250 Hz. This is due to the presence of a number of mechanical services that are present within the large semi-anechoic room. The higher background sound pressure level results in higher pressure-intensity indexes and repeatability indexes in the large test facility; the metrics required by ISO 15186-1 are still met with this higher background noise level.

The presented results indicate that there are significant variations in the measured sound transmission loss related to the sample size, sample construction, niche depth and sample material. The measurements showed a consistent increase in the sound transmission loss as the sample size was decreased. This effect was confounded with the influence of the other partition parameters, each of which has different effects on the measured sound transmission loss. It is necessary for these factors to be better understood in order for the small transmission loss sample results to be directly compared with measurements made using the larger sample size specified by ISO 15186-1. These effects will be discussed in detail in the following sections.

7.3. Panel Surface Pressure Level Measurements

The pressure level near the surface of both the small and large transmission loss partitions was measured. This was achieved by placing the diaphragm of a microphone near the surface of the sample, and measuring sound pressure level in a grid across the surface. These measurements

assessed if other factors were affecting the measured sound transmission loss of the samples. The variation in the sound pressure level within the source room and the variation in sound pressure level across the surface of the sample was investigated. The results of these tests indicated that the pressure variations on the source room side were not major contributors to the variations in measured sound transmission loss.

The sound pressure level near the surface of the large rig was measured at 25 mm from the surface using an array of nine microphones, as shown in Figure 7.13. The measurement array was moved several times, resulting in a 72 point grid measurement across the surface. The sound pressure level near the surface of the small rig was measured at 0 mm and 25 mm from the surface using a panel with 45 holes drilled in a grid, as shown in Figure 7.14. The holes were drilled to be a snug fit for the Brüel and Kjær 4189 microphones utilised in this testing. The microphones were inserted through the holes; this allowed measurements to be made at 0 mm and 25 mm from the surface of the small sample. The small samples were made in a 185 mm × 220 mm grid, and the large grid was measured in a 400 mm × 400 mm grid. A 30 second linear average of the sound pressure level was made at all of the microphone locations. During the tests the un-used holes in the small sample were plugged with wooded plugs.

Figure 7.13: Microphone array for large surface pressure measurements

Figure 7.14: Microphone array for small surface pressure measurements

The average measured sound pressure levels for both the small and large transmission loss samples are presented in Figure 7.15. The large sample has a higher sound pressure 25 mm from the surface of the panel, this variation peaks at approximately three decibels around the 1000 Hz

frequency band. The measurements made at the surface (0 mm) of the pressure level show, a increase in the frequency range above 630 Hz due to the doubling of the pressure that occurs at the surface of the panel. The 25 mm measurements are subject to a similar doubling in pressure below this 630 Hz band.

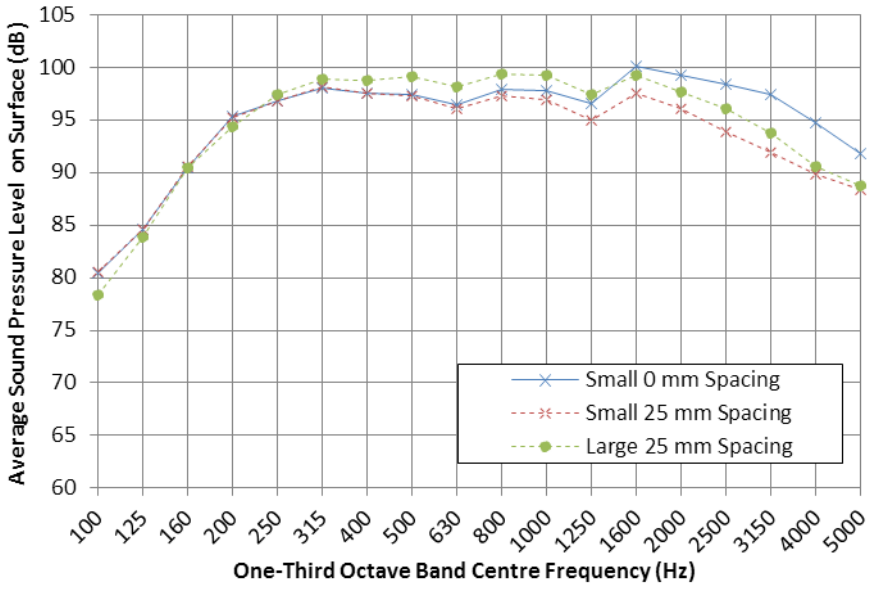

Figure 7.15: Microphone array for small surface pressure measurements

Figure 7.16 shows the pressure variation across the surface of the small transmission loss sample at 100 Hz. There was some level of modal or resonant behaviour evident in the measurement at 100 Hz, this is typical of the sample in the frequency range below 500 Hz. Above this frequency the small panel shows no obvious modal behaviour across the surface. Figure 7.17 presents a typical high frequency response.

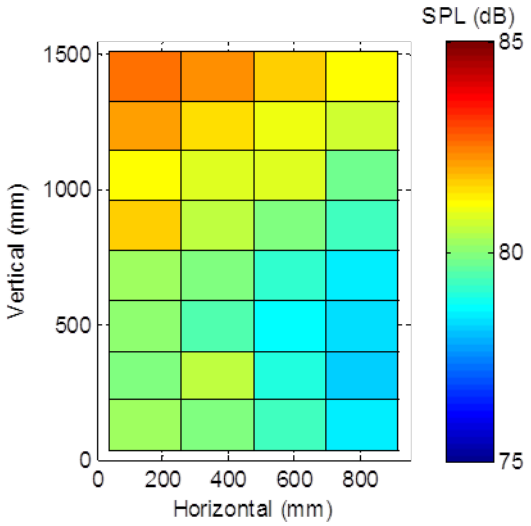

Figure 7.16: Pressure variation 25 mm from surface of small sample at 100 Hz

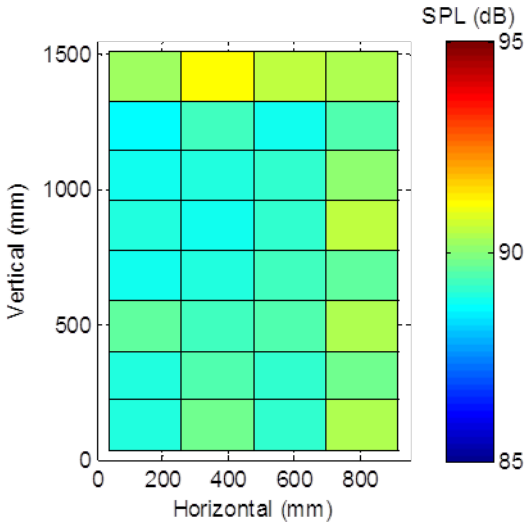

Figure 7.17: Pressure variation 25 mm from surface of small sample at 4000 Hz

The large sample does not show the modal behaviour of the small panel in any of the frequency range evaluated, although there is a reasonably large variation in the sound pressure level throughout the measured frequency range. Figure 7.18 shows the variation across the surface of the large panel at 100 Hz, there is some evidence of a degree of modal or resonant behaviour, but it is not as immediately clear as the small sample behaviour.

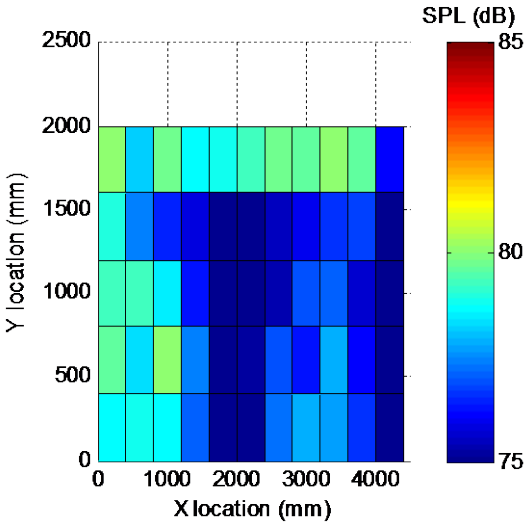

Figure 7.18: Pressure variation 25 mm from surface of large sample at 100 Hz

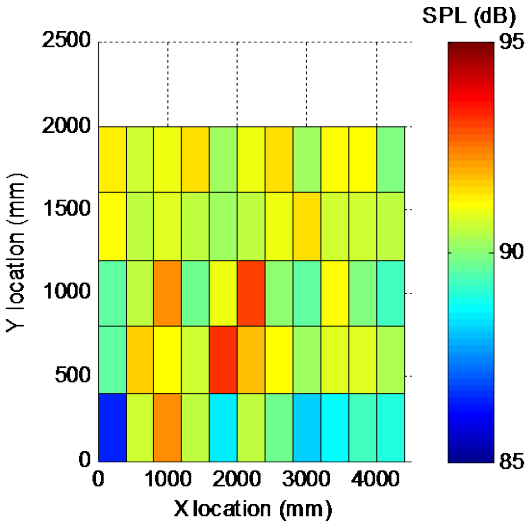

Figure 7.19: Pressure variation 25 mm from surface of large sample at 4000 Hz

The maximum variation and the standard deviation in the measured sound pressure level 25 mm from the surface of the panel was evaluated for both the small and the large test rigs and is presented in Figure 7.20. Both the maximum variation and the standard deviation showed the same trends. The standard deviation was significantly lower than the maximum variation; indicating the presence of some significant outliers in the measured sound pressure level. The small sample has a larger variance in the sound pressure level near the surface than the large sample in the 125 Hz – 400 Hz one third octave bands, with the large sample having a higher variation in the rest of the measured frequency range. There was no clear trend relating the variance of the pressure levels across the surface of the panels to the variatiotionin the measured sound transmission loss behaviour. The large test rig has a relatively consistent variation in the pressure level across the surface at the lower frequencies. At higher frequencies there was an increased variation across the surface which is the result of an increase in the measured sound pressure level near the edges of the panel.

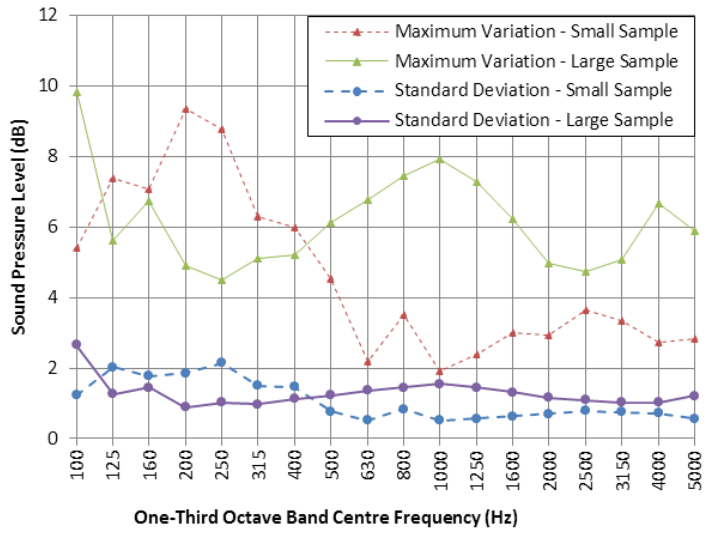

Figure 7.20: Maximum difference and standard deviation in sound pressure levels measured in grid across the surface of both test samples at a distance of 25 mm

Overall the level of variation was relatively consistent across the frequency range and between the different sample sizes. The variation in sound pressure level was also not directly correlated with changes in the measured sound transmission loss. This indicates that the variation in the pressure level across the surface was not a major factor to the variation in the measured sound transmission loss.

A comparison between the measured sound pressure levels 25 mm from the surface of the panel is presented in Figure 7.21. The maximum and minimum pressure levels are also presented for comparison. The maximum variation for the large sample is seen to peak around 1000 Hz. Throughout the measured frequency range the variation of both samples overlaps.

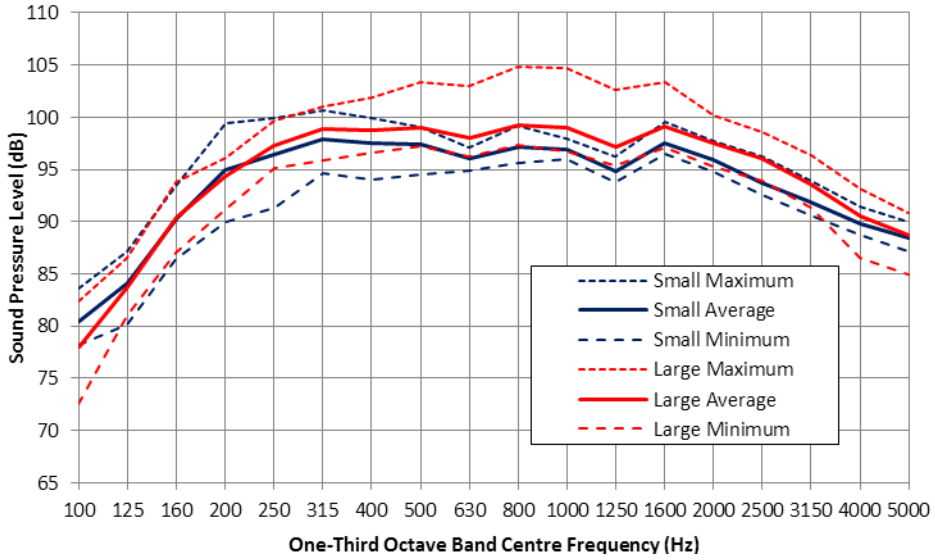

Figure 7.21: Sound pressure level 25 mm from surface of both the small and large transmission loss facilities

The difference between the average sound pressure level values measured at 25 mm from the surface of both samples is presented in Figure 7.22. The difference in average sound pressure level is below 2.5 dB across the frequency range measured. This does not appear to account sufficiently for the variation seen in the sound transmission loss measurements performed.

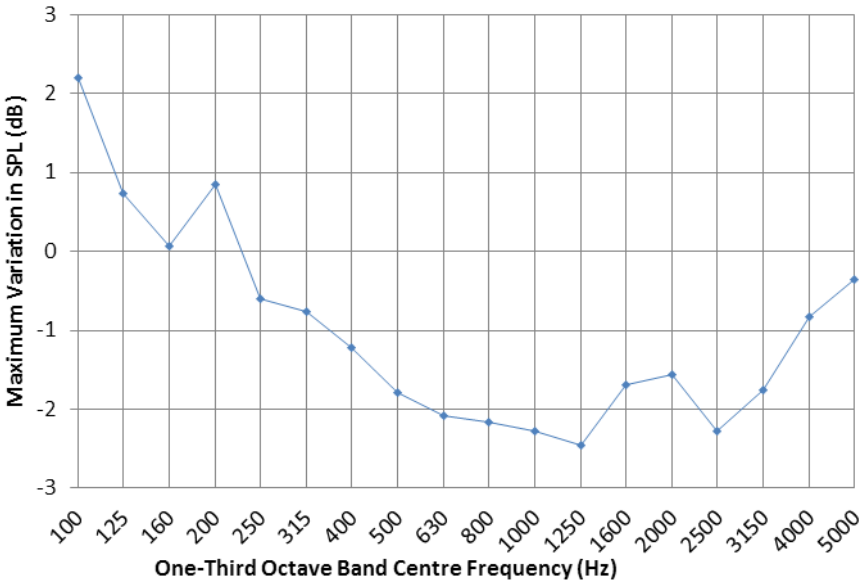

Figure 7.22: Variation between averaged sound pressure levels measured 25 mm from the surface of the small and large transmission loss rigs

These factors may have contributed somewhat to the observed variations in the sound transmission loss of the two sample sizes. The pressure variations were not sufficient to completely describe the variations observed. A further investigation into other contributing factors was also undertaken to further understand the reasons for these variations.

7.4. Room Pressure Level Measurements

The influence of the pressure distribution in the reverberation room on the measured sound transmission loss was evaluated. The uniformity of the pressure levels throughout the reverberation room was assessed. There was a significant difference in the location of the samples within the reverberation room. The location of the small sample indicted that it could have been shielded by the stationary diffusing panel in front of the surface of the small sample (Figure 7.23). The pressure was measured in a 500 mm × 500 mm × 500 mm grid within the room volume using five Brüel & Kjær 4189 microphones on a vertical stand; the microphone array used is shown in Figure 7.24. Measurements were performed using a 30 second linear average at each of the microphone locations.

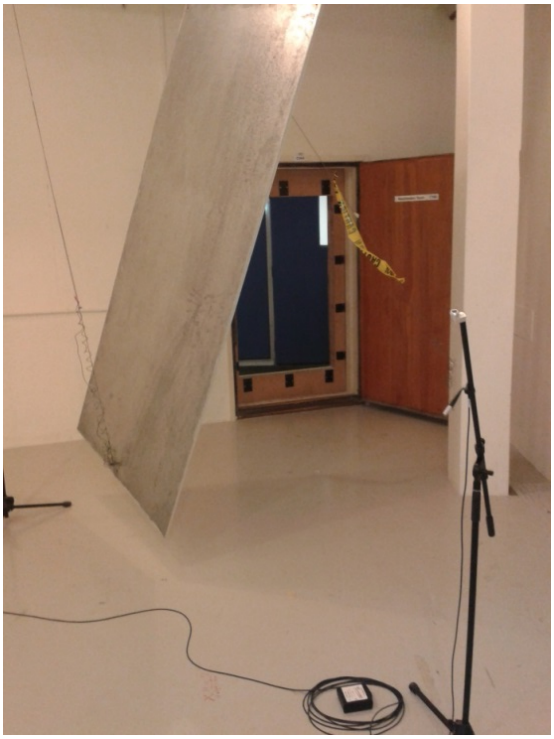

Figure 7.23: Diffuser in front of small transmisison loss rig

Figure 7.24: Vertical micropohne array for volume pressure measurements

The average sound pressure level throughout the reverberation room and near the surfaces of the two samples is presented in Figure 7.25. The measurements near the samples were within 500 mm of the sample surface. There are no large differences between the sound pressure levels near the transmission loss samples and the rest of the room. In the frequency range above 315 Hz the small sample has a slightly lower sound pressure level, although this level difference is less than two decibels across the measured frequency range, as shown in Figure 7.26. In these two data sets the microphones within 1.4 m of the source were neglected.

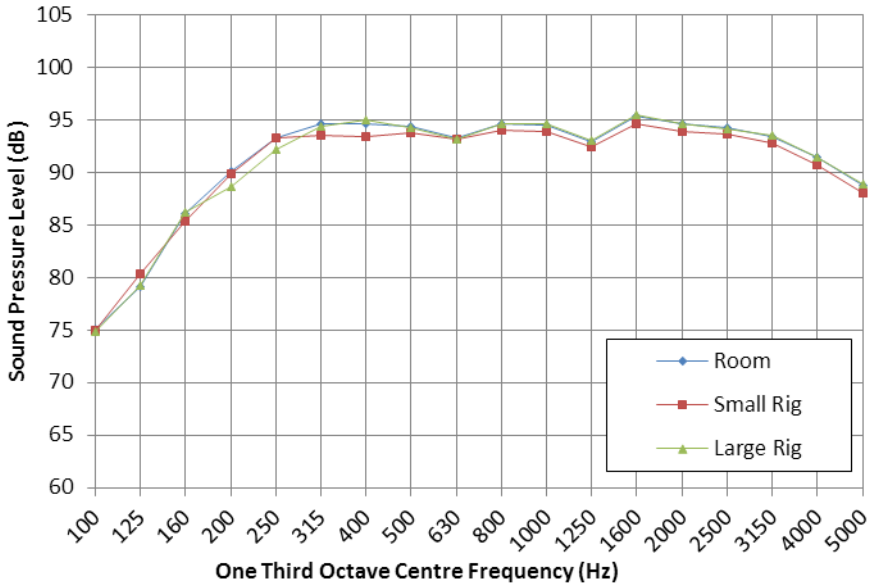

Figure 7.25: Average pressure throughout room volume compared to measurement points within 500 mm of samples

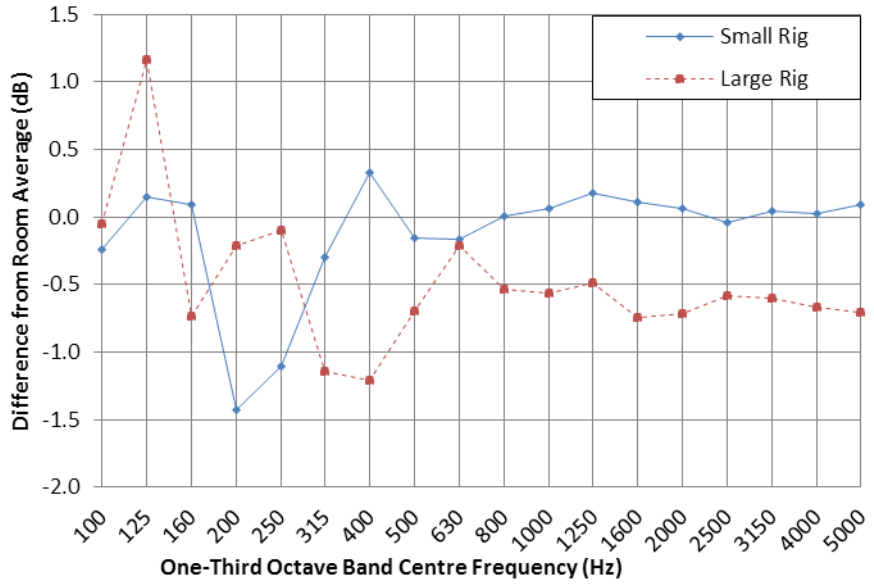

Figure 7.26: Variation between average sound pressure level 500 mm from the surface of the test samples and the average sound pressure level throughout the reverberation room

The measured pressure distributions were evaluated throughout the reverberation room. Figure 7.27 shows the measured pressure variation in the 100 Hz one-third octave band centre frequency. There was an increased sound pressure level near the sound source as expected, but the pressure throughout the rest of the room was relatively constant. The 1000 Hz behaviour is shown in Figure 7.28. As with the small samples there was increased sound pressure level near the sound source, but the sound pressure level throughout the room is relatively constant. The pressure variations near the sound source were ignored as the microphones are placed outside of this region. Of primary

interest were the variations near the surface of the small sample. These measurements indicate that the shielding influence of the diffuser is likely to have a negligible effect on the measured sound transmission loss.

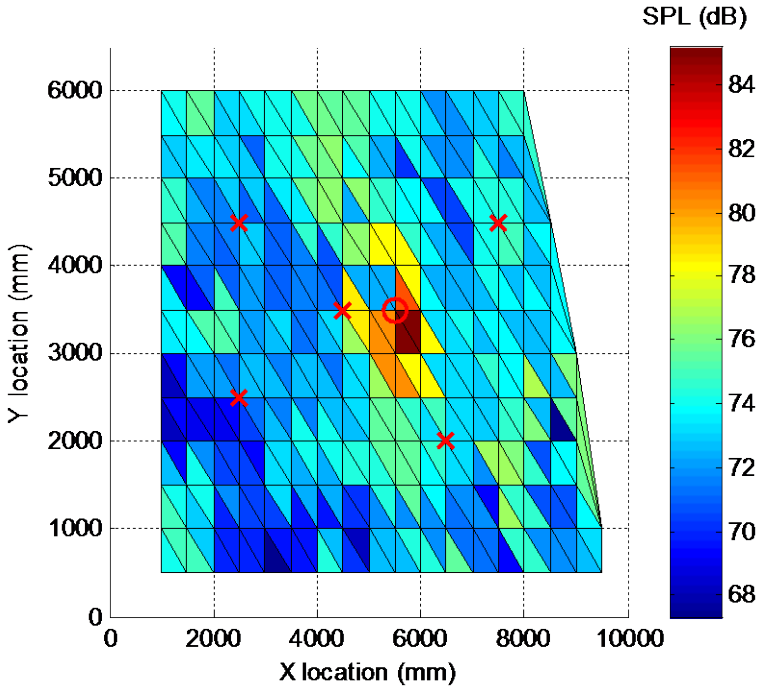

Figure 7.27: Pressure variation throughout the reverberation room, at 1500 mm above the floor, at 100 Hz. The red 'X' mark the standard microphone locations and the red 'O' marks the source location

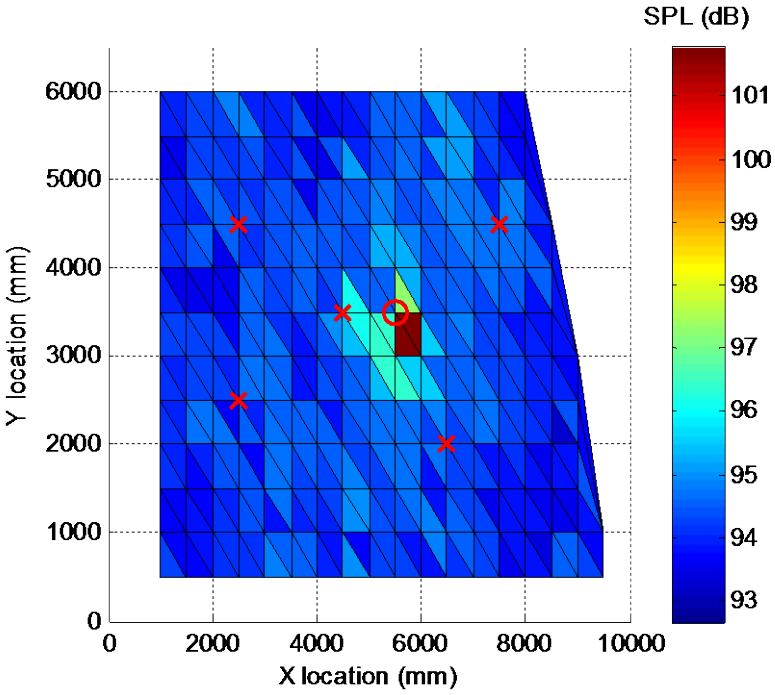

Figure 7.28: Pressure variation throughout the reverberation room, at 1500 mm above the floor, at 1000 Hz. The red 'X' mark the standard microphone locations and the red 'O' marks the source location

These results indicate that the room pressure variations may be a small contributing factor to the differences in the measured sound transmission loss. This variation in the room pressure distribution was predicted to contribute less than two decibels to the variation across the measured frequency range.

7.5. Reasons for Variations in Sound Transmission Loss

There are a large number of factors that may have caused the variations in the observed measured sound transmission loss. The main contributing factors are discussed in this section and the predicted effects are compared with the measured results. The primary finding is that the effect of sample size on transmission loss is strongly related to the construction of the panel. As such a simple correction cannot be applied to all smaller samples as the presence of studs and multiple leaves causes different variations. The trends seen in the small transmission loss measurements are considered to still reflect the trends expected from large samples, but the absolute measurements must be used with care.

The size of a sample affects a number of parameters that can be related to the panel behaviour. Table 7.2 presents the edge ratio, the sample area ratio, the sample perimeter length, and the sample area of the two different sample sizes. The sample area ratio is of more significance when undertaking pressure-pressure measurements, as a lower sample area ratio increases the influence of flanking on the system. The pressure-intensity method utilised in this research is less susceptible to effects caused by changes to the sample area ratio. Kihlman and Nilsson [154] describe some of the effects that the changes to the sample area and edge ratios have on the sound transmission loss. The variations seen in the measurements presented here support the work of Kihlman and Nilsson below the critical frequency. Above the critical frequency Kihlman and Nilsson did not predict any changes due to the sample size and mounting conditions, which is contrary to the results presented here.

Table 7.2: Comparison of parameters between small and large transmission loss suites

Parameter	Small Sample (1.55 m × 0.95 m)	Large Sample (2.4 m × 4.8 m)	Relevant Formula
Panel Area (m^2)	1.47	11.52	$A_{panel}(m^2)=l_x(m)\times l_y(m)$
Panel Perimeter (m)	5.00	14.4	$l_{edge}(m)=2l_x(m)+2l_y(m)$
Edge Ratio (m^{-1})	3.4	1.3	$\frac{l_{edge}(m)}{A_{panel}(m^2)}$
Sample Area Ratio (N/A)	0.06	0.3	$\frac{A_{panel}(m^2)}{A_{wall}(m^2)}$

Table 7.3: Variation in important parameters between small and large transmission loss suites

Sample	Source Room Niche Depth	Receiving Room Niche Depth
Small Single Leaf Samples	350 mm	200 mm (less the panel thickness)
Small Double Leaf Samples	350 mm	200 mm (less the partition thickness)
Large Single Leaf Samples	160 mm	210 mm (less the panel thickness)
Large Double Leaf Samples	70 mm (less the panel thickness)	210 mm (less the partition thickness)

7.5.1. Size Effects

The different sample sizes resulted in a measureable change in the measured sound transmission loss. These size effects are explored in consideration with existing theoretical methods. The sound transmission loss behaviour of a sample is governed by different factors [8] throughout the frequency range of interest. As described in Section 2 the frequency range can be broken into several regions, above, within, and below the coincidence region. Within each of these frequency ranges the sample size affects the sound transmission loss behaviour in different ways; each region must be considered separately when evaluating the size effects. In all the measured cases except that of the twin leaf gypsum plasterboard, the small sample has a higher sound transmission loss across the majority of the frequency range. In general the sound transmission loss curves converge within the coincidence region. Above the coincidence region the sound transmission loss curves generally diverge again with the small sample having a somewhat higher measured sound transmission loss. The variation between measured transmission loss of the small and large samples is reduced above the initial onset of the coincidence region.

The region below the coincidence frequency the sound transmission loss is predominantly governed by the mass of the sample [21].The resonant transmission in this range is heavily affected by the edge conditions as the edges are comparatively efficient radiators. Thus at low frequencies the panel size and edge conditions have a large influence on the sound transmission loss. A number of studies [159, 160] have shown that the sound transmission loss of a sample will increase as the panel size is reduced. Although these studies were focused on the sound transmission loss measured using the pressure-pressure method, the influence of the use of the pressure-intensity method is very unlikely to result in significant changes in the observed trends.

Very little research has been presented on the influence of sample size within the coincidence region. When coincidence occurs the panel radiates sound more efficiently via the coincident modes due to matching between the trace of the incident waves and the panel vibration. The panel itself becomes the dominant radiator and the contributions from edge effects are reduced. The size

effects are also related to the panel's transmission efficiency and as such the very high efficiency that occurs at coincidence causes the size effects to become negligible.

Above the critical frequency the edges provide a link for power to flow into the surrounding structures. This power flow is described in a number of previous studies [154, 172]. The power flow from the sample into the surrounding structure is heavily dependent on the connection between the sample and the structure. All structural connections will provide some level of energy dissipation, with an optimal dissipation frequency based on the stiffness and damping of the system. A more effective coupling will result in a higher sound transmission loss as a greater quantity of the panel's vibrational energy will be dissipated into the surrounding structure. This effect is most pronounced for relatively heavy partitions, but is also present in lightweight partitions, although the glass used in [173] will have very low damping loss factor compared to plywood or plasterboard. The results presented indicate that the sample size can have a large effect on the measured sound transmission loss above the critical frequency. Reducing the sample size increases the edge to area ratio, which in turn increases the amount of energy that can flow into the surrounding structure.

Research by Sewell [47] and later work by Davy [1, 3, 135, 174, 175] investigated the influence of the sample size on the radiation efficiency of samples excited by incident sound. Figure 3 in Davy's 2009 publication indicates that the theoretical diffuse field forced radiation efficiency increases as the sample size is increased for a set frequency. This will result in the smaller samples having a higher sound transmission loss below the coincidence region. The prediction formulas presented by Davy and Sewell indicate that the forced radiation efficiency increases with increasing sample size. This effect will be explored in more detail in Section 8.

Research presented by Sakuma et al [176] demonstrated some reduction in the sound transmission loss of glass panes with increasing sample size. This reduction was shown to occur at frequencies above the coincidence region. The reduction in sound transmission loss was due to a reduction in the edge damping that occurs as the panel size is increased. This pattern of behaviour is similar to that observed in the research presented in this thesis. The behaviour of the glass system is influenced by different factors than the plywood systems, due to the very low internal damping factor of glass. This low internal damping factor increases the relative importance of the boundary conditions as reflected waves are not damped out resulting in higher radiation levels.

7.6. Correction Factor

The variations measured in the pressure distributions within the room were applied to try and correct for the sample size and location. The difference between the pressure levels near the surface of the transmission loss panels (Figure 7.22) were subtracted from the small transmission loss samples. The sound transmission loss was adjusted for a range of different samples; the results of these corrections are presented in Figure 7.29 – Figure 7.31.

The application of the correction factor improved the correlation between the two sample sizes when applied to a 2 kg/m^2 barrier (Figure 7.29). The correlation above 500 Hz was dramatically improved, although the location of the coincidence criterion was shifted significantly. Below 500 Hz the correlation between the two measurements is not improved by the application of this correction factor.

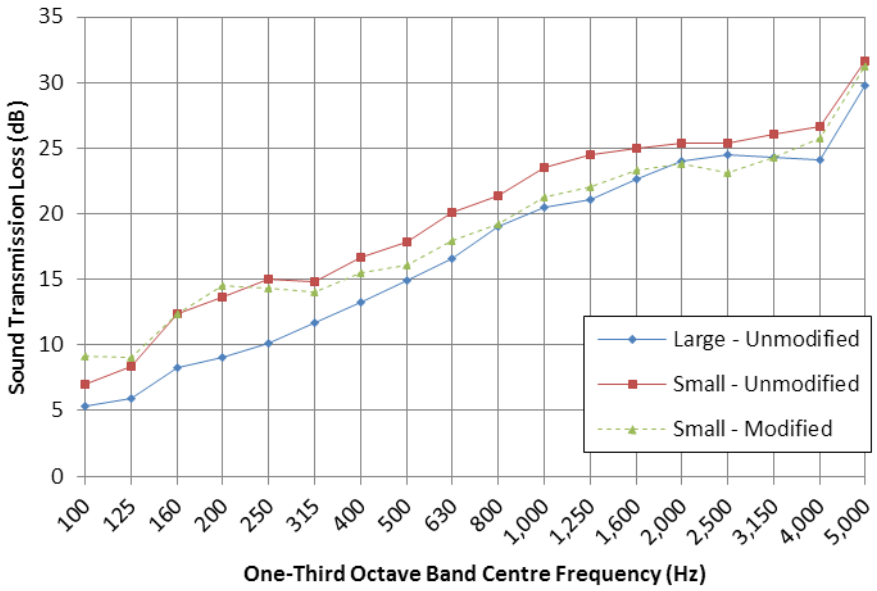

Figure 7.29: Sound transmisisonl loss of 2kg/m^2 mass loaded barrier, modified using the difference in surface pressure levels

The same correction factor was applied to a single leaf 9 mm plywood partition (Figure 7.30) and a single leaf 10 mm gypsum plasterboard partition (Figure 7.31). The correction factor makes the small and large samples correlate better above 500 Hz; as was seen in the 2 kg/m^2 barrier samples. In comparison the correction factor worsens the agreement within the coincidence region and appears and only yields a significant improvement in the frequency bands between 400 Hz and 1600 Hz.

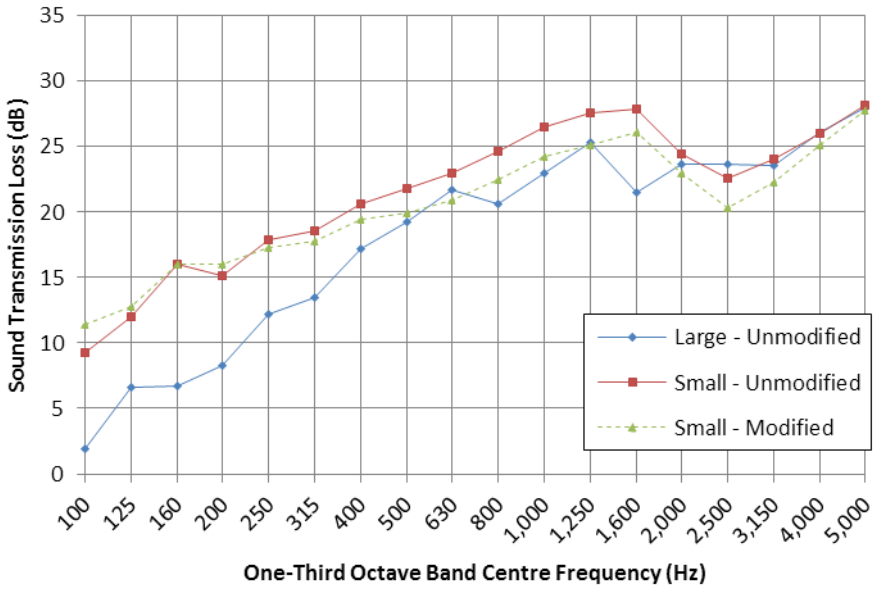

Figure 7.30: Sound transmisison loss of single leaf of 9 mm plywood, modified using the difference in surface pressure levels

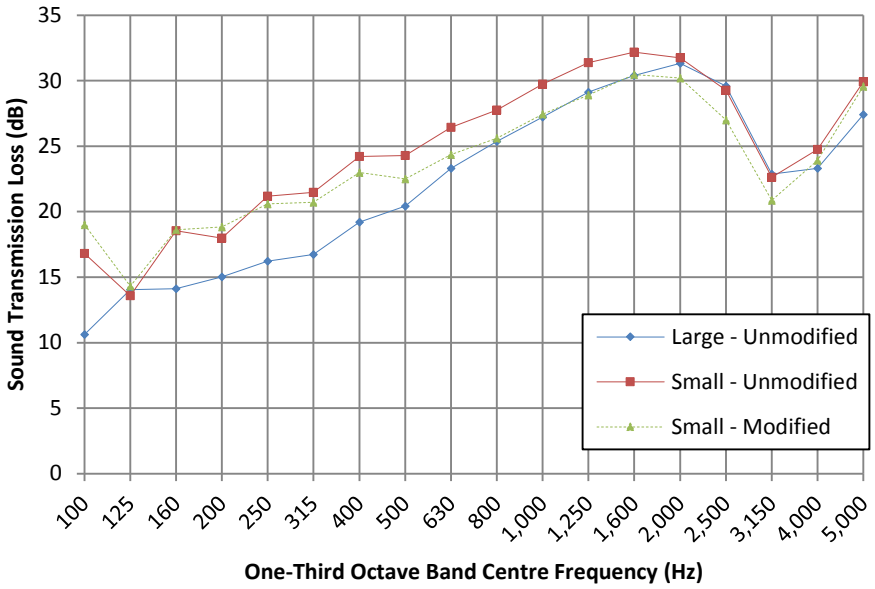

Figure 7.31: Sound transmission loss of single leaf of 10 mm gypsum plasterboard, modified using the difference in surface pressure levels

Whilst accounting for the different surface pressure levels appeared to somewhat improve the correlation between the two sample sizes it was not consistent. This lack of consistency makes this technique less useful for practical applications. The lack of consistency in the correction also indicates that there are other contributing factors affecting the measured sound transmission loss.

7.7. Other Effects

Several other effects that are not directly related to the sample size may also have an effect on the measured sound transmission loss. These effects include; the construction of the sample, the niche effect, the sample edge mounting conditions, and the tunnelling effect. Each of these factors and their relative influence will be discussed in this section.

The observed measurement results indicate that the construction of the sample alters the variation between the small and large transmission loss samples. Reducing the size of a single leaf partition increased the sound transmission loss in almost all cases. In contrast reducing the size of a double leaf partition had a much less pronounced difference on the measured sound transmission loss. The addition of studs adds an additional high radiation area and structural connection path below the critical frequency, which was provided only by the edges of the sample in the case of partitions without studs. Below the critical frequency the resonant radiation of the panel is confined to the edges of the panel. In areas of the panel away from the edges the resonant waves have the effect of cancelling all radiated sound away from the panel. Studs alter this by creating a discontinuity in the panel, this discontinuity results in reflected waves near the studs. The reflected waves are spread over a range of frequency components and are not cancelled, resulting in areas of high radiation near the studs. The inclusion of studs into the test samples dramatically increased the area of the panel that radiates at lower frequencies reducing the effect of the increased edge ratio [59].

There are a number of niche effects that can occur in a sound transmission loss facility. The first niche effect is the change in effective maximum angle of incidence. This is a function of both the sample size and the depth of the niche the sample is mounted in. The exposure of the panel to waves at grazing incidence is directly affected by the depth of the niche on the reverberant source room side. As the niche depth increases the maximum angle of incidence is reduced. This yields an expression for the maximum angle of incidence (θ_{max}), given by Equation 7.1.

$$\theta_{max} = \tan^{-1}\left(\frac{L_x, L_y}{d}\right) \qquad \textbf{7.1}$$

where L_x and L_y are the lengths of the rectangular sample and d is the depth of the sample niche. Theoretically the predicted sound transmission loss of an infinite plate is heavily dependent on the angle of incidence. In the case of the single leaf samples the maximum angles of incidence are given in Table 7.4.

Table 7.4: Maximum angle of incidence on reverberation (source) room side of transmission loss sample

Sample	Horizontal ϑ_{max}	Vertical ϑ_{max}
Large (4.8 m × 2.4 m)	83°	77°
Small (1.5 m × 0.95 m)	77°	69°

The reduced angle of incidence resulted in an increased sound transmission loss, as predicted by the infinite panel theories. This effect is due to the grazing waves being responsible for a significant proportion of the transmitted sound. This explanation accounts for some of the variation in sound transmission loss seen in these measurements.

According to the prediction methods presented in Section 2 the sound transmission loss of a system is very dependent on the maximum angle of incidence. Reducing the angle of incidence will reduce the transmission coefficient for any given partition system, this in turn causes an increase in the sound transmission loss of the system. The grazing incidence waves make a significant contribution to the sound transmission loss of the system, thus reducing the grazing incidence waves increases the sound transmission loss accordingly. This explanation accounts for some of the variation in the sound transmission loss seen in the measurements.

Reducing the maximum angle of incidence influences the onset of the coincidence region. The lowest frequency coincidence occurs ($f_c(\theta)$) when the angle of incidence (θ) is highest, as shown by Equation 7.2.

$$f_c(\theta) = \frac{{c_0}^2}{2\pi \sin^2\theta}\sqrt{\frac{m}{B}} \qquad \textbf{7.2}$$

where m is the surface mass of the panel, B is the bending stiffness of the panel, and c_0 is the speed of sound in air.

The highest possible angle of incidence is theoretically 90 degrees, but the inclusion of a significant sample niche results in a reduction in this maximum angle of incidence. Reducing this angle of incidence increases the lowest frequency at which the coincidence region begins.

Existing research into the effect the niche has on the sound transmission loss has been explored using numerical methods [177]. It was found that the sound transmission loss is reduced below the critical frequency and increased above the critical frequency due to the niches. The niche effect was shown to be greatest when the niches on either side were equal (i.e. the sample was centrally located in the aperture). Further research using wave based methodologies [156] found that the niche effect caused the sound transmission loss to be lower below the critical frequency, and somewhat higher above the critical frequency. The niche causes two smaller volumes within the test

aperture to be coupled, resulting in higher sound transmission at lower frequencies. At higher frequencies this coupling is reduced and the effect of the reduced maximum angle of incidence becomes more important. The niche depth of the large sample is significantly larger than that of the small sample; this may have contributed to the decrease in measured sound transmission loss of the large sample below the critical frequency. The niche effect is also much more evident in samples smaller than 5 m^2 [157], as is the case with the small sample tested in this research. The behaviour measured in this research supports these findings. The niche effect is presumed to be a major contributor to the variations in the observed sound transmission loss.

Research has been undertaken on the tunnelling effect that occurs when there is a niche on both sides of the panel [158]. In this research it was shown that the position of a sample within the aperture can have a significant influence on the measured sound transmission loss. The trends of increasing sound transmission loss with increasing tunnel depth and decreasing panel size appear to agree with the results observed. The smaller transmission loss rig has a deeper niche, and has a higher sound transmission loss.

The method used to secure the sample into the test opening can also affect the measured sound transmission loss. This is especially important at low frequencies where the majority of the sound is radiated at the boundaries of the sample [132]. Furthermore the physical construction of the test opening can also have an effect on the measured sound transmission loss. It has been shown that increasing the rigidity of the mounting condition will increase the sound radiation near the edges. The radiation efficiency for a clamped panel is twice as large as that of a simply supported panel [164]. The difference in measured sound transmission loss can differ by up to 3 dB between different fixture arrangements [173]. Whilst these effects will alter the radiation efficiency at low frequencies when the wavenumber is low it has been shown that over the frequency range measured the influence of the edge conditions plays a relatively minor role in the overall sound transmission loss [132, 178].

The inclusion of the stud frame stiffens the panel which in turn alters the radiation efficiency of the panel. The effect of stiffening members on the radiation efficiency of panels has been explored by Maidanik [166]. This research found that the inclusion of studs results in areas of increased radiation efficiency around the studs. The radiation efficiency below the coincidence frequency is proportional to the perimeter of the boundary of a finite panel. This effect is due to the edges causing a scattering of the plane waves within the panel, resulting in wave components within the panel that may effectively radiate sound. These wave components are not effectively cancelled and are therefore more efficient radiators. The presence of the studs has the same scattering effect,

increasing the radiation efficiency of partitions with studs present. This effect reduces the difference in measured sound transmission loss between the small and large test samples.

The power flow that was discussed earlier can also be affected by the mounting conditions, specifically the rigidity of the mounting conditions. Higher edge losses occur in more firmly mounted structures, whereas elastic mountings result in lower edge losses. The measurements presented in this thesis used small samples that were clamped into a wooden frame, and the large samples were screwed and glued onto a timber frame that was rigidly mounted to a heavyweight concrete wall system. It is possible that because the small sample had a frame that was constructed from timber that there may have had slightly closer impedance matching between the panel and the frame. It is thought that the edge coupling effects were similar for both samples and were unlikely to contribute greatly to the measured variations in sound transmission loss.

All the double leaf samples were constructed on a timber stud frame. The majority of the single leaf samples tested had studs present for the large samples, and did not have studs in the small samples. The inclusion of studs within the test sample increases the overall stiffness of the system. The unsupported area of the small sample was 1550 mm × 950 mm, whereas when the studs were included the unsupported area in a large sample was 600 mm × 2400 mm. The inclusion of studs into the test system has some effect on the transmission loss of the large facility (Figure 7.7). The presented data compares a single leaf of plywood measured with and without studs in the large transmission loss rig.

7.8. Evaluation

The measured sound transmission loss is heavily influenced by the size of the sample, as is expected from the existing theories. The results presented in this section show that there is not a simple correlation between a change in sample size and the change in measured sound transmission loss. There is a number of complicating factors which alter the influence of the sample size on the transmission loss. An effort has been made to explore these factors in relation to the relevant research that has been performed.

A significant increase in the sound transmission loss was seen when the sample size was reduced. The low frequency behaviour of the samples tested was as expected, with the transmission loss of the smaller sample remaining 3 to 5 decibels higher until the coincidence frequency where some convergence occurred. A number of the measured samples produced results which deviated from most current theories on the effects of sample size above the coincidence frequency, with the smaller sample again having a higher sound transmission loss. This effect is likely to be due to the

combination of increased niche depth and reduced sample size, reducing the maximum angle of incidence.

It was found that the general trends seen in both the sample sizes are relatively consistent. This means that the use of the small transmission loss rig for comparative testing appears to be justified. Unfortunately there appears to be no clear method for predicting the change that the variation in the sample size will cause. The models presented in Section 9 will be applied to the smaller transmission loss rig, using an expression for the finite panel radiation efficiency and a limited angle of incidence to adjust the results to fit the smaller samples measurements.

A major finding in this research was the influence that the construction of the partition had on the observed size effects. The change in the sound transmission loss due to the sample size was significantly larger in single leaf, samples without studs than in double leaf samples with studs. Including studs into the system also results in a more similar edge condition which also influences the magnitude of the size effects discussed in sections above. This influence of the construction on the size effects means that the transmission losses measured using the small transmission loss facility cannot have a simple correction factor applied to the measurements.

The overall trends and behaviours measured in both the small and large transmission loss facilities are similar. The coincidence regions for similar constructions occur at a similar frequency. The low and high frequency slopes are similar with the only major variation occurring in the region where the two curves converge, slightly above and below the coincidence frequency.

The measurements and the qualitative analysis performed in this section indicate that the size of the sample has a measureable effect on the measured transmission loss across the entire frequency range. The dependence of these effects on the construction of both the sample and the frame mean that drawing direct comparisons between these measurements is difficult. Despite these issues the small transmission loss facility is still very useful for assessing a large number of transmission loss samples efficiently.

8. Effect of Acoustic Treatments on Sound Transmission Loss

Research concerned with the acoustic treatment of lightweight plywood is presented. Two treatments were investigated in this research: the attachment of decoupled mass loaded barriers onto the panels surface and the insertion of an internal viscoelastic damping layer into the centre of the panel. Each of these treatments was applied and evaluated, and methods for predicting the transmission loss of the treated partitions were developed.

8.1. Overview

Much of Section 8.2 was presented in a journal article "Predicting the sound insulation of plywood panels when treated with decoupled mass loaded barriers" [2] and an associated conference article "Acoustic treatment of panels: Effect of attachment method" [4]. The material presented in these articles is further developed in Section 8.2, and a more detailed analysis of the test methodology, sample construction, and results is presented.

Section 8.3 presents new research into the effects of viscoelastic damping materials on the sound transmission loss. These materials have been applied to a range of materials for vibration damping purposes, but their use within lightweight timber structures is relatively limited. The application of such materials is relevant to high performance lightweight timber systems. Previous research indicates that increasing the internal damping loss factor reduces the severity of the coincidence dip and this hypothesis is evaluated.

8.2. Decoupled Layer Treatments

8.2.1. Introduction

The relatively poor acoustic performance of lightweight timber partitions prompted this investigation into the effectiveness of treating the plywood panels with mass loaded barriers. The relatively lightweight and high stiffness properties of the plywood partitions results in relatively low transmission loss. The treatment method assessed in this section consists of limp mass loaded barriers of different surface densities spaced off a panel by a layer of open cell foam of varying thickness. This investigation was focused on evaluating these barrier materials as sound transmission loss treatments. A simple analytical model for predicting the performance of these materials was also developed. The prediction model presented was based on research undertaken by Davy [74, 75, 77, 78] which presented models for the prediction of the sound transmission loss of double leaf partitions. The thickness of the open celled decoupling foam, and the attachment method used to

attach the treatment to the panel were found to have a large influence on the sound transmission loss of the system. A range of different partitions were evaluated to assess the variation in sound transmission loss as the treatment arrangement and construction were altered. The prediction models were evaluated for a range of different treated partitions.

The theories behind the prediction methods developed in this section are described in Section 2. The prediction method used is a double leaf partition model, in which the cavity depth was altered in order to approximate the sound transmission loss of the treated samples. Past research has investigated the propagation of sound through porous media within multi-layered structures. A transfer matrix method [179, 180] was utilised to predict the impedance and transmission loss of multi-layered porous materials. In the transfer matrix method the system is represented by a set of 2 × 2 matrices that yield the ratio in velocities between the two plates. The results presented show reasonably good agreement except near the coincidence region. This technique was not pursued as the aim was to produce a simple analytical solution that could be implemented within a spreadsheet, for easy application by persons without technical computing capacities such as Matlab.

8.2.2. Measurement Procedure and Sample Details

The transmission loss of the samples was measured using the small transmission loss facility described in Section 4.3. The issues with the use of the small transmission loss facility described in Section 7 are considered in the predictions presented in this section. The trends observed using the small test facility are relatively consistent and as such the use of these results for model development was considered valid. In order to scale the model to full sized partitions a calibration test would be required to evaluate the variation due to the sample size.

All the samples evaluated consisted of an 18 mm thick panel of marine grade plywood with the attached treatment facing towards the reverberation room. The surface density of the plywood was 6 kg/m^2. Samples with two barrier surface densities (8 kg/m^2 and 4 kg/m^2) and five decoupling layer thicknesses (6 mm, 12 mm, 24mm, 50 mm and 100 mm) were evaluated. The sound transmission loss of the untreated plywood was also measured to evaluate the change caused by the decoupled treatment. The arrangement of the barrier, foam and plywood is shown schematically in Figure 8.1.

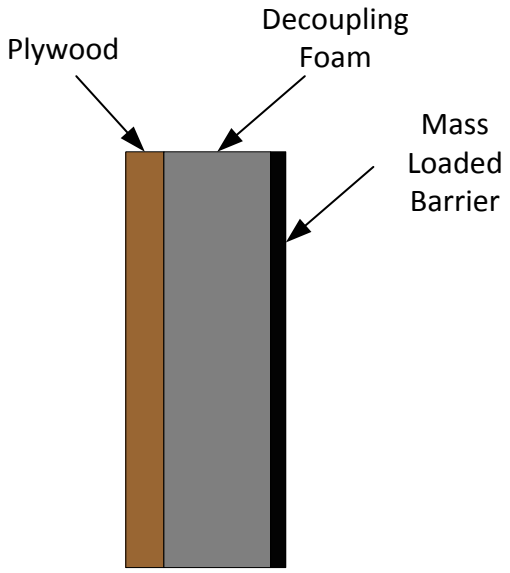

Figure 8.1: Arrangement of test samples treated with decoupling foam

The decoupling foam layer was an open cell polyurethane foam that is normally used for sound absorption. It has a compressional stiffness of 0.025 MPa (see section 3.3) and a density of 28 kg/m^3. The mass loaded barrier was a vinyl layer that was approximately 3 mm thick with varying densities as specified by the surface mass. The mass loaded barrier has a very low bending stiffness, which was unable to be accurately measured using the available test equipment.

Five different methods of attachment between the plywood panel and the treatment were investigated. Two arrangements of steel pins were used, a 300 mm × 400 mm grid (Figure 8.2) and a 500 mm × 600 mm grid (Figure 8.3). Two arrangements of glued samples were constructed; in the first arrangement the decoupling foam layer was glued to the panel using a layer of contact adhesive glue, resulting in the entire surface of the foam being glued to the panel. In the second glued arrangement 50 mm diameter spots of glue applied between the panel and the decoupling foam in a 300 mm × 400 mm grid (as in Figure 8.2). Finally 50 mm wide double sided adhesive was used to secure the foam to the panel; this was run vertically down the length of the panel and spaced horizontally at 300 mm centres (see Figure 8.4). In all cases the mass loaded barrier was glued to the decoupling layer using a full surface layer of contact adhesive. A summary of all the samples tested is presented in Table 8.1.

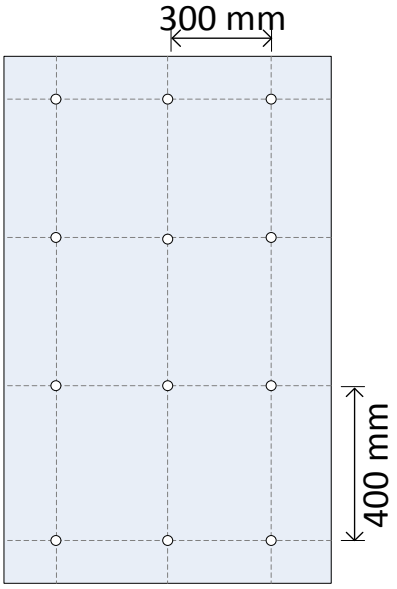

Figure 8.2: Fine pin spacing

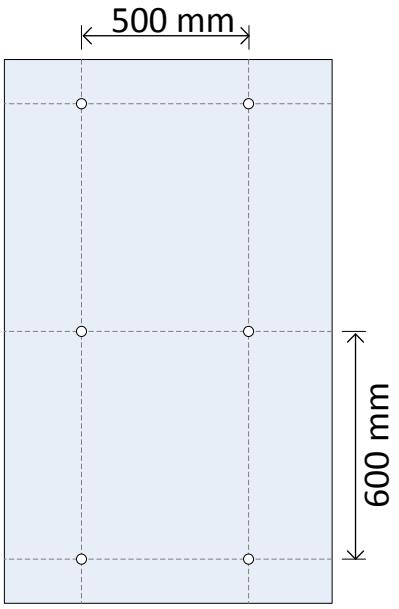

Figure 8.3: Wide pin spacing

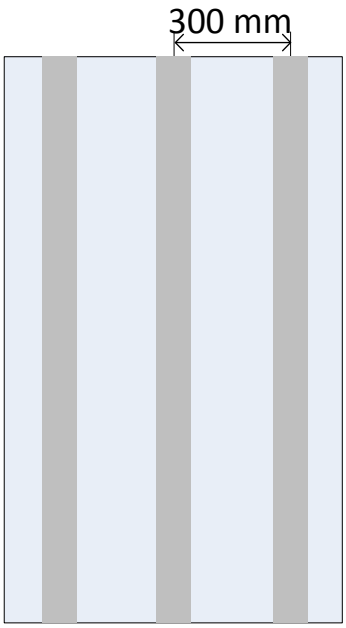

Figure 8.4: Adhesive tape layout

Table 8.1: Description of materials evaluated in decoupled layer tests

Sample #	Barrier Surface Density	Foam Thickness	Attachment Method
1	4 kg/m^2	6 mm	Pinned
2	8 kg/m^2	6 mm	Pinned
3	4 kg/m^2	12 mm	Pinned
4	8 kg/m^2	12 mm	Pinned
5	4 kg/m^2	24 mm	Pinned
6	8 kg/m^2	24 mm	Pinned
7	4 kg/m^2	50 mm	Pinned
8	8 kg/m^2	50 mm	Pinned
9	4 kg/m^2	100 mm	Pinned
10	4 kg/m^2	12 mm	Spot Glued
11	4 kg/m^2	24 mm	Spot Glued
12	4 kg/m^2	12 mm	Wide Spaced Pinned
13	4 kg/m^2	24 mm	Wide Spaced Pinned
14	4 kg/m^2	12 mm	Adhesive Strip
15	4 kg/m^2	24 mm	Adhesive Strip
16	4 kg/m^2	12 mm	Fully Glued
17	4 kg/m^2	24 mm	Fully Glued

Samples one to nine were tested to assess the effect of changing the density of the mass loaded barrier layer, and altering the thickness of the foam decoupling layer. The samples used for evaluating the effect of the decoupling layer thickness were all attached in the same manner. Two

different masses were used in all cases except the sample with 100 mm thick decoupling foam. Samples ten to seventeen were tested to assess the effect the fixture method had on the sound transmission loss of the sample. The sound transmission loss of the 18 mm plywood was also evaluated to assess the improvement caused by the decoupled layer treatments.

The completed samples were clamped into the small transmission loss facility with the decoupled layer treatment facing towards the source room. This clamping process caused the edges of the treatment to be squashed between the clamps, causing a possible structural connection. A constant torque of 10 Nm was applied to all the clamping bolts and the sound transmission loss was then measured. Once these samples were mounted in the transmission loss suite they were tested using the methodology described in Section 4. The results of these measurements are presented in Section 8.2.3. In all cases the pressure-intensity index and repeatability index was checked to ensure the measurements were not contaminated by extraneous noise.

8.2.3. Results and Evaluation

The variations in the measured sound transmission loss due to different attachment methods are shown in Figure 8.5 and Figure 8.6. The addition of the treatments to the plywood partitions results in an increase in the transmission loss above 200 Hz in most cases. The transmission loss below 200 Hz was similar to the untreated partition in most cases with some variations in individual one-third octave frequency bands. The sound transmission losses of samples treated using the different attachment methods were observed to converge above 1600 Hz and a similar convergence occurred below 200 Hz. The sound transmission loss of the samples had a consistent trend, with a significant dip in the transmission loss near 200 Hz, followed by steep 18 decibel per octave increase in the sound transmission loss. Overall the treatment resulted in an improved sound transmission loss and an increase in the STC and R_w values.

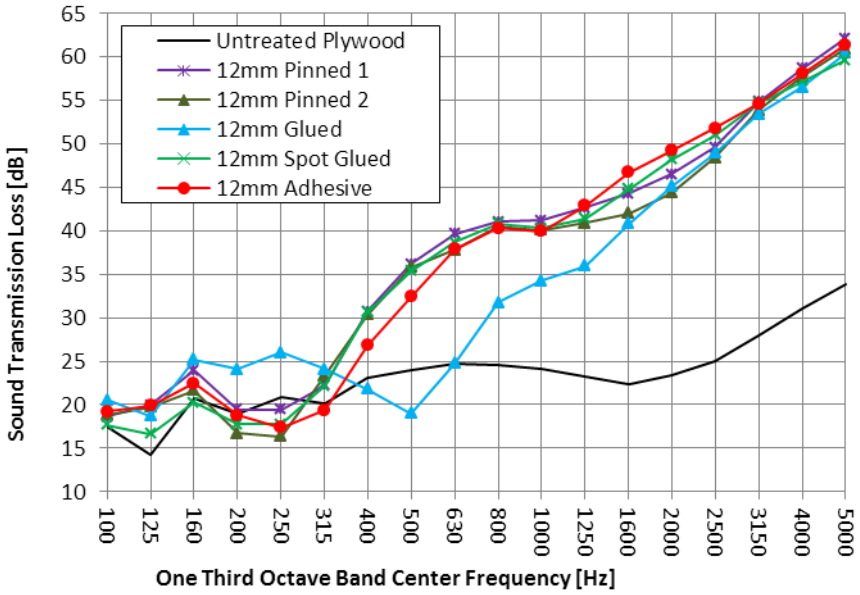

Figure 8.5: Variation in the measured sound transmission loss due to the attachment method. All arrangements consist of a 4 kg/m² mass loaded barrier and a 12 mm thick foam decoupling layer

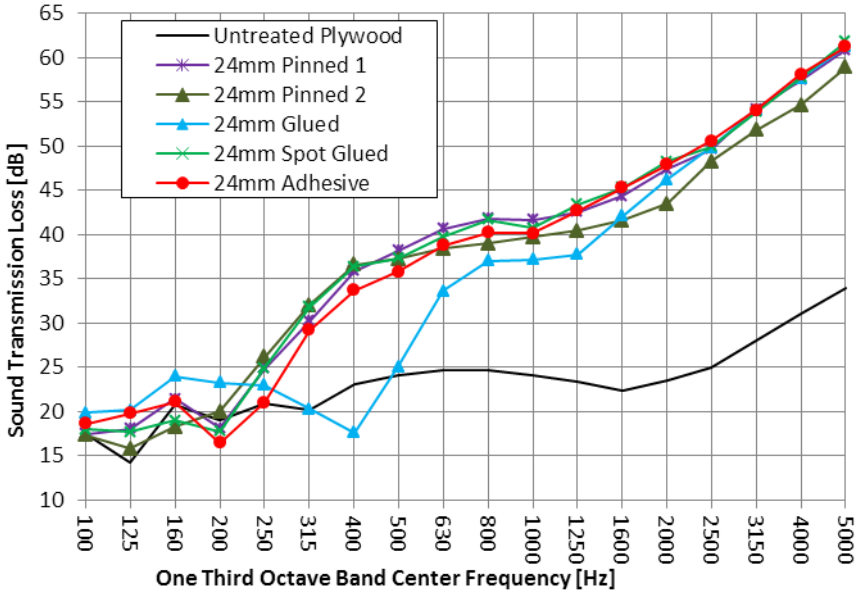

Figure 8.6: Variation in the measured sound transmission loss due to the attachment method. All arrangements consist of a 4 kg/m² mass loaded barrier and a 24 mm thick foam decoupling layer

There is a reduction in the slope of the transmission loss curves between 800 Hz and 1600 Hz. This is related to the flattening of the untreated plywood panel's transmission loss curve caused by the coincidence behaviour. The dip occurs at a lower frequency in the treated samples than the untreated plywood as the underlying plywood transmission loss behaviour is overwhelmed by the high frequency double leaf behaviour.

Theoretically addition of mass loaded barrier with a surface density of 4 kg/m² to the plywood should increase the transmission loss by approximately 4 dB in the mass controlled region [17]. A

similar increase of approximately 4 dB across the rest of the frequency range of interest was expected due only to the application of mass to the system. The decoupling of the mass loaded barrier from the panel was observed to result in a large increase in the sound transmission loss compared to simply increasing the surface density of panel, especially in the frequency range above 200 Hz.

The treated panels had three distinct regions of behaviour similar to a typical double leaf partition. At frequencies below 200 Hz the system had a sound transmission loss curve that appeared to generally increase at 6 decibels per octave, although this was complicated by the presence of a number of resonant “dips”. This region of relatively slow increased was followed by a steep 18 dB per octave region at the mid-range frequencies (200 Hz – 1000 Hz). A third region at higher frequencies exhibits an increase of 12 dB per octave. The sound transmission loss behaviours of the different samples converge between the 18 dB per octave region and the 12 dB per octave region. This appears to be typical double leaf wall behaviour, with the steep increase occurring above an equivalent mass-stiffness-mass frequency. This mass-stiffness-mass is equivalent to a mass-air-mass that is observed in typical double leaf partitions with an air cavity. The calculation of this mass-stiffness-mass frequency will be discussed in Section 8.2.4.

The results indicate that increasing the stiffness of the attachment between the foam and the panel decreases the overall sound transmission loss. The stiffest attachment method used was the fully glued method. This method has a much lower transmission loss across the measured frequency range than less rigid attachment methods like the pinned samples. This was due to the less rigid attachments lowering the equivalent stiffness of the cavity between the two leaves, causing the system to begin acting as a double leaf partition at a lower frequency.

The fully glued samples had a lower transmission loss between 315 Hz and 2000 Hz. The fully glued arrangement also had a higher sound transmission loss below 315 Hz; this was due to the fact that the mass-air-mass resonant frequency of the glued sample was significantly higher than the other samples. The samples with other attachment methods had their mass-stiffness-mass resonance in the 200 Hz – 250 Hz range, which resulted in a decrease in the measured sound transmission loss. In this range the glued sample was not within its mass-stiffness-mass resonance and as such had a higher measured sound transmission loss.

The adhesive strips yielded a somewhat lower transmission loss in the 18 decibel per octave region for both the 12 mm and the 24 mm samples. Outside of this region the transmission loss was very similar to the other attachment methods. There were no clear trends in the other three

attachment methods; all the sound transmission loss behaviours were very similar throughout the frequency range of interest.

The sound transmission loss increases as the thickness of the decoupling foam layer is increased, as shown in Figure 8.7 and Figure 8.8. Five thicknesses of decoupling foam were used with the 4 kg/m^2 barrier and four thicknesses with the 8 kg/m^2 barrier. All of the samples had the treatment pinned to the panel using the closely spaced arrangement (300 mm × 400 mm grid). An increase in sound transmission loss occurs between 250 Hz and 1000 Hz as the thickness of the decoupling layer is increased, this was evident in all of the samples tested. The largest increase in the measured sound transmission loss between the 6 mm and 100 mm samples was 20 decibels in the 315 Hz one-third octave band.

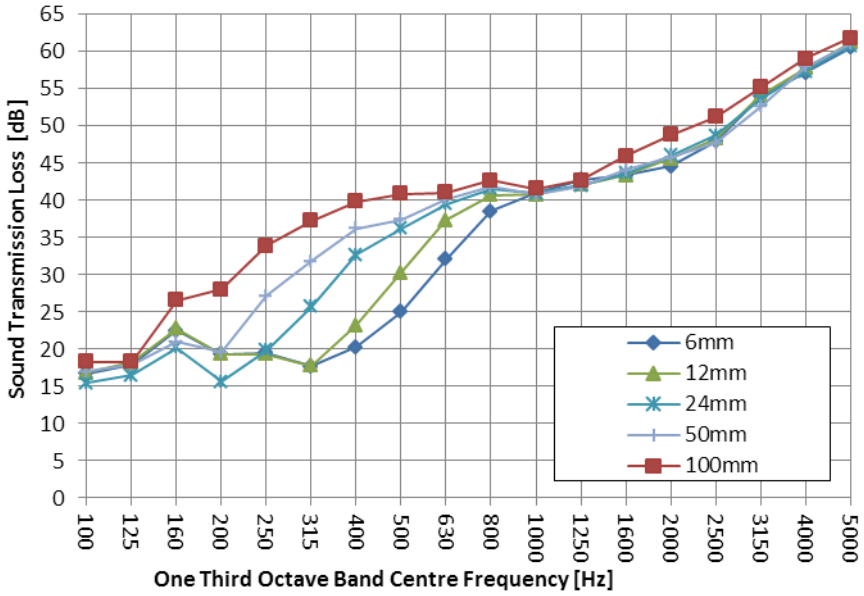

Figure 8.7: Effect of increasing decoupling layer thickness with 4 kg/m^2 mass loaded barrier

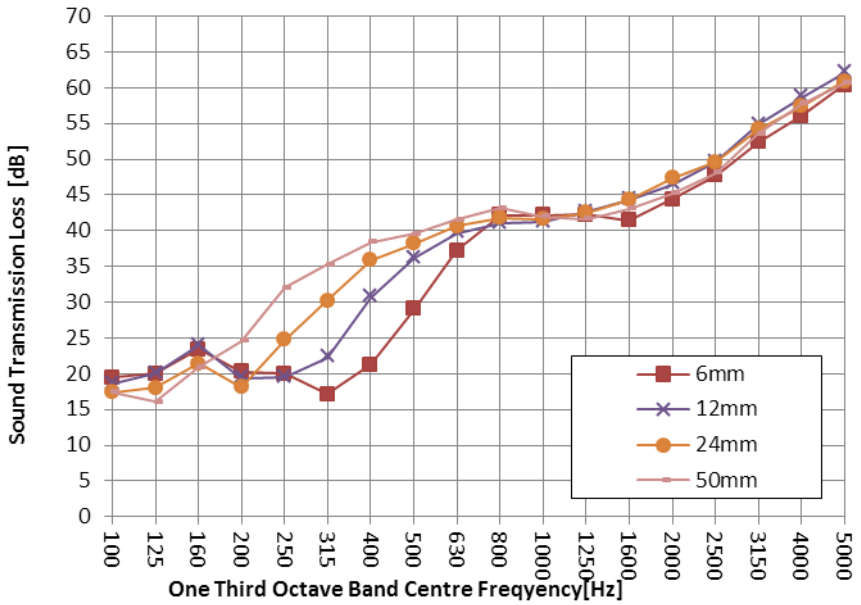

Figure 8.8: Effect of increasing decoupling layer thickness with 8 kg/m² mass loaded barrier

The sound transmission loss behaviour of the samples had the same three distinct regions seen in the fixture arrangement tests. Increasing the thickness of the decoupling layer reduces the frequency at which the steep 18 decibel per octave region begins. This is typical of the behaviour of a double leaf partition with increasing cavity depth; the cavity depth being governed by the decoupling layer thickness. The pins, clamped edges, and the decoupling foam all form structural connections between the two leaves.

The variation in thickness had a similar effect on the sound transmission loss when the decoupling foam was glued to the plywood panel. The glued and pinned behaviour is shown in Figure 8.9. These same similarities are seen between all the different attachments methods. In all cases increasing the thickness of the decoupling foam layer causes the initial dip in the sound transmission loss to occur at a lower frequency. This effect was due to the mass-stiffness-mass occurring at a lower frequency as the decoupling layer thickness was increased. As with the samples presented above the sound transmission loss converges above 2000 Hz. This convergence is the same for arrangements with different thicknesses and different attachment methods.

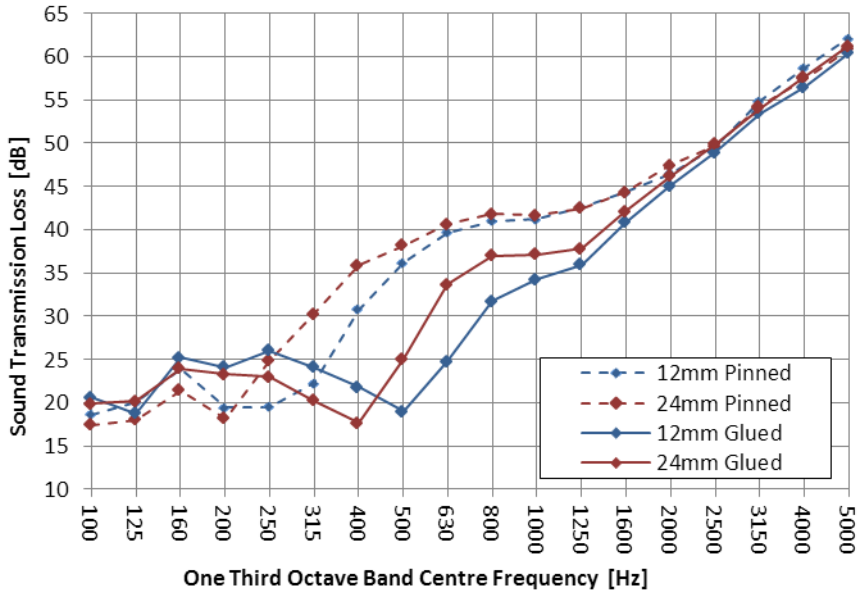

Figure 8.9: Variation in the measured sound transmission loss due to the attachment method for two thicknesses of foam decoupling layer. All the panels are treated with a 4kg/m² mass loaded treatment

The variation in the measured sound transmission loss caused by increasing the barrier surface density 4 kg/m² to 8 kg/m² is presented in Figure 8.10. For both thicknesses presented, the transmission loss increases in the steep 18 dB per octave region when the surface density of the barrier is increased. Increasing the barrier surface density also increased the transmission loss below the 18 dB per octave region by 2 to 3 dB in each one third octave frequency band. These variations in the sound transmission loss due to increasing surface density are consistent with theories concerning both single and double leaf partitions.

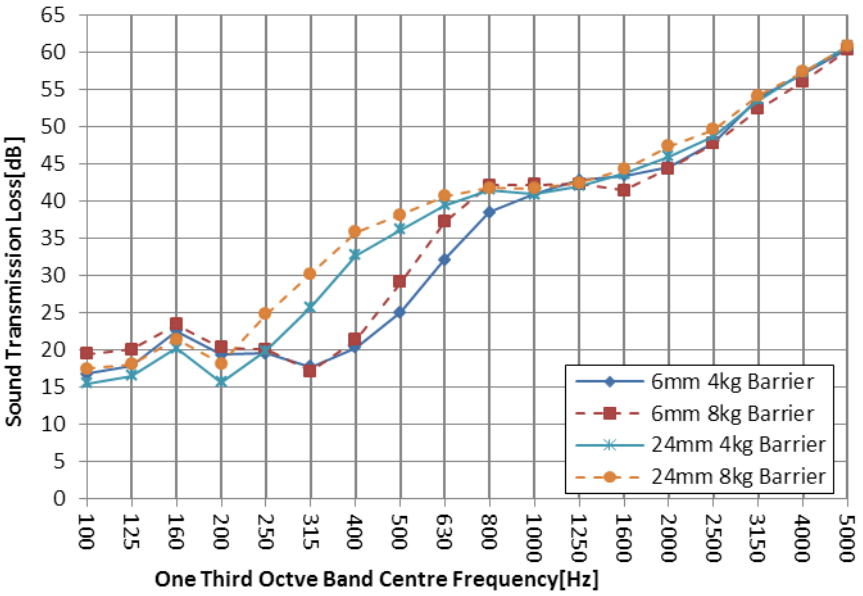

Figure 8.10: Variation in sound transmission loss of sample due to the mass of the treatment for two thicknesses of

foam decoupling layer. The treatment was pinned to the panel using the close pin spacing

The STC and R_w ratings were calculated for all the measured samples to evaluate the improvement in single number ratings that the acoustic treatments cause. The calculated values are shown in Figure 8.11, these values were calculated using the methods described in ASTM E413-10 [181] and ISO 717-1:1996 [44]. The STC and R_w ratings can be heavily affected by a low STL in a single one-third octave band. The STC and R_w of samples 6 and 7 are similar to that of untreated ply, despite the significantly higher STL above 1000Hz.

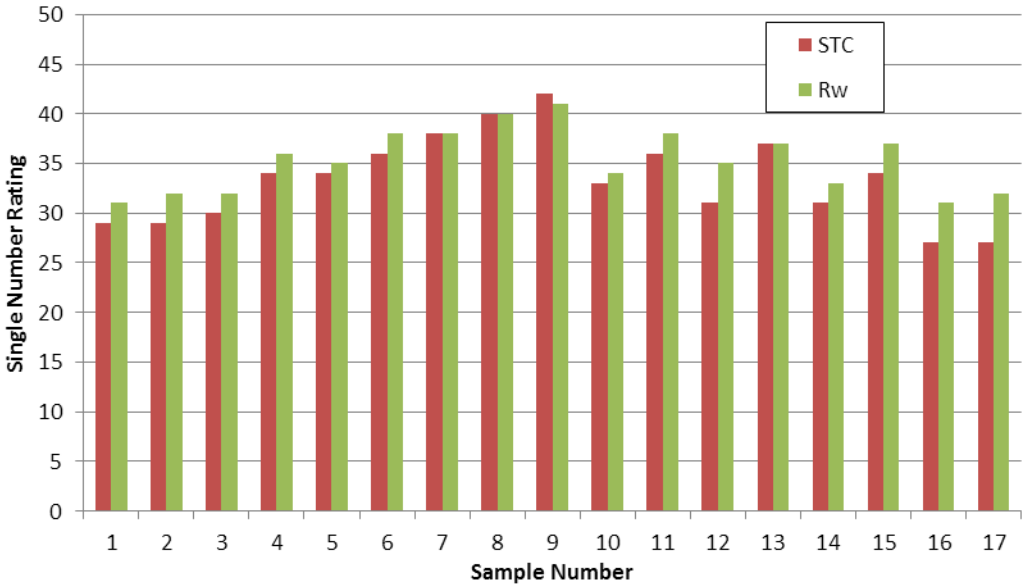

Figure 8.11: Single number ratings (STC and Rw) for the treated materials

8.2.4. Prediction Methods

A method for predicting the sound transmission loss of the treated systems is presented. The frequency range of interest is divided into several sections and different formulae are used in each region to predict the sound transmission loss. The orthotropic properties of the plywood were neglected in this modelling, as the double leaf construction reduced its influence. Furthermore the mass loaded barrier is essentially a limp mass that does not have a coincidence dip, which significantly reduces the overall influence of the coincidence behaviour. In this situation the stiffness of the plywood panel was assumed to be the geometric mean of the two orthotropic bending stiffness values, given by Equation 8.1.

$$E_{mean} = \sqrt{E_x E_y} \qquad \textbf{8.1}$$

Three related models were utilised to model the performance of the partition. An initial model was used for the evaluation of the sound transmission loss of the untreated plywood [77]. A second

model was used for the sound transmission loss of the plywood and barrier system [75], using varied cavity depths to represent the foam thickness. A third model was used to evaluate the transmission due to the connection points [78]. Parameters within these models were altered to predict the behaviour of the tested specimens.

Initially an isotropic single panel model was utilised for the plywood behaviour and the low frequency behaviour of the system. The single panel model used in this work was presented by Davy [77] as an extension to Cremer's [17] model. The sound transmission coefficient when the angular frequency ω is above the angular critical frequency ω_c was calculated using Equation 8.2.

$$\tau_{single,f>f_c} = \frac{\sigma^2(\theta_c)}{2ar(\sigma(\theta_c)+a\eta)}\left\{\arctan\left[\frac{2a}{\sigma(\theta_c)+a\eta}\right]-\arctan\left[\frac{2a(1-r)}{\sigma(\theta_c)+a\eta}\right]\right\} \quad \textbf{8.2}$$

where a is given by Equation 8.3, η is the damping loss factor of the panel, r is the ratio between the frequency being calculated and the critical frequency (ω/ω_c) and $\sigma(\theta_c)$ is the single sided forced radiation efficiency at the coincidence angle $\theta_c$as derived by Davy,

$$a = \frac{\omega m}{2\rho_0 c} \quad \textbf{8.3}$$

where m is the surface density of the panel, ρ_0 is the ambient air density, ω is the angular frequency of interest and c is the speed of sound in air. The total sound transmission coefficient below the critical frequency is given by the summation of the sound transmission coefficients calculated using Equations 8.4 and 8.2.

$$\tau_{single,f<f_c} = \frac{2\langle\sigma\rangle}{a^2} \quad \textbf{8.4}$$

where $\langle\sigma\rangle$ is the diffuse field forced radiation efficiency.

The experimental measurement of the untreated plywood panel is compared to the modelled results in Figure 8.12. The measured data has a significantly shallower coincidence dip than predicted by the modelled data; due to the orthotropic stiffness of the plywood. This prediction is compared in Section 9 to orthotropic prediction methods.

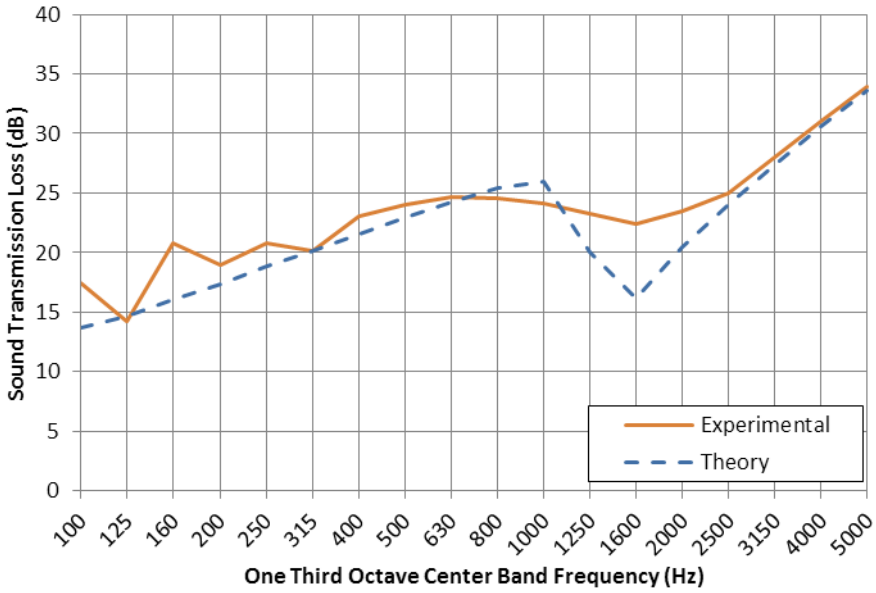

Figure 8.12: Comparison between measured sound transmission loss of 18 mm marine grade plywood and isotropic prediction model

The stiffness of the plywood was measured following the techniques described in Section 3.1. The stiffness in the soft direction was 2 GPa, and the stiffness in the hard direction was 5 GPa. The two stiffness values correspond to a low critical frequency of 1100 Hz and a high critical frequency of 1700 Hz. These stiffness values also allow the first fundamental frequency to be calculated, this was done to assess the range over which the models were likely to be accurate. The first resonance frequency for an orthotropic panel with different edge conditions were calculated using the equation given by Pilkey [10]. A simply supported panel has a first resonant frequency at 51 Hz, and a fully clamped pane has a resonant frequency of 96 Hz. The test facility used had edge conditions that were assumed to sit between these two different conditions. The models presented are considered to be valid above the first resonant frequency, thus the models presented are valid above approximately 100 Hz. The geometric mean of the orthotropic stiffness measurements was 3.2 MPa, the average damping loss factor was 0.021 and the density of the plywood was 340 kg/m^3. The damping loss factor was found to vary with both the frequency and sample tested. The average damping loss factor of the measured samples was used as no specific frequency dependent trend could be identified. It was also assumed that this measured damping loss factor was similar to that of the panel installed in the test facility.

Outside of the coincidence region the single leaf isotropic prediction method performs well, with good agreement with the experimental results at frequencies above 2500 Hz. The variation at the low frequencies may be due to the small sample size influencing the measured sound transmission loss. The small sample size will result in some modal behaviour. The first modal resonance occurs

somewhere below 100 Hz, above this frequency the modal density is constant which allows the model to be utilised for frequencies above this value.

The foam decoupling layer was modelled as an air cavity with a cavity depth that was altered depending on the attachment method and decoupling foam thickness. When modelling the fully glued case the stiffness of the air cavity was assumed to be the same as the stiffness of the foam layer; the modelled cavity depth was adjusted to meet this requirement. The other methods of attachment were modelled using an air cavity with the same thickness as the foam layer, as depicted in Figure 8.13. This method was utilised as it was found to best agree with the experimental response. The glued sample seals the foam against the plywood panel, so air cannot move in and out of the foam. In the other samples the air can move freely between the panel and the foam; the limp attachment methods result in a significant air cavity between the foam and plywood panel. These effects explain to some extent the stiffness behaviour observed. The glued foam was the primary transmission path and thus it was used as the cavity stiffness. In the case of the other attachment methods the airborne path is more significant hence the separation stiffness is equal that of the equivalent thickness air cavity.

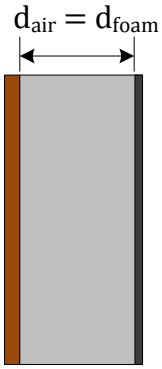

Figure 8.13: Equivalent air gap for all attachment methods except fully glued

The effective air cavity depth (d_{air}) for the fully glued samples was calculated based on the foam decoupling layer thickness (d_{foam}) using Equation 8.5. The stiffness of the foam decoupling layer (E_{foam}) was measured as described in Section 3.3. The measured stiffness was 0.065 MPa, whereas the stiffness used in the calculations was 0.55 MPa. The stiffness value was changed in order to improve the agreement of the model when compared to the experimental data. Possible explanations for this empirical correction are discussed below.

The measured compressional stiffness represents the static stiffness, whereas in practice the foam is undergoing dynamic excitation which results in a deviation from the measured stiffness. The stiffness measurements were also undertaken in a manner which allowed dilatational expansion; this may significantly reduce the measured compressional stiffness.

The equivalent cavity (Equation 8.5) depth is 2.5 mm for the 12 mm fully glued foam decoupling layer and 4.9 mm for the 24 mm fully glued foam decoupling layer. This was derived by setting the stiffness of the cavity equal to the stiffness of an equivalent air cavity.

$$d_{air} = \frac{\rho_0 {c_0}^2 d_{foam}}{E_{foam}} \qquad 8.5$$

The nominal 8 kg/m^2 barrier was modelled using the measured surface density of 9.08 kg/m^2. It was found that accurate measurements of the bending stiffness of the mass loaded barrier were difficult to achieve, furthermore as the damping loss factor was high the standard dynamic tests were unable to be used as the decay times were too short. The other material parameters were set so that the combination of the barrier and the foam layer which was glued to it had a critical frequency of about 32 kHz. The barrier was assumed to act as a limp mass due to its construction. To further justify this assumption the measured transmission loss behaviour of the 8 kg/m^2 barrier is presented in Figure 8.14. The transmission loss curve has no obvious coincidence behaviour within the frequency range of interest; as such the critical frequency was selected to be much higher than the highest measured frequency of 5000 Hz.

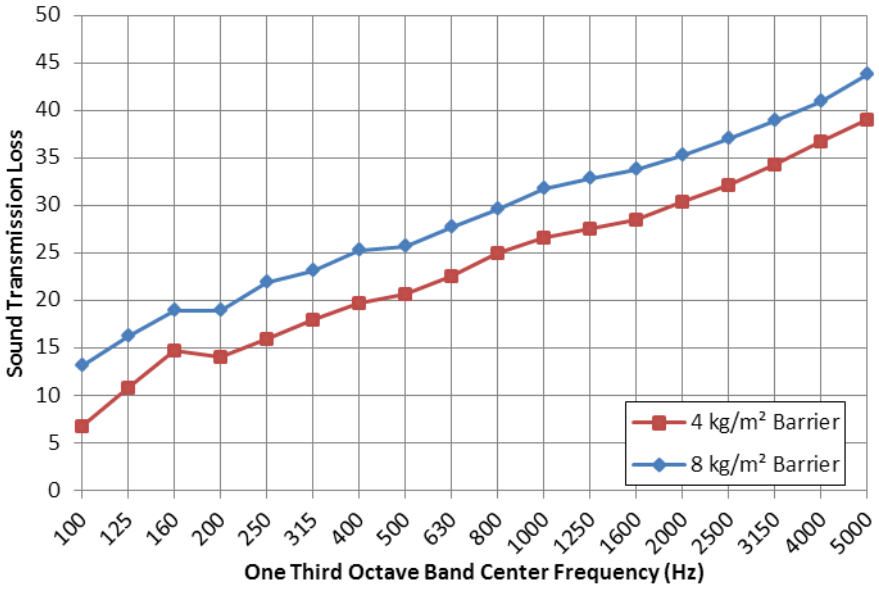

Figure 8.14: Measured sound transmission loss of 4 kg/m² and 8 kg/m² mass loaded vinyl barrier without acoustic foam or plywood panel

The sound transmission coefficient used in evaluating the airborne sound transmission loss of the decoupled systems above the lowest of the two critical frequencies is given by Equation 8.6. This transmission coefficient was presented by Davy in his 2010 paper [75]. The following equations are taken from this publication.

$$\tau_{wall,f>f_{c1}} = \frac{I}{s_1^2 s_2^2 \alpha^2} \quad \textbf{8.6}$$

where the variable s_i is given by Equation 8.7, and α is the sound absorption coefficient of the cavity. The sound absorption in the cavity is set to a small but non-zero value in the case of an empty cavity, otherwise it is the absorption of the material within the cavity.

$$s_i = \frac{2a_i\xi_i}{\sigma(\theta_{ci})} \quad \textbf{8.7}$$

where ξ_i is the ratio between the angular frequency and the critical frequency (see Equation 8.8).

$$\xi_i = \frac{\omega}{\omega_i} \quad \textbf{8.8}$$

If the two leaves have different properties I can be described using Equations 8.9 – 8.13.

$$I = \frac{A + B + C}{D} \quad \textbf{8.9}$$

$$A = q_1 q_2 (p_2 - p_1) \ln\left\{\frac{[q_1^2 + (p_1 - 1)^2](q_2^2 + p_2^2)}{[q_2^2 + (p_2 - 1)^2](q_1^2 + p_1^2)}\right\} \quad \textbf{8.10}$$

$$B = q_1[(p_1 - p_2)^2 + q_1^2 - q_2^2]\left[\arctan\left(\frac{p_2}{q_2}\right) - \arctan\left(\frac{p_2 - 1}{q_2}\right)\right] \quad \textbf{8.11}$$

$$C = q_2[(p_2 - p_1)^2 + q_2^2 - q_1^2]\left[\arctan\left(\frac{p_1}{q_1}\right) - \arctan\left(\frac{p_1 - 1}{q_1}\right)\right] \quad \textbf{8.12}$$

$$D = q_1 q_2[(p_2 - p_1)^2 + (q_2 + q_1)^2][(p_2 - p_1)^2 + (q_2 - q_1)^2] \quad \textbf{8.13}$$

where $p_i$is given by Equation 8.14 and q_i is given by Equation 8.15.

$$p_i = 1 - 1/\xi_i \quad \textbf{8.14}$$

$$q_i = \frac{1 + \frac{a_i\eta_i}{\sigma(\theta_{ci})}}{s_i} \quad \textbf{8.15}$$

If the two leaves have the same properties, $q_1 = q_2 = q$ and $p_1 = p_2 = p$, and Equation 8.9 simplifies to Equation 8.16.

$$I = \frac{q^2 - p(p-1)}{2q^2(q^2+p^2)[q^2+(p-1)^2]} + \frac{\left[\arctan\left(\frac{p}{q}\right) - \arctan\left(\frac{p-1}{q}\right)\right]}{2q^3} \quad \textbf{8.16}$$

where η_i is the damping loss factor of the individual panels, a_i is given by Equation 8.17 and α is the absorption coefficient of the cavity. The sound absorption coefficient is governed by Equation 8.18, which limits the maximum value of the absorption coefficient to 1 and reduces it at lower frequencies.

$$a_i = \frac{\omega m_i}{2\rho_0 c} \quad \textbf{8.17}$$

$$\alpha = \begin{cases} kd \; if \; kd < 1 \\ 1 \; if \; kd \geq 1 \end{cases} \quad \textbf{8.18}$$

where m_i is the surface density of the i^{th} leaf and ω_i is the critical frequency of the i^{th} panel.

Equation 8.18 is utilised in order to account for the reduced absorption coefficient at low frequencies when the thickness of the absorption is small in comparison with the wavelength of the incident sound waves. $\sigma(\theta_{ci})$ is the single sided forced radiation efficiency at the coincidence angle (θ_{ci}) of the i^{th} leaf. To obtain better agreement with experimental results, the radiation efficiency is set equal to 1 if the frequency is greater than or equal to the lower of the two critical frequencies. If the frequency is between 0.9 times and 1 times the lower of the two critical frequencies, the radiation efficiency is linearly interpolated in the frequency domain between the value of the radiation efficiency at 0.9 times the lower of the two critical frequencies and a value of 1 at the lower of the two critical frequencies.

Below the lower of the two critical frequencies the methodology set out by Davy [74] is used, with some slight modifications as described in [75]. This frequency range is broken down further into two sections; the range below the mass-air-mass resonance frequency and the range above the mass-air-mass resonance frequency. For the case where the foam is fully glued to the plywood, the mass-air-mass resonance frequency is replaced by the mass-stiffness-mass resonance, where the stiffness is that of the foam decoupling layer. Below the mass-air-mass frequency resonance the system acts as a single leaf system with a total mass of $m = m_1 + m_2$. Between this mass-air-mass frequency resonance and the lower of the two critical frequencies the transmission coefficient is given by the sum of Equation 8.19 and Equation 8.6.

$$\tau = \frac{1 - cos^2\theta_l}{(q + pcos^2\theta_l)(p+q)} \quad \textbf{8.19}$$

Where p is given by Equation 8.20.

$$p = a_1 a_2 \alpha \tag{8.20}$$

and α is given by Equation 8.18.

The variables q and $cos^2\theta_l$ are given by Equations 8.21 and 8.22, and d_{foam} is the thickness of the decoupling foam layer.

$$q = \frac{1}{2}\left(\frac{a_2}{a_1} + \frac{a_1}{a_2}\right) \tag{8.21}$$

$$cos^2\theta_l = \begin{cases} 0.9 \; if \; \dfrac{1}{2ke} > 0.9 \\ \dfrac{1}{2ke} \; if \; 0.9 \geq \dfrac{1}{2ke} \geq cos^2 61° \\ cos^2 61° \; if \; cos^2 61° > \dfrac{1}{2ke} \end{cases} \tag{8.22}$$

where e can be calculated using Equation 8.23.

$$2e = 4S/U \tag{8.23}$$

and S is the area of the partition, U is the perimeter of the partition and k is the wave number of the sound in air.

The structure borne transmission is predicted using a third model. Davy [78] gives a detailed theory for the structure borne transmission contribution to the overall airborne sound transmission. The sound transmission coefficients are derived for both line and point connections.

The sound transmission coefficient for a resilient massless point connection is given by Equation 8.24.

$$\tau_{point} = \frac{256 n \rho_0^2 c^4 Q R}{\pi \omega^2 [(m_1 \omega_{c2} + m_2 \omega_{c1})^2 + 64 \omega^2 m_1^2 m_2^2 c^4 C^2]} \tag{8.24}$$

where Q is calculated based on the ratio of resonant vibrational energy of the first leaf to its mass law vibrational energy (Equations 8.25 and 8.26). C is the compliance of the point connections and was assumed to be zero for this model. n is the number of point connections per unit area. The surface density of the i^{th} leaf is m_{i} and $\omega_{c\mathrm{i}}$ is the critical frequency of the i^{th} leaf. The fact that the expressions for the structure borne transmission are not symmetric with leaf number is addressed in

Davy [78]. The order of leaves are numbered such that $\omega_{c1} < \omega_{c2}$. As such the first leaf is the plywood in all cases.

$$e = \frac{\pi \omega_{c1} \sigma_1}{4\omega \eta_1} \quad \textbf{8.25}$$

$$Q = \begin{cases} 1 + e & \text{if } \omega < \omega_{c1} \\ e & \text{if } \omega \geq \omega_{c1} \end{cases} \quad \textbf{8.26}$$

R is calculated using the ratio, r. For point connections the r can be calculated using Equation 8.27.

$$r = \frac{P_S}{P_n} = \frac{\pi \omega_{c2} \sigma_2}{4\omega \eta_2} \quad \textbf{8.27}$$

Equation 8.28 gives the equivalent calculation for line connections.

$$r = \frac{P_S}{P_n} = \frac{\sigma_2}{2\eta_2} \sqrt{\frac{\omega_{c2}}{\omega}} \quad \textbf{8.28}$$

where P_S, and the power radiated by the vibrational field in the second leaf generated by the connection, P_n. These equations allow R to be calculated using Equation 8.29.

$$R = \begin{cases} 1 + r & \text{if } \omega < \omega_{c2} \\ r & \text{if } \omega \geq \omega_{c2} \end{cases} \quad \textbf{8.29}$$

The sound transmission coefficient for parallel resilient massless line connections is given by Equation 8.30 where the leaves are ordered such that $\omega_{c1} < \omega_{c2}$.

$$\tau_{stud} = \frac{64 \rho_0^2 c^4 Q R}{b\omega^2 [G^2 + (4\omega^{3/2} m_1 m_2 c C - G)^2]} \quad \textbf{8.30}$$

where G is calculated using Equation 8.31.

$$G = m_1 \sqrt{\omega_{c2}} + m_2 \sqrt{\omega_{c1}} \quad \textbf{8.31}$$

b is the distance between the centre lines of adjacent line connections. For the calculation of the sound insulation due to the structure borne transmission between the leaves, the radiation efficiency of a freely propagating bending wave in the i^{th} leaf is limited to a maximum value of 1 [182]. The line connection theory is used to model the connecting effect of the frame around the edge of the sample.

The prediction model developed in this section was implemented in Matlab and Excel. The prediction method does not require any computationally expensive calculations (such as numerical integrations). There are a number of parameters in this prediction method that can be "tuned" to fit experimental data better; unfortunately these have not been found to be directly related to material properties measured using static approaches. The following section presents a number of comparisons between the measured and predicted sound transmission loss measurements.

8.2.5. Comparisons between Predictions and Measurements

The prediction method presented in the previous section was evaluated against the measured results. The predicted sound transmission loss was calculated from 100 Hz to 5000 Hz for all of the samples measured. A wide range of comparisons are presented between the predicted methods and the various measured attachment methods.

The performance of the prediction methods when applied to the closely pinned samples is shown in Figure 8.15 and Figure 8.16. In both the 12 mm and the 24 mm samples the airborne transmission model predicts the behaviour of the treated system reasonably well until the end of the steep 18 decibel per octave section of the curve. Above this frequency the airborne model dramatically overestimates the sound transmission loss of the partition.

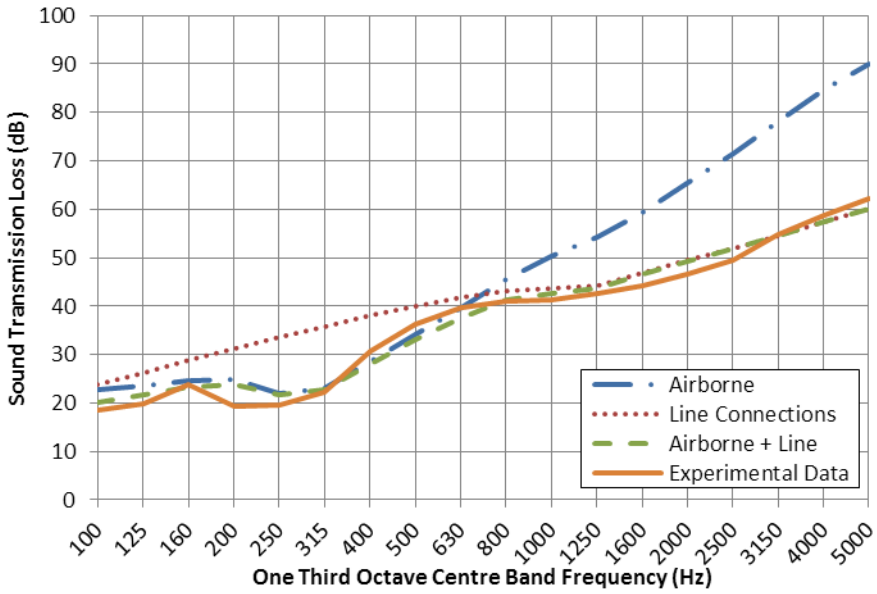

Figure 8.15: Comparison of different prediction methods when applied to the prediction of the closely pinned samples, with a decoupling foam thickness of 12 mm

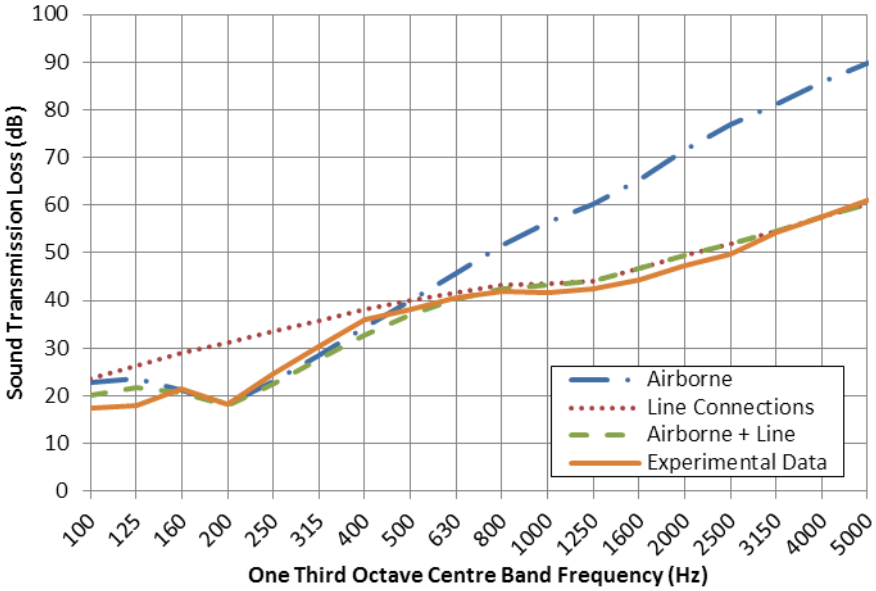

Figure 8.16: Comparison of different prediction methods when applied to the prediction of the closely pinned samples, with a decoupling foam thickness of 24 mm

Similar performance is seen when the same prediction methods are applied to the wide pinned samples. The performance for the 12 mm and 21 mm samples which were attached using a widely spaced pin arrangement are presented in Figure 8.17 and Figure 8.18. The agreement between the predicted and measured results is somewhat worse. The reduction in accuracy is due to the prediction method being unable to account for the altered location of the mass-stiffness-mass frequency that occurs when the pin spacing is changed. The cavity depth could be altered to make the mass-stiffness-mass dip in the predicted results match the dip in the measured results, but this would imply that the cavity stiffness was lower than a purely air filled cavity of the same thickness which appears counter intuitive.

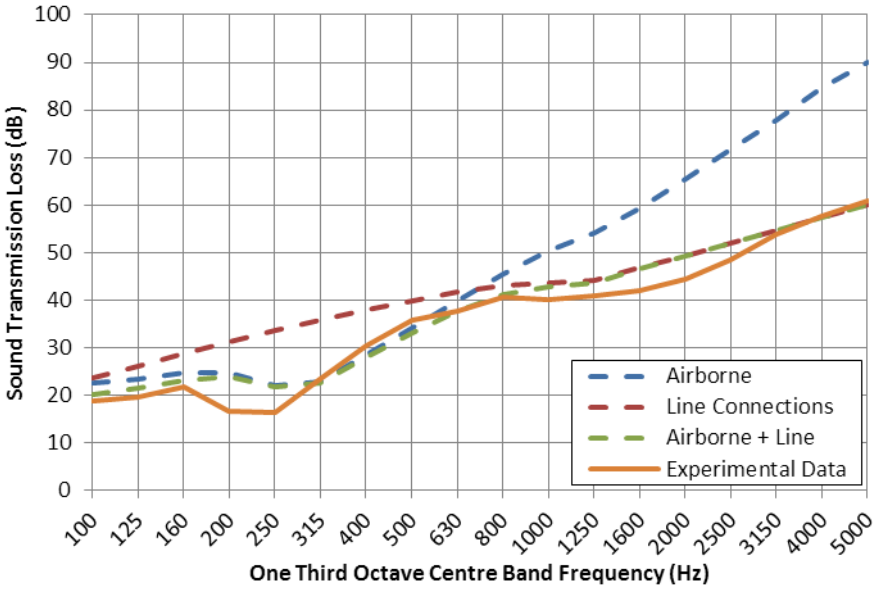

Figure 8.17: Comparison of different prediction methods when applied to the prediction of the widely pinned samples, with a decoupling foam thickness of 12 mm

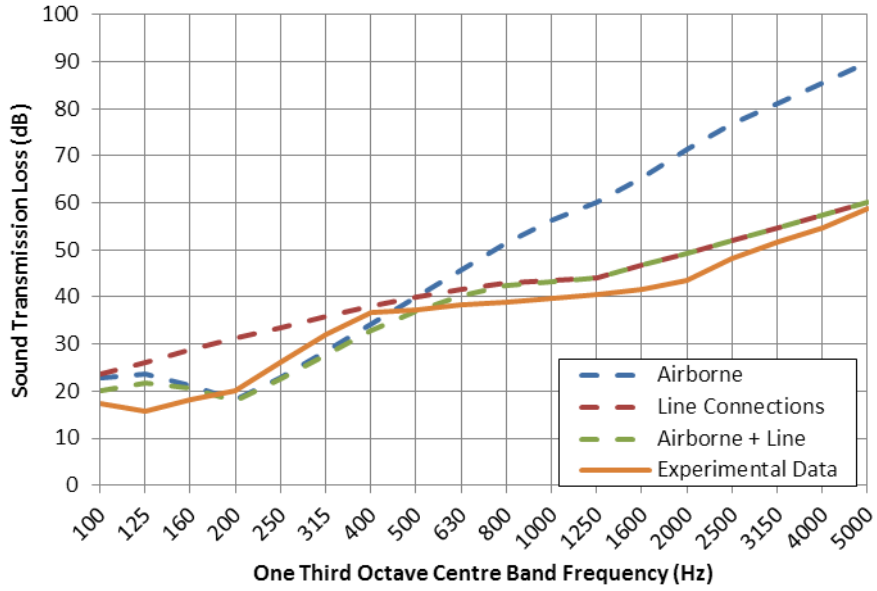

Figure 8.18: Comparison of different prediction methods when applied to the prediction of the widely pinned samples, with a decoupling foam thickness of 24 mm

The results of the predictions applied to the fully glued sample are presented in Figure 8.19 and Figure 8.20. The agreement in these cases was significantly worse. This was partially due to the difficulties encountered in correctly calculating an equivalent air gap thickness (using Equation 8.5). The airborne model manages to predict the transmission loss behaviour below 630 Hz to within 4 decibels, although the location of the mass-air-mass resonance predicted to be two thirds of an octave higher than measured. As with the pinned samples the point connections dramatically overestimate the entire transmission loss curve. The line connections yield poor agreement above

the 18 decibel per octave region. Again a combination of the airborne and line connection prediction methods yields the best agreement with the measured data, to within 4 decibels across the majority of the frequency range. Overall the performance is much worse across most of the frequency range when compared to the agreement achieved for the pinned samples.

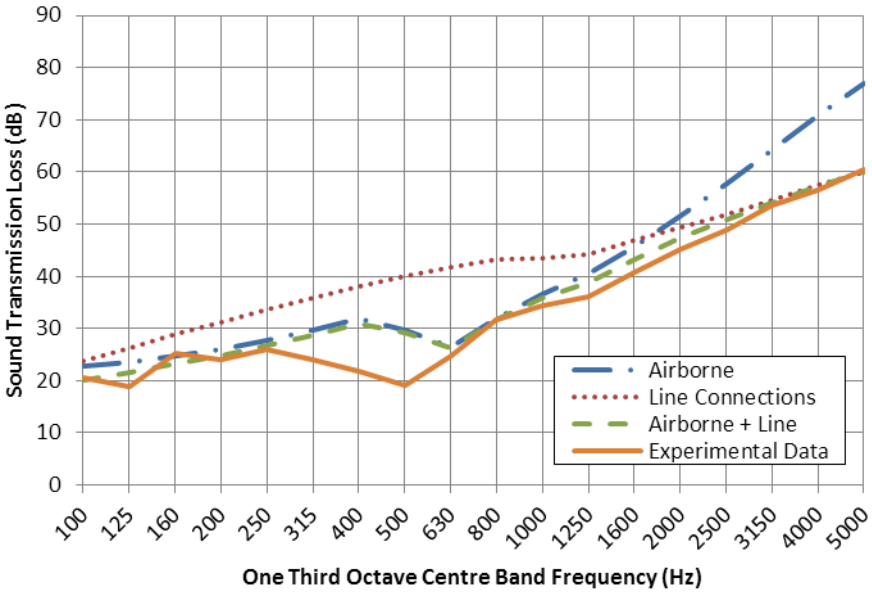

Figure 8.19: Comparison of different prediction methods when applied to the prediction of the fully glued samples, with a decoupling foam thickness of 12 mm

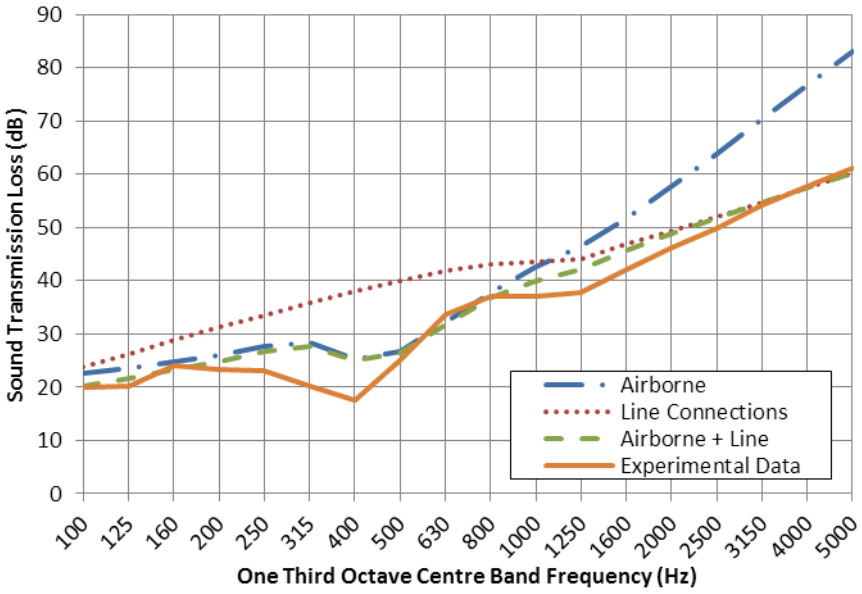

Figure 8.20: Comparison of different prediction methods when applied to the prediction of the fully glued samples, with a decoupling foam thickness of 24 mm

The prediction methods were reasonably accurate when modelling the behaviour of the other attachment methods such as the adhesive strips. In all cases the agreement between the airborne

model and the measurements is reasonably good below the end of the 18 decibel per octave region, and the line connection models achieved a reasonable agreement above this region.

The structure borne transmission models have a similar shape to the higher frequency behaviour of the measured results. Both the point and line connections have a plateau in the mid – high frequency range with a shallow slope above this frequency. The point connection model has a significantly higher sound transmission loss than the measured across the entire frequency range; the line connection models predictions are only slightly higher than the measured sound transmission loss.

As was the case in the two previous examples the combination of the airborne and line transmission paths yields the closest agreement to the measured results. In all the alternative attachment methods the frequency range below the lowest part of the mass-air-mass resonance is poorly modelled, possibly because the stiffness of the cavity was modelled as an equivalent air gap. The inclusion of the open cell foam, even when loosely bonded, will affect the effective stiffness of the cavity.

To achieve good agreement a number of factors had to be selected within the model. The line spacing model is used to model the connection of the plywood and the barrier at the edge of the specimen due to the frame in which the sample was mounted. This connection is used to explain why all the results are so similar at high frequencies. Flanking sound transmission was rejected as a cause of the similar results at higher frequency because this rig has previously been used to establish higher sound insulation values within the frequency range of interest. It was found that the line connection spacing had a large effect on the final modelled results; a final spacing of 1.5 m was selected. It is thought that a stud spacing wider than that of the double leaf partition system is required due to the radiation efficiency at the edges being lower than the radiation efficiency of a stud at the centre of a panel. Cremer and Heckl [183] showed that the mobility of a beam excited by a point force at the centre is four times that of beam excited at the edge (This can be seen in Table 5.1. of [183]). This can be related to the sound transmission coefficient utilising Equation 38 and the related equations presented in [78], which suggests that a variation in the plate mobility at the studs results in a variation in the transmission coefficient. The wider stud spacing is an empirical fix to improve the agreement; the justification for this fix is due to the variations in plate mobility at the edges.

The analytical model predicts the measured sound transmission loss of the pinned samples very well. The most accurate model combined the airborne transmission model for transmission across the cavity and the stud-borne transmission. The good agreement between the measured results and

the model in the pinned case indicates that the structure borne transmission is similar to the transmission seen with stud connections. The large stud spacing indicates that the transmission at the edges is dominant.

The variation between the predicted and measured sound transmission loss for the glued samples indicates that the approach taken was not entirely appropriate. The model development still provides some interesting insights into the behaviour of the system. The variation occurs around the mass-air-mass resonance frequency. The frequency of the measured mass-air-mass resonance was predicted to within one third octave band by the models evaluated. All the models evaluated generally over predict the location by one third octave band but this is not consistent in all the systems modelled.

8.2.6. Conclusions

The experimental data presented shows the importance of system design when developing noise treatment products. The effects of decoupling layer thickness, the mass of the barrier and the attachment method all need to be considered if the treatment product is to be optimised. As the decoupling layer thickness increases, the sound transmission loss increases in the 250 – 1250 Hz frequency range. The fixture method also had an effect on the measured sound transmission loss; increasing the stiffness of the fixture method decreased the sound transmission loss in the 250 – 1250 Hz frequency range. This combination of factors can be related to the typical restraints put on treatment products; the volume of space available, the maximum allowable mass, and the means by which the product may be attached to the material to be treated. These decoupled mass loaded barriers, attached via low stiffness methods, can be utilised to provide effective sound treatments for lightweight panels with optimal weight and thickness parameters.

The models developed in this section allow for reasonable predictions to be performed for the transmission loss of a plywood panel treated with a decoupled mass loaded barrier. The model required a number of parameters to be calculated, measured or estimated. . Good agreement was seen between the modelled and measured results in the case of pinned attachments, with poorer agreement when the treatment was attached with a layer of glue. It was found that measuring the dynamic stiffness of the foam layers and the mass loaded barriers was a significant hurdle. Although these variables could be back calculated reasonably easily from one initial measurement, allowing the following configurations to be predicted reasonably accurately. It may be possible to develop alternative methods for the evaluation of the dynamic properties of highly damped, low stiffness materials.

The development of the model allowed the behaviour of the system to be understood in more detail. It was shown that panels treated with decoupled mass loaded barriers act like double leaf partitions, with a modified effective air cavity. A mass-air-mass resonance is evident with a rapid increase in sound transmission loss above the mass-air-mass resonance frequency. It was found that the transmission loss of these systems is heavily dependent on the attachment method used. The model developed in this section is significantly simpler than other models designed to predict the behaviour of systems with porous materials in their construction. Other models, such as those developed in Section 9 require significantly more computational time for their evaluation.

8.3. Viscoelastic Damping Materials

8.3.1. Theory and Methodology

The addition of viscoelastic damping materials was explored as a method of improving the overall transmission loss properties of the plywood, both as a single panel and within a double leaf partition. The theories described in Section 2.2 presented the current formulae used to calculate the sound transmission loss of a sample. In Cremer's model the damping loss factor only has an effect around and above the coincidence frequency. This effect near the critical frequency was of significant interest, as the plywood has a relatively broad coincidence "dip". This broad coincidence "dip" is due to the orthotropic nature of the plywood. The damping loss factor has a large effect within the coincidence region [20], because of this it was believed that increasing the damping loss factor would significantly improve the transmission loss of the plywood.

The damping loss factor of the plywood panels was increased by adding a layer of viscoelastic material between two 6 mm plywood sheets. A viscoelastic paste was used for the construction of the samples; this was spread onto the plywood sheets with glue trowels. The layer of viscoelastic damping is shown in Figure 8.21. A second sheet was placed on this layer and the two sheets were pressed together to ensure a cohesive bond. This resulted in a panel of damped plywood that has a central layer of viscoelastic. The overall thickness of the finished panel was approximately 12.5 mm, with a mass slightly higher to that of a 12 mm plywood panel.

Figure 8.21: Layer of damping material applied to plywood panel

The effect of the viscoelastic layer of the damping loss factor was measured via the free-free test methodology presented in Section 3.1.2. Several sample lengths were evaluated to spread the frequency responses over a wide range. The test arrangement of the largest beam tested is shown in Figure 8.22.

Figure 8.22: Largest damped plywood beam set up for damping and stiffness test

The damping loss factor and the measured stiffness of the damped plywood beams are shown in Figure 8.23 and Figure 8.24.

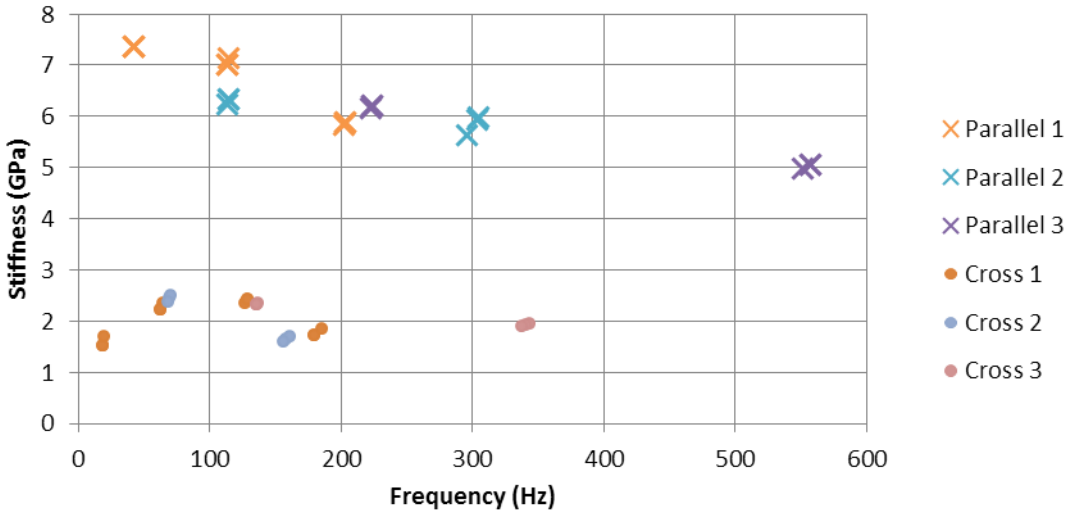

Figure 8.23: Dynamic stiffness of the damped plywood

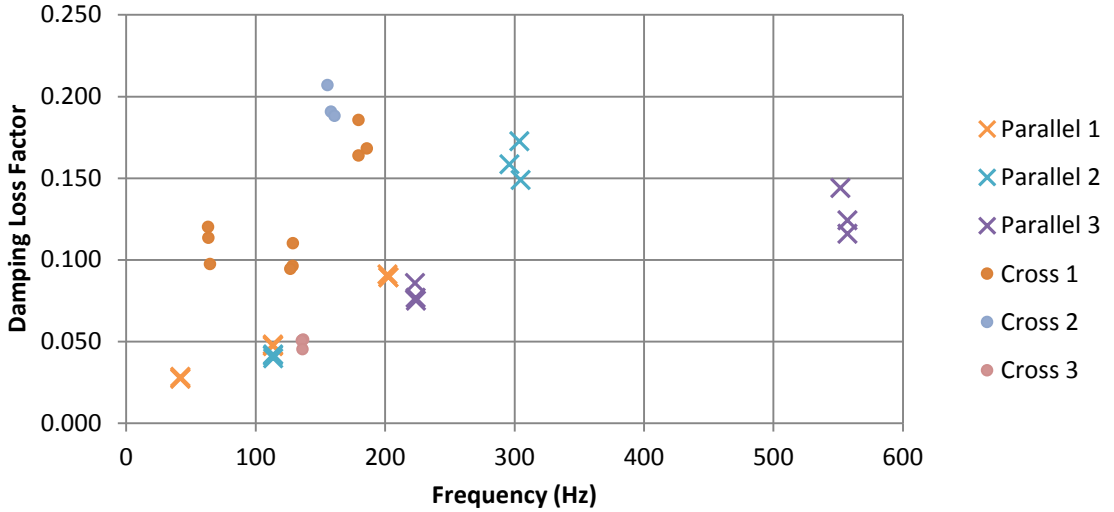

Figure 8.24: Damping loss factor of the damped plywood

The effective damping loss factor is significantly higher than the equivalent untreated plywood panel in the all of the samples tested. The geometric mean of the damping loss factor of the untreated plywood was 0.017, whereas the treated plywood had an average damping loss factor of 0.101. The measured stiffness values are very close for both the treated and untreated plywood panels. In both samples the stiffness of the plywood was observed to have a significant frequency dependence.

Figure 8.25 shows the difference in the sound transmission loss between a single leaf of un-damped 12 mm plywood and a single leaf of 12 mm damped plywood. The transmission loss of the damped plywood is somewhat higher across most of the frequency range between 100 Hz and 5000 Hz. Of specific interest is the apparent disappearance of the coincidence dip around the 1600 Hz

one-third octave frequency range. This has a reasonably large effect on the STC and Rw ratings, with an increase of two STC points and two R_w points.

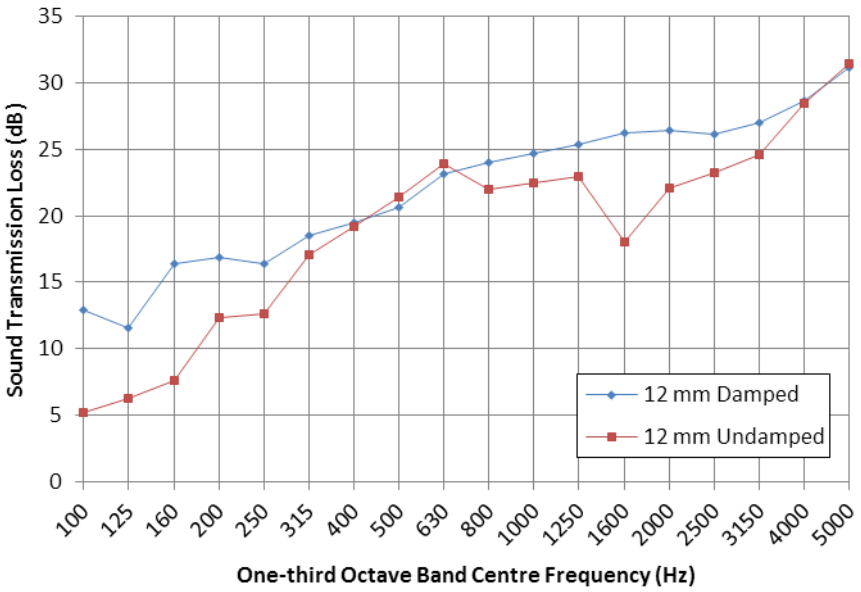

Figure 8.25: Sound transmission loss of damped and un-damped 12 mm single leaf plywood partitions

The transmission loss of a damped double leaf partition is compared to the equivalent un-damped double leaf partition in Figure 8.26. The damped sample has a higher transmission loss at all frequencies between 160 Hz and 5000 Hz. It was predicted that the addition of damping material would have a large effect on the sound transmission loss, due to the increased damping reducing the effectiveness of the structure borne vibrations. The increased damping reduces the influence of the coincidence region, this caused the improved sound transmission loss at high frequencies. The inclusion of the damping material results in an increase of four STC and R_w points.

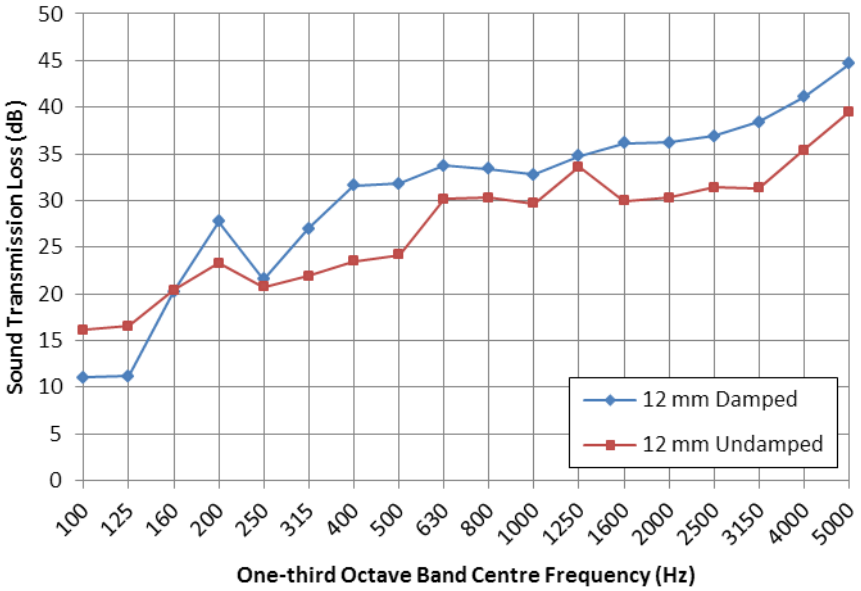

Figure 8.26: Sound transmission loss of damped and un-damped 12 mm double leaf plywood partitions

The damped panels are modelled using the new prediction method developed in the following section. The results presented here clearly show that the incorporation of the constrained viscoelastic damping layer results in a significant improvement in the sound transmission loss performance of the plywood. The combination of both the orthotropic stiffness and the increased damping loss factor result in an almost non-existent coincidence dip.

9. Prediction of Sound Transmission Loss of Orthotropic Materials

The development of several analytical models for the prediction of the sound transmission loss of orthotropic finite panels is presented. These prediction methods are compared to measured data and existing models. The finite sample size was accounted for using an expression for the radiation for a finite panel. The influence of variable material properties was also incorporated in the model.

9.1. Introduction

This section presents the development and evaluation of a prediction method for the prediction of the sound transmission loss of systems constructed from orthotropic materials. The work presented in Section 2.5 is expanded and the performance of the prediction models is evaluated and examined. The resulting prediction methods are expanded to allow the transmission loss behaviour of a simplified double leaf partition to be predicted.

As discussed in Section 2 most of the existing methods for the prediction of sound transmission loss assume the materials are isotropic in nature. This field of research is very well developed, but still lacks an effective universal prediction method as highlighted by Hongisto [93]. There has been a comparatively limited amount of research on systems constructed from orthotropic materials. The effects of orthotropic material properties on the transmission loss are qualitatively understood but a more detailed understanding is lacking. The research presented in this section (and the rest of this thesis) aims to improve the level of understanding of the influence of the behaviour of orthotropic materials on the sound transmission loss of single and double leaf partitions.

The existing models for the prediction of orthotropic sound transmission loss are focussed on very highly orthotropic materials, such as Hansen's [120, 121] prediction method for the transmission loss of corrugated sheets. These highly orthotropic materials have hard stiffness values that can be upwards of ten times the soft stiffness values. The plywood stiffness is less orthotropic, with hard stiffness values that are typically 2 to 10 times the soft stiffness values. This smaller variation between the two stiffness values compromised the use of existing prediction methods designed for higher variations. Highly orthotropic materials have two coincidence frequencies (Equation 2.71) which are relatively distinct. The less orthotropic materials considered in this thesis have two coincidence frequencies that are relatively close, resulting in a wide coincidence region that is generally poorly predicted.

The sound transmission loss was initially predicted with existing isotropic and orthotropic methods, utilising the measured material properties presented in Section 3. The results of these predictions are presented in Section 9.2. The predicted sound transmission loss values were compared to the measurements presented in Sections 5 and 6.

Section 9.3 describes the development of a model for the transmission loss of a finite orthotropic panel. This derivation is based on the model developed by Lyon and Ordubadi [122] which was presented in Section 2.5.1. This is combined with a number of expressions for the finite panel radiation impedance to develop a model for the transmission loss of a finite orthotropic panel. These models are used to predict the sound transmission loss of the materials measured in this research, using the measured material properties.

A further modification is made to the prediction methods via the inclusion of a frequency dependent stiffness value. This was undertaken to account for the frequency dependent stiffness values identified in Section 3. The frequency dependent stiffness was incorporated into the transmission loss model in an effort to better approximate the transmission loss, especially around the coincidence frequency. The results of these models are compared with the measured transmission loss values in Sections 5 and 6.

9.2. Existing Models

9.2.1. Isotropic Model

The sound transmission loss of single leaf plywood partitions was modelled using the prediction method presented by Davy [77]. This model assumes that the materials are orthotropic. The geometric mean of the stiffness properties presented in Appendix 0 was used in the calculations presented in this section. This provided a basis for alterations to the sound transmission loss predictions to be compared to. It was expected that the high and low frequency behaviour of the samples would be modelled with reasonable accuracy. It was also expected that the predicted coincidence region would be significantly narrower and deeper than measured.

The measured sound transmission loss of a 7 mm plywood partition is compared to the predicted isotropic sound transmission loss in Figure 9.1. The behaviour below the coincidence region is reasonably well modelled, although the transmission loss of the large sample is under-predicted throughout this entire region. A significant divergence occurs just below the coincidence region, where the modelled results predict a much deeper and narrower coincidence region. The predicted coincidence region was also predicted to occur two-thirds of an octave below the measured results. Some convergence is seen above the coincidence region.

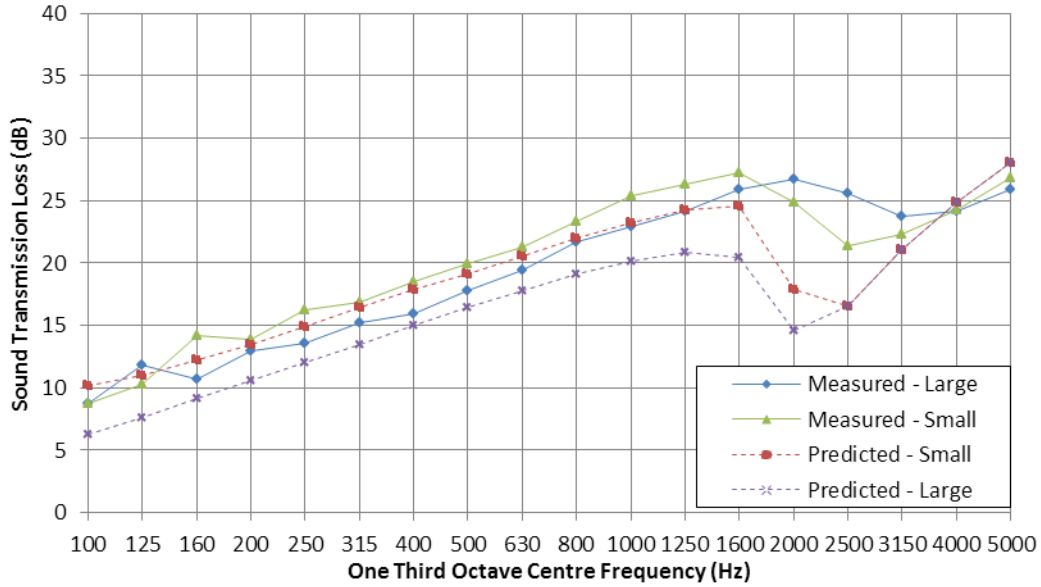

Figure 9.1: Comparison between measured transmission loss of 7 mm plywood samples and Davy's 2009 isotropic model

The prediction of a 9 mm plywood partition is presented in Figure 9.2. The frequency range below the coincidence region is modelled well for both the small and large test samples. As with the 7 mm sample the coincidence region is predicted to be significantly narrower and deeper than measured. Above the coincidence region some convergence between the predicted and measured results is observed.

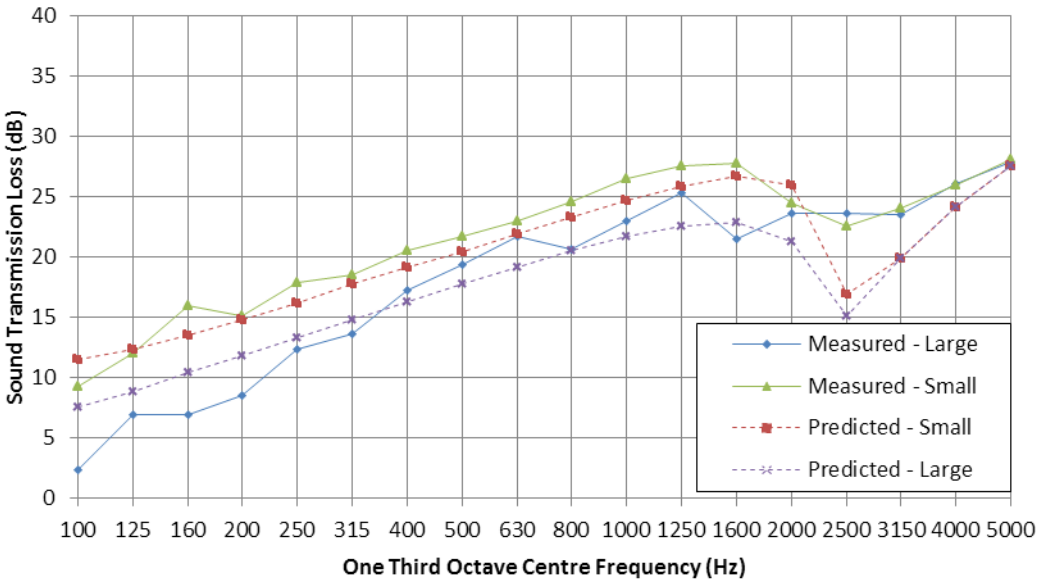

Figure 9.2: Comparison between measured transmission loss of 9 mm plywood samples and Davy's 2009 isotropic model

Similar trends were seen between the predicted and measured sound transmission loss of a 12 mm plywood sample (Figure 9.3). There was good agreement above the coincidence region, although the modelled data under-predicted the measured results by 2-3 decibels. The location of the coincidence region was reasonably well predicted. As expected the predicted coincidence "dip"

was much narrower and deeper than measured. The low frequency prediction of the large sample was reasonably good, but the small sample was under-predicted throughout the measured frequency range.

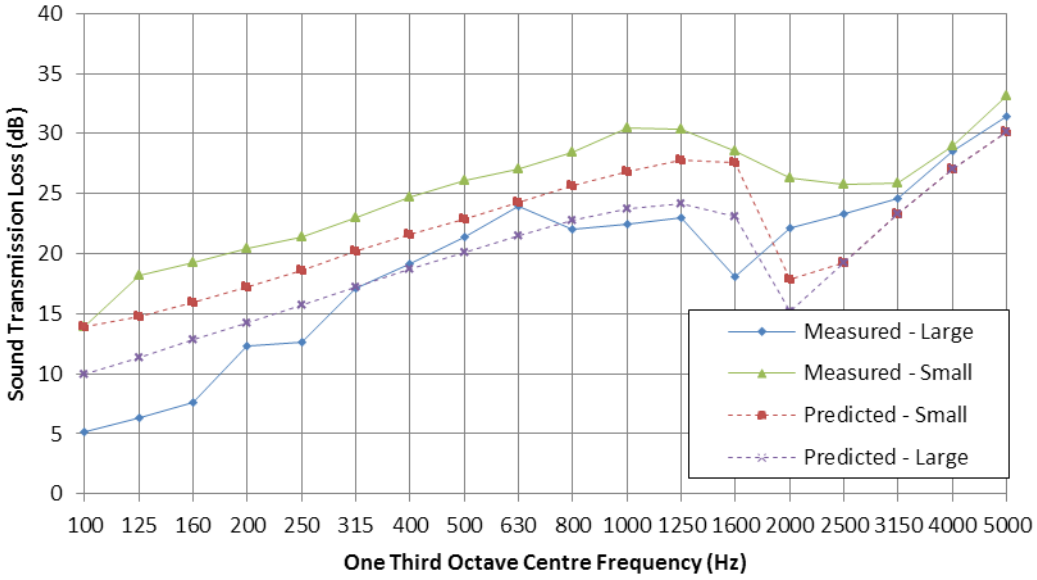

Figure 9.3: Comparison between measured transmission loss of 12 mm plywood samples and Davy's 2009 isotropic model

The sound transmission loss of a 21 mm plywood panel was predicted using the isotropic model and the results of the predictions are presented in Figure 9.4. The high frequency behaviour of the small sample was predicted with high accuracy, and the large sample was over-predicted by two to four decibels. The coincidence behaviour was very poorly predicted, occurring at a higher frequency and being significantly deeper and narrower than the measured results. Some of the low frequency behaviour of the small sample was predicted reasonably well. The large sample was over-predicted by 2-5 decibels throughout the low frequency range measured.

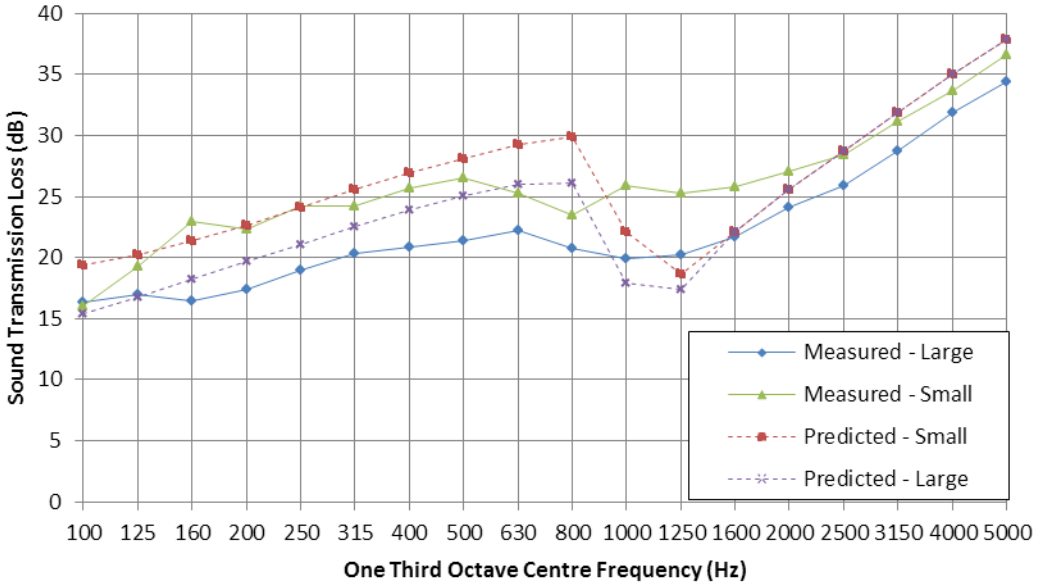

Figure 9.4: Comparison between measured transmission loss of 21 mm plywood samples and Davy's 2009 isotropic model

Overall the prediction method achieved a reasonable agreement with a number of the measured samples. In all cases the coincidence region was poorly modelled; and was predicted to be significantly narrower and deeper than measured. The high frequency behaviour was predicted to exhibit more convergence between the two sample sizes than was observed from the measurements. The prediction method both over-predicted and under-predicted the low frequency behaviour of both the small and large samples, despite this the predicted trends were similar to what was measured.

The poor agreement within the coincidence region is attributed to the assumption of an isotropic, frequency independent stiffness. The isotropic stiffness will result in a single critical frequency, unlike orthotropic materials which have a range of critical frequencies due to the orthotropic stiffness behaviour. The orthotropic behaviour means that at each azimuthal angle a different coincidence frequency, this range of coincidence frequencies is bounded by that predicted for the hard and soft stiffness values. The assumption that the stiffness of the material is frequency independent also narrows the coincidence region, as the frequency dependent stiffness causes the transmission loss behaviour to be spread over a wider frequency range. The following sections study the inclusion of these parameters into an analytical prediction method.

9.2.2. Ordubadi and Lyon's Orthotropic Model

The first orthotropic model discussed was presented in Section 2.5.1. This model was developed by Ordubadi and Lyon [122]. The model does not have an analytical solution to the integration of the transmission coefficient. The integration was performed in Matlab using the adaptive integration

"*integral2*" function. The integration was initially performed using the material properties from Ordubadi and Lyon's original paper, given in Table 9.1.

Table 9.1: Material properties used by Lyon

Property	1/4 Inch Plywood	3/8 Inch Plywood	1/2 Inch Plywood
h (mm)	6.35	9.525	12.7
ρ_s (kg/m^2)	3.81	5.175	7.62
E_x (MPa)	1.0534	5.0508	2.7649
E_y (MPa)	6.4817	6.4288	5.6280
E_{xy} (MPa)	2.9555	5.6991	3.9556
η	0.028	0.028	0.028
ν	0.3	0.3	0.3

These material properties allowed the transmission loss to be calculated, these calculated values were compared to the calculated values presented by Ordubadi and Lyon. The calculated transmission loss values were only presented in a graph in the original manuscript, as such these values were read off the graph with limited accuracy. The approximate sound transmission loss values from Ordubadi and Lyon's paper are presented in Table 9.2.

Table 9.2: Sound transmission loss values presented by Lyon

Property	1/4 Inch Plywood	3/8 Inch Plywood	1/2 Inch Plywood
250 Hz	10 dB	12 dB	15 dB
500 Hz	16 dB	18 dB	21 dB
1000 Hz	26 dB	24 dB	22 dB
2000 Hz	27 dB	19 dB	22 dB
4000 Hz	25 dB	35 dB	39 dB

Figure 9.5 presents the calculated transmission loss compared with the values listed in Table 9.2. The location of the coincidence region is relatively consistent between the calculated values and Ordubadi and Lyon's graphical data. There is some discrepancy between the values calculated and those presented in the original paper. This was because the original paper did not specify the limiting angle of incidence that was used for the numerical calculations. This angle of incidence has a significant effect on the predicted sound transmission loss as it alters the amount of waves incident at grazing angles of incidence.

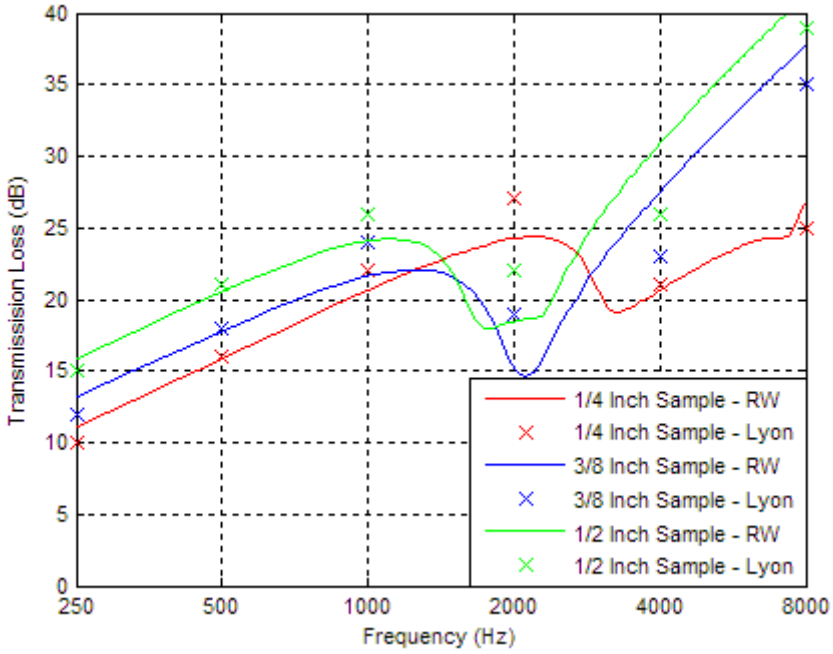

Figure 9.5: Comparison between calculated transmission loss (RW) and values from Ordubadi and Lyon's manuscript (LYON)

A number of different limiting angles of incidence were applied to the numerical integration of the model. The integration limits utilised to generate the predicted sound transmission loss curves presented in Figure 9.5 are given in Table 9.3.

Table 9.3: Limits of integration used in calculating comparative measurements to Ordubadi and Lyon's data

Angle of Incidence: θ_{lim}	90° (π/2 rad)
Azimuthal Angle: ϕ_{lim}	90° (π/2 rad)

The variations seen between the data presented in the original paper and the values calculated here may also be due to inaccuracies in measuring the data off the original graph which had relatively low resolution. The correlation is close and can be improved by making small adjustments to the angle of incidence. If the integration limit to the angle of incidence was reduced by five degrees to 85, significantly better agreement was seen. The effect of the altered angle of incidence is shown in Figure 9.6.

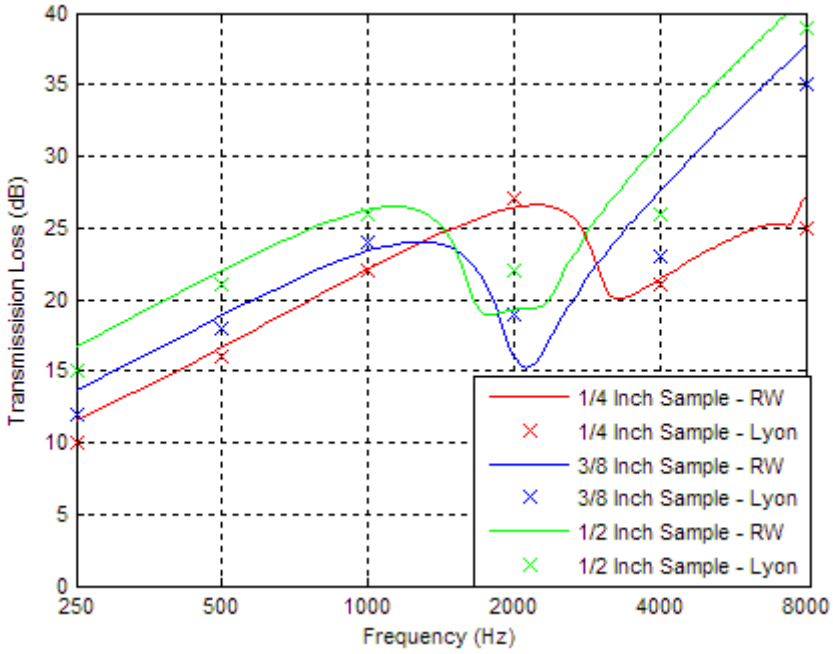

Figure 9.6: Comparison between calculated transmission loss (RW) and values from Ordubadi and Lyon's manuscript (LYON)

The model developed by Lyon was then compared with the measured plywood sound transmission loss values. The calculated transmission loss for each plywood thickness is presented in Figure 9.7. The general trends exhibited by Ordubadi and Lyon's model are similar to those of the measured samples. All these predictions were performed using a maximum angle of incidence of 85°.

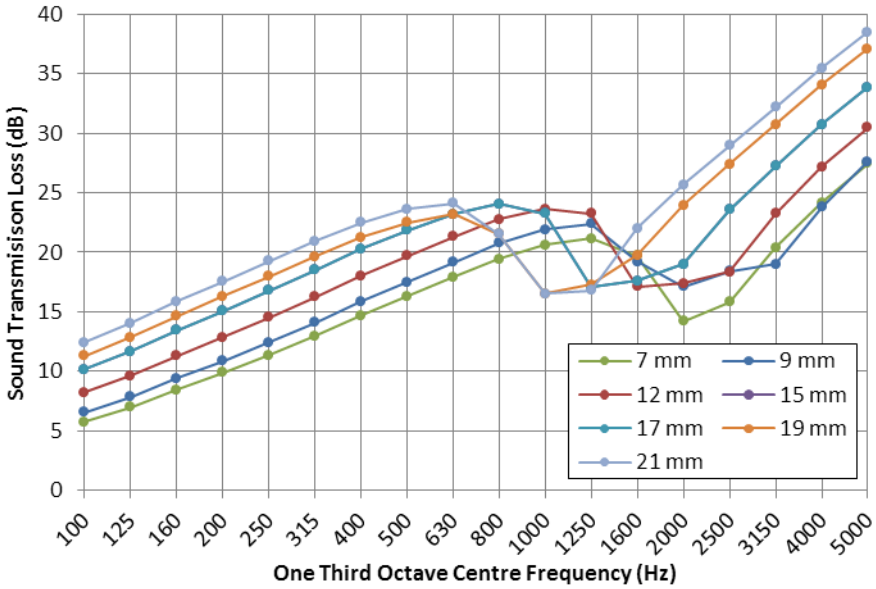

Figure 9.7: Ordubadi and Lyon's calculated sound transmission loss for measured plywood samples

The predicted data is compared with the measured plywood data for four single leaf plywood samples in Figure 9.8 - Figure 9.11.The transmission loss of both the small and large samples are presented to assess the model's ability to predict finite sized panels. These initial models are presented with a maximum angle of incidence of 85°.

The transmission loss of the 7 mm plywood is modelled relatively poorly by Ordubadi and Lyon's model. This is suspected to be due to the difficulties in accurately measuring the stiffness and damping loss factor of the 7 mm plywood. The low frequency behaviour is relatively well modelled, although the predictions are approximately two decibels below the measured sound transmission loss. Once the prediction method enters the coincidence region the agreement between the predicted and measured data is very poor. This poor correlation is compounded by the prediction of a relatively narrow and deep coincidence region, which is not typical for the sound transmission loss of orthotropic materials. The prediction of the location of the coincidence region is also between one third and two thirds of an octave below the measurements. Above the coincidence region (from 3150 Hz upward) the predicted results appear to converge closely with the measured results.

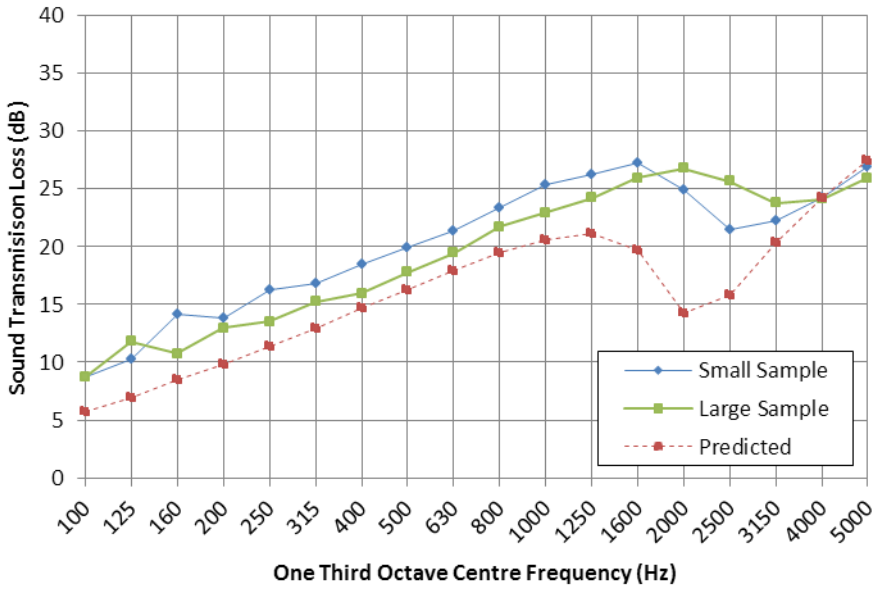

Figure 9.8: Comparison between Ordubadi and Lyon's model and the sound transmission loss of 7 mm plywood

The agreement between the large 9 mm sample and Ordubadi and Lyon's model is somewhat better than for the 7 mm sample. This may have been due to the more reliable measurements of the material properties, due to the high variability and cracking in the 7 mm samples. The location of the large samples coincidence dip was predicted reasonable well, whereas the location of the coincidence region of the small 9 mm plywood is under predicted by two thirds of an octave.

The prediction appears to converge with the measured results at 5000 Hz, but this may be transient behaviour. The high frequency limit of the measurements and calculations stops this convergence being assessed further. The low frequency behaviour is also reasonably well predicted for the large transmission loss samples. The worst agreement is seen within the coincidence region between 1600 Hz and 4000 Hz.

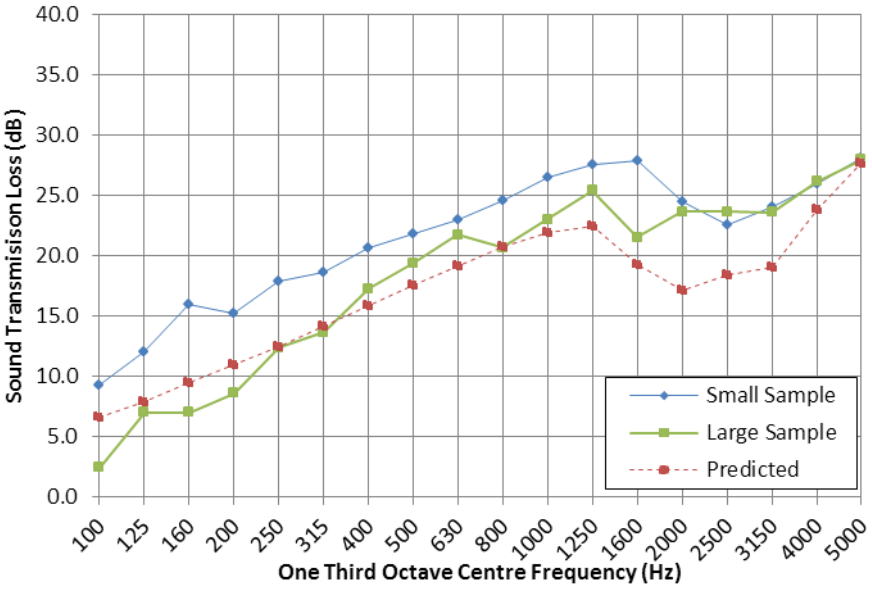

Figure 9.9: Comparison between Ordubadi and Lyon's model and the sound transmission loss of 9 mm plywood

Reasonable agreement was seen between the large 12 mm sample and Lyon's model. The coincidence region is predicted well for the large sample, but the smaller sample is under predicted. The large sample has a transmission loss curve that is steeper than Ordubadi and Lyon's modelled data. Again the prediction model appears to have a significantly deeper coincidence region than the measured data, although in this prediction it is wider than the 7 mm and 9 mm predictions. Above the coincidence region the predicted transmission loss converges closely with the measured transmission loss values for both the small and large samples.

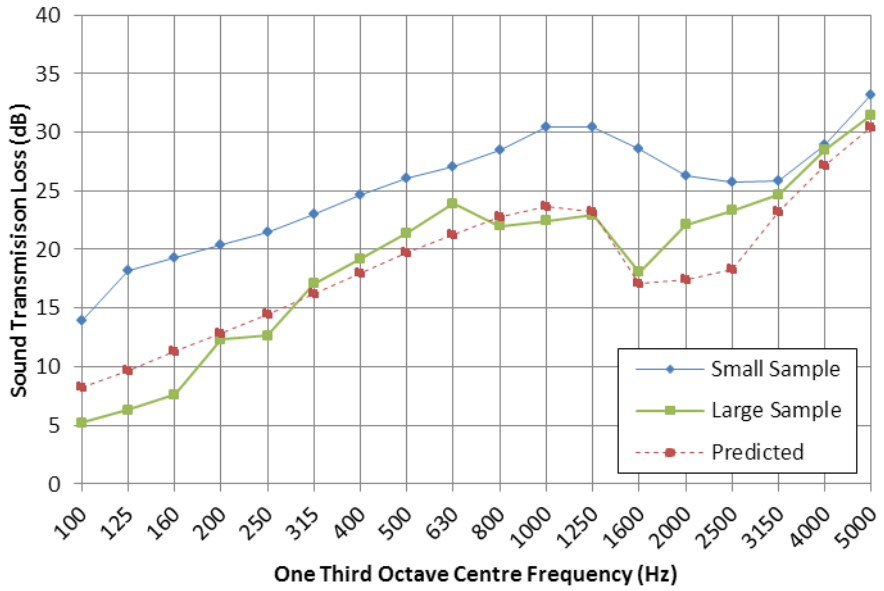

Figure 9.10: Comparison between Ordubadi and Lyon's model and the sound transmission loss of 12 mm plywood

The agreement between Ordubadi and Lyon's model and the 21 mm plywood sample is predicted with varying levels of accuracy both above and below the coincidence region. The large sample is modelled to within three decibels below the coincidence region, and above the coincidence region the both sample sizes are modelled to within two decibels. The predicted sound transmission loss above the coincidence region is parallel to both the small and large samples, indicating that the prediction error may be due to an inaccuracy in the material properties used for the prediction. The location of the coincidence region is predicted to within one third of an octave for both the small and large samples. The shape of the coincidence region is narrower and significantly deeper than that of the plywood samples.

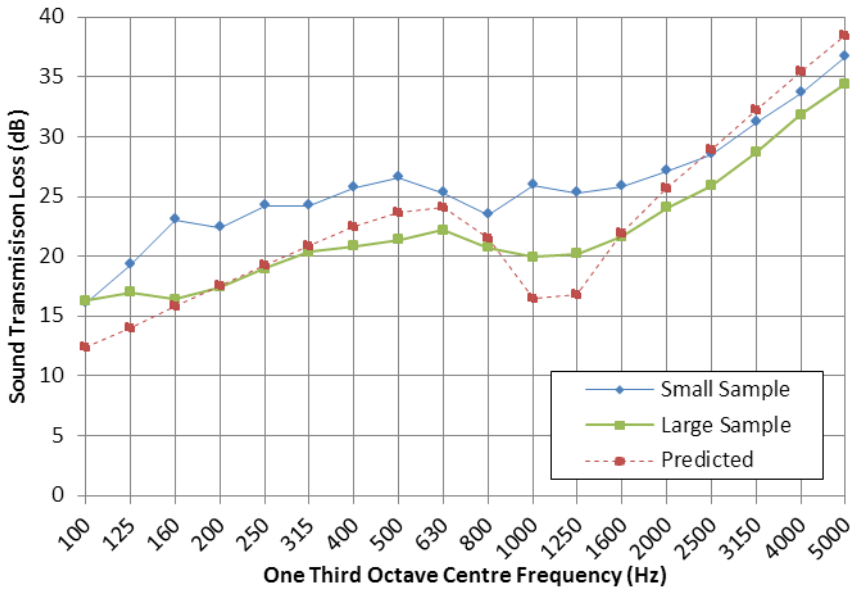

Figure 9.11: Comparison between Ordubadi and Lyon's model and the sound transmission loss of 21 mm plywood

Ordubadi and Lyon's model was shown to predict the behaviour of plywood panels with varying degrees of accuracy. The coincidence region is poorly predicted with all the predictions presented having a coincidence region that is narrower and deeper than that of the measured data.

The value of the maximum angle of incidence causes a significant variation in the predicted sound transmission loss results. The variation in predicted sound transmission loss due to variations in the maximum angle of incidence is shown in Figure 9.12. This maximum angle of incidence can be affected by the sample size and niche depth as described in Section 7.

As the maximum angle of incidence is reduced the coincidence region occurs at higher frequencies, due to the grazing angles of incidence being responsible for the lowest frequency at which the coincidence criterion is met. This also causes the coincidence region to be shallower as the ranges of angles of incidence that are combining to cause coincidence are reduced, reducing the accumulative effects. The low frequency behaviour is typical of reduced maximum angle of incidence and is due to less forcing waves being incident on the partition's surface.

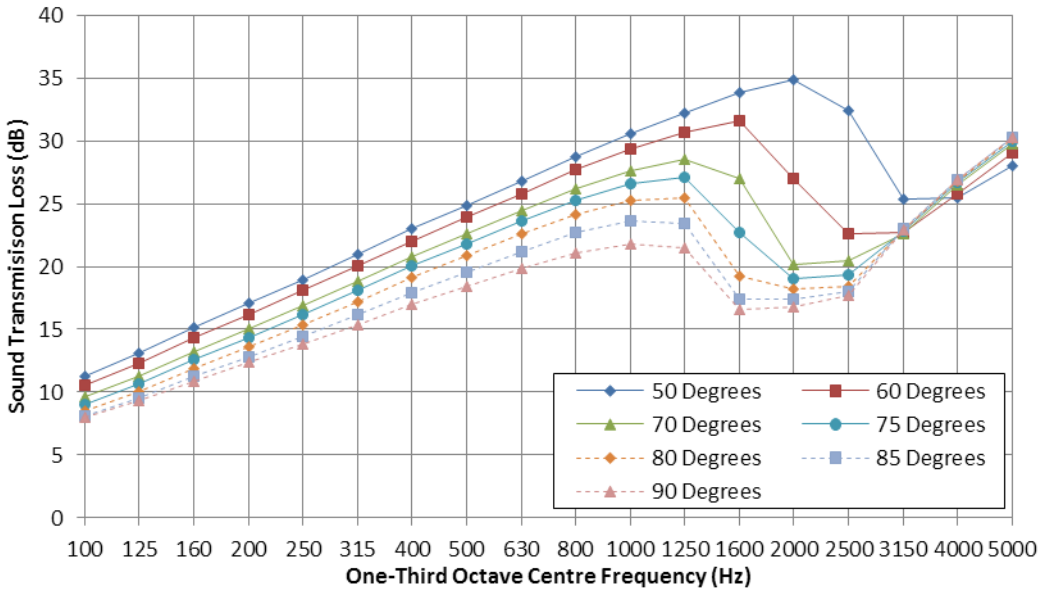

Figure 9.12: Influence of varying maximum angle of incidence on Lyon and Ordubadi's prediction model

The small transmission loss facility has a significantly lower maximum angle of incidence as a result of the sample size and the depth of the source room niche. The maximum angle of incidence was calculated to be approximately 73 degrees in the small sample and 80 degrees in the large sample. The effect of this reduced angle of incidence on the predicted sound transmission losses of 9 mm, 12 mm, and 21 mm samples are described below.

The predicted transmission losses for small and large samples of 9 mm plywood are presented in Figure 9.13. The predicted values were evaluated using Lyon and Ordubadi's model combined with a limiting angle of incidence, designed to account for the niche conditions in the transmission loss facilities. The inclusion of the limiting angle of incidence improved the performance of the prediction model for both the small and large samples. The region below the coincidence region is predicted well for the large sample, but the small sample is still significantly under-predicted in this region. The coincidence region is predicted to be deeper than the measured coincidence regions. The largest variation between the predicted and measured values for the large sample is approximately five decibels.

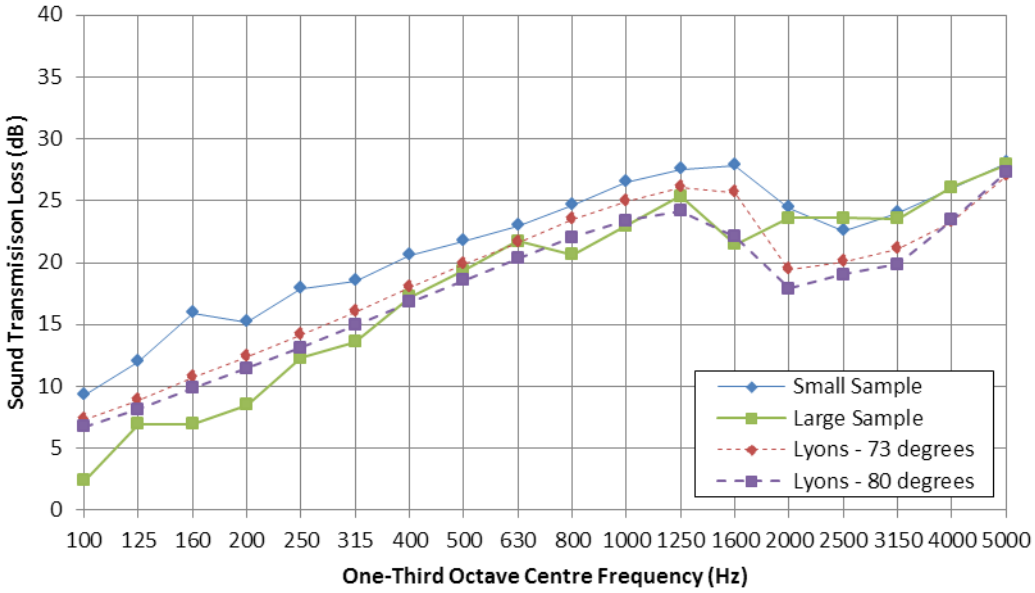

Figure 9.13: Lyon and Ordubadi's prediction (Lyons) for 9 mm plywood, with maximum angle of incidence adjusted for sample size

Figure 9.14 compares the measured and predicted sound transmission loss of a 12 mm plywood panel. The reduced maximum angle of incidence provides somewhat better agreement for both the small and large samples; although the small sample is again largely under predicted. The prediction of the coincidence region is slightly better, although the coincidence region is still significantly deeper and wider than the measured behaviour. Above the coincidence region the predicted transmission loss converges relatively closely with the measured results.

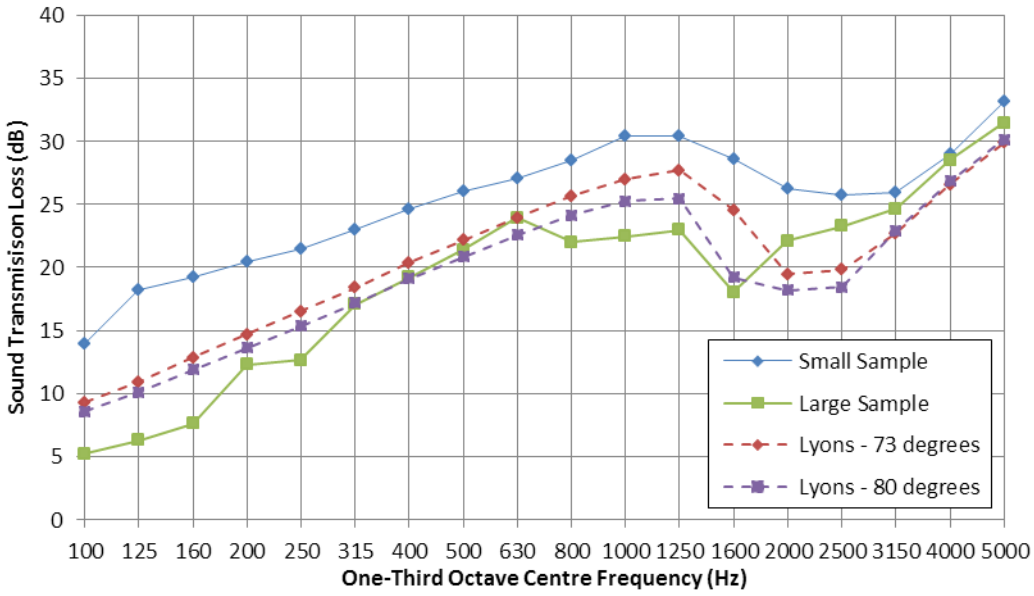

Figure 9.14: Lyon and Ordubadi's prediction (Lyons) for 12 mm plywood, with maximum angle of incidence adjusted for sample size

Similar trends are seen in the 21 mm plywood sample; as shown in Figure 9.15. The coincidence dips in both the predicted sound transmission loss curves are significantly deeper and narrower than the measured results. The predicted data deviates widely from the measured results across much of the frequency range, with a significantly higher gradient in the predicted sound transmission loss curve below the coincidence region. Above the coincidence region the predicted transmission loss is higher than both the small and large samples, but the gradient of this curve is similar to both the measured samples.

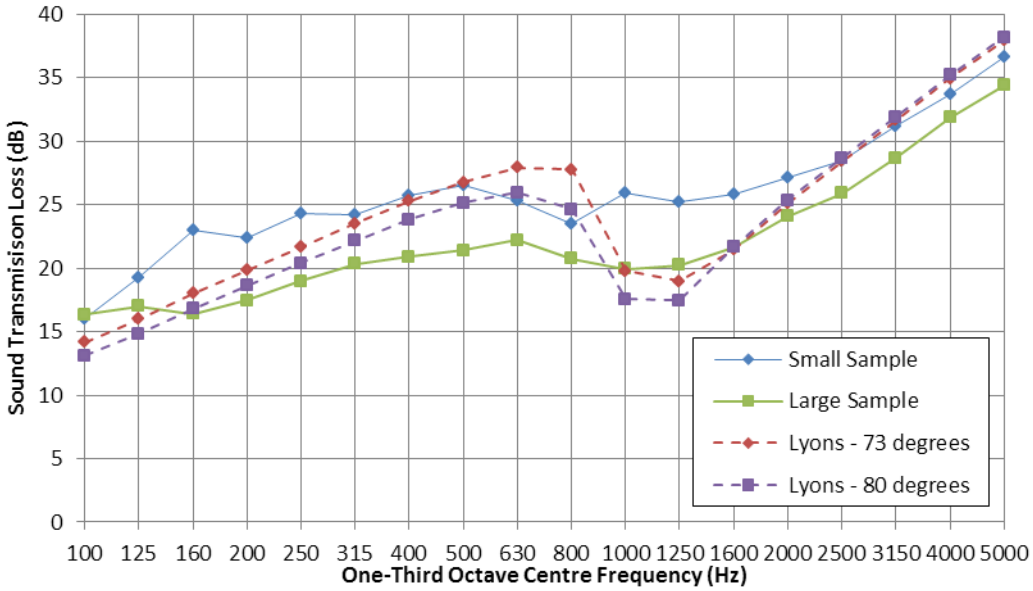

Figure 9.15: Lyon and Orbidue's prediction (Lyons) for 21 mm plywood, with maximum angle of incidence adjusted for sample size.

Some of the observed variation is probably due to the variation in material properties with frequency, and the way the smaller samples were modelled. The limit applied to the maximum angle of incidence is a relatively crude method for approximating the effect of a finite sample size. The finite panel size will significantly alter the radiation efficiency of the sample from the radiation efficiency of an infinite panel. The following section explores the influence of incorporating an expression for the finite panel radiation efficiency into the prediction model.

The finite sample introduces numerous other effects including; boundary effects, modal behaviour, and it also alters the influence of the niche conditions. These effects compound with the reduction in maximum angle of incidence used above. The variation in bending stiffness with excitation frequency (as shown in Section 3) further alters the actual transmission loss; reducing the accuracy of the orthotropic prediction methods. Some of these factors are incorporated in the model presented in the following Section. These changes improve the agreement between the measured and predicted transmission losses for samples of various sizes.

9.3. Finite Orthotropic Model

9.3.1. Finite Panel Radiation Impedance Prediction

The prediction method presented by Ordubadi and Lyon is modified and incorporated into a model that can account for a finite panel size, by the introduction of an expression for the finite panel radiation impedance. An analytical expression for the finite panel radiation impedance was incorporated into the transmission coefficient, and an approximation to this radiation impedance was also implemented. The approximate model for the radiation impedance and the associated approximation was presented in several publications by Davy *et al.* [1, 6, 7]. This allowed the transmission coefficient of a finite panel to be calculated numerically. The impedance at the surface of a vibrating panel is a ratio between the pressure at the surface (p) and the normal velocity (u_n) of the panel.

$$Z_w = \frac{p}{u_n} \qquad \textbf{9.1}$$

For a plane wave incident at an angle, θ, Figure 9.16 shows the relationship between the variables described in Equation 9.1.

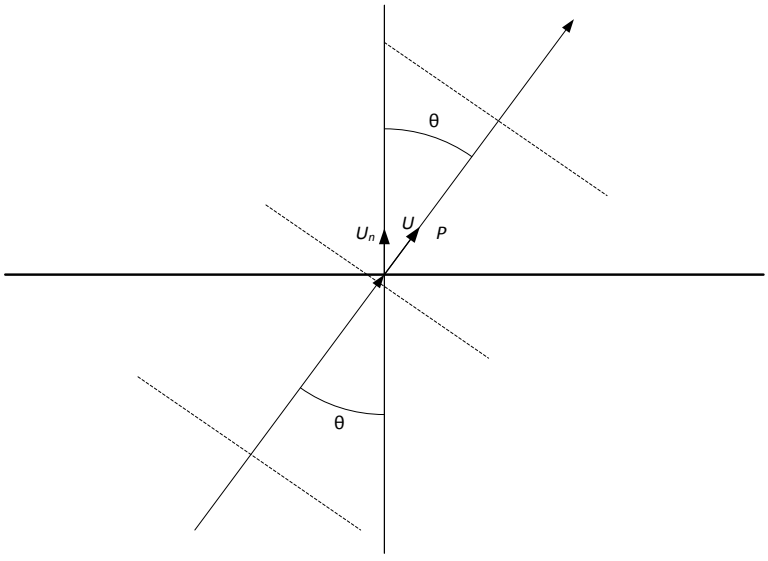

Figure 9.16: Plane wave behaviour when incident on a panel at an angle of incidence θ

This relationship allows the wave impedance to be expressed in terms of the pressure, p, and particle velocity of the incident wave, u, and the angle of incidence; as shown by Equation 9.2.

$$Z_w = \frac{p}{u\cos\theta} \quad \textbf{9.2}$$

In the case of an infinite isotropic panel the ratio of pressure to particle velocity is given by Equation 9.3.

$$\frac{p}{u} = \rho_0 c_0 \quad \textbf{9.3}$$

where ρ_0 is the density of air and c_0 is the speed of sound in air. This allows the plane wave impedance of an infinite, isotropic panel to be expressed as Equation 9.4.

$$Z_w = \frac{\rho_0 c_0}{\cos\theta} \quad \textbf{9.4}$$

The radiation impedance for a finite panel mounted in an infinite baffle is derived. The radiation impedance can be incorporated into the expression for the transmission coefficient (τ), accounting for the finite panel behaviour.

$$\tau = \frac{Z_p}{Z_w} \quad \textbf{9.5}$$

A surface, S, mounted in an infinite baffle has a transverse wave velocity that can be expressed as Equation 9.6.

$$u(\boldsymbol{r}_0) = u_0 e^{-i\boldsymbol{k_b}\cdot\boldsymbol{r_0}} \quad \textbf{9.6}$$

where $\boldsymbol{k_b}$ is the wave number vector of the incoming plane wave (Equation 9.8), u_0 is the amplitude of the transverse wave propagating in the plate and $\boldsymbol{r_0}$ is a location on the surface.

$$\boldsymbol{r_0} = (x_0, y_0, z_0) \quad \textbf{9.7}$$

$$\boldsymbol{k_b} = \left(k_x, k_y, 0\right) \quad \textbf{9.8}$$

$$\boldsymbol{r} = (x, y, z) \quad \textbf{9.9}$$

The bending wavenumber in each direction is defined by Equation 9.10.

$$k_{b(x,y,z)} = \sqrt[4]{\frac{12\rho_s\omega(1-\nu^2)}{E_{(x,y,z)}h^3}} \quad \textbf{9.10}$$

The sound pressure at a position in space, $\boldsymbol{r}$, is given by Equation 9.11.

$$p(\boldsymbol{r}) = ikZ_c \iint_S g_\omega(\boldsymbol{r}, \boldsymbol{r}_0) u(\boldsymbol{r}_0) d\boldsymbol{r}_0 \quad \textbf{9.11}$$

Where $g_\omega(\boldsymbol{r}, \boldsymbol{r}_0)$ is the Green's function [184] for a point source on an infinite rigid baffle which is given by Equation 9.12.

$$g_\omega(\boldsymbol{r}, \boldsymbol{r_0}) = \frac{e^{-ikR}}{2\pi R} \quad \textbf{9.12}$$

R is the difference between a location on the surface of the panel ($\boldsymbol{r}_0$) and a point in space ($\boldsymbol{r}$), given by Equation 9.13.

$$R = |\boldsymbol{r} - \boldsymbol{r_0}| = \sqrt{(x - x_0)^2 + (y - y_0)^2 + (z - z_0)^2} \quad \textbf{9.13}$$

Thus the normalised specific wave impedance at a point on the surface can be expressed as:

$$Z_w(\boldsymbol{r}) = \frac{p(\boldsymbol{r})}{Z_c u(\boldsymbol{r})} = ik \iint_S g_\omega(\boldsymbol{r}, \boldsymbol{r_0}) e^{-i\boldsymbol{k_b}\cdot(\boldsymbol{r}-\boldsymbol{r_0})} d\boldsymbol{r_0} \quad \textbf{9.14}$$

This double integral is the result of averaging the pressure contributions of all the points across the surface of the panel. To calculate the average normalised specific acoustic wave impedance the value of the point impedance is then averaged across the surface of the panel, resulting in Equation 9.15. This was evaluated numerically in a publication by Thomasson [129], the values of this evaluation are used for comparison with the values calculated in this section.

$$Z_w = \frac{ik}{S} \iint_S \iint_S g_\omega(\boldsymbol{r}, \boldsymbol{r_0}) e^{-i\boldsymbol{k_b}\cdot(\boldsymbol{r}-\boldsymbol{r_0})} d\boldsymbol{r} d\boldsymbol{r_0} \quad \textbf{9.15}$$

where S is the surface of the panel being integrated across.

This quadruple integral would incur significant computational costs when incorporated into the transmission coefficient as this results in a sextuple integral. In order to reduce the computational effort required to evaluate the transmission coefficient the reduction presented by Li and Gibeling [130] is utilised. This reduction requires that the surface is a rectangle defined by Equation 9.16.

$$|x| \leq l_x, |y| \leq l_y, z = 0 \quad \textbf{9.16}$$

The reduction yields Equation 9.17, which is equivalent to Equation 9.15 via the coordinate transformation variables κ and ς given by Equations 9.18 and 9.19.

$$Z_\omega = \frac{ik}{2\pi l_x l_y}\int_0^{2l_y}\int_0^{2l_x}\cos(k_x\kappa)\cos(k_y\varsigma)\frac{e^{-ik\sqrt{\kappa^2+\varsigma^2}}}{\sqrt{\kappa^2+\varsigma^2}}(2l_y-\kappa)(2l_x-\varsigma)d\kappa d\varsigma \quad \textbf{9.17}$$

$$\kappa = x - x' \quad \textbf{9.18}$$

$$\varsigma = y - y' \quad \textbf{9.19}$$

Other methods exist for the reduction of the radiation impedance but this form was found to be relatively stable for numerical integration. A singularity exists at $\kappa = \varsigma = 0$ but modern automatic adaptive numerical integration methods appear to handle this singularity reasonably well. The diffuse field transmission coefficient for an orthotropic panel, considering the effect of the finite panel radiation impedance can be expressed as:

$$\tau_d = \frac{2}{\pi}\int_0^{\frac{\pi}{2}}\int_0^{1}\left|\frac{d(\sin^2\theta)d\phi}{1+\frac{\frac{\{D'(\phi){k_p}^4-\rho_s\omega^2\}}{j\omega}}{2\frac{ik}{2\pi ab}\int_0^{2l_y}\int_0^{2l_x}\cos(k_x\kappa)\cos(k_y\varsigma)\frac{e^{-ik\sqrt{\kappa^2+\varsigma^2}}}{\sqrt{\kappa^2+\varsigma^2}}(2a-\kappa)(2b-\varsigma)d\kappa d\varsigma}}\right| \quad \textbf{9.20}$$

This fourth order integral does not admit an analytical solution but it can be solved using numerical methods. Due to the complexity of solving this entire integral the behaviour of the integrand within the expression for the radiation efficiency was investigated. This analysis was designed to develop an understanding on the integral and assess the limitations of the numerical integration routines used.

The real and imaginary components of the integrand in Equation 9.17 were calculated at different wavenumbers. Figure 9.17 presents the imaginary component of the integrand at $k = k_x = k_y = 1$, and Figure 9.18 presents the real component of the integrand at the same wavenumber.

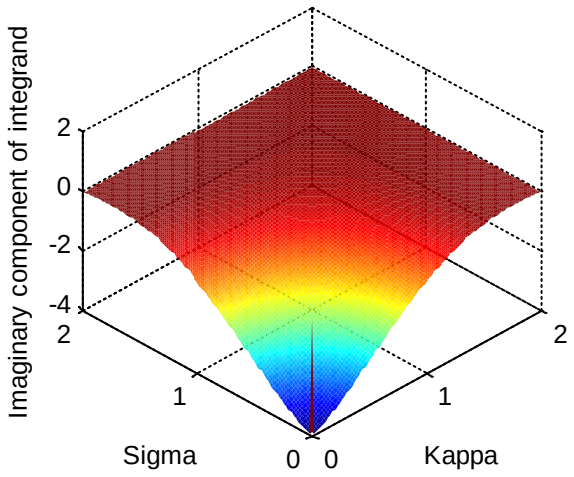

Figure 9.17: Imaginary component of the integrand in Equation 9.17 at $\boldsymbol{k = k_x = k_y = 1}$

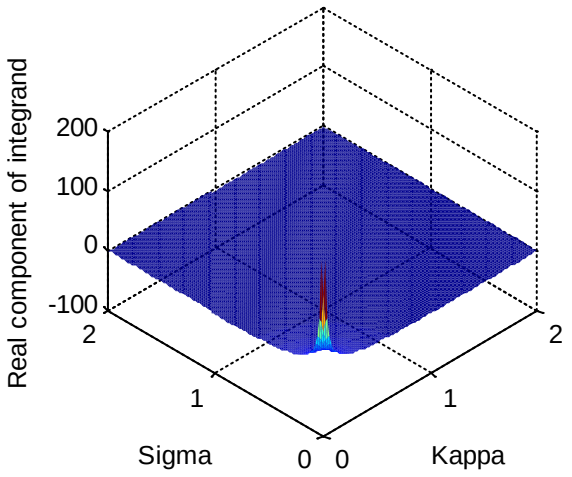

Figure 9.18: Real component of the integrand in Equation 9.17 at $\boldsymbol{k = k_x = k_y = 1}$

Figure 9.17 and Figure 9.18 demonstrate the location of the singularity at $\kappa = \varsigma = 0$, aside from this singularity the impedance equation is smooth across the integration range. This indicates that this function will be relatively efficient to integrate numerically at low frequencies.

The behaviour of the integrand at higher frequencies was assessed by calculating the same equation with $k = k_x = k_y = 100$. The results of these calculations are presented in Figure 9.19 and Figure 9.20. It is evident in these figures that the radiation impedance behaviour has become significantly more complex with the increased wavenumber. This increase in complexity will result in dramatic increases in the time required to perform numerical evaluations of Equation 9.20.

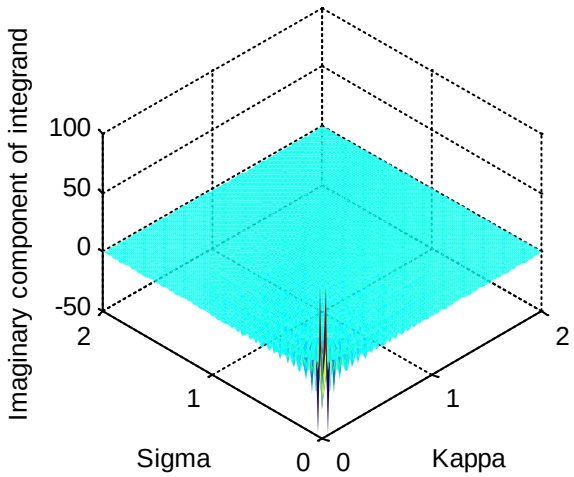

Figure 9.19: Imaginary component of the integrand in Equation 9.17 at $\boldsymbol{k = k_x = k_y = 100}$

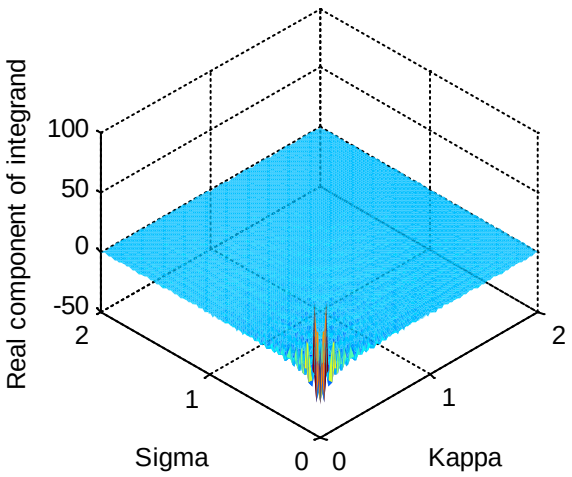

Figure 9.20: Real component of the integrand in Equation 9.17 at $\boldsymbol{k = k_x = k_y = 100}$

The time taken to evaluate the second order integral for the radiation impedance, given in Equation 9.17 was evaluated. This example utilised an edge length of one metre and evaluated the integral across a range of wavenumbers from $k = 0.1 \rightarrow 100$. The integral was evaluated using Matlab's *integral2* function. Figure 9.21 shows the variation in evaluation time with increasing wavenumber.

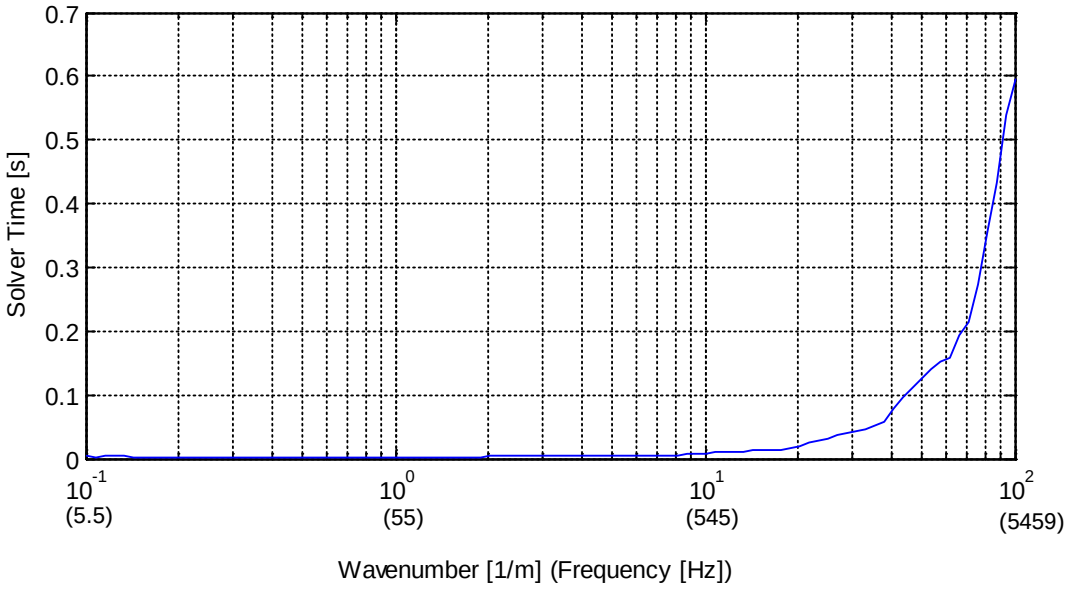

Figure 9.21: Variation in time taken to evaluate Equation 9.17 across the range: $k = 0.1 \rightarrow 100$

Figure 9.21 shows a clear and dramatic increase in the solver time required as the wavenumber is increased. The radiation impedance lies within a double integral in the transmission loss coefficient (Equation 9.20), thus increases in the time required to evaluate the radiation impedance have a very large effect on the time required to evaluate the transmission coefficient.

The difference between the radiation efficiency values calculated via a numerical integration of Equations 9.17 – 9.20 were compared with the numerically calculated values presented by Thomasson. The ratio between the real components of the two calculated radiation efficiencies is presented in Figure 9.22 and the imaginary component is presented in Figure 9.23. These were calculated for a square panel with sides $l_x = l_y = l = 1\ m$.

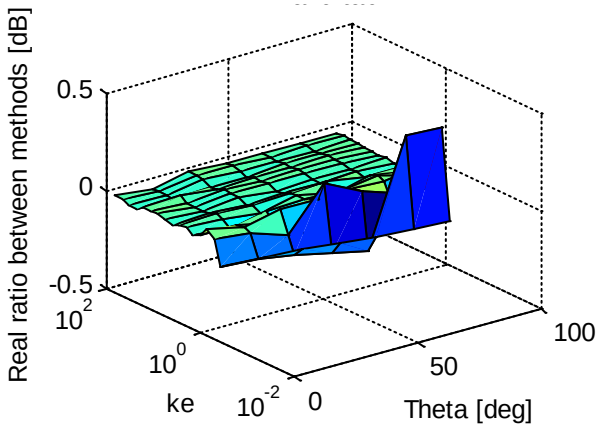

Figure 9.22: Real component of ratio between Thomasson's tabulated radiation efficiency and the radiation efficiency calculated using Li and Gibeling's formulation

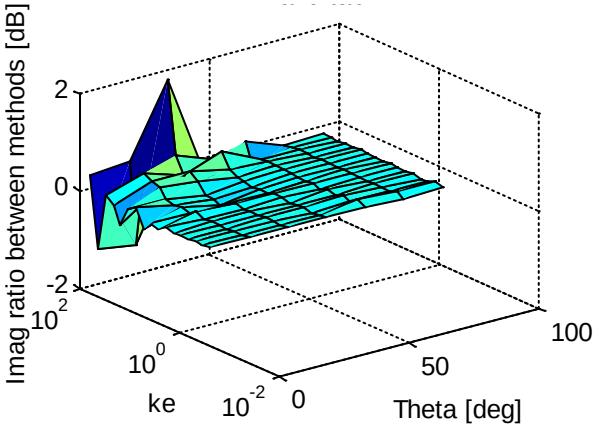

Figure 9.23: Imaginary component of ratio between Thomasson's tabulated radiation efficiency and the radiation efficiency calculated using Li and Gibeling's formulation

The variations between the both the real and imaginary components were primarily due to the rounding of Thomasson's tabulated data. The tabulated data in Thomasson's original manuscript is presented to two decimal places, whereas Matlab calculates the results to 12 decimal places. If the calculated values are rounded to the same accuracy in Matlab the correlation is very close, as shown in Figure 9.24 and Figure 9.25.

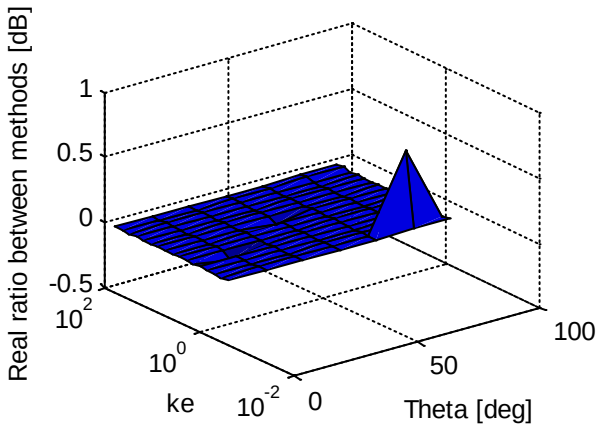

Figure 9.24: Real component of ratio between Thomasson's tabulated radiation efficiency and the radiation efficiency calculated using Li and Gibeling's formulation, rounded to 2 decimal places

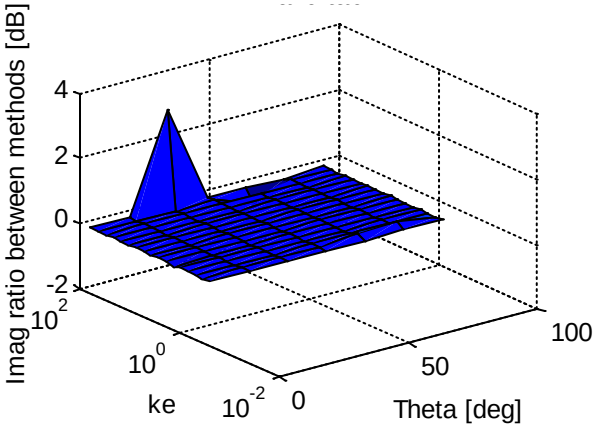

Figure 9.25: Imaginary component of ratio between Thomasson's tabulated radiation efficiency and the radiation efficiency calculated using Li and Gibeling's formulation, rounded to 2 decimal places

Some of the variations seen between the two predictions are due to the numerical integration performed in Matlab. At high frequencies convergence to the desired tolerances was not always achieved within Matlab's 10,000 iteration limit. Better convergence could be achieved by forcing Matlab's "integral2" function to use a tiled integration method.

The remaining variations are due to the method of calculation and the accuracy of the integration. Thomasson integrated the radiation efficiency across all azimuthal angles, whereas the values calculated above took a sample of 20 azimuthal angles and averaged these. This normally has little influence on the calculations, but when the absolute values are very small these differences can result in large changes in decibels especially when rounding errors are included.

A recent paper by Davy *et al.* [1] and several submitted conference articles by Davy *et al.* [6, 7] presented an approximation for the radiation coefficient that was able to dramatically reduce the time required for evaluation whilst still retaining reasonable accuracy. The real and imaginary components of the approximate radiation efficiency were calculated separately and then combined. The final form of the approximation is presented here; details of the derivation are presented in the above references.

The approximation presented combines a high frequency and low frequency approximation using Equation 9.22. The ratio (μ) between the bending wavenumber in the panel and the wavenumber of the incident sound is calculated, as shown in Equation 9.21, and is utilised to divide the prediction model into different sub-ranges.

$$\mu = \frac{k_b}{k} \qquad \textbf{9.21}$$

where k_b is the wavenumber of the bending waves in the panel, and k is the wavenumber of the incident sound.

The derivation presented below assumes that $\mu \leq 1$. The original paper also presents an approximation for calculating the finite panel radiation efficiency when $\mu > 1$, this is not presented here as the calculations performed assume forced vibrations. In Equation 9.22, Z_{ω_l} is the low frequency approximation, Z_{ω_h} is the high frequency approximation, and n is an integer that is altered depending on the value being calculated. This equation can be used to combine both the real and imaginary components of the radiation efficiency.

$$Z_\omega = \frac{1}{\sqrt[n]{{Z_{\omega_l}}^n + {Z_{\omega_h}}^n}} \qquad \textbf{9.22}$$

The low frequency, real component of the radiation efficiency ($Z_{\omega_{l:real}}$) is calculated utilising Equation 9.23, and the high frequency, real component ($Z_{\omega_{h:real}}$) is calculated using Equation 9.24. The integer, n, is set to 2 for the real component calculations. These variables are combined in Equation 9.22 to calculate the total real component of the radiation efficiency ($Z_{\omega_{real}}$).

$$Z_{\omega_{l:real}} = 2k^2\, l_x l_y/\pi \quad \textbf{9.23}$$

$$Z_{\omega_{h:real}} = \mathrm{Re}\left(\frac{1}{\sqrt{1+\left({}^{0.956}/_{ke} - i\mu\right)^2}}\right) \quad \textbf{9.24}$$

where e is the characteristic length of the panel given by Equation 9.25. Equations 9.23 and 9.24 are combined to yield Equation 9.26.

$$e = \frac{2l_x l_y}{l_x + l_y} \quad \textbf{9.25}$$

$$Z_{\omega_{real}} = \frac{1}{\sqrt[2]{{Z_{\omega_{l:real}}}^2 + {Z_{\omega_{h:real}}}^2}} \quad \textbf{9.26}$$

The imaginary component of the radiation impedance is calculated using a similar method, as described below. The low frequency component that corresponds to the real component given in Equation 9.23 ($Z_{\omega_{l:imag}}$) is calculated using Equation 9.27.

$$Z_{\omega_{l:imag}} = \frac{2k}{\pi}[\mathscr{b}H(a/\mathscr{b}) + aH(\mathscr{b}/a)] \quad \textbf{9.27}$$

where $H(x)$is given by Equation 9.28. a and $\mathscr{b}$ are the side lengths of the panel.

$$H(x) = \ln\left(\sqrt{1+x^2} + x\right) - \frac{\sqrt{1+x^2} - 1}{3x} \quad \textbf{9.28}$$

The high frequency imaginary component of the radiation impedance when the incident wave is normally incident ($Z_{\omega_{h:imag\_0}}$) is calculated using Equation 9.29.

$$Z_{\omega_{h:imag\_0}} = \frac{0.67}{ke} \quad \textbf{9.29}$$

The high frequency imaginary component for all angles of incidence ($Z_{\omega_{h:imag}}$) is calculated using Equation 9.30.

$$Z_{\omega_{h:imag}} = \mathrm{Im}\left(\frac{1}{\sqrt{1+\left({}^{0.956}/_{ke} - i\mu\right)^2}}\right) \quad \textbf{9.30}$$

The overall normal incidence component of the finite radiation efficiency ($Z_{\omega_{imag\_0}}$) is given by combining Equations 9.29 and 9.27.

$$Z_{\omega_{imag\_0}} = \frac{1}{\sqrt[3]{{Z_{\omega_{l:imag}}}^3 + {Z_{\omega_{h:imag\_0}}}^3}} \quad \textbf{9.31}$$

Finally the resulting imaginary component of the radiation impedance ($Z_{\omega_{imag}}$) is calculated using Equation 9.32.

$$Z_{\omega_{imag}} = \max\begin{Bmatrix} Z_{\omega_{h:imag}} \\ Z_{\omega_{imag\_0}} \end{Bmatrix} \quad \textbf{9.32}$$

The combination of Equation 9.26 and 9.32 yields the total finite panel radiation efficiency of the panel (Z_{ω}), given by Equation 9.33.

$$Z_{\omega} = Z_{\omega_{real}} + iZ_{\omega_{imag}} \quad \textbf{9.33}$$

The results of these approximations were shown to be reasonably close to Thomasson's tabulated data [1, 6, 7]. This model dramatically reduces the calculation time as it can be expressed analytically in Matlab, and as such does not require numerical integration. The computational requirements of this approximation are independent of the wavenumber of the incident wave (k), avoiding changes in the computational time with wavenumber. A comparison between Thomasson's data and the approximation presented in Equations 9.22 – 9.32 is show in Figure 9.26 and Figure 9.27. It is clear that the variation between the predicted and tabulated data is relatively small; with the only significant variation occurring when ke is near 2.

The variation between the two predictions of the real component of the radiation efficiency is not a consistent under prediction or over prediction. This indicates that the variations seen are a result of the approximation method utilised. The approximation attempts to model the radiation impedance as closely as possible across a wide range, resulting in variations under certain conditions. At an angle of incidence of zero degrees the largest variation occurs at $ke = 2$; the location of this maximum variation shifts to higher values of ke as the angle of incidence is increased.

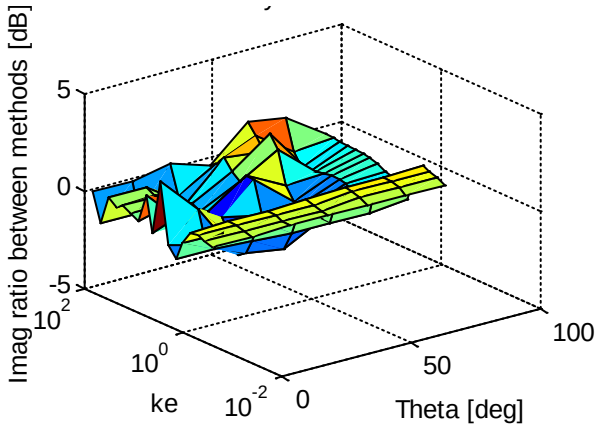

Figure 9.26: Imaginary component of the ratio between Davy's approximation and Thomasson's tabulated data

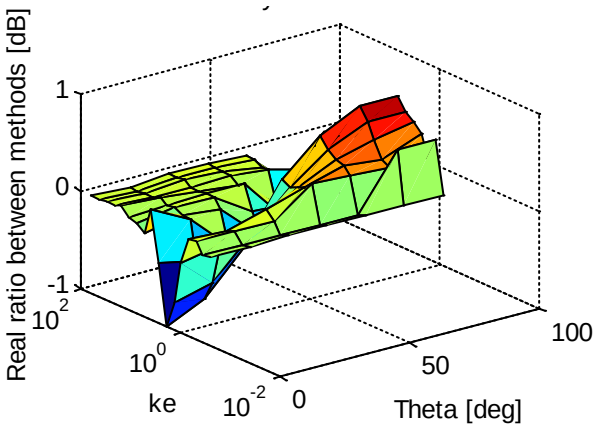

Figure 9.27: Real component of the difference between Davy's approximation and Thomasson's tabulated data

Overall the approximation achieves a representation of the radiation impedance across a wide frequency range to within three decibels. This will result in significant computational savings for the evaluation of the transmission coefficient as the radiation impedance is nested within a double integral; as such the computational requirement for the radiation impedance calculations will be significantly magnified in the overall calculations. The computational savings are summarised in Figure 9.28, the average computational time for the approximate formulation was 1.4×10^{-4} seconds.

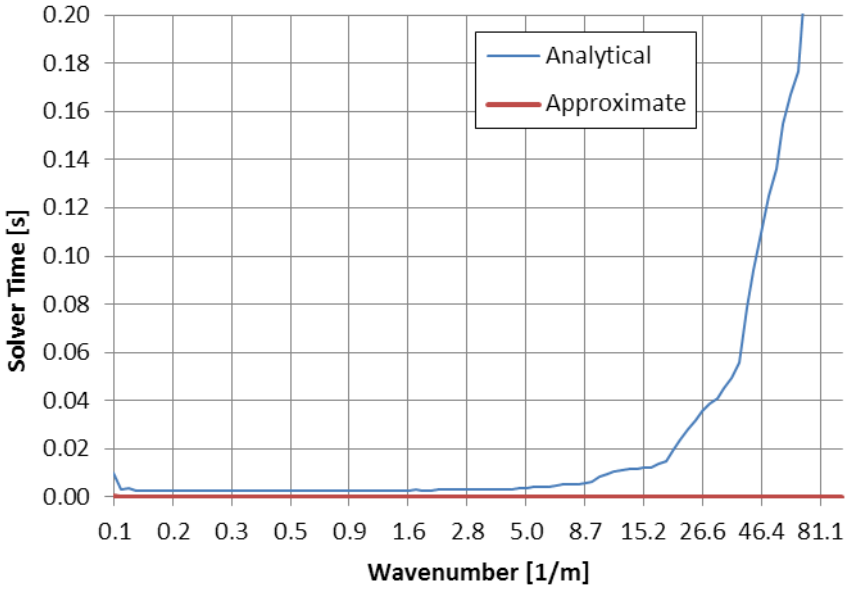

Figure 9.28: Comparison of computational times for approximate and analytical calculations of the radiation impedance

The small variations between the approximation and the analytical solution combined with the large savings in computational time justify the use of this approximation in calculations of the sound transmission loss. The differences between the transmission loss calculated using both the analytical

and approximate formulations for the radiation impedance will be presented in the following sections.

9.3.2. Orthotropic Sound Transmission Loss with Finite Panel Radiation Impedance

The transmission coefficient and the associated transmission loss were calculated using both the calculated radiation efficiencies presented above. The expression for the transmission coefficient is rewritten as Equation 9.34. The plane wave radiation impedance derived in the preceding section is inserted into this equation to develop an expression for the transmission coefficient that incorporates the finite panel radiation impedance. In both cases the plane wave bending wave impedance was set equal to that used in Ordubadi and Lyon's orthotropic model.

$$\tau_{\mathrm{d}} = \frac{2}{\pi}\int_0^{\phi_{lim}}\int_0^{\theta_{lim}} \left|1 + {Z_p}/{2Z_w}\right|^{-2} d(\sin^2\theta)d\phi \qquad \textbf{9.34}$$

The numerical solutions that utilised Li and Gebeling's formulation for the finite panel radiation efficiency required significant computational time. The computational time was affected by the frequency of the incident sound, the size of the panel and the thickness of the panel. The increases in the computational time due to the increasing frequency, increasing panel thicknesses, and increasing panel size are shown in Figure 9.29 and Figure 9.30

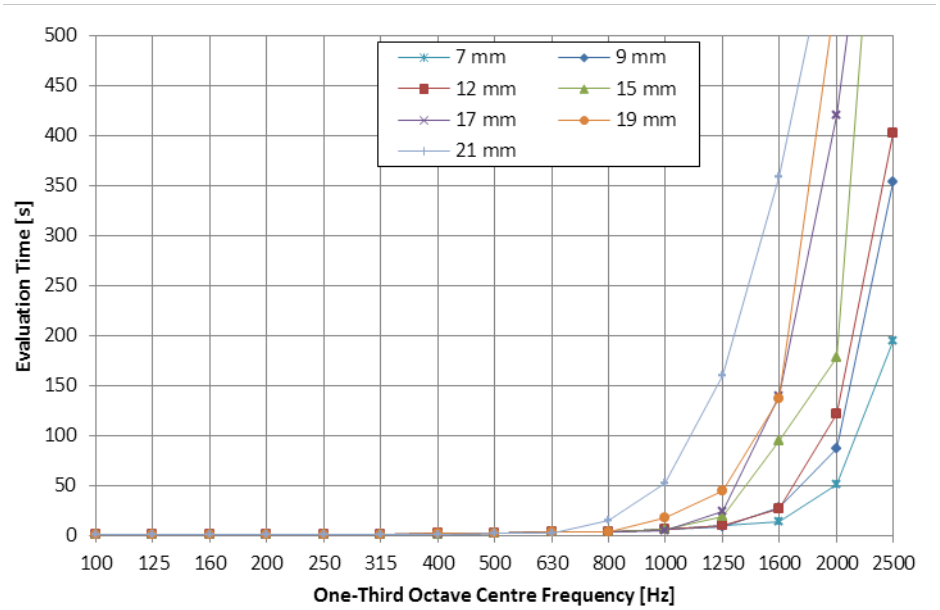

Figure 9.29: Effect of increasing frequency on computational requirements for calculation of sound transmission loss of small sample

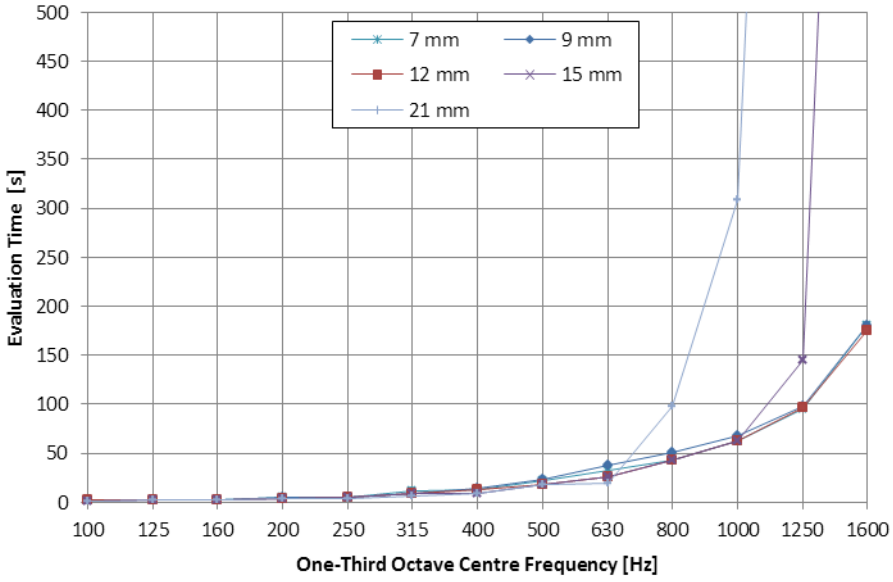

Figure 9.30: Effect of increasing frequency on computational requirements for calculation of sound transmission loss of large sample

The computational time increases in a near exponential manner as the frequency is increased. This is due to the increasing complexity of the integrand that was discussed previously. Increasing the sample size also dramatically increases the time required to integrate the integral, this is evident in the two figures presented above. The large sample was only evaluated up to 1600 Hz as the solver times increased significantly with the frequency. As the thickness of the panel increases the time required to solve the integral increases, this is especially evident as the frequency increases. This effect is predominantly due to the earlier onset of the coincidence region that occurs in the thicker samples, calculations within this region require a large increase in the computational effort.

The predicted sound transmission loss for both the small and large samples was evaluated using adaptive numerical methods. These evaluations were performed using the measured material properties presented in Section 3. The model of the small sample was calculated between 100 Hz and 3150 Hz due to the computational limitations encountered at higher frequencies. Similarly the large sample was calculated between 100 Hz and 2500 Hz again due to the computational limitations. It was found that Matlab's adaptive integration "*integral2*" function failed to converge when evaluating the large sample at frequencies greater than 2500 Hz. Convergence could be forced by significantly increasing the absolute and relative tolerances, resulting in reduced numerical accuracy. The absolute tolerance used was 1×10^{-8} and the relative tolerance was 1×10^{-4}. The maximum number of iterations performed by the integration routine was 10,000. Further improvements in the convergence could be achieved by forcing the integration routine to use a tiled integration method.

A comparison between the predicted and measured results for a 7 mm plywood panel is presented in Figure 9.31. The low frequency predictions are within three decibels, although significant variation of up to 14 decibels occurs between the predicted and measured results near the coincidence frequency. Unfortunately the high frequency behaviour cannot be assessed due to the limited frequency range of the predictions. The effect of changing the sample size shows a similar effect in both the predicted and measured results.

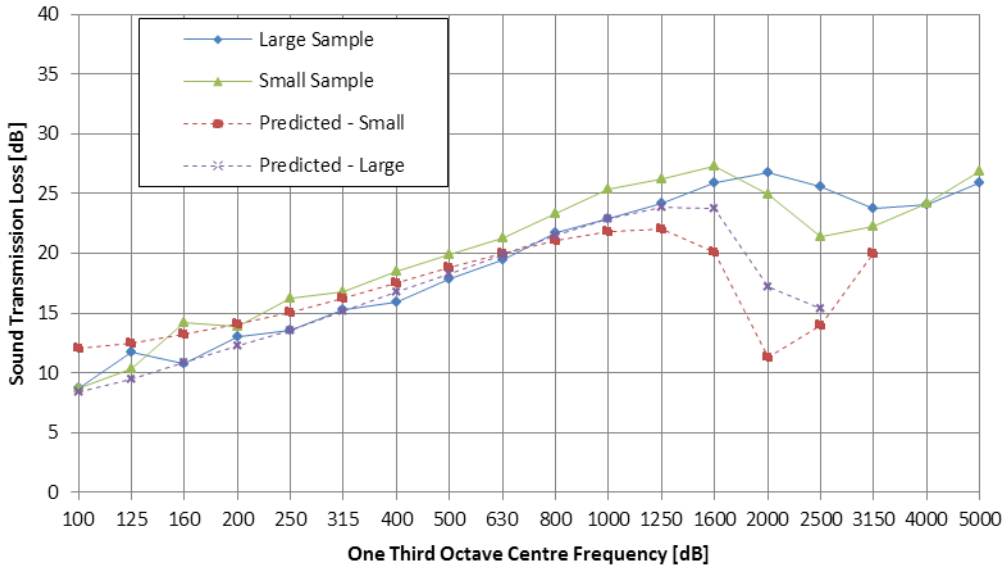

Figure 9.31: Comparison between prediction method using Li and Gebling's formulation and the sound transmission loss of 7 mm plywood

Comparisons between the predicted and measured results of 9 mm and 12 mm plywood samples are presented in Figure 9.32 and Figure 9.33. In general the low frequency behaviour is modelled somewhat better than the frequency range around the coincidence region. The best agreement is seen in the predictions of the 12 mm plywood transmission loss. This agreement is still relatively poor and is not appreciably better than the agreement seen in Lyon's results (Section 9.2.2). The integration limits were 90 degrees for both sample sizes. In all cases the coincidence region is predicted to be significantly narrower and deeper than that measured in both the sample sizes. The location of the lowest point in the coincidence region appears to shift down approximately one third of an octave between the small and large samples.

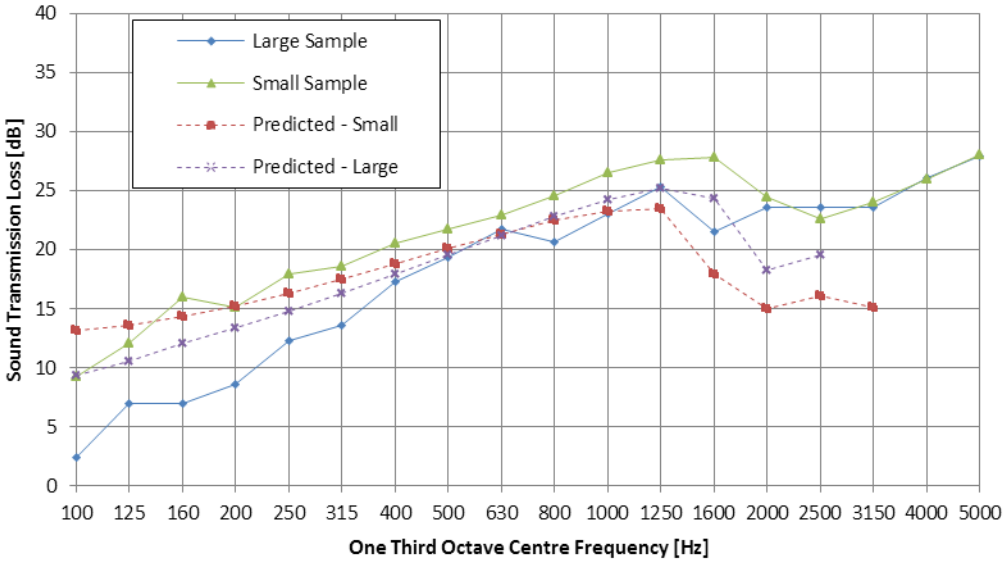

Figure 9.32: Comparison between prediction method using Li and Gebling's formulation and the sound transmission loss of 9 mm plywood

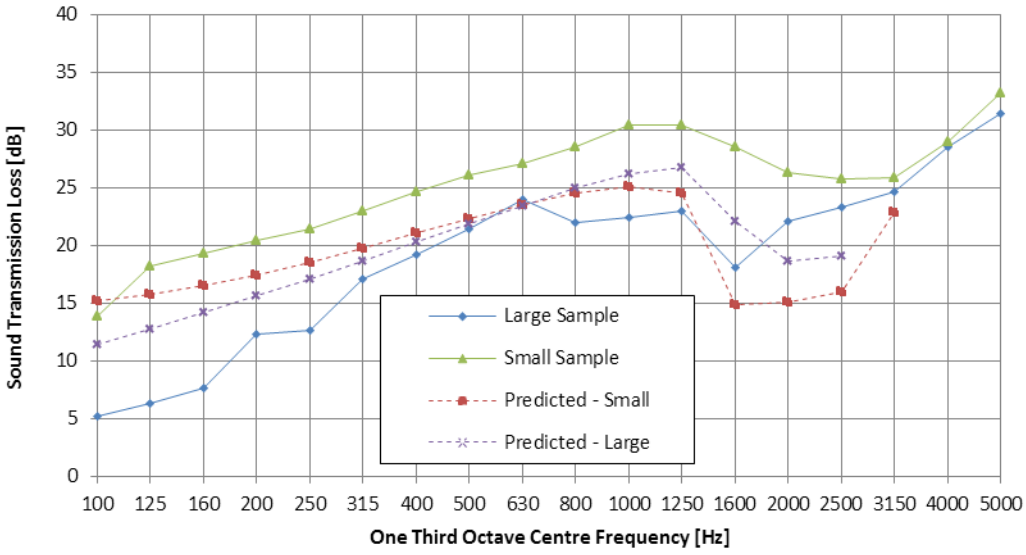

Figure 9.33: Comparison between prediction method using Li and Gebling's formulation and the sound transmission loss of 12 mm plywood

The predicted and measured sound transmission losses of a 21 mm plywood panel are presented in Figure 9.34. The low frequency behaviour is modelled very well, including the variation between the small and large samples. Above this region the prediction performs very poorly, with the predicted coincidence dip being much deeper than measured. The location of the coincidence region is predicted reasonably well for the small samples and convergence occurs between the

predicted and measured results above the coincidence region. The location of the coincidence dip is over-estimated by two thirds of an octave for the large sample.

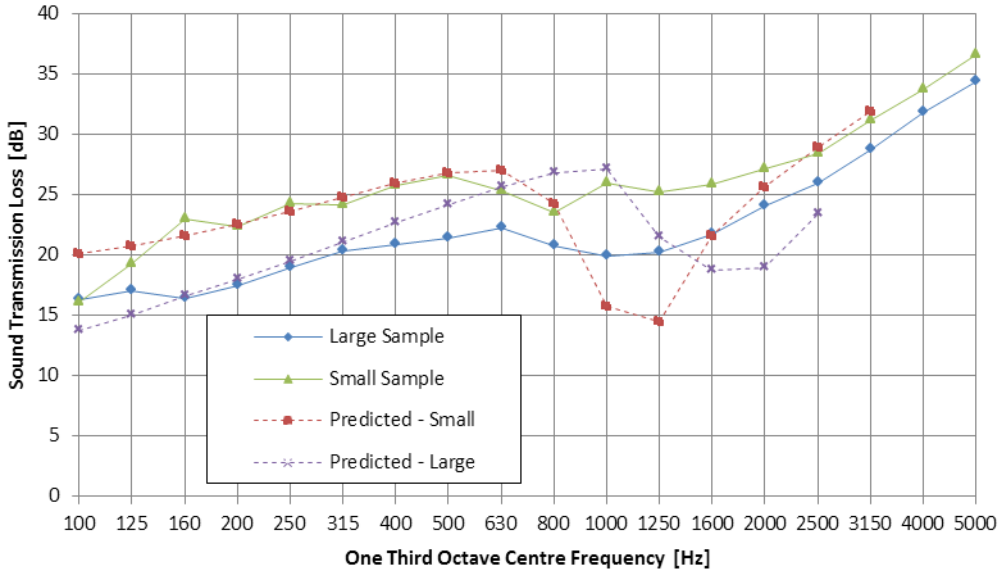

Figure 9.34: Comparison between prediction method using Li and Gebling's formulation and the sound transmission loss of 21 mm plywood

The large sample has an upper frequency limit of 2500 Hz, and the small sample has an upper frequency limit of 3150 Hz. This limitation prevents the high frequency behaviour from being compared to the measured results.

The transmission losses of the same partitions were also evaluated using the approximation of the radiation impedance. The calculations were performed with the limits of integration set to 90 degrees. This was done because the finite panel radiation impedance should account for the finite panel size. These calculations were performed for the full measured frequency range (100 Hz – 5000 Hz), this was possible due to the reduction in computational effort as a result of the approximation.

The predicted sound transmission loss of a 7 mm plywood sample is presented in Figure 9.35. The sound transmission loss was modelled relatively well across most of the frequency range. The low frequency behaviour of the small sample is predicted very well, but the large sample is over-predicted by approximately 4 decibels. The predicted coincidence region occurs earlier than measured in the frequency range, resulting in a large underestimation of the sound transmission loss between 1600 Hz and 2500 Hz. The predicted coincidence region also appears to be somewhat narrower than measured. Above the coincidence region the predicted sound transmission loss is higher than measured but follows the measured results.

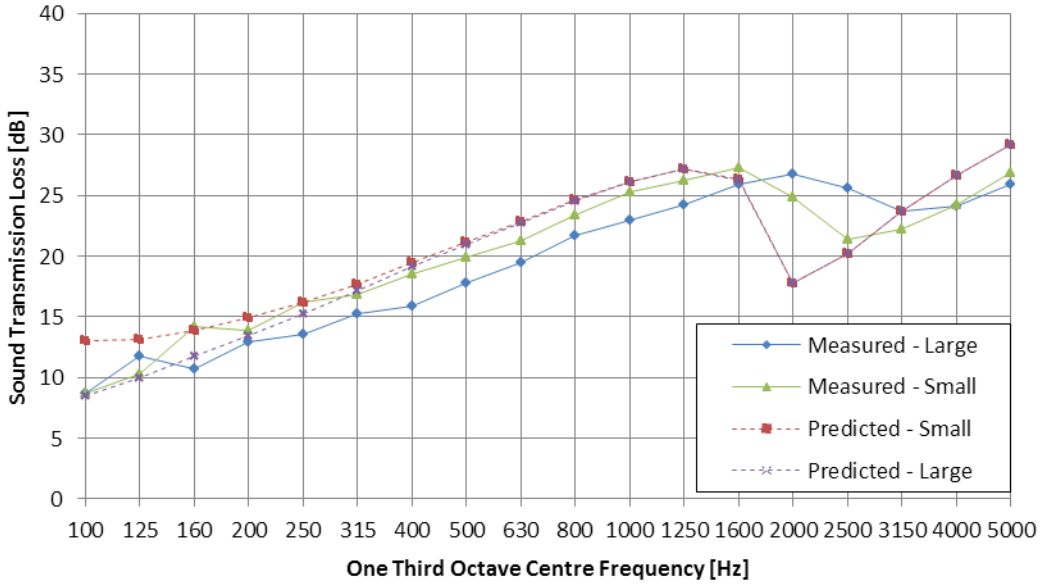

Figure 9.35: Comparison between prediction method using Davy's approximation and the sound transmission loss of 7 mm plywood

The same general trends are seen in the 9 mm plywood samples; as shown in Figure 9.36. The prediction model predicts the behaviour of the small sample well below the coincidence region. The location of the coincidence region is somewhat lower than measured in both cases. The coincidence region is predicted to be relatively wide and shallow, which is similar to that observed in the measured results. The effect of changing the sample size appears to have a relatively limited influence on the predicted sound transmission loss of the 9 mm sample, except for frequencies below 200 Hz,

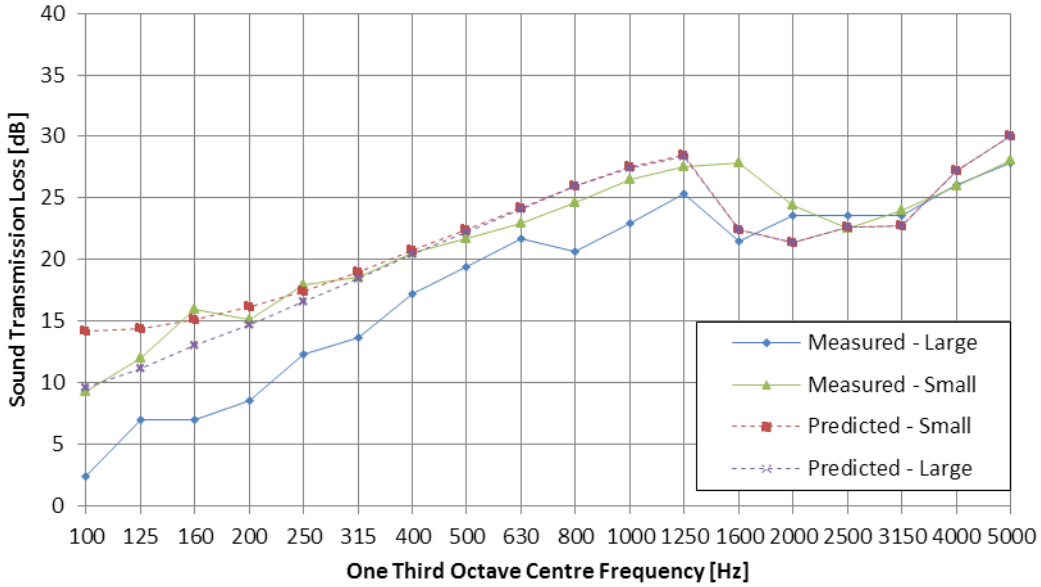

Figure 9.36: Comparison between prediction method using Davy's approximation and the sound transmission loss of 9 mm plywood

The predicted behaviour of the 12 mm plywood samples are presented in Figure 9.37. At frequencies above and below the coincidence region the sound transmission loss appears to be modelled reasonably well for the small sample, although for the large sample the sound transmission loss is significantly over-predicted below the coincidence region. Above the coincidence region the agreement between the modelled and predicted samples is very good. The coincidence region causes a dip that appears to be much deeper than the measured results. The location of the deepest point of the coincidence region appears to be under-estimated by approximately two thirds of an octave in the case of the small sample, but the initial onset of the coincidence region is predicted to within one third of an octave.

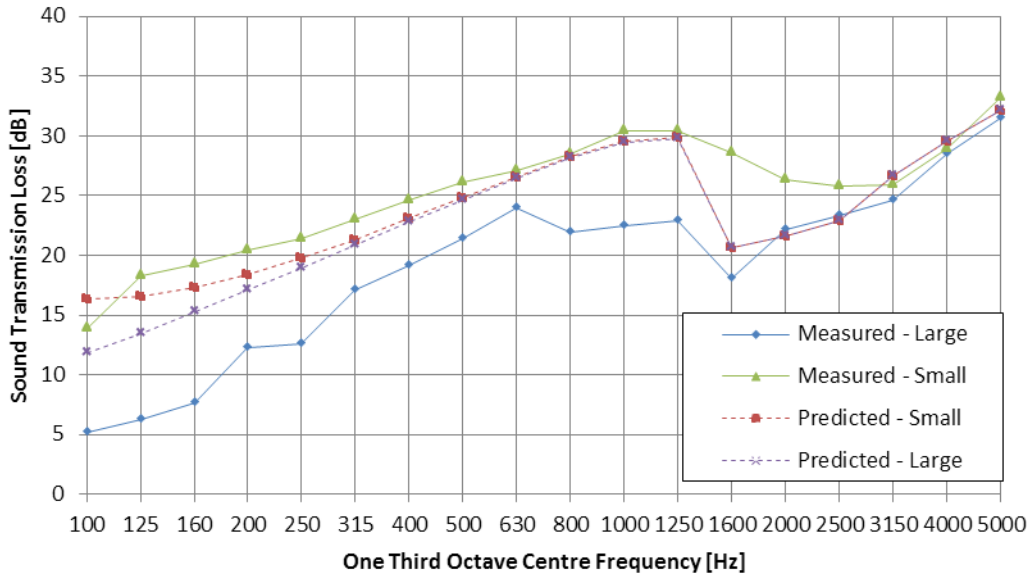

Figure 9.37: Comparison between prediction method using Davy's approximation and the sound transmission loss of 12 mm plywood

The predictions are presented for 21 mm plywood samples in Figure 9.38. This prediction is influenced heavily by the sample size. The prediction model does reasonably well below the coincidence region for the small sample, but for the large sample there is considerable deviation from the observed results. The coincidence region is much narrower and deeper than measured in both the small and large samples. Above the predicted coincidence region the transmission loss of both the small and large samples is predicted reasonably well.

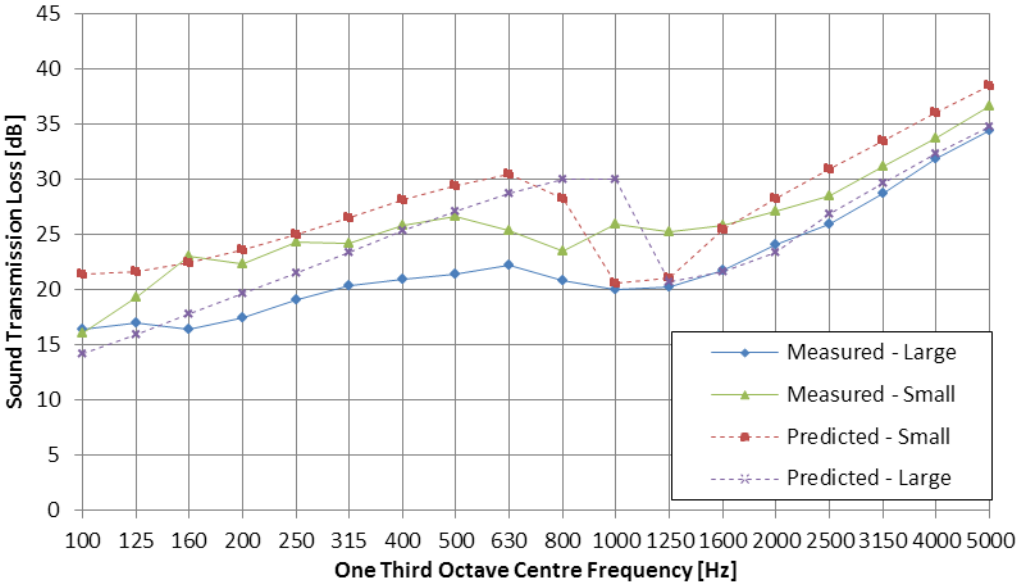

Figure 9.38: Comparison between prediction method using Davy's approximation and the sound transmission loss of 21 mm plywood

The inclusion of the finite panel radiation impedance qualitatively improved the overall agreement between measured and predicted sound transmission loss. Predictions for the large sample were generally less successful than for the small sample. In all cases the coincidence region was not well predicted. The approximate formulation of the radiation impedance was an efficient method for including an expression for the finite panel radiation impedance. The analytical model did yield significantly better results than the approximate formulation, but the computational requirements limited the calculations to below 2500Hz.

9.3.3. Adjusted Angle of Incidence

The inclusion of the finite panel radiation impedance was an improvement on the initial treatment of the system. The finite radiation impedance appears to account for a certain amount of the behaviour caused by the finite sample size. The presence of the niche has a large effect on the measured sound transmission. To account for this factor the maximum angle of incidence was limited based on the niche depth. The calculations performed using the approximate radiation impedance were repeated; with a limited maximum angle of incidence. The small samples had a maximum angle of incidence of 73 degrees, and the large samples had a maximum angle of incidence of 85 degrees.

The predicted sound transmission loss for the 9 mm plywood samples is presented in Figure 9.39. The agreement between the predicted and measured transmission loss of a small sample is very good, the maximum variation is less than five decibels across the measured frequency range.

The agreement for the large sample is not as good as the low frequency behaviour is over-estimated, but the transmission loss within and above the coincidence region is modelled well.

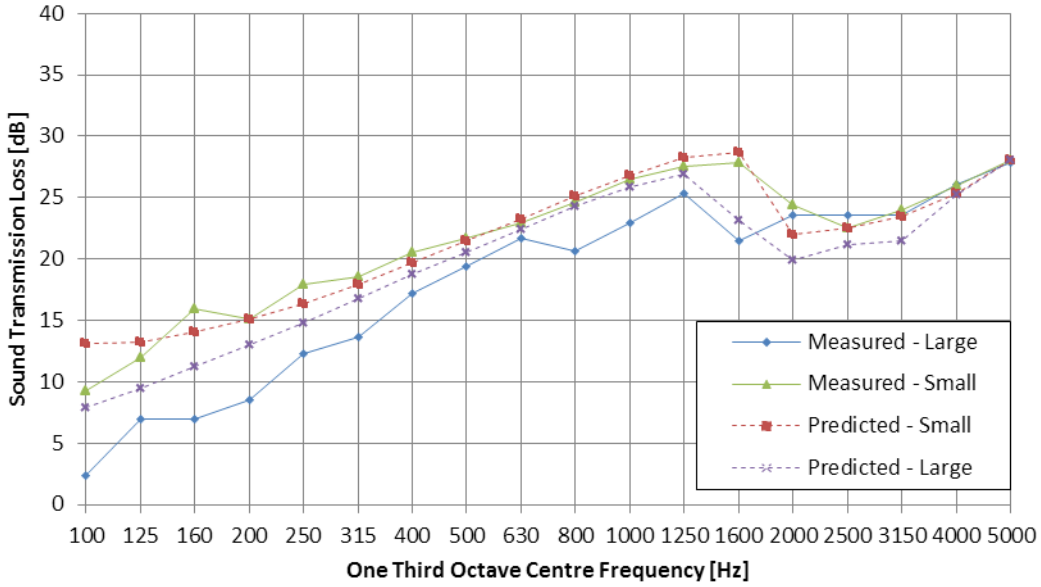

Figure 9.39: Comparison between prediction method using Davy's approximation and the sound transmission loss of 9 mm plywood with limited angle of incidence

There is less agreement between the predicted and measured transmission loss for 12 mm plywood; as shown in Figure 9.40. The behaviour above the coincidence region is predicted very closely. The predicted coincidence region is deeper than measured but the location and the width is accurately predicted. The low frequency behaviour is predicted relatively poorly, the transmission loss of large sample is over-predicted and the transmission loss of the small sample is under-predicted.

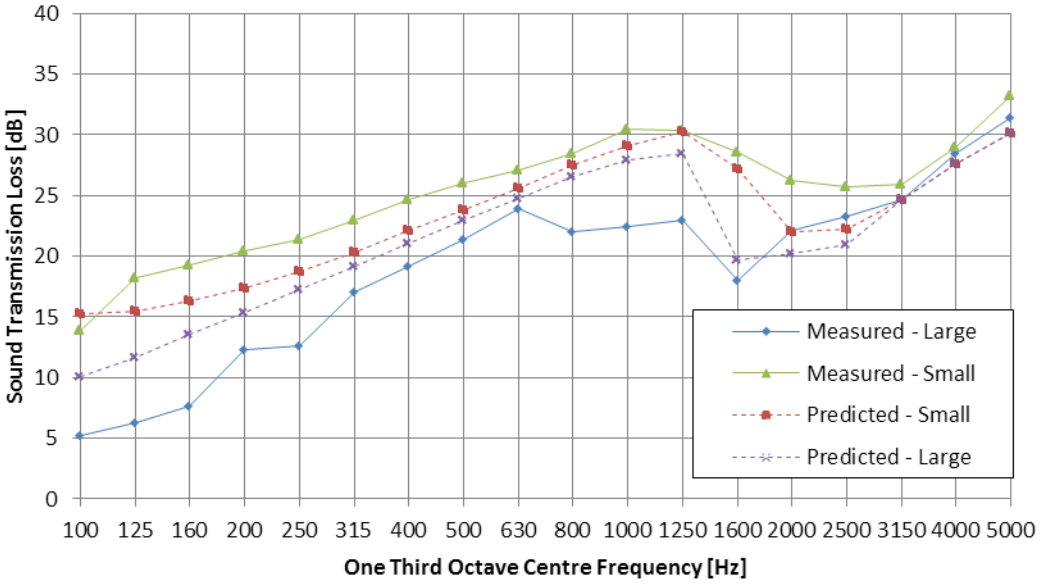

Figure 9.40: Comparison between prediction method using Davy's approximation and the sound transmission loss of

12 mm plywood with limited angle of incidence

The addition of the limiting angle of incidence did not improve the prediction of the 21 mm plywood transmission loss significantly (see Figure 9.41). The coincidence region is still predicted poorly for both the small and large samples. Above and below the coincidence region the transmission loss is predicted reasonably well for the small sample, but there are large discrepancies in the prediction for the large sample in these frequency ranges.

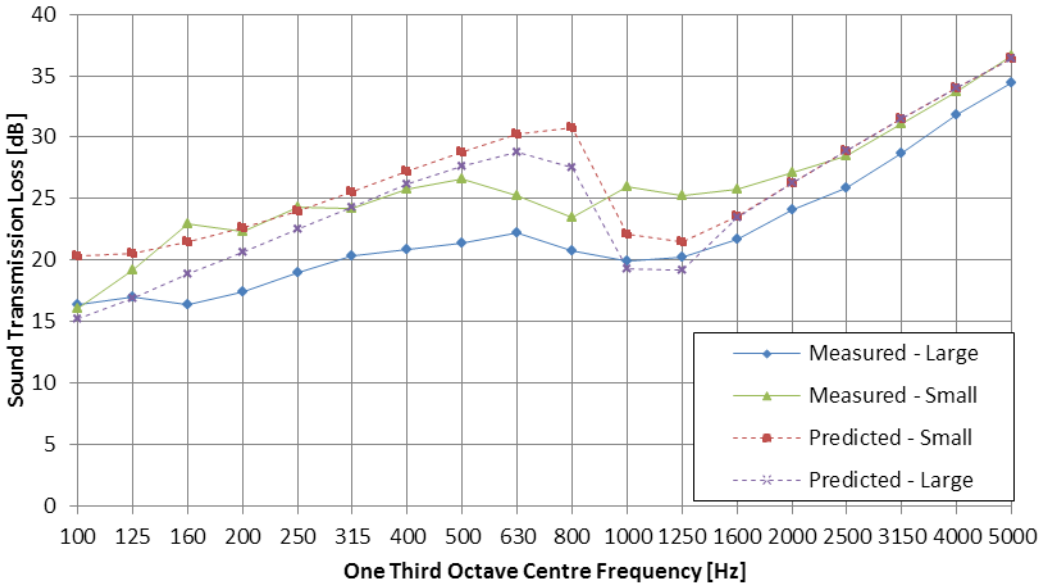

Figure 9.41: Comparison between prediction method using Davy's approximation and the sound transmission loss of 21 mm plywood with limited angle of incidence

The addition of a limiting angle based on the niche depth appears to improve the transmission loss predictions in many cases. The cases in which significant improvements were not seen were generally modelled poorly before the limiting angle was introduced. The observed changes which occur with small changes in the material properties indicate that any inaccuracies in the measurement of these properties will adversely alter the predicted transmission loss.

9.4. Frequency Dependent Variables

As described in Section 3, the stiffness of the plywood was found to be frequency dependent. The stiffness was calculated across a wide frequency range for 12 mm and 21 mm samples, and a narrower frequency range for the other samples measured. It was found that this frequency dependence could be replicated reasonably using an exponential decay of the form given in Equation 9.35.

$$\boldsymbol{B}(f) = \boldsymbol{B_i} e^{\boldsymbol{Q}f} \qquad \textbf{9.35}$$

where *f* is the one third octave band centre frequency of interest, $\boldsymbol{B}(f)$ is a stiffness matrix given by Equation 9.36, $\boldsymbol{B_i}$ is the corresponding initial stiffness matrix and $\boldsymbol{Q}$ is the corresponding rate of reduction of the stiffness values with frequency.

$$\boldsymbol{B}(f) = \begin{bmatrix} \boldsymbol{B_{low}}(f) \\ \boldsymbol{B_{high}}(f) \end{bmatrix} \qquad \textbf{9.36}$$

$$f_{low,high} = \frac{c^2}{2\pi}\sqrt{\frac{m}{B_{low,high}}} \qquad \textbf{9.37}$$

This variation has the effect of increasing the width of the coincidence dip. The coincidence frequencies of the panel (Equation 9.37) are inversely proportional to the square root of the bending stiffness. Thus as the dynamic stiffness of the panel decreases with increasing frequency of excitation, the critical frequencies increase correspondingly. This effectively spreads the frequency behaviour of the system across a wider range, resulting in a somewhat later onset, and significantly wider coincidence region.

The frequency dependent stiffness was used to calculate the sound transmission loss of the plywood using both the original orthotropic model (Section 9.2.2) and the prediction models that incorporate the finite panel radiation impedances (Section 9.3). The frequency dependent stiffness was calculated at each one third octave band centre frequency utilising the exponential curves given in Appendix 0. The sound transmission loss was calculated for 7 mm, 9 mm, 12 mm, and 21 mm plywood samples; as these were measured for both the small and large transmission loss sample sizes.

9.4.1. Original Model

The frequency dependent stiffness was included in Ordubadi and Lyon's model that was presented in Section 9.2.2. The stiffness was updated at each one third octave band centre frequency. This was performed in Matlab and the required integration was performed using the *"integral2"* function. In all the presented results the intermediate stiffness parameter (H) was assumed to be the geometric mean of the two stiffness values at each one third octave band centre frequency. The adjusted maximum angle of incidence was also included in an effort to account for the finite panel behaviour.

The predicted sound transmission loss of a 7 mm single leaf panel is compared with the measured results in Figure 9.42. The agreement with the measured results is improved by the addition of the frequency dependent stiffness. This frequency dependence has the effect of widening the coincidence dip significantly. Below the coincidence region the predicted sound transmission loss is very close to the measured results.

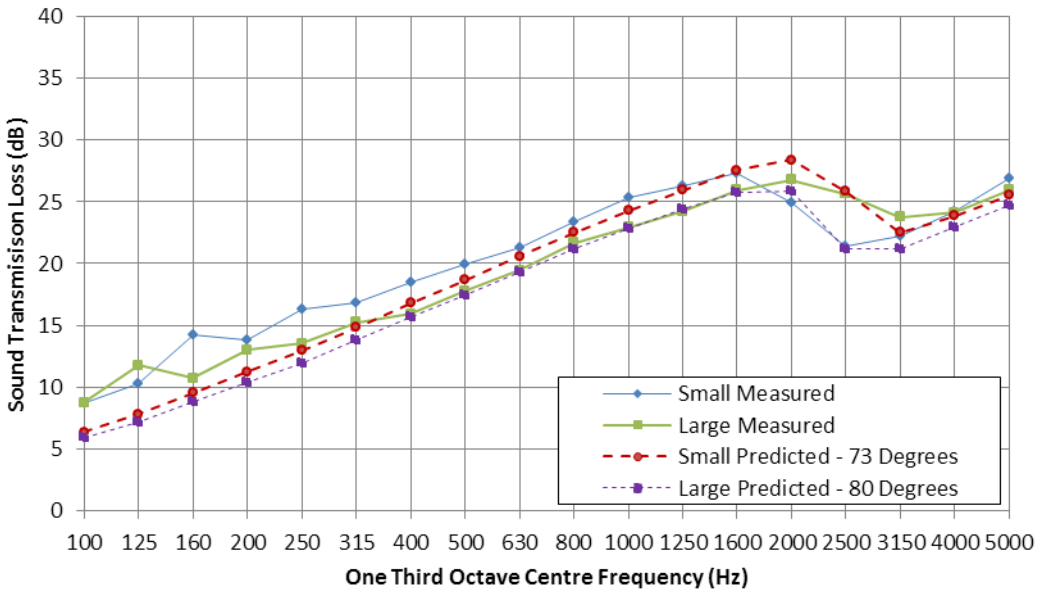

Figure 9.42: Transmission loss calculated for a 7 mm single leaf plywood panel when the frequency dependent stiffness is utilised, calculated using Ordubadi and Lyon's model

The predicted sound transmission loss of a 9 mm plywood panel is presented in Figure 9.43. The prediction was somewhat improved by the inclusion of the frequency dependent stiffness; although the small sample prediction is poor in the frequency range above the coincidence region. The significant discrepancy in this frequency range was probably due to an error in the way the frequency dependent stiffness was modelled. There is a very large deviation between the predicted and measured sound transmission loss above the coincidence region for the small sample. This indicates that the stiffness model is likely to be incorrect.

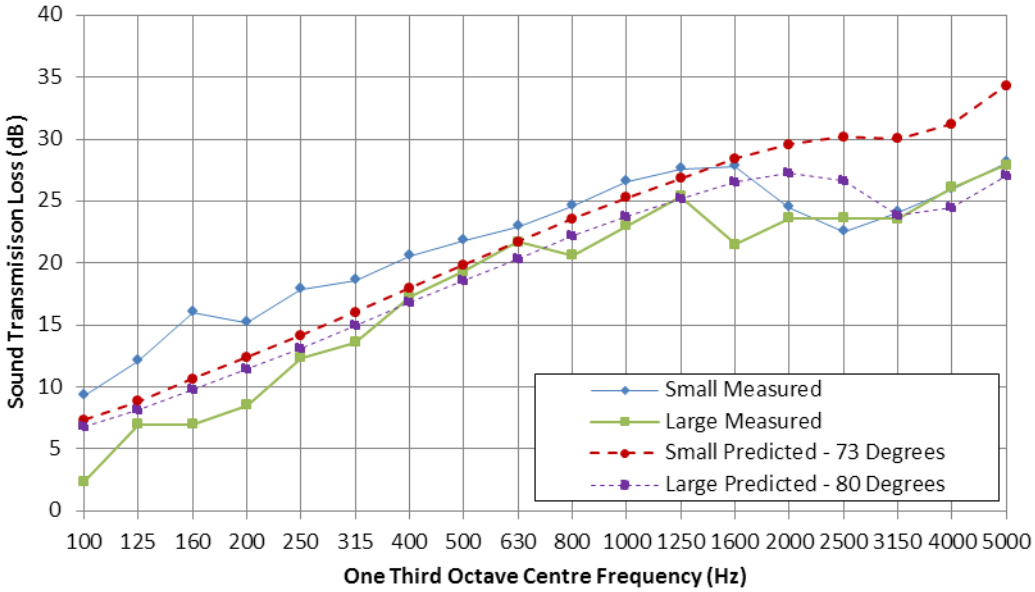

Figure 9.43: Transmission loss calculated for a 9 mm single leaf plywood panel when the frequency dependent stiffness is utilised, calculated using Ordubadi and Lyon's model

The accuracy of the prediction model for the 12 mm plywood samples was significantly reduced by the inclusion of the frequency dependent stiffness (Figure 9.44). This effect is especially clear just below the predicted coincidence region. There is a large under-estimation by the prediction model above the coincidence region. The width and depth of the coincidence region appears to be modelled relatively well for the large sample, but the entire curve appears to be too low.

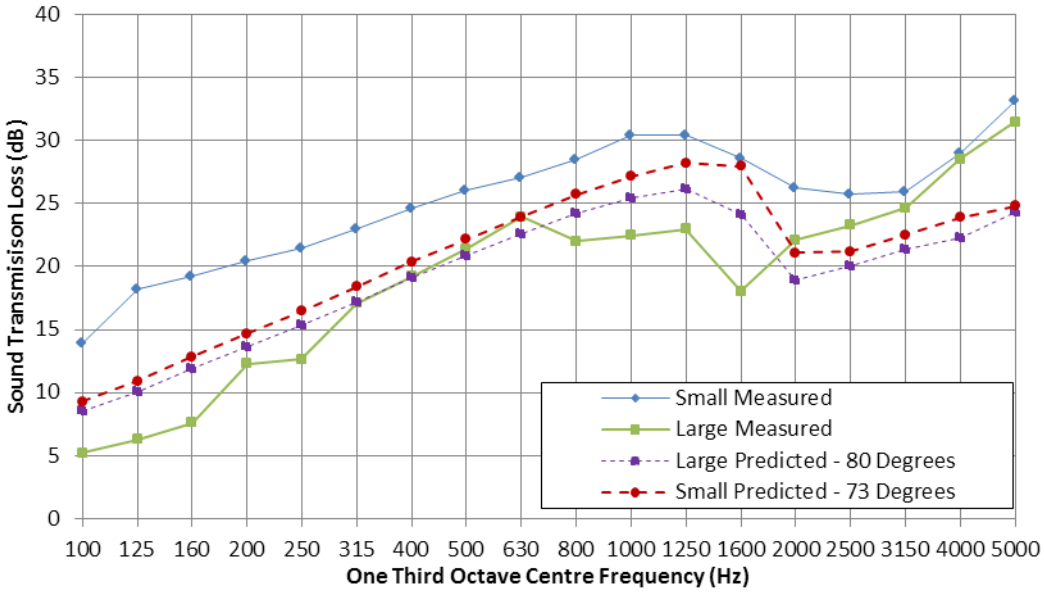

Figure 9.44: Transmission loss calculated for a 12 mm single leaf plywood panel when the frequency dependent stiffness is utilised, calculated using Ordubadi and Lyon's model

The 21 mm plywood is predicted with varying degrees of accuracy when the frequency dependent stiffness is incorporated; as shown in Figure 9.45. The high frequency behaviour above

the coincidence region is well modelled. There is a large deviation between the predicted and measured results below the coincidence region.

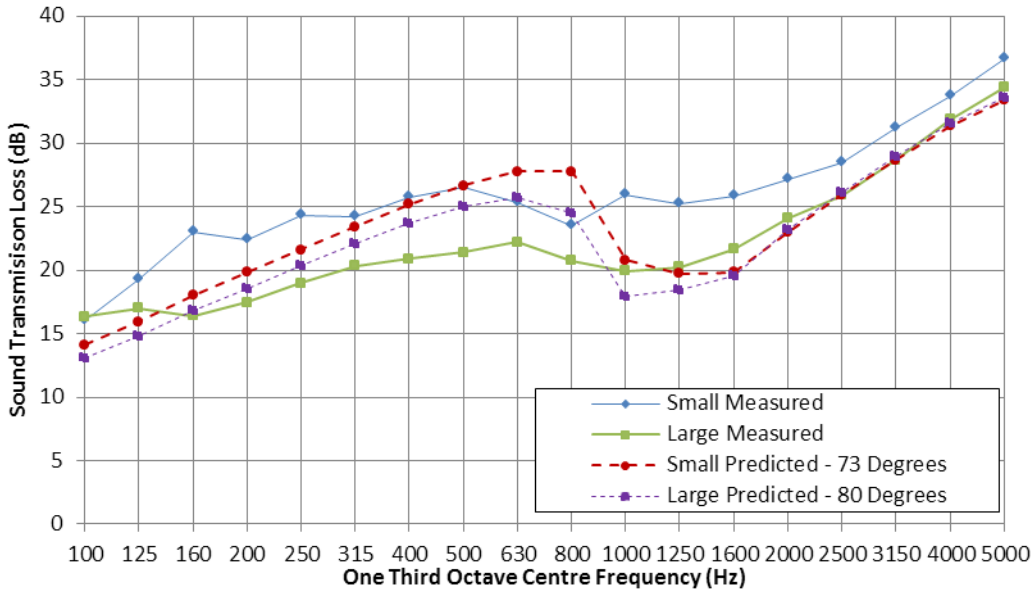

Figure 9.45: Transmission loss calculated for a 21 mm single leaf plywood panel when the frequency dependent stiffness is utilised, calculated using Ordubadi and Lyon's model

The inclusion of a variable stiffness generally improved the prediction of the sound transmission loss using Lyon and Ordubadi's model for some of the measured panels. The quality of the prediction is heavily dependent on the equation used to predict the stiffness at each one third octave centre frequency. The exponential curve utilised to predict the frequency dependent stiffness is reasonable in some cases but did not achieve a good fit in all cases; this may have an adverse effect on the predicted sound transmission loss.

In all cases the variable bending stiffness was seen to widen the coincidence region by a large amount. It appears that this variable stiffness has a larger contribution to the wide coincidence region seen in the plywood samples than the orthotropic stiffness. This is contrary to the initial hypothesis of this research that assumed that the orthotropic stiffness was the main cause of the wide and shallow coincidence region. The combination of both the orthotropic and frequency dependent stiffness properties causes the very wide coincidence region that was observed in most of the measured results. These effects combine to yield a panel that has a much shallower and wider coincidence dip than standard linings, the variable stiffness also reduces the gradient of the transmission loss curve across the entire frequency range.

As discussed in Section 9.2.2 the assumption that the panel is of infinite extent will also have an adverse effect on the predicted sound transmission loss. The reduction in the maximum angle of incidence accounts somewhat for the finite panel size. The following section will implement the

frequency dependent stiffness into a model with radiation impedance that accounts for the finite panel size.

9.4.2. Finite Radiation Impedance Model

The frequency dependent stiffness was incorporated into the prediction methods that utilise the finite radiation impedance. The predictions were only performed using the approximate formula for the radiation impedance that was presented in 9.3.1. The analytical model for the radiation impedance requires a large increase in the computational requirements, and did not show any improvements in the prediction of the sound transmission loss. As such it was removed from the following evaluations.

The predicted transmission loss of the 9 mm plywood samples is presented in Figure 9.46. The low frequency behaviour is predicted well for the small sample. The coincidence region is predicted poorly with the onset occurring one third of an octave above the measured results, resulting in a significant overestimation of the sound transmission loss in the beginning of the coincidence region. Above the coincidence region the prediction schemes converge closely, and appear to predict a transmission loss that is approximately two decibels above the measured results.

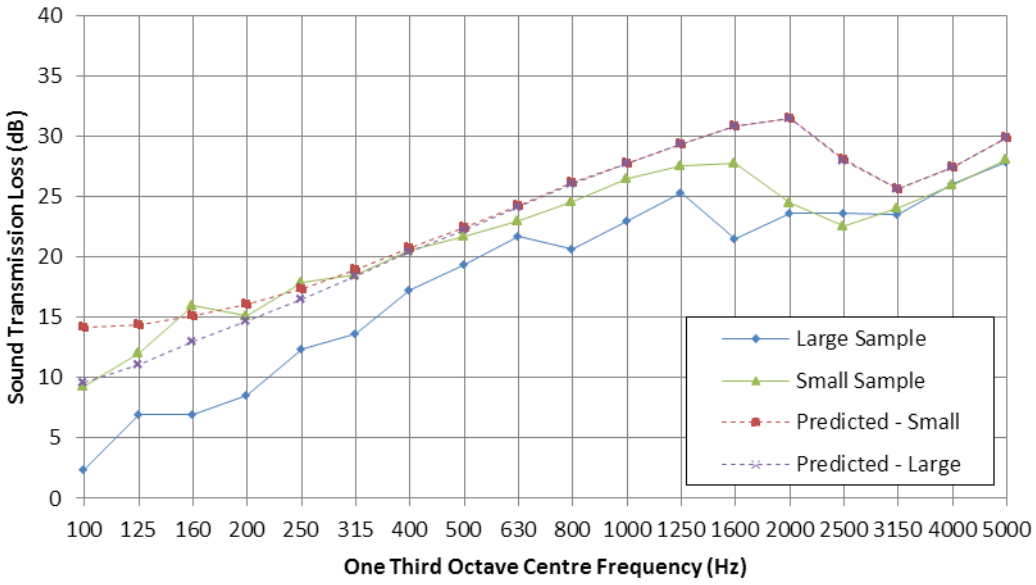

Figure 9.46: Transmission loss calculated for a 9 mm single leaf plywood panel when the frequency dependent stiffness is utilised in conjunction with the approximate finite panel radiation impedance

The transmission loss of a 12 mm sample calculated using the approximate finite panel impedance and a variable bending stiffness is presented in Figure 9.47. The prediction method under predicts the transmission loss of the small sample across the entire frequency range by 2 – 3 dB, with a larger variation around the coincidence region. In contrast the large sample predictions somewhat over predict the transmission loss at low frequency, and under predict the transmission

loss at higher frequencies. The location of the small sample's coincidence region is predicted reasonably well, but the predicted location of the large sample's coincidence region is one third of an octave higher than measured. The shape of the small transmission loss sample's coincidence region is predicted well, with the prediction having a similar width and a slightly deeper coincidence dip. The coincidence region of the large sample is poorly predicted.

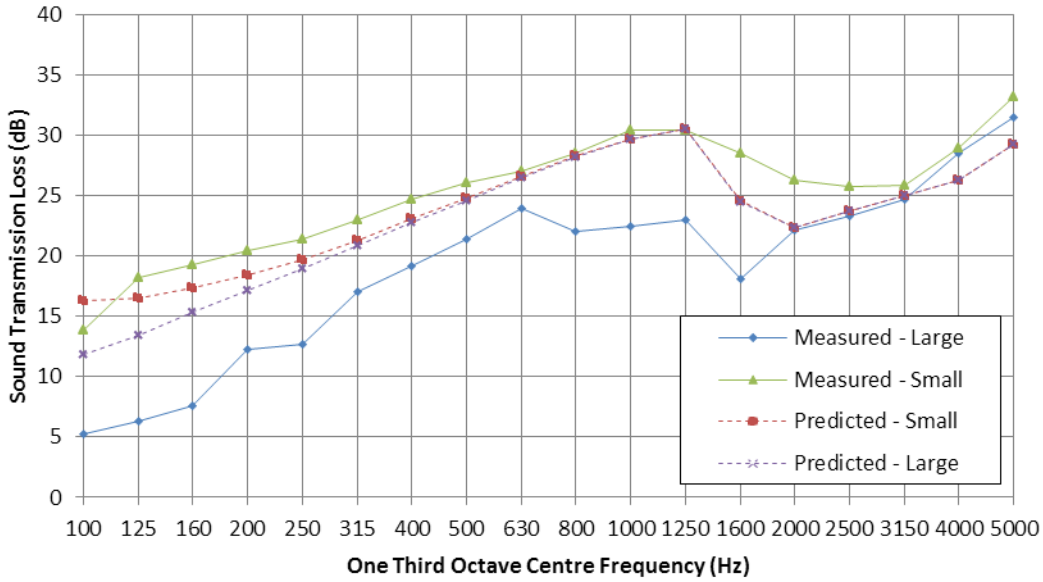

Figure 9.47: Transmission loss calculated for a 12 mm single leaf plywood panel when the frequency dependent stiffness is utilised in conjunction with the approximate finite panel radiation impedance

The predicted sound transmission loss of a 21 mm plywood panel with a variable stiffness is compared to experimentally measured data in Figure 9.48. The high frequency behaviour is relatively well predicted especially for the small sample. The coincidence region is predicted poorly, the predicted coincidence region is significantly deeper and narrower than measured. The transmission loss of both the small and large transmission loss samples is over-predicted across much of the frequency range below the coincidence region.

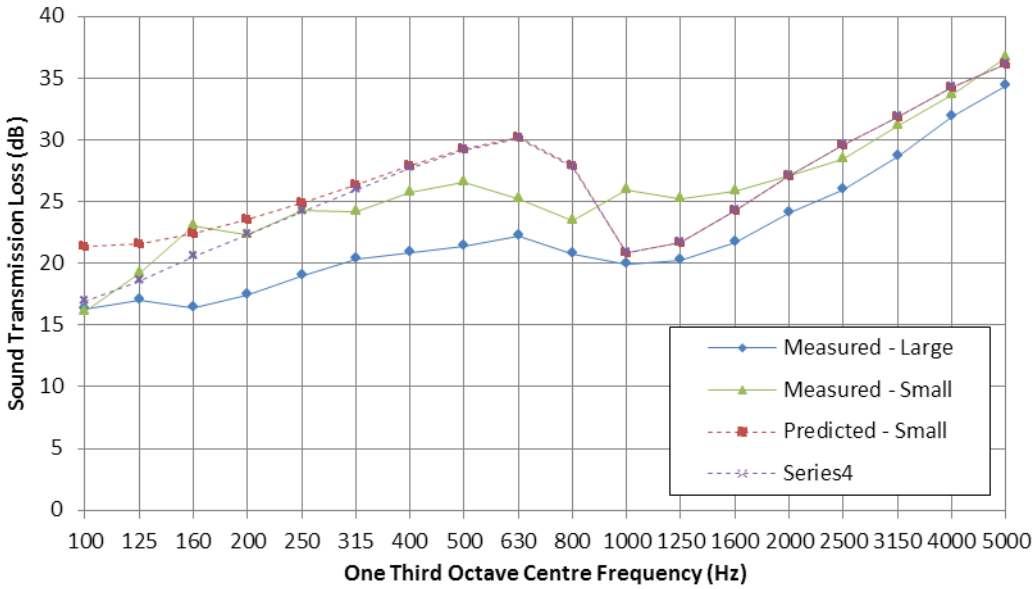

Figure 9.48: Transmission loss calculated for a 21 mm single leaf plywood panel when the frequency dependent stiffness is utilised in conjunction with the approximate finite panel radiation impedance

The same limiting angles were incorporated into the previous calculations to account for some of the niche effects present in the measured results. The small sample had a niche depth of 73 degrees, and the large sample had a niche depth of 85 degrees. The calculations of the transmission loss were performed using the approximate model for the radiation impedance and a frequency dependent bending stiffness.

The predicted sound transmission loss for a 7 mm plywood panel is presented in Figure 9.49. Reasonably good agreement is seen throughout the frequency range, with the largest variations occurring within the coincidence region. The coincidence region is predicted to occur one third of an octave later than measured in the small samples and one third of an octave earlier than measured in the large samples.

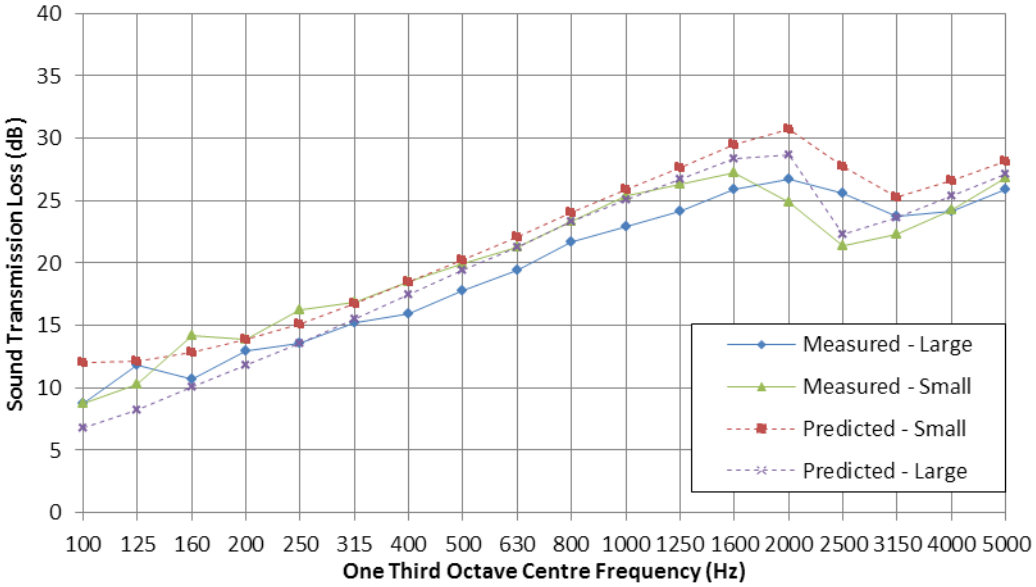

Figure 9.49: Transmission loss calculated for a 7 mm single leaf plywood panel using a frequency dependent bending stiffness, finite radiation impedance and a limiting maximum angle of incidence

The predicted transmission loss for a 12 mm plywood panel is presented in Figure 9.50. The prediction methods agree reasonably with the small sample but the sound transmission loss of large sample is not especially well predicted. The region above the coincidence region appears to diverge from the measured results. The coincidence region has been widened significantly but was predicted to occur somewhat later than measured.

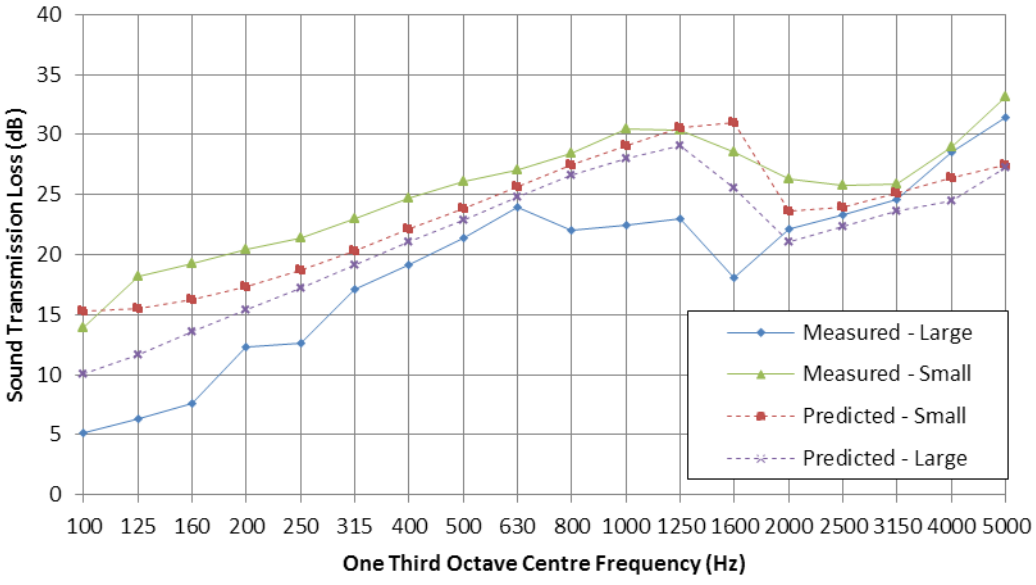

Figure 9.50: Transmission loss calculated for a 12 mm single leaf plywood panel using a frequency dependent bending stiffness, finite radiation impedance and a limiting maximum angle of incidence

The 21 mm plywood is relatively well modelled in the case of the small sample, but the low frequency behaviour of the large sample is poorly modelled. The combination of the different

prediction methods gives an improved prediction of the behaviour of the coincidence region. The coincidence region is still deeper than measured, and displays a later, less gradual onset than observed.

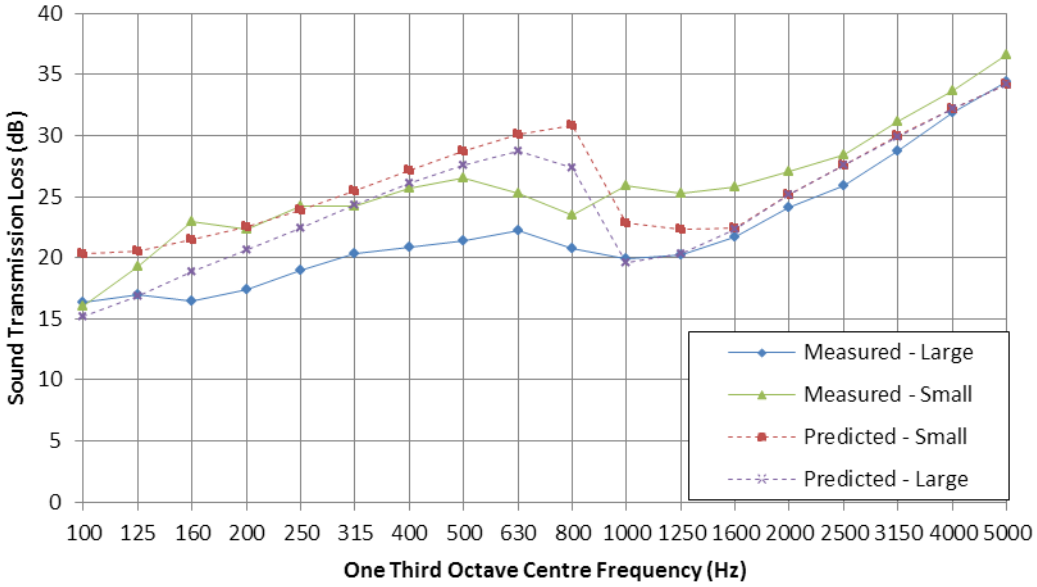

Figure 9.51: Transmission loss calculated for a 21 mm single leaf plywood panel using a frequency dependent bending stiffness, finite radiation impedance and a limiting maximum angle of incidence

The combination of a frequency dependent bending stiffness, a finite radiation impedance, and a niche dependent limiting angle of incidence results in a reasonably effective prediction of the sound transmission loss. The influence of a variable bending stiffness was much larger than anticipated and contributed a large amount to the widened coincidence region observed in the measurements. The limiting maximum angle of incidence results in a number of changes which explain some of differences in the measurements obtained using the two different sample sizes. The low frequency transmission loss is seen to increase as the maximum angle of incidence is decreased, and the onset of the coincidence region is delayed by reductions in the maximum angle of incidence.

9.5. Damped Plywood Panels

The damped panels presented in Section 8.3 had significantly higher damping loss factors than the equivalent un-damped plywood panels. The transmission loss of the modified panels is evaluated utilising the prediction methods presented in this section.

Figure 9.52 compares the predicted transmission loss with the measured results for the 12 mm damped plywood. This prediction assumed that the stiffness of the panel was independent of frequency. Below the coincidence region the sound transmission loss of the panel was modelled very well by the prediction method. The predicted coincidence region occurs two thirds of an octave

below the measured coincidence region. The predicted coincidence region is also deeper than measured. Above the coincidence region the predicted results are significantly higher than the measured results, but they appear to show a similar general trend.

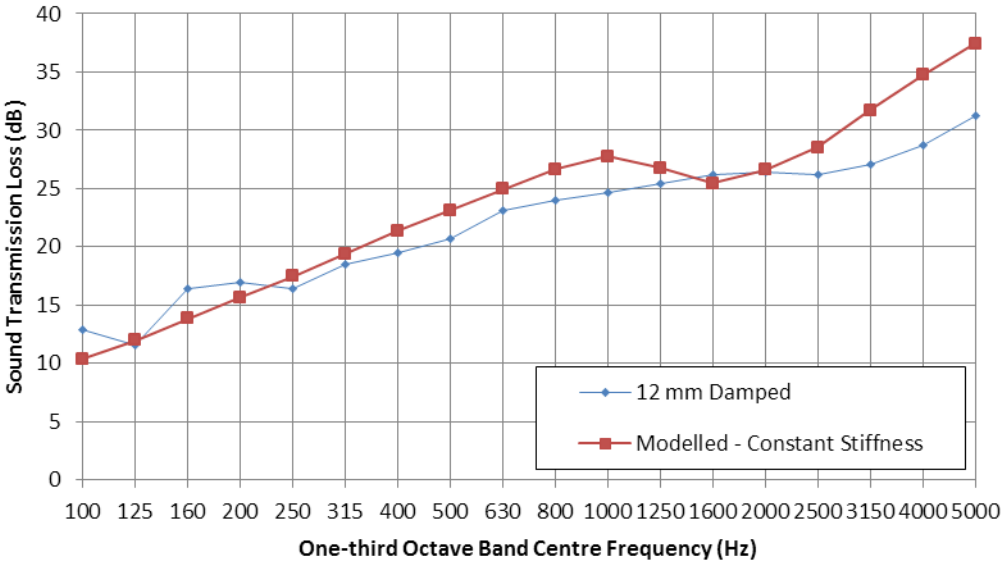

Figure 9.52: Transmission loss of a 12 mm single leaf plywood partition with internal damping. Predicted using a finite radiation impedance and a limiting maximum angle of incidence

The predicted transmission loss of a 7 mm plywood panel that incorporates a frequency dependent stiffness is presented in Figure 9.53. Again the behaviour below the coincidence region is modelled well. The location of the coincidence region occurs two thirds of an octave later than measured, resulting in a relatively large divergence between the predicted and measured results. Above the coincidence region the curves appear to converge.

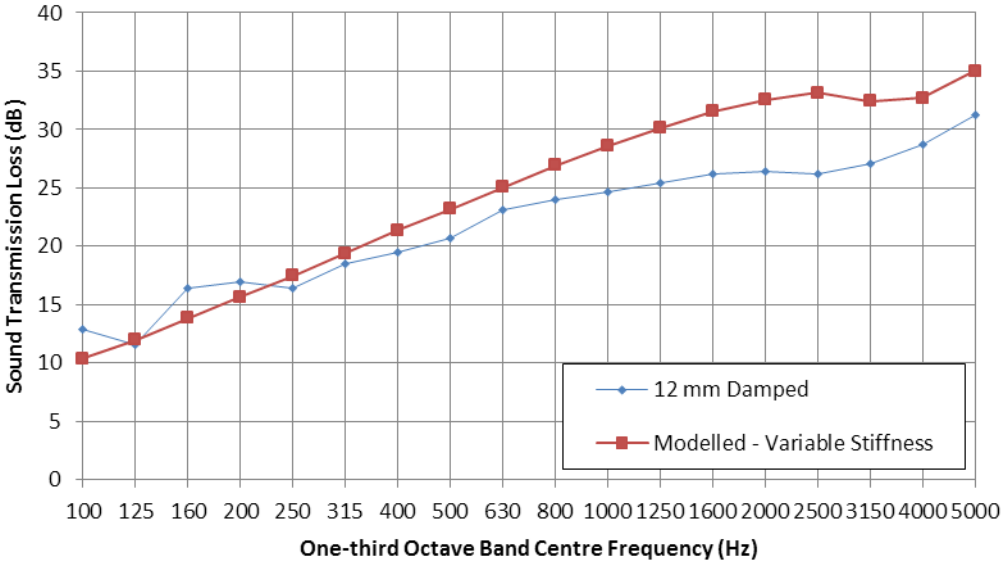

Figure 9.53: Transmission loss of a 12 mm single leaf plywood partition with internal damping. Predicted using a frequency dependent bending stiffness, finite radiation impedance and a limiting maximum angle of incidence

Overall the agreement between the predicted and measured results is generally within five decibels outside of the coincidence region and 10 decibels within the coincidence region. The observed discrepancies is likely to be due to the likely variations in both the stiffness and damping loss factor of the panels due to variations in the construction process. The modelled results appeared to predict the general shape of the curve correctly and yielded similar coincidence dips as measured.

9.6. Double Leaf Partitions

9.6.1. Derivation

A prediction model is presented in this section for an infinite double leaf partition with mismatched orthotropic leaves. This is based on the derivation developed by London and presented in Section 2.2.2. The system is the same as described in Figure 2.6 where the variables are defined. The continuity conditions and the boundary conditions are the same as listed in Equations 2.24 - 2.29. These yield the following formulas (Equations 9.38 and 9.39) for the pressure on either side of the partition and between the leaves.

$$(P_i + P_r) - (P_+ + P_-) = 2\gamma_1(P_i - P_r) \quad \textbf{9.38}$$

$$P_+ e^{-i\beta} + P_- e^{-i\beta} - P_t e^{-i\beta} = 2\gamma_2 P_t e^{-i\beta} \quad \textbf{9.39}$$

Where $\gamma_{n=1,2}$ is defined by Equation 9.40 and β is given by Equation 9.41.

$$\gamma_{n=1,2} = \frac{Z_{p(n=1,2)}}{2Z_{w(n=1,2)}} \quad \textbf{9.40}$$

$$\beta = kd\cos\theta \quad \textbf{9.41}$$

Where d is the cavity depth, $Z_{p(n=1,2)}$ is the plate impedance of each panel, and β is a factor related to the cavity depth. These equations can be solved to calculate the ratio between the incident sound power and the transmitted sound power, which represents the inverse of the transmission coefficient. In the first case it is assumed that the panels are mismatched, allowing a generic equation to be developed. The ratio of interest is given by Equation 9.42.

$$\frac{P_i}{P_t} = 1 + \gamma_1 + \gamma_2 + \gamma_1\gamma_2\left(1 - e^{-2i\beta}\right) \quad \textbf{9.42}$$

This equation can be shown to be consistent with the previously derived expression for the single panel transmission coefficient if the cavity depth is set to zero and the mass of each panel is set to one half. This will result in Equation 2.15 for the transmission coefficient.

If the partitions are assumed to be equal in all ways Equation 9.42 reduces to Equation 9.43. This is the case for matched partitions.

$$\frac{P_i}{P_t} = 1 + 2\gamma + \gamma^2\left(1 - e^{-2i\beta}\right) \qquad \textbf{9.43}$$

Assuming that the partitions have a bending wave impedance that can be modelled as a pure mass reactance (Equation 2.16) and that the partition is of infinite extent (the radiation impedance is given by Equation 9.4). This yields Equation 2.30 for the transmission coefficient as expected.

If the effect of an orthotropic stiffness component is added using Equation 2.77 for the bending wave impedance value Equation 9.43 can be rewritten as Equation 9.44. This expression assumes that the radiation impedance of both partitions is that of an infinite panel.

$$\frac{P_i}{P_t} = 1 + 2\left\{\frac{\left[k_0^4 \sin^4\theta D'(\phi) - \rho_s\omega^2\right]}{\frac{i\omega}{2\left(\frac{\rho c}{\cos\theta}\right)}}\right\} + \left\{\frac{\left[k_0^4 \sin^4\theta D'(\phi) - \rho_s\omega^2\right]}{\frac{i\omega}{2\left(\frac{\rho c}{\cos\theta}\right)}}\right\}^2 \left(1 - e^{-2i\beta}\right) \qquad \textbf{9.44}$$

This can then also be expressed utilising the finite panel radiation impedance derived in Section 9.3.1. This yields Equation 9.45 for the transmission ratio, where the panel radiation impedance is given by either Equation 9.17 or the approximation developed by Davy.

$$\frac{P_i}{P_t} = 1 + 2\left\{\frac{\left[k_0^4 \sin^4\theta D'(\phi) - \rho_s\omega^2\right]}{\frac{i\omega}{2Z_w}}\right\} + \left\{\frac{\left[k_0^4 \sin^4\theta D'(\phi) - \rho_s\omega^2\right]}{\frac{i\omega}{2Z_w}}\right\}^2 \left(1 - e^{-2i\beta}\right) \qquad \textbf{9.45}$$

The effect of a variable bending stiffness is included in the prediction model utilising the method described in Section 9.4. This results in a frequency dependent stiffness $D'(f,\phi)$ that can be evaluated at each one third octave centre frequency.

Finally the same process is applied to mismatched plywood panels. This alteration means that Equation 9.42 must be utilised, yielding alternative formulations for the transmission ratio. These formulations are given in Equations 9.46 and 9.47. This can also be combined with the frequency dependent stiffness as described in the previous paragraph.

$$\frac{P_i}{P_t} = 1 + \frac{\frac{\left[k_0^4 \sin^4\theta D_1'(\phi) - \rho_{s1}\omega^2\right]}{i\omega} + \frac{\left[k_0^4 \sin^4\theta D_2'(\phi) - \rho_{s2}\omega^2\right]}{i\omega}}{2\left(\frac{\rho c}{\cos\theta}\right)} + \frac{\frac{\left[k_0^4 \sin^4\theta D_1'(\phi) - \rho_{s1}\omega^2\right]\left[k_0^4 \sin^4\theta D_2'(\phi) - \rho_{s2}\omega^2\right]}{-\omega^2}}{4\left(\frac{\rho c}{\cos\theta}\right)^2} \times \left(1 - e^{-2i\beta}\right) \quad \textbf{9.46}$$

$$\frac{P_i}{P_t} = 1 + \frac{\frac{\left[k_0^4 \sin^4\theta D_1^{'}(\phi) - \rho_{s1}\omega^2\right]}{i\omega} + \frac{\left[k_0^4 \sin^4\theta D_2^{'}(\phi) - \rho_{s2}\omega^2\right]}{i\omega}}{2Z_w} + \frac{\frac{\left[k_0^4 \sin^4\theta D_1^{'}(\phi) - \rho_{s1}\omega^2\right]\left[k_0^4 \sin^4\theta D_2^{'}(\phi) - \rho_{s2}\omega^2\right]}{-\omega^2}}{4{Z_w}^2} \times \left(1 - e^{-2i\beta}\right) \quad \textbf{9.47}$$

The transmission coefficient is thus calculated using

$$\tau_d = 2\int \frac{\sin\theta\cos\theta}{\left|\frac{P_i}{P_t}\right|^2} \quad \textbf{9.48}$$

A major limitation in the theoretical derivation is related to the infinite extent of the panels. Despite the finite panel radiation impedance being included there is a fundamental issue in the assumption that the lateral extent of the cavity is infinite. Once the mass-air-mass frequency is achieved there will always be some combination of frequency and coincidence angle at which this criterion is present.

9.6.2. Comparison with Measured Values

The formulas for the prediction of the sound transmission coefficient are non-integrable. As such the transmission coefficient must be calculated using a numerical method; in this case Matlab's *integral2* function was used again to perform this integration. The evaluation of the analytical expressions encounters similar computational issues to those discussed in Section 9.3.1. The evaluation of models in which the radiation impedance was an analytical solution were faster than those that required the evaluation of a second double integral for the radiation impedance (Equation 9.17).

The first prediction model evaluated was the infinite panel case, Equation 9.44. It was found that a singularity occurs around the critical frequency. The transmission coefficient is presented across the integration range in Figure 9.54 and Figure 9.55, showing the singularity that occurs near the critical frequency. Figure 9.54 shows the transmission coefficient across the integration range when the frequency is below the coincidence region. It is clear that the transmission coefficient function is smooth across the range of interest; as such the numerical integration is fast and accurate. In contrast Figure 9.55 shows the transmission coefficient near the coincidence frequency, where the numerical integration methods were unable to find a solution. It is clear that a significant singularity is occurring and thus the numerical approaches taken will encounter difficulties in evaluating the total integral.

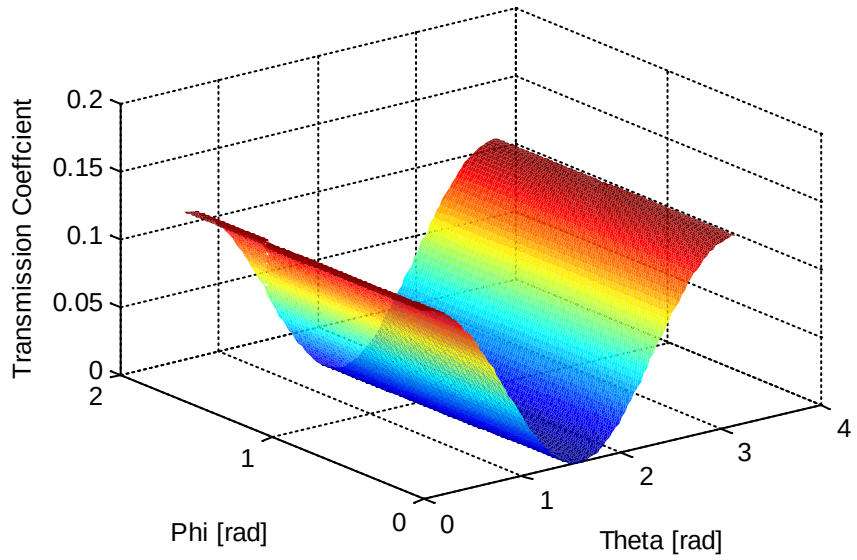

Figure 9.54: Transmission coefficient of 12 mm double leaf partition using infinite radiation impedance at 100 Hz.

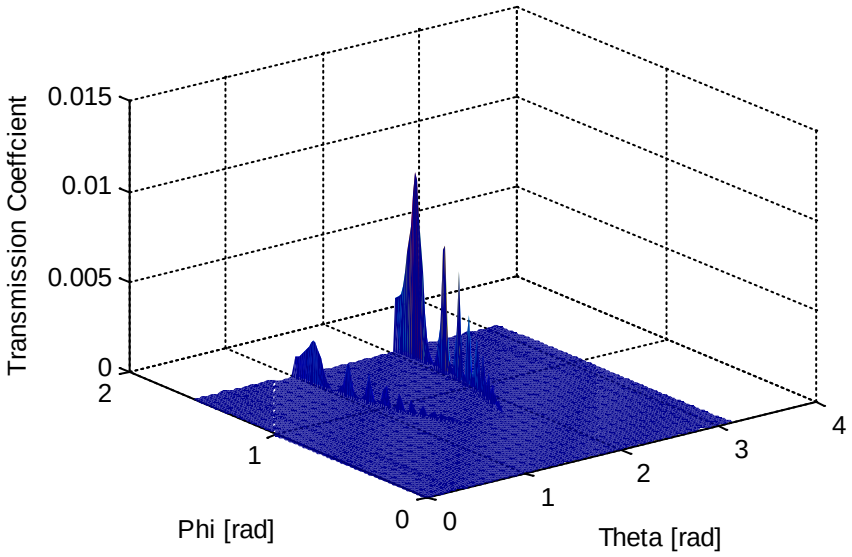

Figure 9.55: Transmission coefficient of 12 mm double leaf partition using infinite radiation impedance at 2000 Hz

The calculated transmission loss is presented in Figure 9.56, Figure 9.57, and Figure 9.58. In the 9 mm double leaf partition the prediction method does not accurately predict the sound transmission loss of the double leaf partition (Figure 9.56). The coincidence region is very poorly modelled and the low frequency region has a slope which is significantly less than the measured data. The low frequency behaviour was well modelled but above 1250 Hz the prediction is very poor, although the gradient of the low frequency transmission loss is 3 decibels per octave lower than the measured data.

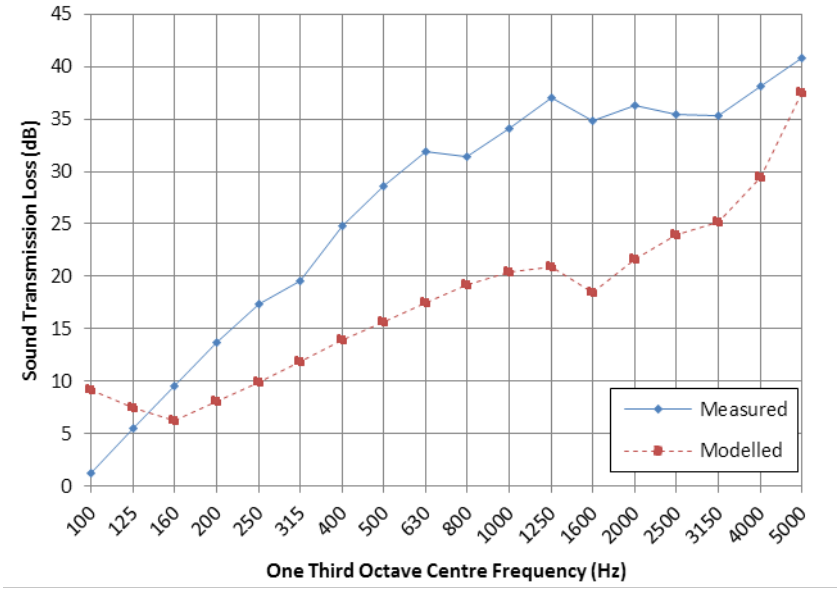

Figure 9.56: Transmission loss coefficient of 9 mm double leaf partition using infinite radiation impedance

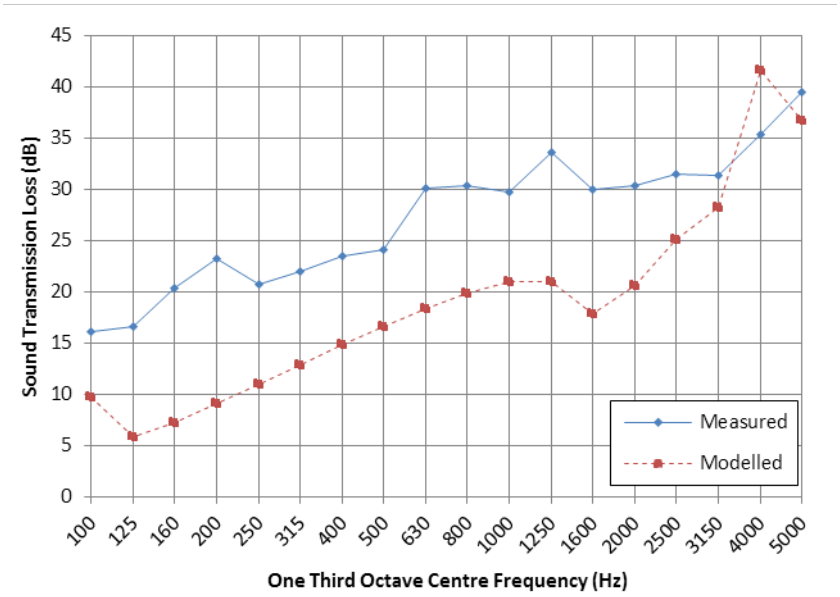

Figure 9.57: Transmission loss of 12 mm double leaf partition using infinite radiation impedance

The transmission loss behaves in a very similar manner when the approximation of the finite radiation impedance is applied. The numerical integration techniques struggle to converge around the critical frequency, again due to the singularity or near singularity that occurs. In all cases the integration routine reaches the maximum allowed number of iterations without achieving the desired convergence near the critical frequency.

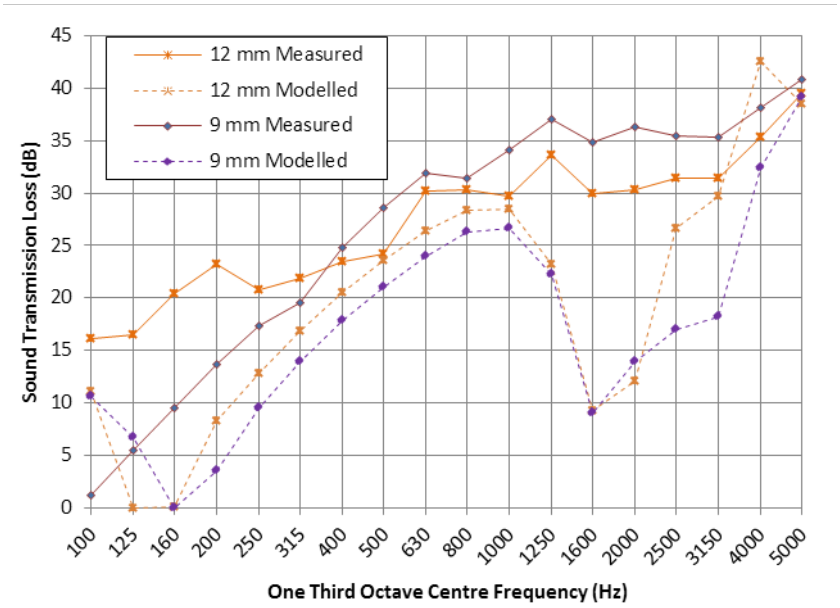

Figure 9.58: Transmission loss of 9 mm and 12 mm double leaf partitions calculated using approximated finite panel radiation impedance

The effect of including the variable stiffness in the evaluation of the double leaf sound transmission prediction method is presented in Figure 9.59. Results calculated using the approximate model of the radiation impedance are presented as the analytical solution appears to

offer no significant improvements in the prediction accuracy. The model that incorporates the frequency dependant bending stiffness appears to perform worse than the model that utilises a constant stiffness value. As with the previous results the correlation above the critical frequency is very poor.

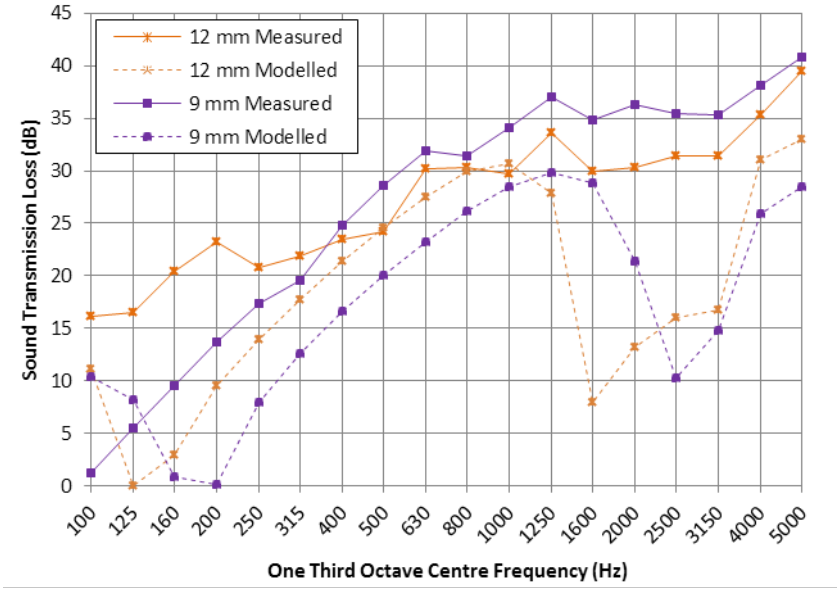

Figure 9.59: Transmission loss coefficient of 9 mm and 12 mm double leaf partitions calculated using approximated finite panel radiation impedance, and including a variable material stiffness

9.6.3. Conclusions

The transmission loss of all the double leaf wall systems was not predicted well using the analytical approach presented. This is due to the assumed absence of any cavity absorption and the assumption that no structural connection paths exist. Many commonly used prediction methods for the evaluation of the sound transmission loss of double leaf partitions require some small non-zero value for the absorption of an empty cavity. This absorption in the cavity significantly increases the predicted sound transmission loss.

The evaluation of the integral required to calculate the transmission coefficient encountered difficulties at frequencies at and above the coincidence frequency. The numerical integration routine used in this research was unable to converge within the specified number of iterations. This indicated that the high frequency results may not be a good representation of the actual sound transmission loss.

The incorporation of the analytical expression for the radiation impedance was not used due to computational requirements. The use of the approximate radiation impedance was shown earlier to be similar to the analytical solution. This was utilised as the error associated with the approximation was much lower than that caused by other assumptions used in the model.

Despite the large inaccuracies in the presented models it is hoped that it forms a good basis for developing a more comprehensive model for the performance of double leaf orthotropic partitions. This improvement may be achieved by the inclusion of cavity absorption, the incorporation of structural connection paths and the optimisation of the numerical integration method. These changes to the model should have different effects; the absorption in the cavity will cause an increase in the sound transmission loss whereas the inclusion of structure-borne transmission paths will result in a reduction in the sound transmission loss. Overall the changes should result in better agreement throughout the frequency range of interest.

10. Conclusions and Future Work

This section presents a conclusion of the findings made in this thesis. Paths and directions for future research are identified and discussed.

10.1. Conclusions

10.1.1. Sound Transmission Loss of Plywood

The sound transmission loss of different thicknesses of plywood panels were measured in both single and double leaf partitions, with various stud arrangements. The influence of the orthotropic, frequency dependent stiffness properties on the transmission loss was investigated. The combination of these factors causes the shape of the transmission loss curve to be spread out across a the frequency range. Figure 10.1 shows the typical effects caused by the orthotropic and frequency dependant stiffness on the sound transmission loss.

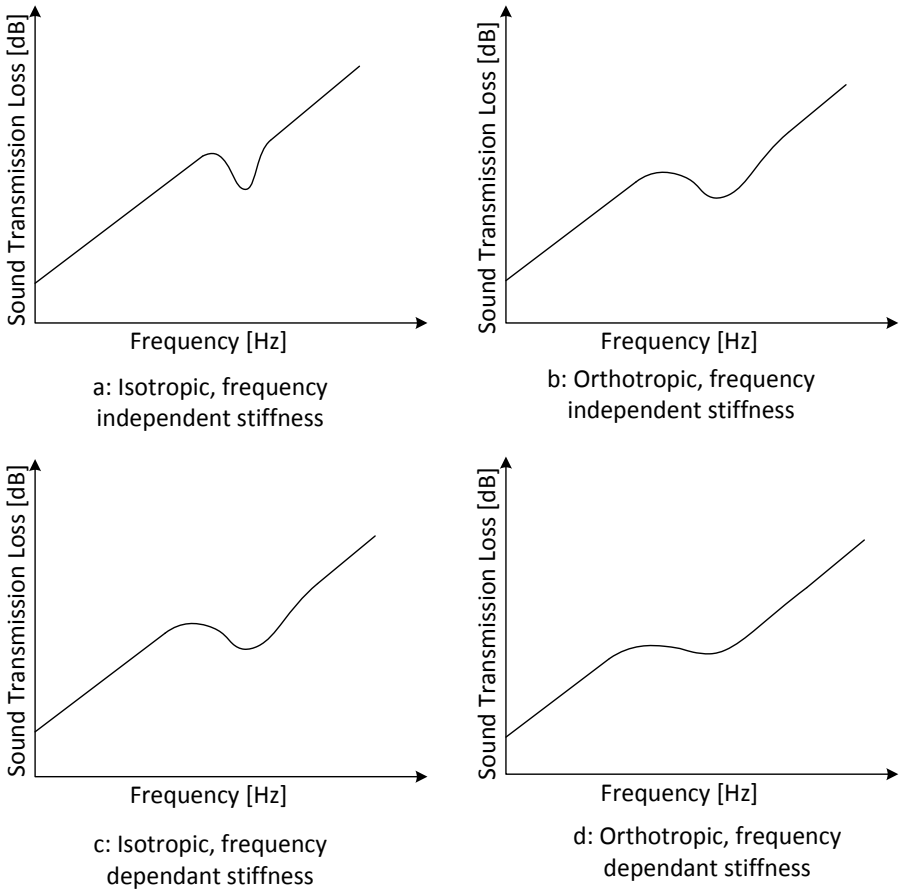

Figure 10.1: Typical influence of various stiffness parameters on the sound transmission loss

The influence of the orthotropic, frequency dependant stiffness on the sound transmission loss was evident in both single and double leaf partitions.

10.1.2. Size Effects

The influence of sample size on the measured sound transmission loss was evaluated for the partitions. The combined influence of the sample size, sample construction, and sample materials were investigated. A qualitative analysis of these factors was performed and was compared to published research.

It was found that decreasing the sample size increased the measured sound transmission loss. This change in the measured sound transmission loss due to the sample size was found to depend on the construction of the sample. The addition of a second leaf, with internal studs significantly reduced the change observed between the two sound transmission loss measurements. Further confounding the size effects was the increased influence of the sample niche for the smaller samples.

The sample size had the largest influence on the transmission loss below the coincidence region. The smaller samples had a significantly higher sound transmission loss below the coincidence region in all of the measured samples. Reducing the sample size caused the niche effect to become more pronounced, which in turn reduced the maximum angle that sound can be incident on the sample. As the maximum angle of incidence is reduced the start of the coincidence region occurred at higher frequencies.

The smaller sample size resulted in a slightly higher transmission loss above the coincidence region in most cases. The trends observed above the coincidence region were less consistent than those observed within and below the coincidence region. In the case of double leaf walls with studs the transmission loss above the coincidence region was observed to be very similar for both sample sizes.

Applying a correcting factor that adjusted for the different sound pressure levels on the surface of the two sample sizes resulted in an improved correlation between the results. This improvement was primarily in the frequency range within and above the coincidence region. This indicates that other factors, such as the reduced maximum angle of incidence, cause a significant amount of the variation between the two sample sizes.

10.1.3. Acoustic Treatment of Plywood

Two forms of acoustic treatments were explored. The first was a mass loaded barrier, spaced off the plywood with a layer of acoustic foam. The second treatment was a thin layer of viscoelastic

material sandwiched between two 6 mm plywood panels. The sound transmission losses of these treatments were measured to evaluate their effectiveness.

The addition of the decoupled mass loaded barrier was found to significantly influence the sound transmission loss. The thickness of the decoupling layer and the method by which the treatment was attached to the underlying panel were observed to have a large influence on the transmission loss of the system.

Increasing the thickness of the decoupling layer resulted in an increased sound transmission loss. This increase occurred above the effective mass-stiffness-mass resonance frequency that occurred between the underlying panel and the mass loaded barrier. Increasing the density of the mass loaded barrier also results in an increase in the sound transmission loss above the mass-stiffness-mass resonant frequency.

The attachment method was observed to alter the location of the mass-stiffness-mass resonant frequency, which resulted in changes to the overall sound transmission loss. Reducing the rigidity of the attachment method reduced the frequency at which the mass-stiffness-mass resonance occurred. Reducing this resonant frequency causes the system to enter a region where the sound transmission loss increased rapidly with frequency. Reducing the rigidity of the attachment method increases the sound transmission loss performance significantly.

A prediction method was developed using published theories to predict the transmission loss of the treated samples. The treated partitions were modelled as a double leaf wall system with a modified stiffness between the leaves. The attachment method was modelled using a range of different structural connection paths. The predicted transmission loss was generally within five decibels of the measured results, although in the case of fully glued samples the location of the mass air mass resonance was over predicted by approximately two thirds of an octave.

The treatment of the plywood with a thin layer of internal viscoelastic material significantly increased the sound transmission loss of the plywood. The inclusion of the viscoelastic into the plywood panels increased the damping loss factor by a factor of ten with very little change in the stiffness of the material. This increased damping loss factor acts primarily within the coincidence region by reducing the depth of the coincidence dip. This increased damping loss factor has a significant influence on the transmission loss of the double leaf plywood wall systems due to the increased importance of structural connection paths.

The damped plywood panels were modelled using the prediction methods developed in this thesis. The predicted results achieved agreement with the measured results to within five decibels

across much of the measured frequency range. Poor agreement was seen in some of the cases near the coincidence region.

10.1.4. Orthotropic, Frequency Dependent Prediction Methods

Several methods for predicting the sound transmission loss of single leaf orthotropic partitions were developed and evaluated. Analytical solutions for the bending wave impedance of an orthotropic panel, and the radiation impedance of a finite rectangular panel were utilised in the prediction of the sound transmission loss. These analytical forms required the use of adaptive numerical integration as the formation of the transmission coefficient did not admit an analytical solution.

The sound transmission loss of all the samples was predicted using the measured material properties. These predicted results were evaluated against the measured results for both the small and large transmission loss facilities. A comprehensive comparison of the results has been presented.

It was found that the introduction of an orthotropic stiffness into the transmission loss model improved the agreement between the measured and predicted results to a small degree. Introducing frequency dependent stiffness parameters resulted in a significant improvement of the accuracy of the predicted results.

The incorporation of a finite panel radiation impedance improved the agreement between the measured and predicted results, especially for the small sample size. This improvement is further enhanced by imposing a limitation on the maximum angle of incidence that the transmission coefficient is integrated across. This limiting angle is due to the finite sample size and the presence of the sample niche; which reduces the sound transmission contributions due to incoming waves from near grazing angles of incidence.

The use of an approximation for the finite radiation impedance reduced the required computational time significantly. This approximation removed the requirement to solve a double integral for the transmission coefficient which has a large influence on the computational requirements. This approximation of the finite panel radiation impedance was shown to produce reasonable agreement with the analytical solution.

The model developed in this thesis provides an effective and relatively efficient means for predicting the sound transmission loss of single leaf partitions constructed with orthotropic materials.

10.1.5. Overview

This research aimed to experimentally and analytically assess the sound transmission loss behaviour of plywood in both single and double leaf wall constructions. The sound transmission loss of a range of different plywood panels was evaluated experimentally using the pressure – intensity method. The material properties of all the samples evaluated were also evaluated. These measurements provide a comprehensive database to characterise the sound transmission behaviour of plywood.

The analytical models developed form the basis for the development of a comprehensive model of the sound transmission loss. The inclusion of frequency dependent and orthotropic stiffness properties, and an expression for the radiation impedance of a finite panel reduce the requirement for empirical corrections by introducing real-world constraints. Furthermore the application of existing double leaf wall models to the decoupled layer treatments provide a useful tool for predicting the performance of these systems.

10.2. Future Work

This section covers areas of research that should be pursued in order to improve the general understanding of the sound transmission loss of lightweight, orthotropic construction materials. Some of this research will be undertaken following the submission of this thesis.

10.2.1. Inhomogeneous Material Properties

The material properties of the plywood panels were assumed to be constant throughout the extent of the panel. This assumption was required for the presented derivations, but it may not be representative of the actual system behaviour. The models developed in this thesis did not account for the inhomogeneous material properties, and these may have an impact on the calculated sound transmission loss [137, 185]. These effects should be explored as it is an important factor that is not well understood. The material properties need to be assessed using both static and dynamic testing methodologies. If possible point wise intensity and vibration measurements should be used to identify the effects on inhomogeneity on the sound radiated from the panel.

10.2.2. Approximations for the Orthotropic Transmission Coefficient

The evaluation of the transmission coefficient derived in Section 9 required a relatively intensive numerical integration that was undertaken using Matlab's *integral2* function. Whilst this function is relatively simple to utilise it means that the calculations cannot be performed in a manner that does

not require relatively extensive computing capacity. If a suitable approximation could be developed then the calculations could be implemented in a spreadsheet, making the predictions easier.

10.2.3. Offset Damped Panels

In the damped material presented in Section 8.3 the damping layer is between two equal thickness panels. The location of the damping layer within the panel may affect the level of damping achieved. Offsetting the location of the damping layer may increase the shear applied to the layer, resulting in higher effective damping. Increasing the internal damping of the panels was shown to increase the sound transmission loss considerably.

10.2.1. Optimisation of Numerical Integration

The relatively smooth behaviour of the transmission coefficient curve indicates that alternative methods may be used to perform the numerical integration. Recent work by Ballagh *et al.* [186] indicated that the use of a Gauss-Legendre method for performing the integration of the transmission coefficient. The technique described in this paper may be applicable to the more complex problem described in this thesis, as its implementation may allow for significant reductions in the computational effort required.

10.2.1. Completion of Double Leaf Model

A number of changes should be made to the double leaf model to improve the agreement with measured results. These changes are the inclusion of a cavity finite level of absorption and the introduction of structural transmission paths. Further changes should be implemented to improve the numerical integration for the double leaf partition model.

References

1. Davy, J.L., et al., *The average specific forced radiation wave impedance of a finite rectangular panel.* Journal of the Acoustical Society of America, 2014. **136**(2): p. 525-536.
2. Wareing, R.R., J.L. Davy, and J.R. Pearse, *Predicting the sound insulation of plywood panels when treated with decoupled mass loaded barriers*. 2014. p. 1 - 38.
3. Wareing, R.R., J.R. Pearse, and J.L. Davy, *Variationins in the measured sound transmissin loss due to sample size and construction parameters*. 2014: Journal of Applied Acoustics. p. 20.
4. Wareing, R.R., et al., *Acoustic treatment of panels: Effect of attachment method*, in *Internoise*. 2013: Innsubruck, Austria. p. 1-9.
5. Wareing, R.R., J.L. Davy, and J.R. Pearse, *Effects of sample construction, sample size and niche depth on measured sound transmission loss* in *Internoise 2014*. 2014: Melbourne, Australia.
6. Davy, J.L., et al., *Approximate formulae for the average specific forced radiation wave impedance of a finite rectangular panel*, in *Internoise 2014*. 2014: Melbourne, Australia. p. 1 - 10.
7. Davy, J.L., et al., *The specific forced radiation wave impedance of a finite rectangular panel excited by a plane sound wave*, in *ICSV 21*. 2014: Beijing, China. p. 1-8.
8. Bies, D.A. and C.H. Hansen, *Engineering noise control*. 2nd ed. 1996, Cornwall: TJ Press (Padstow) Ltd. 736.
9. Kang, H.-J., et al., *An experimental investigation on the directional distribution of incident energy for the prediction of sound transmission loss.* Applied Acoustics, 2002. **63**(3): p. 283-294.
10. Pilkey, W.D., *Stress, Strain, and Structural Matricies*. Vol. 1. 1994, New York: John Wiley & Sons, Inc. 1458.
11. Gagliardini, L., J. Roland, and J. Guyader, *The use of a functional basis to calculate acoustic transmission between rooms.* Journal of Sound and Vibration, 1991. **145**(3): p. 457-478.
12. Kropp, W., A. Pietrzyk, and T. Kihlman, *On the meaning of the sound reduction index at low frequencies.* Acta Acustica, 1994. **2**(5): p. 379-392.
13. Magalhaes, M. and N. Ferguson, *Low frequency airborne sound transmission.* 2001.
14. Osipov, A., P. Mees, and G. Vermeir, *Low-frequency airborne sound transmission through single partitions in buildings.* Applied Acoustics, 1997. **52**(3): p. 273-288.
15. Mulholland, K. and R. Lyon, *Sound insulation at low frequencies.* The Journal of the Acoustical Society of America, 1973. **54**(4): p. 867-878.
16. Bravo, T. and S.J. Elliott, *Variability of low frequency sound transmission measurements.* The Journal of the Acoustical Society of America, 2004. **115**(6): p. 2986-2997.
17. Cremer, L., *Theorie der schalldämmung wände bei schrägem einfall.* Akustische Zeitschrift., 1942. **7**: p. 81-104.
18. Bhattacharya, M. and M. Crocker, *Forced vibration of a panel and radiation of sound into a room.* Acta Acustica united with Acustica, 1969. **22**(5): p. 275-294.
19. Bhattacharya, M., R. Guy, and M. Crocker, *Coincidence effect with sound waves in a finite plate.* Journal of Sound and Vibration, 1971. **18**(2): p. 157-169.

20. Fahy, F.J. and P. Gardonio, *Sound and structural vibration: radiation, transmission and response*. 2007, London: Academic press. 633.

21. Hopkins, C., *Sound insulation*. 2012: Routledge. 622.

22. Sharp, B.H., *Prediction methods for the sound transmission of building elements.* Noise Control Engineering, 1978. **11**(2): p. 53-63.

23. Thomson, W.T., *Transmission of elastic waves through a stratified solid medium.* Journal of applied Physics, 1950. **21**(2): p. 89-93.

24. Schmidt, H. and F.B. Jensen, *A full wave solution for propagation in multilayered viscoelastic media with application to Gaussian beam reflection at fluid–solid interfaces.* The Journal of the Acoustical Society of America, 1985. **77**(3): p. 813-825.

25. DiNapoli, F.R. and R.L. Deavenport, *Theoretical and numerical Green's function field solution in a plane multilayered medium.* The Journal of the Acoustical Society of America, 1980. **67**(1): p. 92-105.

26. Folds, D. and C. Loggins, *Transmission and reflection of ultrasonic waves in layered media.* The Journal of the Acoustical Society of America, 1977. **62**(5): p. 1102-1109.

27. Lee, C.M. and Y. Xu, *A modified transfer matrix method for prediction of transmission loss of multilayer acoustic materials.* Journal of Sound and Vibration, 2009. **326**(1-2): p. 290-301.

28. Brouard, B., D. Lafarge, and J.-F. Allard, *A general method of modelling sound propagation in layered media.* Journal of Sound and Vibration, 1995. **183**(1): p. 129-142.

29. Papadopoulos, C.I., *Development of an optimised, standard-compliant procedure to calculate sound transmission loss: design of transmission rooms.* Applied Acoustics, 2002. **63**(9): p. 1003-1029.

30. Papadopoulos, C.I., *Redistribution of the low frequency acoustic modes of a room: a finite element-based optimisation method.* Applied Acoustics, 2001. **62**(11): p. 1267-1285.

31. Trevathan, J., *Sound transmission through walls: A coupled BEM/FEM approach*, in *Mechanical Engineering*. 2005, University of Canterbury: Christchurch. p. 1-664.

32. del Coz Diaz, J., et al., *Sound transmission loss analysis through a multilayer lightweight concrete hollow brick wall by FEM and experimental validation.* Building and Environment, 2010. **45**(11): p. 2373-2386.

33. del Coz Diaz, J., et al. *Evaluation of the acoustic behaviour of the light concrete hollow bricks by FEM and experimental validation*. in *Proceedings of the CIATEA conference, Ediuno*. 2007.

34. Kang, Y.J. and J.S. Bolton, *A finite element model for sound transmission through foam-lined double-panel structures.* Journal of the Acoustical Society of America, 1996. **99**: p. 2755.

35. Maluski, S. and B. Gibbs, *A finite element method as a complementary tool for sound transmission between dwellings at low frequencies*. 2002, ICSV9.

36. Maluski, S.P. and B.M. Gibbs, *Application of a finite-element model to low-frequency sound insulation in dwellings.* The Journal of the Acoustical Society of America, 2000. **108**(4): p. 1741-1751.

37. Arjunan, A., et al., *Finite element acoustic analysis of a steel stud based double-leaf wall.* Building and Environment, 2013. **67**: p. 202-210.

38. Davidsson, P., et al., *Analysis of sound transmission loss of double-leaf walls in the low-frequency range using the finite element method.* Building Acoustics, 2004. **11**(4): p. 239-257.

39. Fahy, F.J., *Statistical energy analysis: a critical overview.* Philosophical Transactions of the Royal Society of London. Series A: Physical and Engineering Sciences, 1994. **346**(1681): p. 431-447.

40. Lyon, R.H. and G. Maidanik, *Power flow between linearly coupled oscillators.* The Journal of the Acoustical Society of America, 1962. **34**(5): p. 623-639.

41. Scharton, T.D. and R.H. Lyon, *Power flow and energy sharing in random vibration.* The Journal of the Acoustical Society of America, 1968. **43**(6): p. 1332-1343.

42. Hodges, C. and J. Woodhouse, *Theories of noise and vibration transmission in complex structures.* Reports on Progress in Physics, 1986. **49**(2): p. 107.

43. International, A., *ASTM E413 - 10*, in *Classification for Rating Sound Insulation*. 2003, ASTM Standards.

44. ISO, *ISO 717-1:1996*, in *Acoustics -- Rating of sound insulation in buildings and of building elements -- Part 1: Airborne sound insulation*. 1996.

45. London, A., *Transmission of reverberant sound through single walls.* J. Research Nat. Bur. of Stand, 1949. **42**(605): p. 2.

46. Heckl, M., *Untersuchungen an orthotropen Platten.* Acta Acustica united with Acustica, 1960. **10**: p. 109-115.

47. Sewell, E., *Transmission of reverberant sound through a single-leaf partition surrounded by an infinite rigid baffle.* Journal of Sound and Vibration, 1970. **12**(1): p. 21-32.

48. Cremer, L., *Theory of sound attenuation of thin walls at oblique incidence.* Architectual Acoustics, 1977. **10**: p. 367-399.

49. Davy, J.L. *A model for predicting the sound transmission loss of walls*. in *Australian Vibration and Noise Conference 1990: Vibration and Noise-measurement Prediction and Control; Preprints of Papers*. 1990. Institution of Engineers, Australia.

50. Buckingham, E., *Theory and interpretation of experiments on the transmission of sound through partition walls*. 1925: Govt. Print. Off.

51. Beranek, L.L. and G.A. Work, *Sound transmission through multiple structures containing flexible blankets.* The Journal of the Acoustical Society of America, 1949. **21**(4): p. 419-428.

52. Kimball, A., *Theory of transmission of plane sound waves through multiple partitions.* The Journal of the Acoustical Society of America, 1936. **7**(3): p. 222-224.

53. Antonio, J., A. Tadeu, and L. Godinho, *Analytical evaluation of the acoustic insulation provided by double infinite walls.* Journal of Sound and Vibration, 2003. **263**(1): p. 113-129.

54. Tadeu, A.J. and D.M. Mateus, *Sound transmission through single, double and triple glazing. Experimental evaluation.* Applied Acoustics, 2001. **62**(3): p. 307-325.

55. London, A., *Transmission of reverberant sound through double walls.* Journal of the Acoustical Society of America, 1950. **22**: p. 270-279.

56. London, A., *Transmission of reverberant sound through single walls.* Journal of Research of the National Bureau of Standards, 1949. **42**(6): p. 605-615.

57. Hongisto, V., M. Lindgren, and R. Helenius, *Sound insulation of double walls–An experimental parametric study.* Acta Acustica united with Acustica, 2002. **88**(6): p. 904-923.

58. Rinsk, A. and R.H. Lyon, *Effect of Studs and Cavity Absorption on the Sound Transmission Loss of Plasterboard Walls.* The Journal of the Acoustical Society of America, 1973. **53**(1): p. 387-387.

59. Poblet-Puig, J., et al., *The role of studs in the sound transmission of double walls.* Acta Acustica united with Acustica, 2009. **95**(3): p. 555-567.

60. Davy, J.L. *The sound transmission of cavity walls due to studs*. in *INTERNOISE*. 1993. NOISE CONTROL FOUNDATION.

61. Clive, L.D., C.S. Ventres, and A.L. Mark, *Transmission of sound through sandwich panels: A reconsideration.* Journal of the Acoustical Society of America, 1976. **59**(2): p. 364-367.

62. Brunskog, J., *The influence of finite cavities on the sound insulation of double-plate structures.* The Journal of the Acoustical Society of America, 2005. **117**(6): p. 3727-3739.

63. Ford, R., P. Lord, and P. Williams, *The influence of absorbent linings on the transmission loss of double-leaf partitions.* Journal of Sound and Vibration, 1967. **5**(1): p. 22-28.

64. Trochidis, A. and A. Kalaroutis, *Sound transmission through double partitions with cavity absorption.* Journal of Sound and Vibration, 1986. **107**(2): p. 321-327.

65. Loney, W., *Effect of cavity absorption and multiple layers of wallboard on the sound-transmission loss of steel-stud partitions.* The Journal of the Acoustical Society of America, 1973. **53**(6): p. 1530-1534.

66. Uris, A., et al., *Influence of screw spacings on sound reduction index in lightweight partitions.* Applied Acoustics, 2002. **63**(7): p. 813-818.

67. Warnock, A., *Influence of specimen frame on sound transmission loss measurement.* Applied Acoustics, 1982. **15**(4): p. 307-314.

68. Nightingale, T. and J. Quirt, *Effect of electrical outlet boxes on sound insulation of a cavity wall.* The Journal of the Acoustical Society of America, 1998. **104**(1): p. 266-274.

69. Kurtze, G. and B. Watters, *New wall design for high transmission loss or high damping.* The Journal of the Acoustical Society of America, 1959. **31**(6): p. 739-748.

70. Rao, M.D., *Recent applications of viscoelastic damping for noise control in automobiles and commercial airplanes.* Journal of Sound and Vibration, 2003. **262**(3): p. 457-474.

71. Tohyama, M. and T. Itow, *Theoretical Interpretation of the Mass Law Based on the Wave Theory.* Acta Acustica united with Acustica, 1974. **30**(1): p. 1-11.

72. Sharp, B.H., *A study of techniques to increase the sound insulation of building elements*. 1973, US Department of Commerce, National Technical Information Service (NTIS).

73. Josse, R. and C. Lamure, *Transmission du son par une paroi simple.* Acta Acustica united with Acustica, 1964. **14**(5): p. 266-280.

74. Davy, J.L., *Predicting the sound insulation of walls.* Building Acoustics, 2009. **16**(1): p. 1-20.

75. Davy, J.L., *The improvement of a simple theoretical model for the prediction of the sound insulation of double leaf walls.* Journal of the Acoustical Society of America, 2010. **127**: p. 841-849.

76. Davy, J.L. *Predicting the sound insulation of stud walls*. in *Proceedings of Internoise*. 1991.

77. Davy, J.L., *Predictiong the sound insulation of single leaf walls: Extension of Cremer's model.* Journal of the Acoustical Society of America, 2009. **126**(4): p. 1871-1877.

78. Davy, J.L., *Sound transmission of cavity walls due to structure borne transmission via point and line connections.* Journal of the Acoustical Society of America, 2012. **132**: p. 814-821.

79. Sato, H., *On the mechanism of outdoor noise transmission through walls and windows.* Journal of the Acoustical Society of Japan, 1973. **29**: p. 509-516.

80. Heckl, M. and U. Donner, *Schalldämmung dicker Wände (Sound insulation of thick walls).* Rundfunktech Mitt, 1985. **29**: p. 287-291.

81. Mulholland, K., H. Parbrook, and A. Cummings, *The transmission loss of double panels.* Journal of Sound and Vibration, 1967. **6**(3): p. 324-334.

82. Tadeu, A. and J. António, *Acoustic insulation of single panel walls provided by analytical expressions versus the mass law.* Journal of Sound and Vibration, 2002. **257**(3): p. 457-475.

83. Tadeu, A., J. António, and D. Mateus, *Sound insulation provided by single and double panel walls—a comparison of analytical solutions versus experimental results.* Applied Acoustics, 2004. **65**(1): p. 15-29.

84. Bradley, J. and J. Birta, *A simple model of the sound insulation of gypsum board on resilient supports.* Noise Control Engineering Journal, 2001. **49**(5): p. 216-223.

85. Fringuellino, M. and C. Guglielmone, *Progressive Impedance Method for the classical analysis of acoustic transmission loss in multilayered walls.* Applied Acoustics, 2000. **59**(3): p. 275-285.

86. Mangiarotty, R., *Optimization of the Mass Distribution and the Air Spaces in Multiple-Element Soundproofing Structures.* The Journal of the Acoustical Society of America, 1963. **35**(7): p. 1023-1029.

87. Cummings, A. and K. Mulholland, *The transmission loss of finite sized double panels in a random incidence sound field.* Journal of Sound and Vibration, 1968. **8**(1): p. 126-133.

88. Mulholland, K., A. Price, and H. Parbrook, *Transmission loss of multiple panels in a random incidence field.* Journal of the Acoustical Society of America, 1968. **43**: p. 1432.

89. Utley, W. and K. Mulholland, *The transmission loss of double and triple walls.* Applied Acoustics, 1968. **1**(1): p. 15-20.

90. Price, A. and M.J. Crocker, *Sound transmission through double panels using statistical energy analysis.* Journal of the Acoustical Society of America, 1970. **47**: p. 683.

91. Craik, R.J., *Sound transmission through buildings: using statistical energy analysis.* Journal of Sound and Vibration, 1969. **9**(3): p. 469-486.

92. Craik, R.J., *The prediction of sound transmission through buildings using statistical energy analysis.* Journal of sound and Vibration, 1982. **82**(4): p. 505-516.

93. Hongisto, V., *Sound insulation of double panels-comparison of existing prediction models.* Acta acustica united with acustica, 2006. **92**(1): p. 61-78.

94. Haskell, N.A., *The dispersion of surface waves on multilayered media.* Bulletin of the Seismological Society of America, 1953. **43**(1): p. 17-34.

95. Dorman, J., *Period equation for waves of Rayleigh type on a layered, liquid-solid half space.* Bulletin of the Seismological Society of America, 1962. **52**(2): p. 389-397.

96. Knopoff, L., *A matrix method for elastic wave problems.* Bulletin of the Seismological Society of America, 1964. **54**(1): p. 431-438.

97. Rosenbaum, J., *The long-time response of a layered elastic medium to explosive sound.* Journal of Geophysical Research, 1960. **65**(5): p. 1577-1613.

98. Lowe, M.J., *Matrix techniques for modeling ultrasonic waves in multilayered media.* Ultrasonics, Ferroelectrics and Frequency Control, IEEE Transactions on, 1995. **42**(4): p. 525-542.

99. Sastry, J. and M. Munjal, *A transfer matrix approach for evaluation of the response of a multi-layer infinite plate to a two-dimensional pressure excitation.* Journal of sound and vibration, 1995. **182**(1): p. 109-128.

100. Lee, C.-M. and Y. Wang, *A prediction method of the acoustical properties of multilayered noise control materials in standing wave-duct systems.* Journal of sound and vibration, 2006. **298**(1): p. 350-365.

101. Vigran, T., *Sound transmission in multilayered structures–Introducing finite structural connections in the transfer matrix method.* Applied Acoustics, 2010. **71**(1): p. 39-44.

102. Vigran, T., *Sound insulation of double-leaf walls–Allowing for studs of finite stiffness in a transfer matrix scheme.* Applied Acoustics, 2010. **71**(7): p. 616-621.

103. Munjal, M.L., *Acoustics of ducts and mufflers*. 2014: John Wiley & Sons.

104. Villot, M., C. Guigou, and L. Gagliardini, *Predicting the acoustical radiation of finite size multi-layered structures by applying spatial windowing on infinite structures.* Journal of Sound and Vibration, 2001. **245**(3): p. 433-455.

105. Villot, M. and C. Guigou-Carter, *Using spatial windowing to take the finite size of plane structures into account in sound transmission.* NOVEM, 2005.

106. Norrie, D.H. and G. De Vries, *The finite element method.* 1973.

107. Cook, R.D., *Concepts and applications of finite element analysis*. 2007: John Wiley & Sons.

108. Everstine, G., *Finite element formulatons of structural acoustics problems.* Computers & Structures, 1997. **65**(3): p. 307-321.

109. Bathe, K., C. Nitikitpaiboon, and X. Wang, *A mixed displacement-based finite element formulation for acoustic fluid-structure interaction.* Computers & Structures, 1995. **56**(2): p. 225-237.

110. Wang, X. and K.J. Bathe, *Displacement/pressure based mixed finite element formulations for acoustic fluid-structure interaction problems.* International Journal for Numerical Methods in Engineering, 1997. **40**(11): p. 2001-2017.

111. Watters, B., *Impact-Noise Characteristics of Female Hard-Heeled Foot Traffic.* Journal of the Acoustical Society of America, 1965. **37**: p. 619.

112. Ihlenburg, F., *Finite element analysis of acoustic scattering*. Vol. 132. 1998: Springer.

113. Tezaur, R., et al., *Three-dimensional finite element calculations in acoustic scattering using arbitrarily shaped convex artificial boundaries.* International journal for numerical methods in engineering, 2002. **53**(6): p. 1461-1476.

114. Rienstra, S.W. and W. Eversman, *A numerical comparison between the multiple-scales and finite-element solution for sound propagation in lined flow ducts.* Journal of Fluid Mechanics, 2001. **437**: p. 367-384.

115. Langlet, P., A.C. Hladky-Hennion, and J.N. Decarpigny, *Analysis of the propagation of plane acoustic waves in passive periodic materials using the finite element method.* The Journal of the Acoustical Society of America, 1995. **98**(5): p. 2792-2800.

116. Krajči, L., et al., *Airborne sound transmission of a cross-laminated timber plate with orthotropic stiffness.*

117. Guyader, J. and C. Lesueur, *Acoustic transmission through orthotropic multilayered plates, part ii: Transmission loss.* Journal of Sound and Vibration, 1978. **58**(1): p. 69-86.

118. Guyader, J. and C. Lesueur, *Acoustic transmission through orthotropic multilayered plates, part i: plate vibration modes.* Journal of Sound and Vibration, 1978. **58**(1): p. 51-68.

119. Frederiksen, P.S., *Experimental procedure and results for the identification of elastic constants of thick orthotropic plates.* Journal of Composite Materials, 1997. **31**(4): p. 360-382.

120. Hansen, C.H., *Sound transmission loss of corrugated panels.* Noise Control Engineering Journal, 1993. **40**(2): p. 187-197.

121. Hansen, C., *Sound Transmission Loss of Fluted and Corrugated Panels-Damped and Undamped.* Proceedings of Interior Noise Climates, Australian Acoustical Society, Perth, 1990: p. 19-20.

122. Ordubadi, A. and R.H. Lyon, *Effect of orthotropy on the sound transmission through plywood panels.* Journal of the Acoustical Society of America, 1979. **65**(1): p. 133-139.

123. Leissa, A.W., *Vibration of plates*. 1969, DTIC Document. p. 1-353.

124. Rasmussen, B. and J.H. Rindel, *Sound insulation between dwellings–Descriptors applied in building regulations in Europe.* Applied Acoustics, 2010. **71**(3): p. 171-180.

125. Rasmussen, B., *Sound insulation between dwellings–Requirements in building regulations in Europe.* Applied Acoustics, 2010. **71**(4): p. 373-385.

126. ASTM, *ASTM E413 - 10*, in *Classification for Rating Sound Insulation*. 2003, ASTM Standards. p. 1-4.

127. Wallace, C., *Radiation resistance of a rectangular panel.* Journal of the Acoustical Society of America, 1972. **51**: p. 946.

128. Thomasson, S.-I., *On the absorption coefficient.* Acta Acustica united with Acustica, 1980. **44**(4): p. 265-273.

129. Thomasson, S.-I., *Theory and experiments on the sound absorption as function of the area*. 1982: Department of Acoustics, Royal Institute of Technology. p. 1-43.

130. Li, W. and H. Gibeling, *Determination of the mutual radiation resistances of a rectangular plate and their impact on the radiated sound power.* Journal of Sound and Vibration, 2000. **229**(5): p. 1213-1233.

131. Allard, J. and N. Atalla, *Propagation of Sound in Porous Media: Modelling Sound Absorbing Materials 2e*. 2009: John Wiley & Sons.

132. Berry, A., J.L. Guyader, and J. Nicolas, *A general formulation for the sound radiation from rectangular, baffled plates with arbitrary boundary conditions.* Journal of the Acoustical Society of America, 1990. **88**: p. 2792.

133. Novak, R., *Radiation from partially excited plates.* ACTA ACUSTICA-LES ULIS-, 1995. **3**: p. 561-568.

134. Ljunggren, S., *Airborne sound insulation of thin walls.* The Journal of the Acoustical Society of America, 1991. **89**(5): p. 2324-2337.

135. Davy, J.L. *The radiation efficiency of finite size flat panels*. in *Annual Conference of the Australian Acoustical Society*. 2004. Australian Acoustical Society.

136. International, A., *ASTM E756 - 05(2010)*, in *Standard test method for measuring vibration-damping properties of materials*. 2010.

137. Kouyoumji, J.L. and L. Vermois. *An exploratory study about taking into account heterogeneity of a material in the calculation of it's sound transmission loss*. in *INTER-NOISE and NOISE-CON Congress and Conference Proceedings*. 2005. Institute of Noise Control Engineering.

138. Ghinet, S. and N. Atalla, *Sound transmission loss of insulating complex structures.* Canadian Acoustics, 2001. **29**(3): p. 26-27.

139. ASTM, *ASTM D1621-10: Test method for compressive properties of rigid cellular plastics*. 2010.

140. ISO, *ISO 15186-1:2000*, in *Acoustics -- Measurement of sound insulation in buildings and of building elements using sound intensity -- Part 1: Laboratory measurments*. 2000. p. 1-14.

141. ISO, *ISO 10140-5:2010*, in *Acoustics -- Laboratory measurement of sound insulation of building elements -- Part 5: Requirements for test facilities and equipment*. 2010. p. 1-35.

142. Fahy, F.J., *Sound intensity*. 2002: CRC Press. 295.

143. Fahy, F., *A technique for measuring sound intensity with a sound level meter.* Noise Control Engineering, 1977. **9**(3): p. 155-162.

144. Pascal, J. and C. Carles, *Systematic measurement errors with two microphone sound intensity meters.* Journal of Sound and Vibration, 1982. **83**(1): p. 53-65.

145. Thompson, J. and D. Tree, *Finite difference approximation errors in acoustic intensity measurements.* Journal of Sound and Vibration, 1981. **75**(2): p. 229-238.

146. Elliott, S., *Errors in acoustic intensity measurements.* Journal of Sound and Vibration, 1981. **78**(3): p. 439-443.

147. Watkinson, P., *The practical assessment of errors in sound intensity measurement.* Journal of sound and vibration, 1986. **105**(2): p. 255-263.

148. Tandon, N., *A brief summary of sound intensity measurements and their application to noise control.* Applied Acoustics, 1989. **28**(1): p. 37-47.

149. Pavić, G., *Measurement of sound intensity.* Journal of Sound and Vibration, 1977. **51**(4): p. 533-545.

150. Jacobsen, F., *A simple and effective correction for phase mis-match in intensity probes.* Applied Acoustics, 1991. **33**(3): p. 165-180.

151. Jacobsen, F., V. Cutanda, and P.M. Juhl, *A numerical and experimental investigation of the performance of sound intensity probes at high frequencies.* The Journal of the Acoustical Society of America, 1998. **103**(2): p. 953-961.

152. ISO, *ISO 10140-4:2010*, in *Acoustics -- Laboratory measurement of sound insulation of building elements -- Part 4: Measurement procedures and requirements*. 2010. p. 1-12.

153. ISO, *10140-4:2010*, in *ISO Acoustics -- Laboratory measurement of sound insulation of building elements -- Part 4: Measurement procedures and requirements*. 2010.

154. Kihlman, T. and A.C. Nilsson, *The effects of some laboratory designs and mounting conditions on reduction index measurements.* Journal of Sound and Vibration, 1972. **24**(3): p. 349-364.

155. Sakuma, T., K. Adachi, and Y. Yasuda. *Numerical investigation of the niche effect in sound insulation measurement*. in *INTER-NOISE and NOISE-CON Congress and Conference Proceedings*. 2011. Institute of Noise Control Engineering.

156. Dijckmans, A. and G. Vermeir, *A wave based model to predict the niche effect on sound transmission loss of single and double walls.* Acta Acustica united with Acustica, 2012. **98**(1): p. 111-119.

157. Vinokur, R., *Mechanism and calculation of the niche effect in airborne sound transmission.* The Journal of the Acoustical Society of America, 2006. **119**(4): p. 2211-2219.

158. Kim, B.-K., et al., *Tunneling effect in sound transmission loss determination: Theoretical approach.* The Journal of the Acoustical Society of America, 2004. **115**(5): p. 2100-2109.

159. Michelsen, N., *Effect of size on measurements of the sound reduction index of a window or a pane.* Applied Acoustics, 1983. **16**(3): p. 215-234.

160. Yoshimura, J., S. Sugie, and E. Toyoda. *Effects of size and edge damping on measurement results for sound reduction index of glass pane*. in *INTER-NOISE and NOISE-CON Congress and Conference Proceedings*. 2006. Institute of Noise Control Engineering.

161. Bhattacharya, M. and R. Guy, *The influence of the measuring facility on the measured sound insulating property of a panel.* Acta Acustica united with Acustica, 1972. **26**(6): p. 344-348.

162. Nilsson, A., *Reduction index and boundary conditions for a wall between two rectangular rooms. Part I: Theoretical results.* Acta Acustica united with Acustica, 1972. **26**(1): p. 1-18.

163. Guy, R., A. De Mey, and P. Sauer, *The effect of some physical parameters upon the laboratory measurements of sound transmission loss.* Applied Acoustics, 1985. **18**(2): p. 81-98.

164. Leppington, F., E. Broadbent, and K. Heron, *Acoustic radiation from rectangular panels with constrained edges.* Proceedings of the Royal Society of London. A. Mathematical and Physical Sciences, 1984. **393**(1804): p. 67-84.

165. Nilsson, A., *Reduction index and boundary conditions for a wall between two rectangular rooms. Part II: Experimental results.* Acta Acustica united with Acustica, 1972. **26**(1): p. 19-23.

166. Maidanik, G., *Response of ribbed panels to reverberant acoustic fields.* the Journal of the Acoustical Society of America, 1962. **34**(6): p. 809-826.

167. ISO, *ISO 10140-2:2010*, in *Acoustics -- Laboratory measurement of sound insulation of building elements -- Part 2: Measurement of airborne sound insulation*. 2010. p. 1-13.

168. Van Zyl, B., P. Erasmus, and G. van der Merwe, *A comparative study of the classic method and the sound intensity method for determining sound insulation.* NPRL Report FIS 320 Council for Scientific and Industrial Research, Pretoria, Republic of South Africa, 1985.

169. Van Zyl, B., P. Erasmus, and F. Anderson, *On the formulation of the intensity method for determining sound reduction indices.* Applied Acoustics, 1987. **22**(3): p. 213-228.

170. Halliwell, R. and A. Warnock, *Sound transmission loss: Comparison of conventional techniques with sound intensity techniques.* Journal of the Acoustical Society of America, 1985. **77**(6): p. 2094-2103.

171. Hansen, C.H. *Effect of size on the sound transmission loss of both heavily and lightly damped orthotropic panels*. in *INTER-NOISE Conference Proceedings*. 1991. Institute of Noise Control Engineering.

172. Kihlman, T., *Sound transmission in building structures of concrete.* Journal of Sound and Vibration, 1970. **11**(4): p. 435-445.

173. Utley, W. and B. Fletcher, *Influence of edge conditions on the sound insulation of windows.* Applied Acoustics, 1969. **2**(2): p. 131-136.

174. Davy, J.L., *The directivity of the forced radiation of sound from panels and openings including the shadow zone.* Journal of the Acoustical Society of America, 2008. **123**(5): p. 3499-3499.

175. Davy, J.L., *The forced radiation efficiency of finite size flat panels that are excited by incident sound.* The Journal of the Acoustical Society of America, 2009. **126**(2): p. 694-702.

176. Sakuma, T., K. Egawab, and Y. Yasudac, *Numerical analysis of sound transmission loss of glass pane-On the treatment of edge damping.* moment, 2008. **500**: p. 2w.

177. Tetsuya, S., *Numerical Investigation of the Niche Effect in Sound Insulation Measurement.* Inter-noise 2011, INCE, 2011.

178. Lomas, N. and S. Hayek, *Vibration and acoustic radiation of elastically supported rectangular plates.* Journal of Sound and Vibration, 1977. **52**(1): p. 1-25.

179. Lai, H.-Y., et al., *Layered fibrous treatments for a sound absorption and sound transmission*. 1997, SAE Technical Paper. p. 3311-3318.

180. Song, B.H. and J.S. Bolton, *A transfer-matrix approach for estimating the characteristic impedance and wave numbers of limp and rigid porous materials.* Journal of the Acoustical Society of America, 2000. **107**(3): p. 1131-1152.

181. ASTM, *E413-10*, in *Classification for rating sound insulation*.

182. Ver, I.L., *Interaction of sound waves with solid structures*, in *Noise and Vibration Control Engineering: Principles and Applications, Second Edition*. 1971, John Wiley & Sons, Inc.: Hoboken, NJ, USA. p. 389-515.

183. Cremer, L. and M. Heckl, *Structure-borne sound: structural vibrations and sound radiation at audio frequencies.* Berlin and New York, Springer-Verlag, 1988, 590 p., 1988. **1**.

184. Morse, P.M., *Theoretical acoustics*. 1986: Princeton University Press.

185. Kouyoumji, J.L. and L. Vernois. *Experimental and analytic study about non-homogeneous plate sound transmission loss*. in *INTER-NOISE and NOISE-CON Congress and Conference Proceedings*. 2006. Institute of Noise Control Engineering.

186. Ballagh, K.O. and H. Chung, *Prediction of Acoustic Performance of Composite Steel Floors*, in *Internoise 2014*. 2014: Melbourne, Australia. p. 1 - 5.

Appendices

Three appendices are included that provide detailed sets of results of the sound transmission loss measurements and the vibration performance measurements. Appendix A presents the transmission loss results from the small transmission loss facility. Appendix B presents the transmission loss results from the large transmission loss facility. Appendix C presents the vibration results used to evaluate the material properties of the plywood.

A. Detailed Results of Small Transmission Loss Tests

This appendix presents all the transmission loss measurements performed in the small transmission loss rig referred to in Section 5. These measurements are presented with their respective pressure-intensity indexes, repeatability indexes, transmission loss curves, transmission loss values, and single number ratings.

A.1. Single Leaf 7 mm Plywood

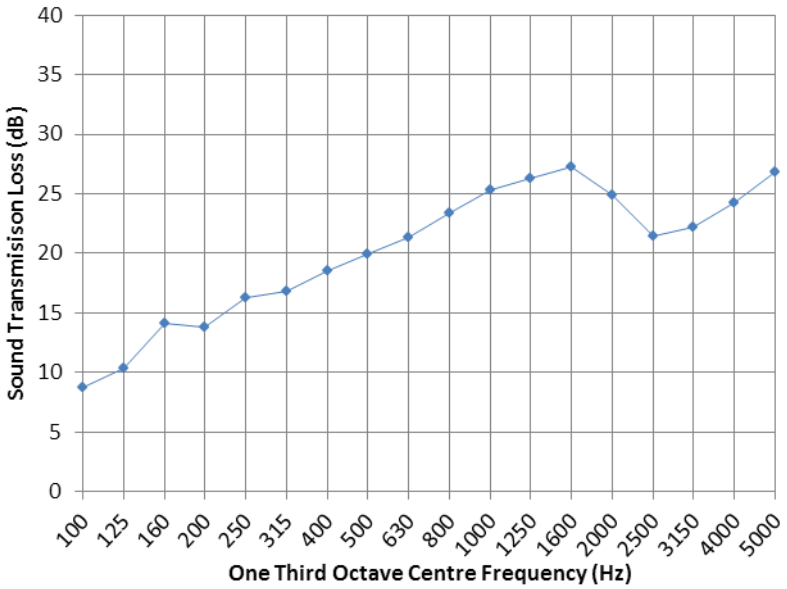

Figure A.1: Measured sound transmission loss of single leaf 7 mm plywood panel, measured in the small transmission loss facility

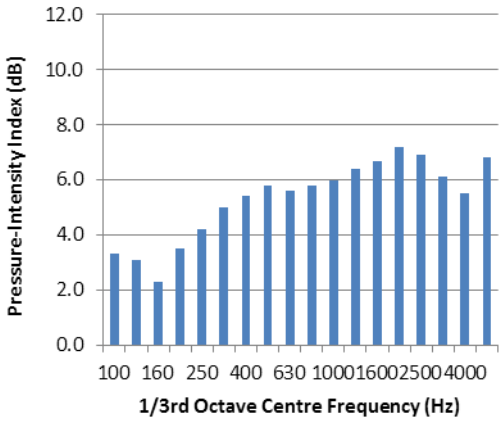

Figure A.2: Pressure-intensity index of intensity measurements for a single leaf 7 mm plywood sample

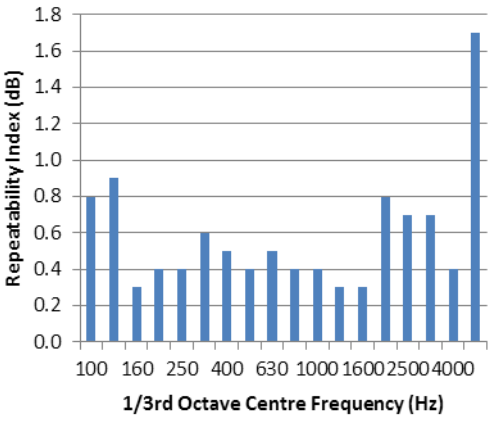

Figure A.3: Repeatability index of intensity measurements for a single leaf 7 mm plywood sample

Table A.1: Single number ratings of 7 mm single leaf plywood sample, measured in small transmission loss facility

Single Number Rating	Result
STC	23
R_w	23

A.2. Single Leaf 9 mm Plywood

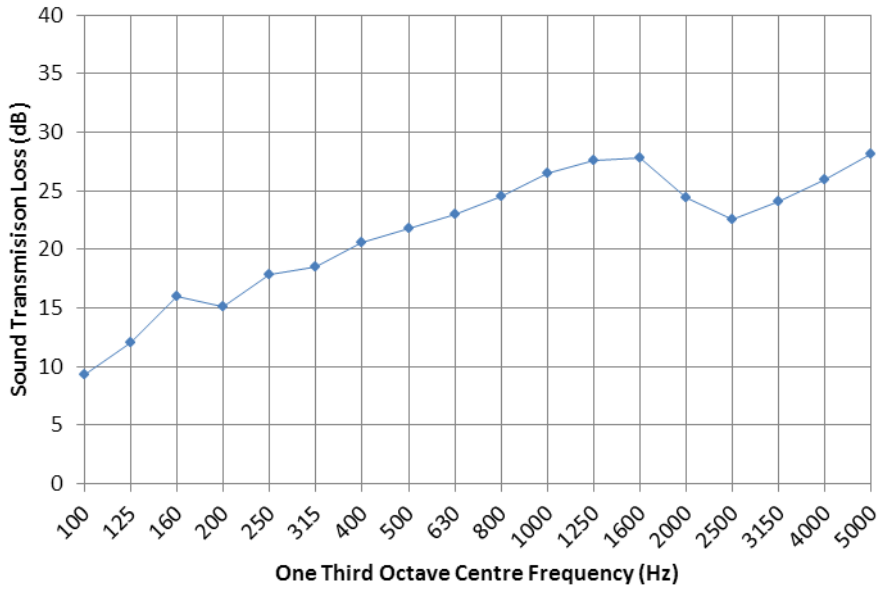

Figure A.4:Measured sound transmission loss of single leaf 9 mm plywood panel, measured in the small transmission loss facility

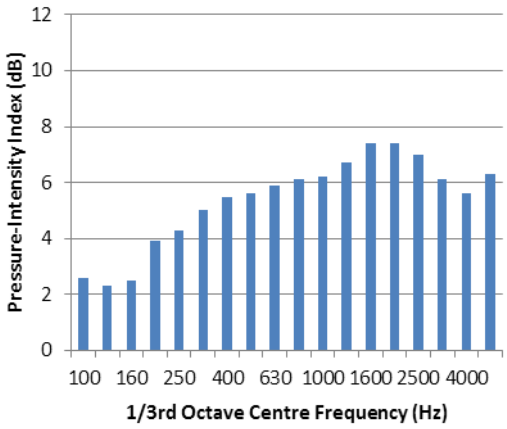

Figure A.5: Pressure-intensity index of intensity measurements for a single leaf 9 mm plywood sample

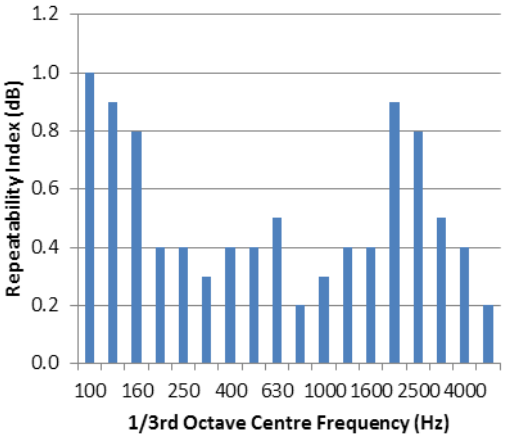

Figure A.6: Repeatability index of intensity measurements for a single leaf 9 mm plywood sample

Table A.2: Single number ratings of 9 mm single leaf plywood sample, measured in small transmission loss facility

Single Number Rating	Result
STC	24
R_w	24

A.3. Single Leaf 12 mm Plywood

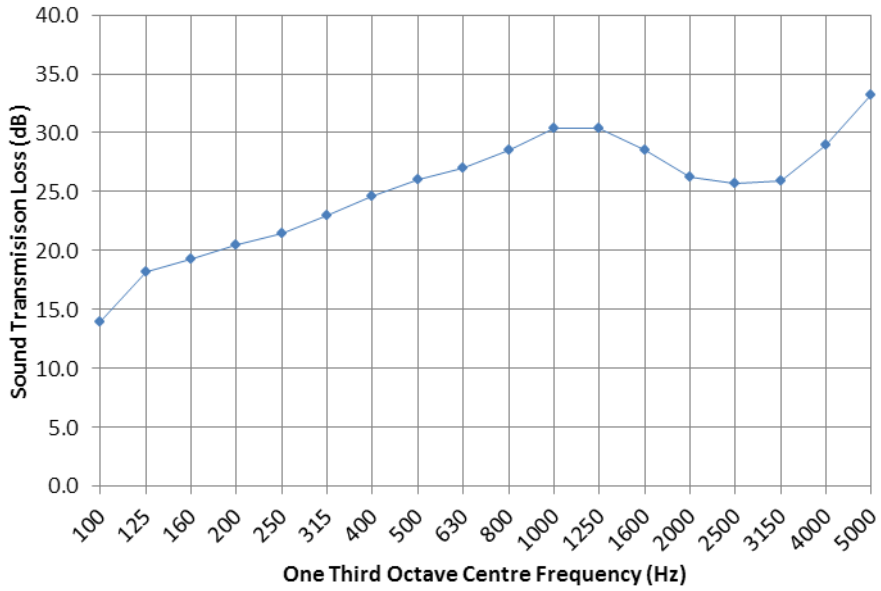

Figure A.7: Measured sound transmission loss of single leaf 12 mm plywood panel, measured in the small transmission loss facility

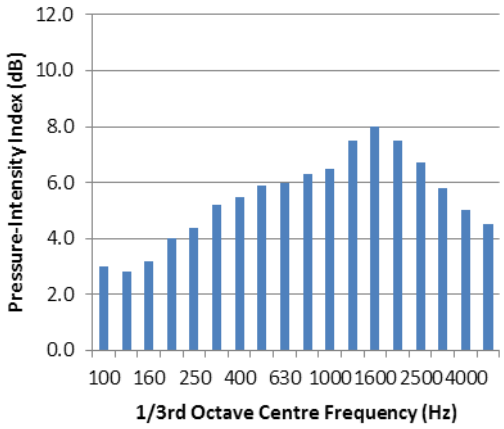

Figure A.8: Pressure-intensity index of intensity measurements for a single leaf 12 mm plywood sample

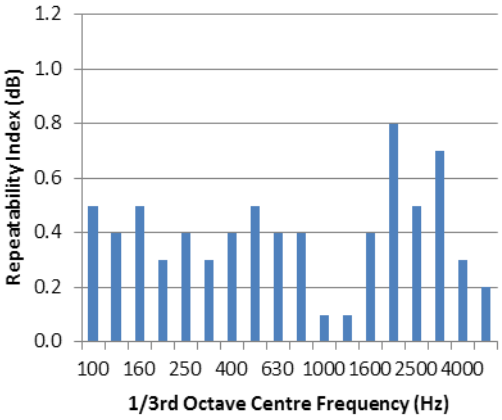

Figure A.9: Repeatability index of intensity measurements for a single leaf 12 mm plywood sample

Table A.3: Single number ratings of 12 mm single leaf plywood sample, measured in small transmission loss facility

Single Number Rating	Result
STC	27
R_w	27

A.4. Single Leaf 15 mm Plywood

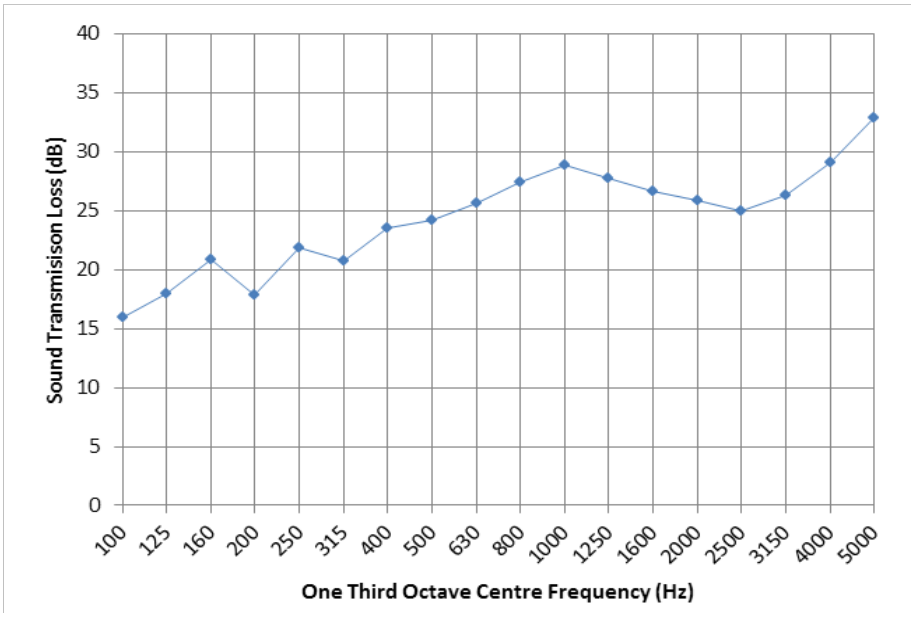

Figure A.10: Measured sound transmission loss of single leaf 15 mm plywood panel, measured in the small transmission loss facility

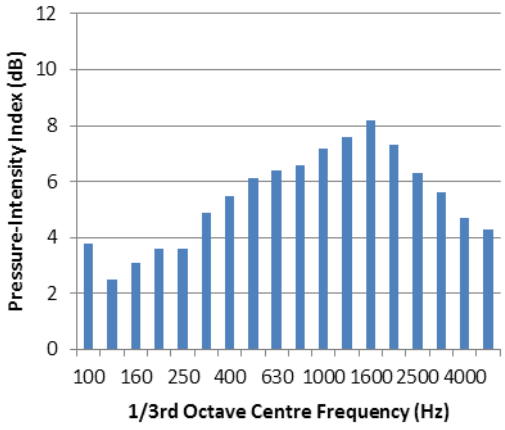

Figure A.11: Pressure-intensity index of intensity measurements for a single leaf 15 mm plywood sample

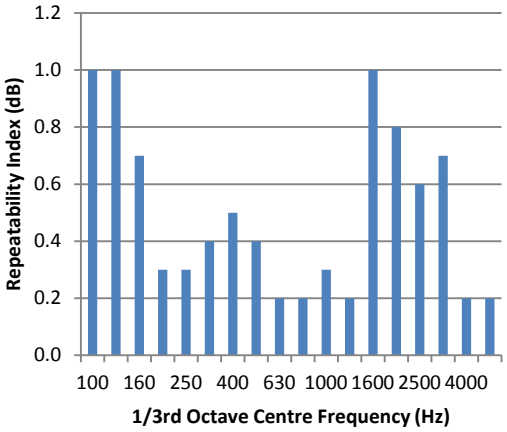

Figure A.12: Repeatability index of intensity measurements for a single leaf 15 mm plywood sample

Table A.4: Single number ratings of 15 mm single leaf plywood sample, measured in small transmission loss facility

Single Number Rating	Result
STC	27
R_w	27

A.5. Single Leaf 17 mm Plywood

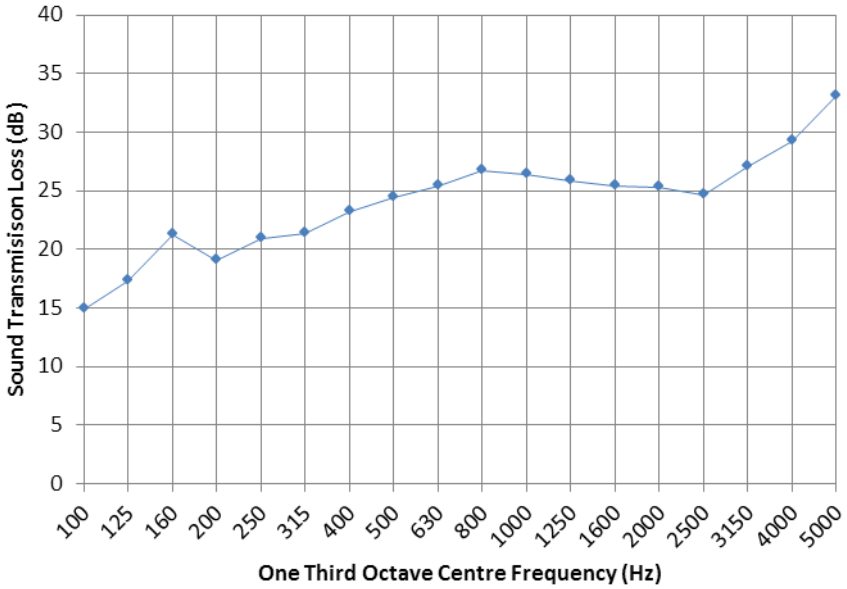

Figure A.13: Measured sound transmission loss of single leaf 17 mm plywood panel, measured in the small transmission loss facility

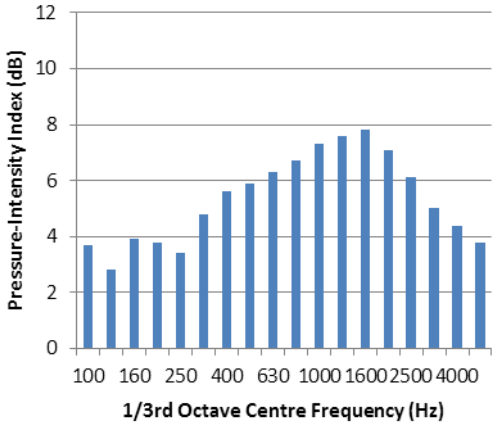

Figure A.14: Pressure-intensity index of intensity measurements for a single leaf 17 mm plywood sample

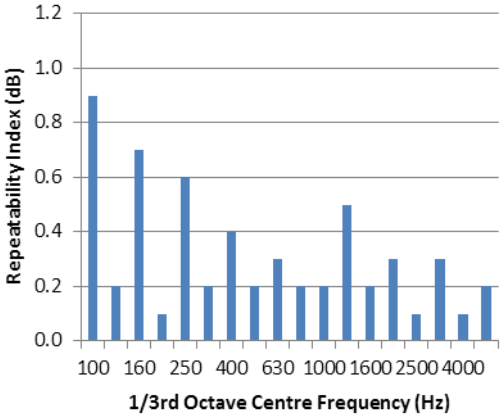

Figure A.15: Repeatability index of intensity measurements for a single leaf 17 mm plywood sample

Table A.5: Single number ratings of 17 mm single leaf plywood sample, measured in small transmission loss facility

Single Number Rating	Result
STC	25
R_w	26

A.6. Single Leaf 19 mm Plywood

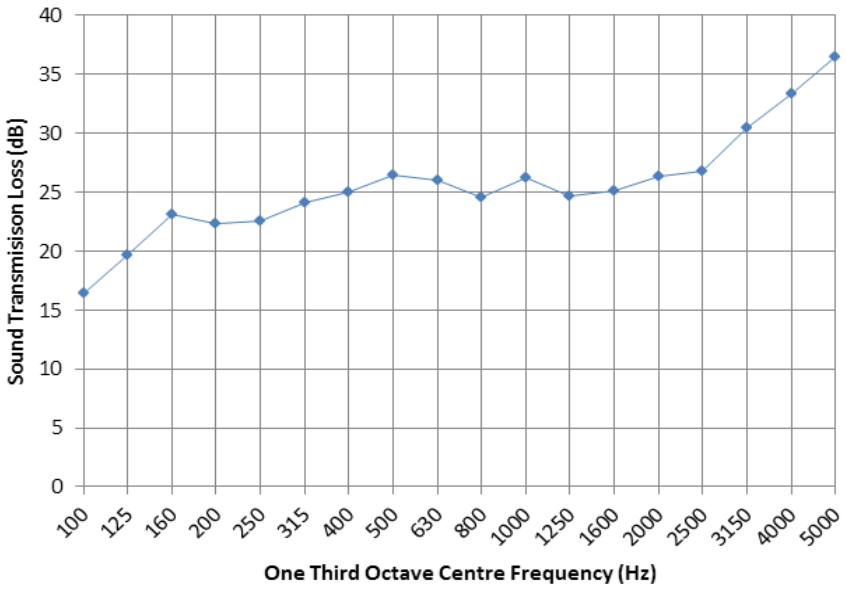

Figure A.16: Measured sound transmission loss of single leaf 19 mm plywood panel, measured in the small transmission loss facility

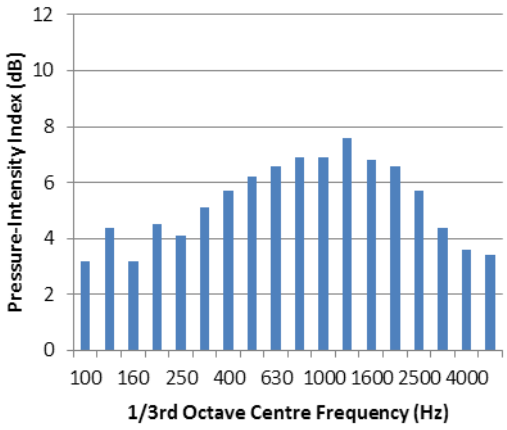

Figure A.17: Pressure-intensity index of intensity measurements for a single leaf 19 mm plywood sample

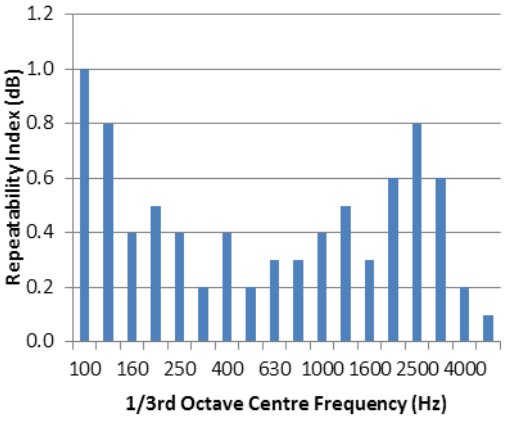

Figure A.18: Repeatability index of intensity measurements for a single leaf 19 mm plywood sample

Table A.6: Single number ratings of 19 mm single leaf plywood sample, measured in small transmission loss facility

Single Number Rating	Result
STC	26
R_w	26

A.7. Single Leaf 21 mm Plywood

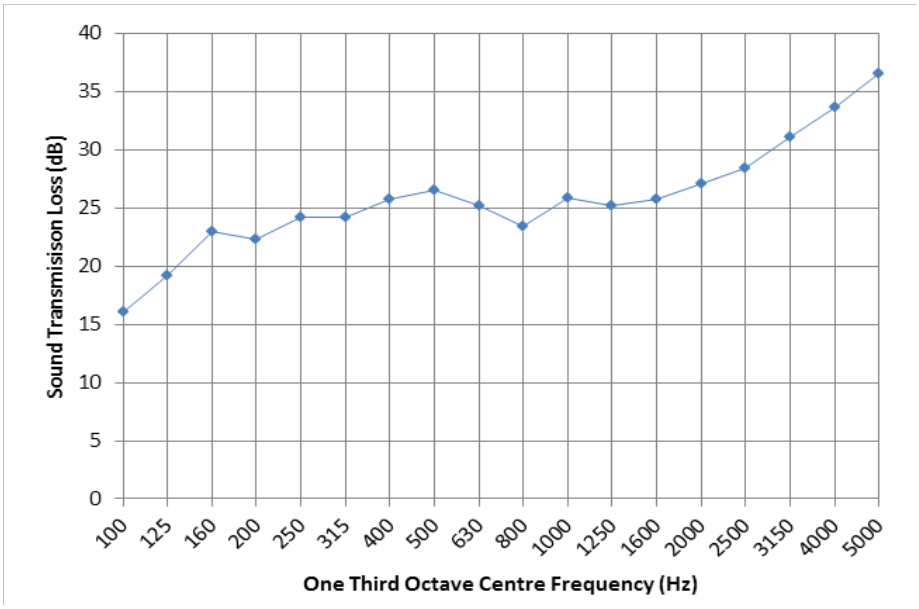

Figure A.2: Measured sound transmission loss of single leaf 21 mm plywood panel, measured in the small transmission loss facility

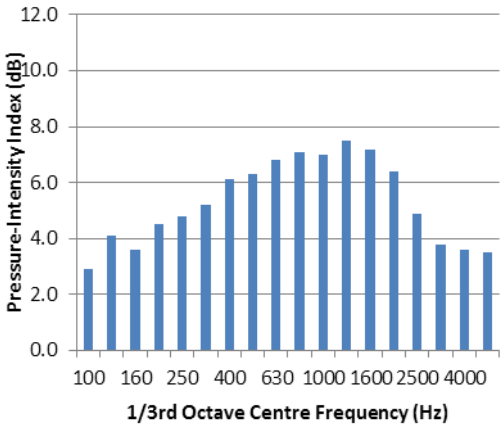

Figure A.20: Pressure-intensity index of intensity measurements for a single leaf 21 mm plywood sample

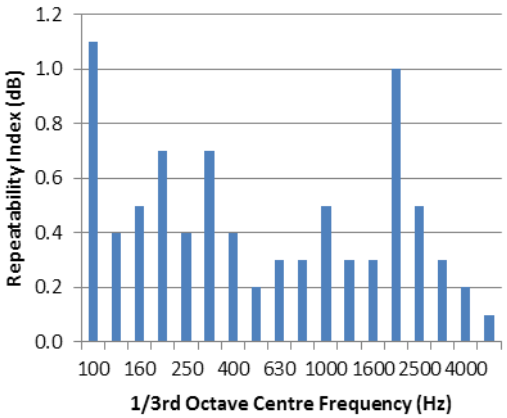

Figure A.3: Repeatability index of intensity measurements for a single leaf 21 mm plywood sample

Table A.7: Single number ratings of 21 mm single leaf plywood sample, measured in small transmission loss facility

Single Number Rating	Result
STC	27
R_w	27

A.8. Single Leaf 10 mm Gypsum Plasterboard

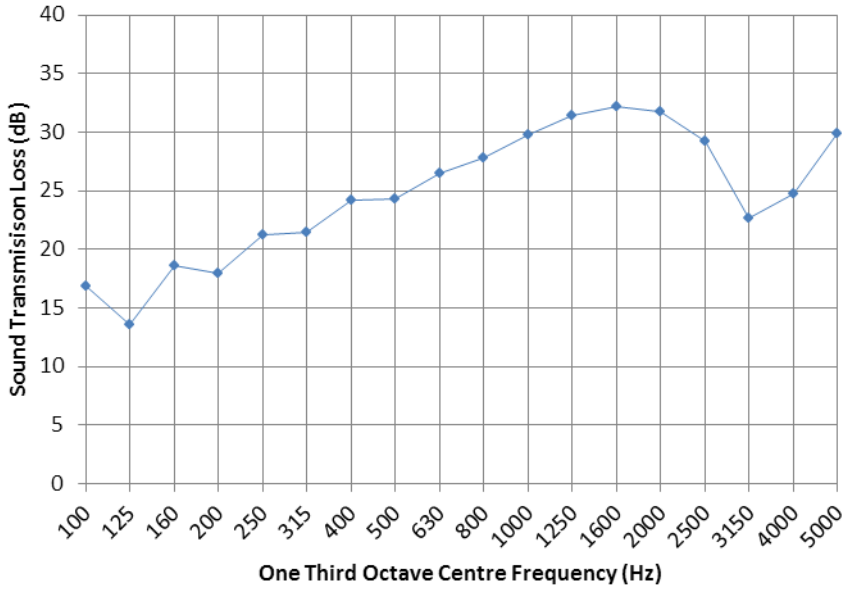

Figure A.22: Measured sound transmission loss of single leaf 10 mm gypsum plasterboard panel, measured in the small transmission loss facility

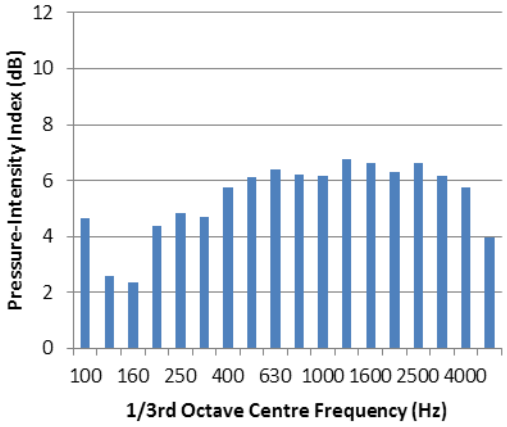

Figure A.23: Pressure-intensity index of intensity measurements for a single leaf 10 mm gypsum plasterboard sample

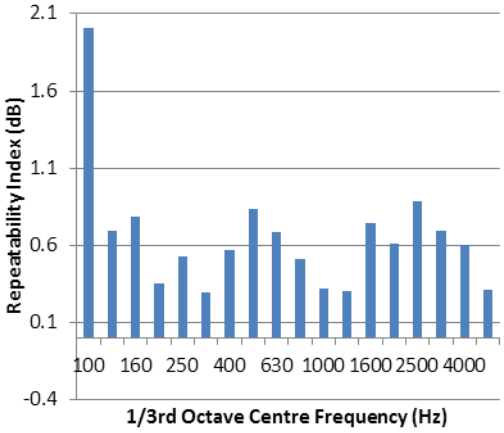

Figure A.24: Repeatability index of intensity measurements for a single leaf 10 mm gypsum plasterboard sample

Table A.8: Single number ratings of 10 mm single leaf gypsum plasterboard sample, measured in small transmission loss facility

Single Number Rating	Result
STC	27
R_w	28

A.9. Double Leaf 12 mm Plywood

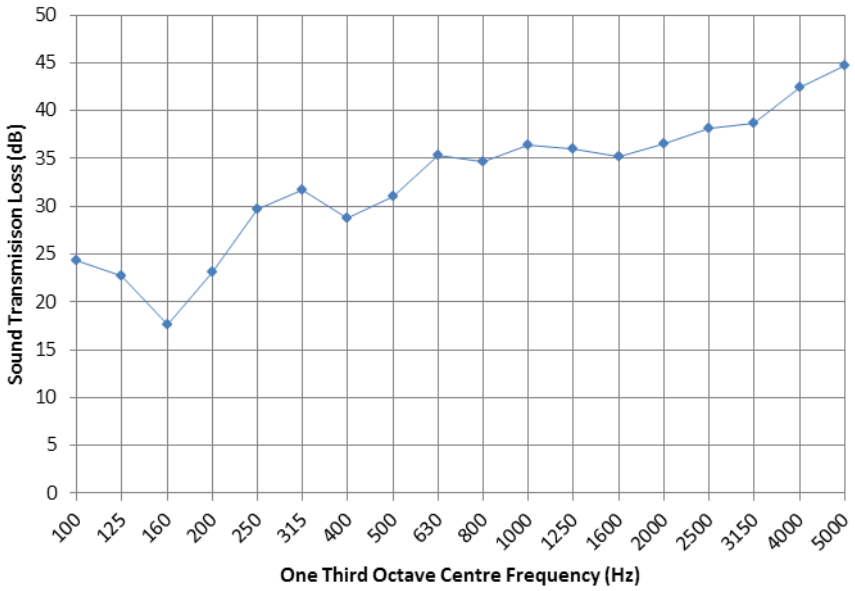

Figure A.25: Measured sound transmission loss of double leaf 12 mm plywood sample, measured in the small transmission loss facility

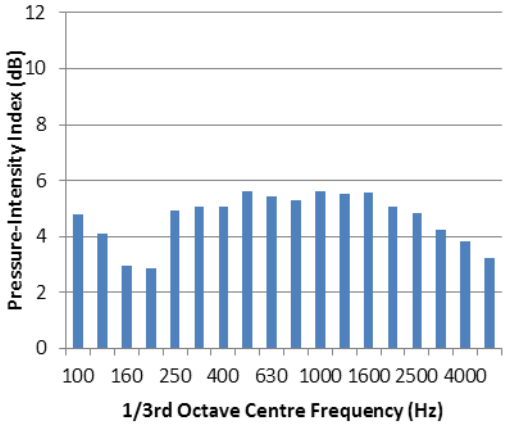

Figure A.26: Pressure-intensity index of intensity measurements for a double leaf 12 mm plywood sample

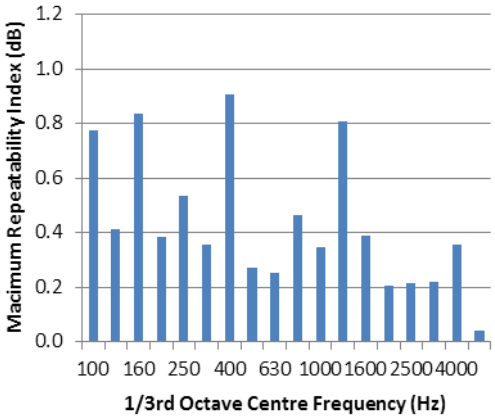

Figure A.27: Repeatability index of intensity measurements for a double leaf 12 mm plywood sample

Table A.9: Single number ratings of double leaf 12 mm plywood sample, measured in small transmission loss facility

Single Number Rating	Result
STC	35
R_w	35

A.10. Single Leaf Studded 12 mm Plywood

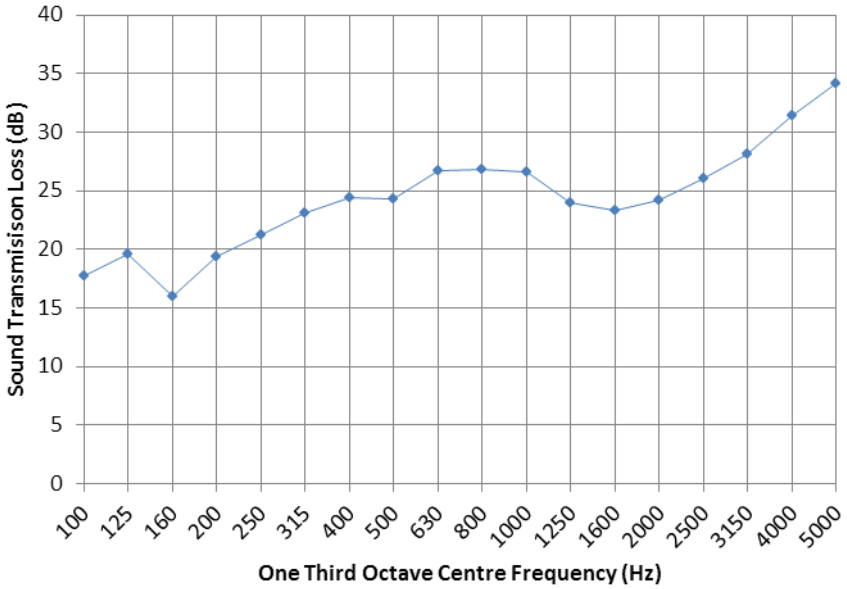

Figure A.28: Measured sound transmission loss of single leaf 12 mm studded plywood panel, measured in the small transmission loss facility

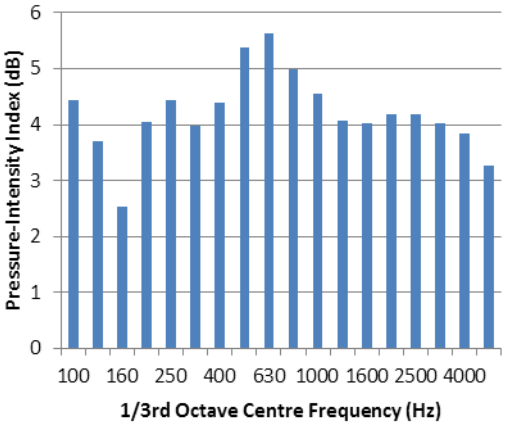

Figure A.29: Pressure-intensity index of intensity measurements for a single leaf 12 mm studded plywood sample

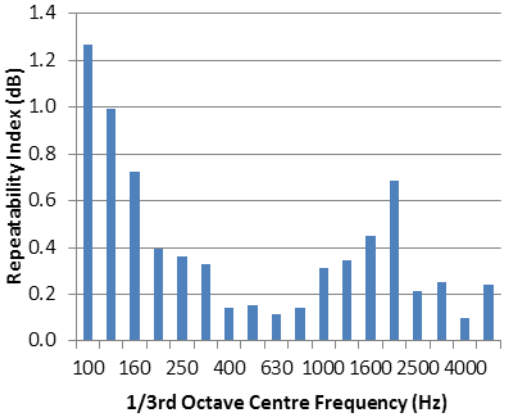

Figure A.30: Repeatability index of intensity measurements for a single leaf 12 mm studded plywood sample

Table A.10: Single number ratings of single leaf 12 mm studded plywood sample, measured in small transmission loss facility

Single Number Rating	Result
STC	26
R_w	26

B. Detailed Results of Large Transmission Loss Tests

This appendix presents all the transmission loss measurements performed in the large transmission loss rig referred to in Section 6. These measurements are presented with their respective pressure-intensity indexes, repeatability indexes, transmission loss curves, transmission loss values, and single number ratings.

B.1. Single Leaf 7 mm Plywood

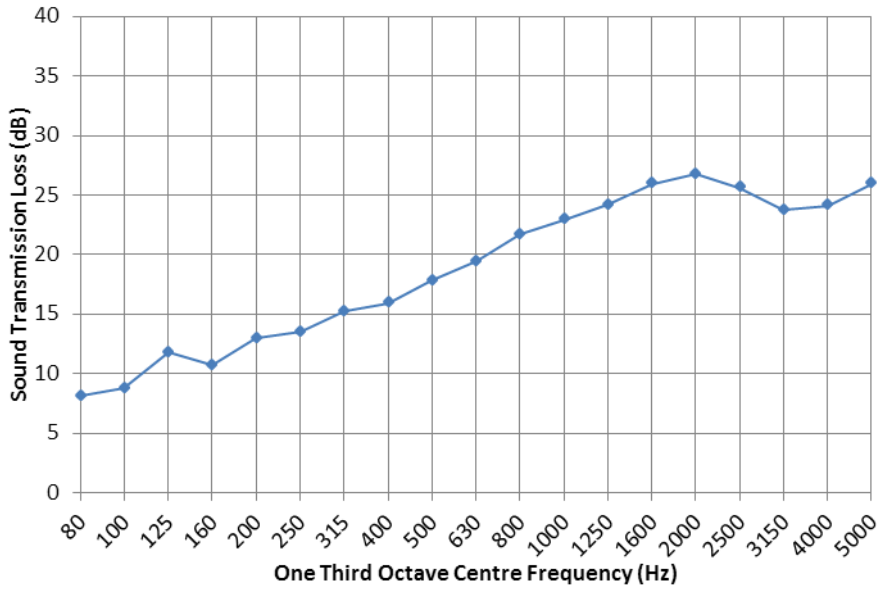

Figure B.1: Measured sound transmission loss of single leaf 7 mm plywood panel, measured in the large transmission loss facility

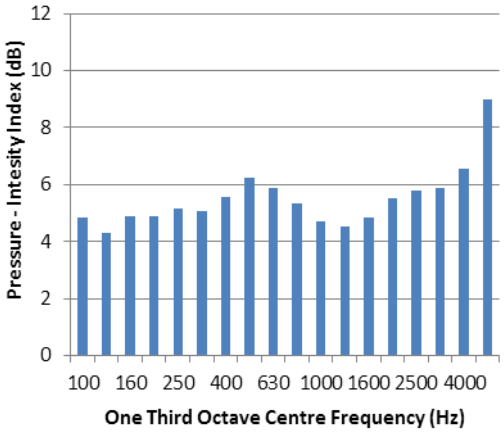

FigureB.2: Pressure-intensity index of intensity measurements for a single leaf 7 mm plywood sample

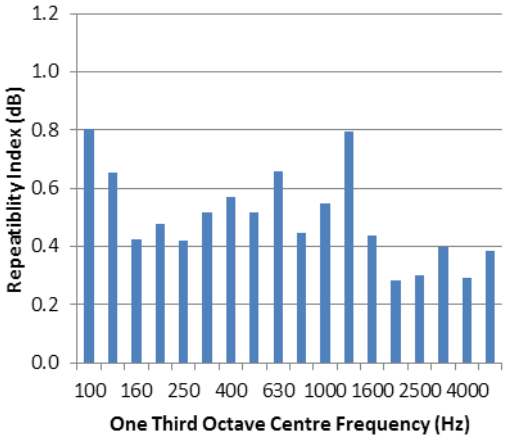

Figure B.3: Repeatability index of intensity measurements for a single leaf 7 mm plywood sample

Table B.1: Single number ratings of 7 mm single leaf plywood sample, measured in large transmission loss facility

Single Number Rating	Result
STC	22
R_w	22

B.2. Single Leaf 9 mm Plywood

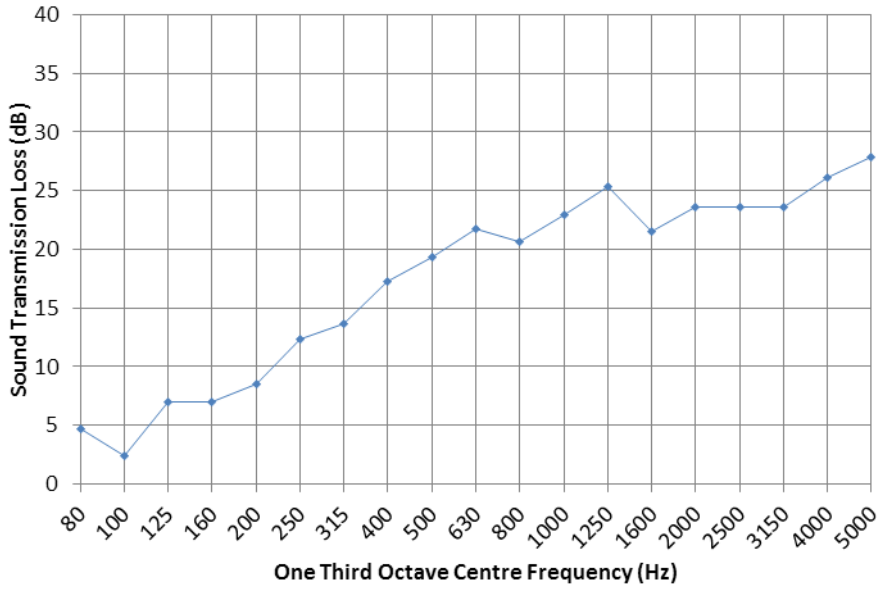

Figure B.4: Measured sound transmission loss of single leaf 9 mm plywood panel, measured in the large transmission loss facility

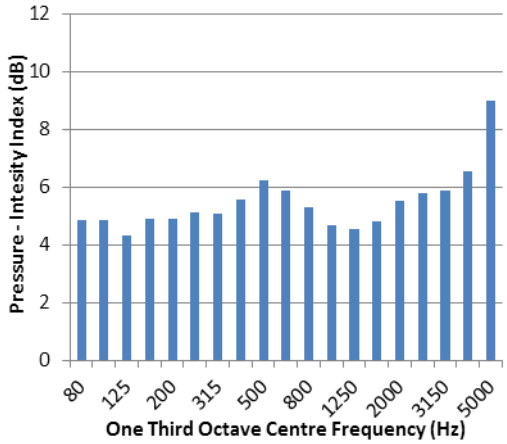

Figure B.5: Pressure-intensity index of intensity measurements for a single leaf 9 mm plywood sample

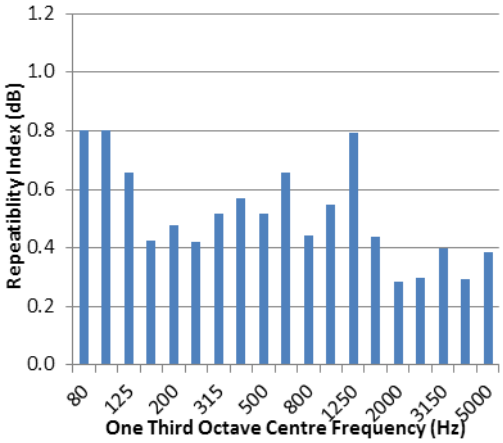

Figure B.6: Repeatability index of intensity measurements for a single leaf 9 mm plywood sample

Table B.2: Single number ratings of 9 mm single leaf plywood sample, measured in large transmission loss facility

Single Number Rating	Result
STC	21
R_w	21

B.3. Single Leaf 12 mm Plywood

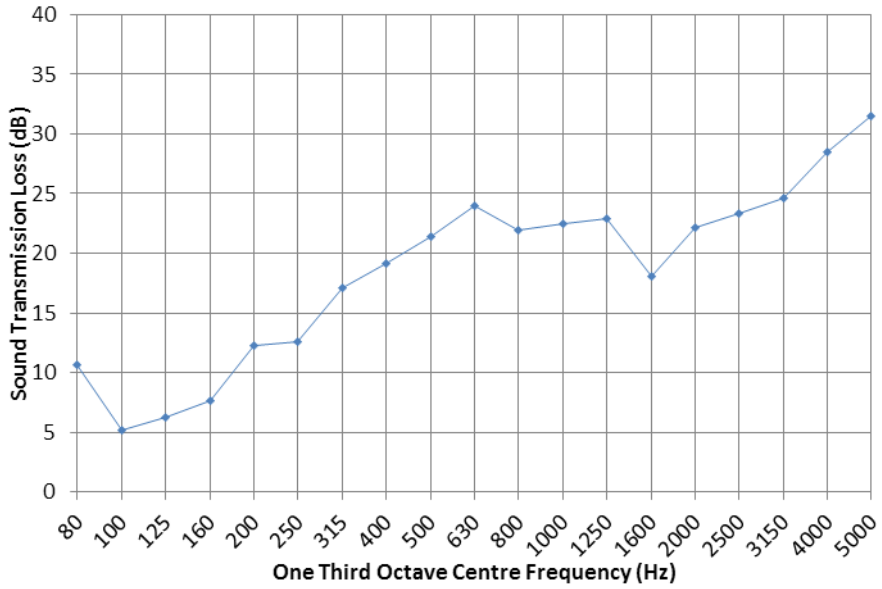

Figure B.7: Measured sound transmission loss of single leaf 12 mm plywood panel, measured in the large transmission loss facility

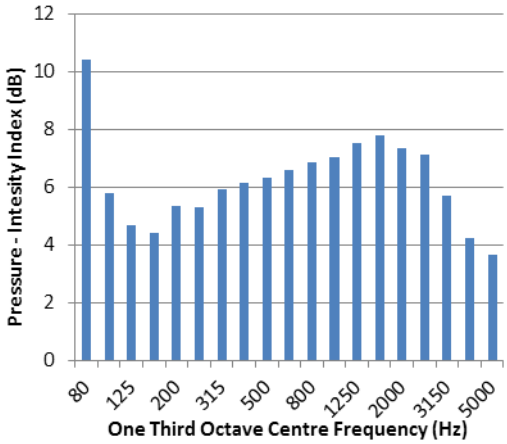

Figure B.8: Pressure-intensity index of intensity measurements for a single leaf 12 mm plywood sample

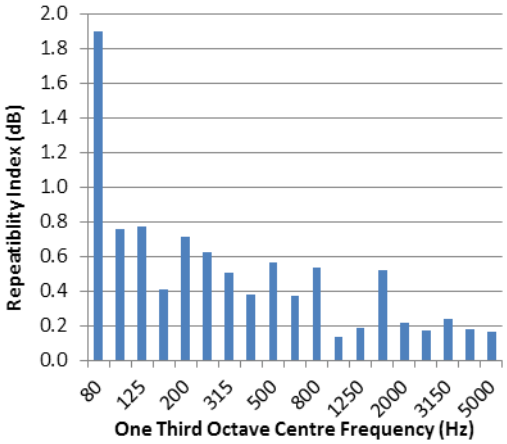

Figure B.9: Repeatability index of intensity measurements for a single leaf 12 mm plywood sample

Table B.3: Single number ratings of 12 mm single leaf plywood sample, measured in large transmission loss facility

Single Number Rating	Result
STC	22
R_w	22

B.4. Single Leaf 21 mm Plywood

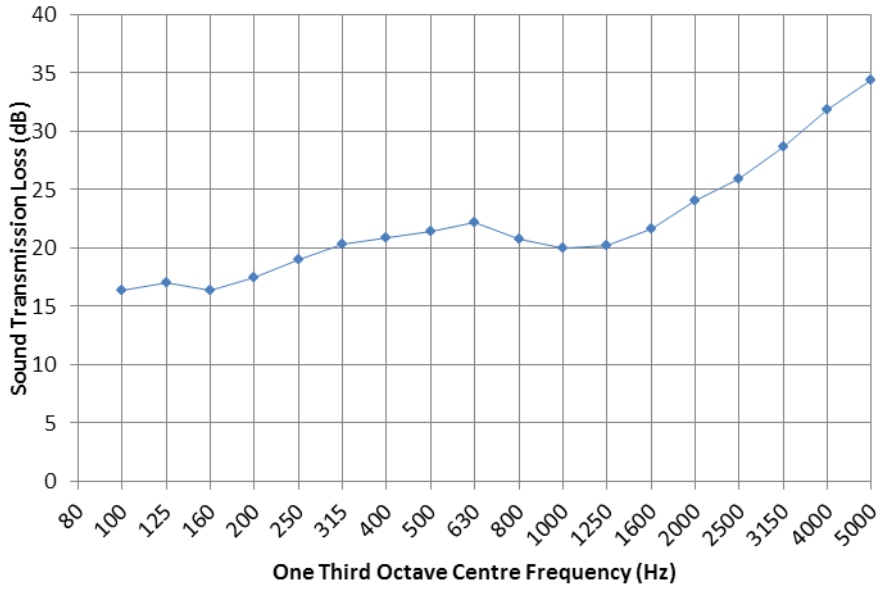

Figure B.10: Measured sound transmission loss of single leaf 21 mm plywood panel, measured in the large transmission loss facility

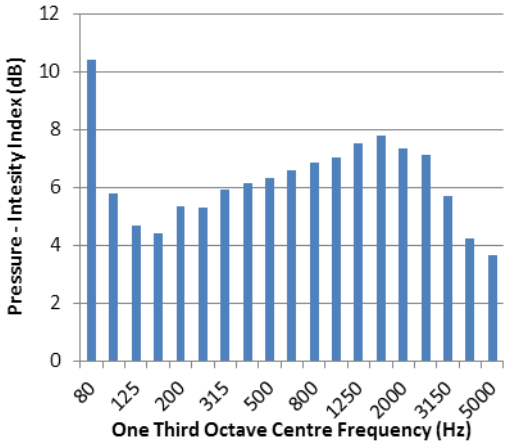

Figure B.11: Pressure-intensity index of intensity measurements for a single leaf 21 mm plywood sample

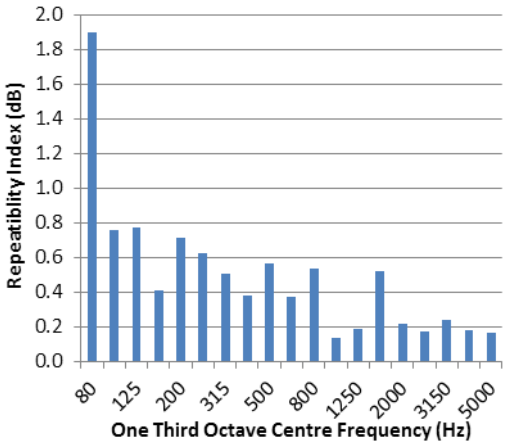

Figure B.12: Repeatability index of intensity measurements for a single leaf 21 mm plywood sample

Table B.4: Single number ratings of 21 mm single leaf plywood sample, measured in large transmission loss facility

Single Number Rating	Result
STC	23
R_w	23

B.5. Double Leaf 9 mm Plywood

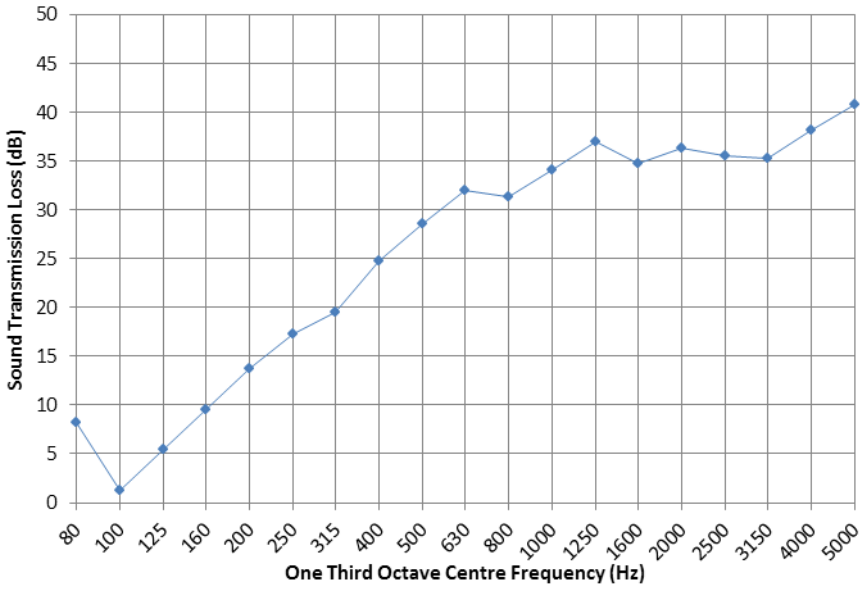

Figure B.13: Measured sound transmission loss of double leaf 9 mm plywood partition, measured in the large transmission loss facility

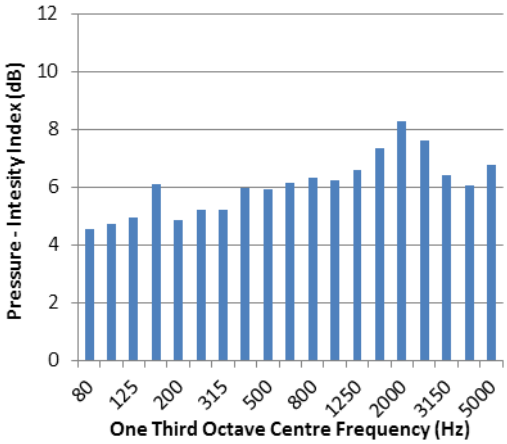

Figure B.14: Pressure-intensity index of intensity measurements for a double leaf 9 mm plywood partition

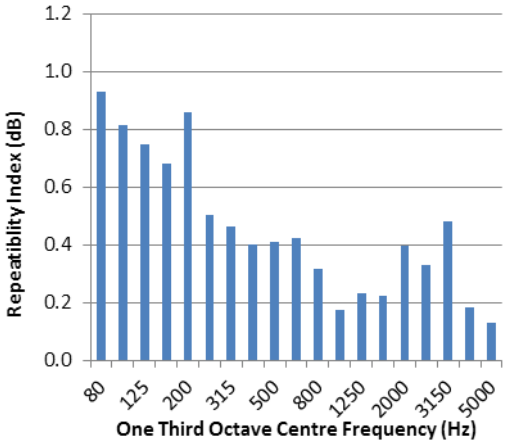

Figure B.15: Repeatability index of intensity measurements for a double leaf 9 mm plywood partition

Table B.5: Single number ratings of a double leaf 9 mm plywood partition, measured in large transmission loss facility

Single Number Rating	Result
STC	29
R_w	27

B.6. Double Leaf 12 mm Plywood

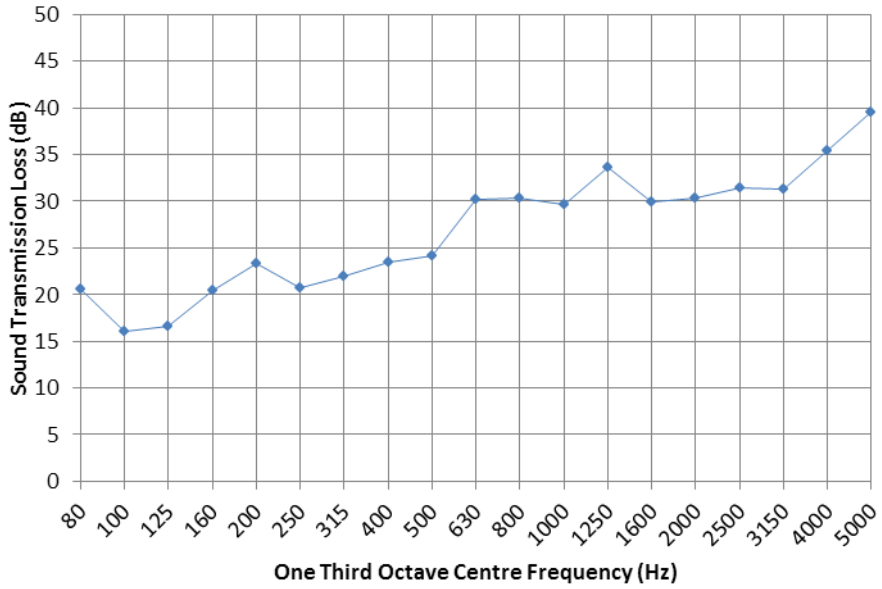

Figure B.16: Measured sound transmission loss of double leaf 12 mm plywood partition, measured in the large transmission loss facility

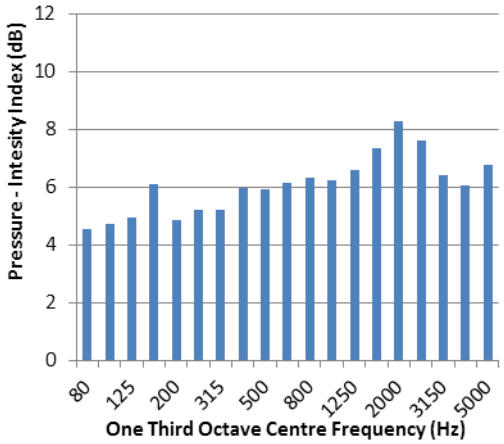

Figure B.17: Pressure-intensity index of intensity measurements for a double leaf 12 mm plywood partition

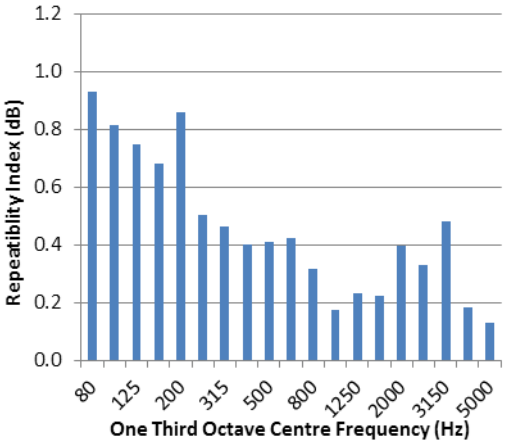

Figure B.18: Repeatability index of intensity measurements for a double leaf 12 mm plywood partition

Table B.6: Single number ratings of a double leaf 12 mm plywood partition, measured in large transmission loss facility

Single Number Rating	Result
STC	29
R_w	29

B.7. Double Leaf 21 mm Plywood

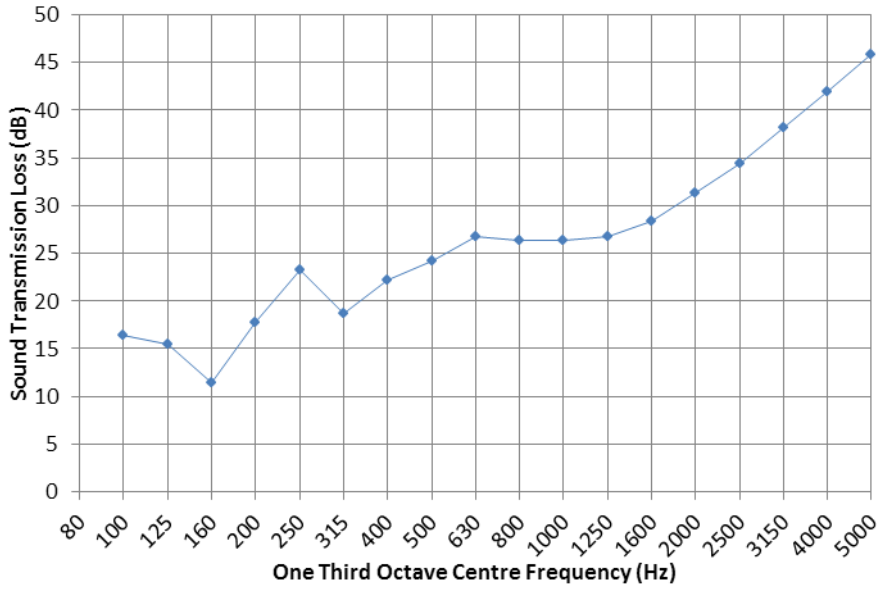

Figure B.19: Measured sound transmission loss of a double leaf 21 mm plywood partition, measured in the large transmission loss facility

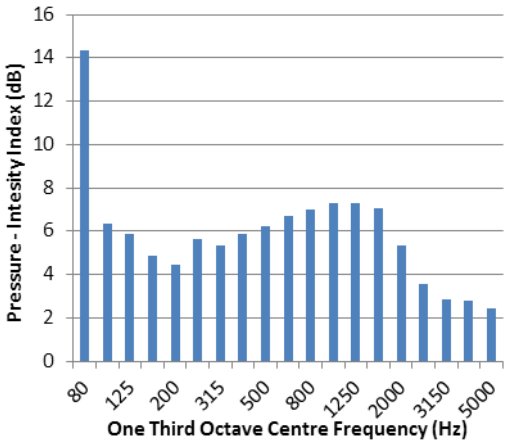

Figure B.20: Pressure-intensity index of intensity measurements for a double leaf 21 mm plywood partition

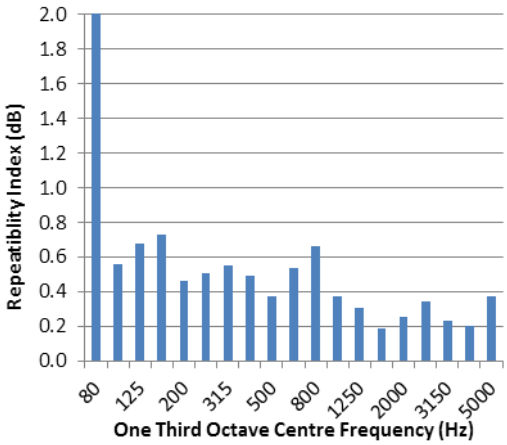

Figure B.21: Repeatability index of intensity measurements for a double leaf 21 mm plywood partition

Table B.7: Single number ratings of a double leaf 21 mm plywood partition, measured in large transmission loss facility

Single Number Rating	Result
STC	27
R_w	27

B.8. Mismatched Double Leaf 7 mm Plywood + 9 mm Plywood

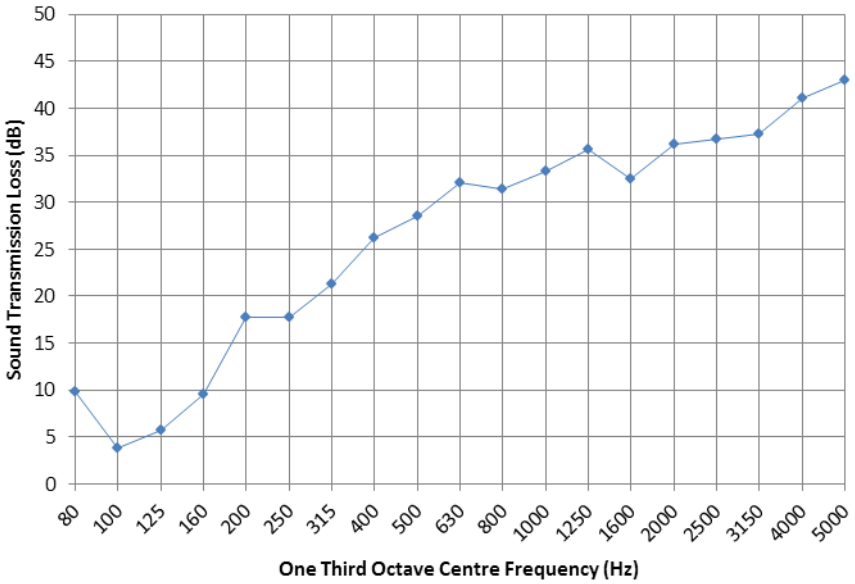

Figure B.22: Measured sound transmission loss of a mismatched double leaf 7 mm plywood + 9 mm plywood partition, measured in the large transmission loss facility

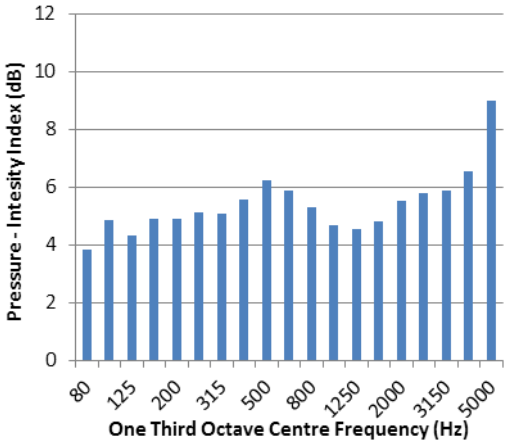

Figure B.23: Pressure-intensity index of intensity measurements for a mismatched double leaf 7 mm plywood + 9 mm plywood partition

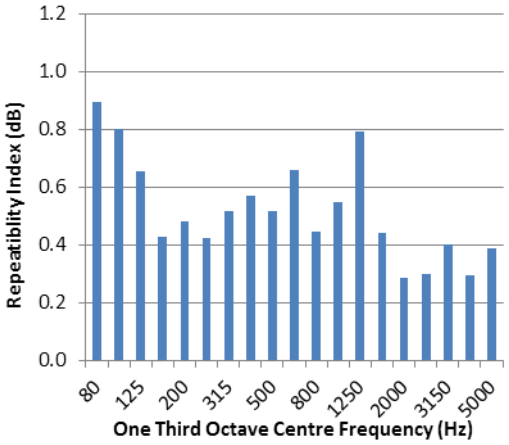

Figure B.24: Repeatability index of intensity measurements for a mismatched double leaf 7 mm plywood + 9 mm plywood partition

Table B.8: Single number ratings of a mismatched double leaf 7 mm plywood + 9 mm plywood partition, measured in large transmission loss facility

Single Number Rating	Result
STC	32
R_w	31

B.9. Mismatched Double Leaf 9 mm Plywood + 12 mm Plywood

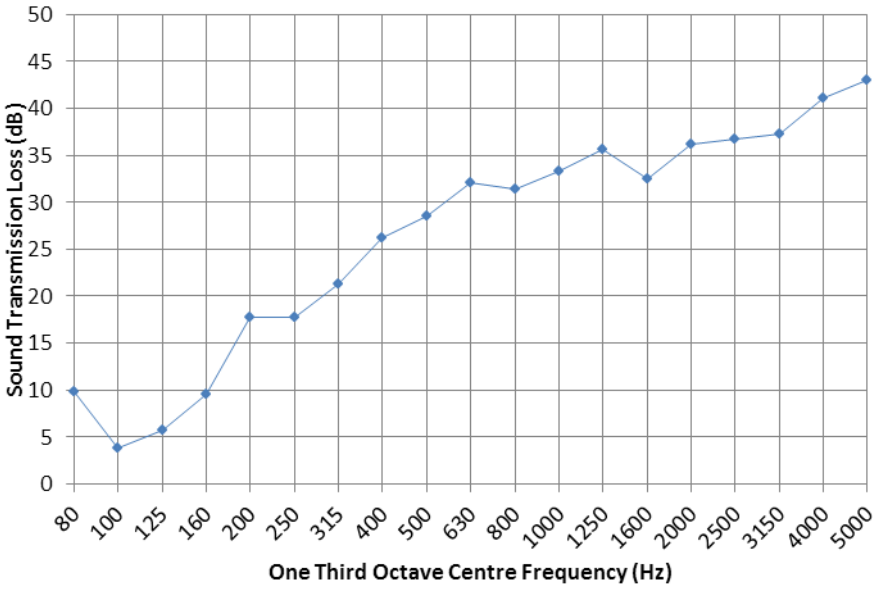

Figure B.25: Measured sound transmission loss of a mismatched double leaf 9 mm plywood + 12 mm plywood partition, measured in the large transmission loss facility

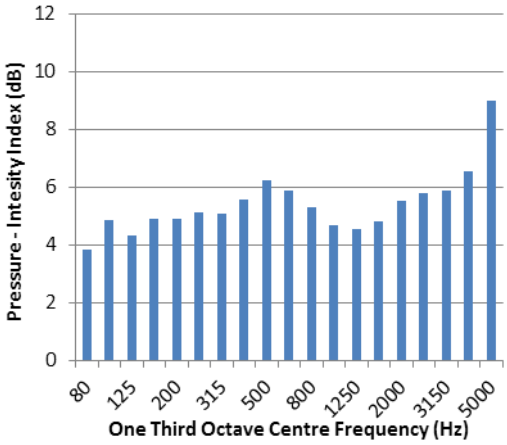

Figure B.26: Pressure-intensity index of intensity measurements for a mismatched double leaf 9 mm plywood + 12 mm plywood partition

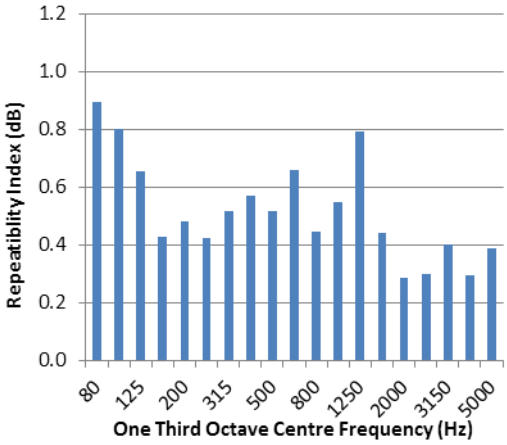

Figure B.27: Repeatability index of intensity measurements for a mismatched double leaf 9 mm plywood + 12 mm plywood partition

Table B.9: Single number ratings of a mismatched double leaf 9 mm plywood + 12 mm plywood partition, measured in large transmission loss facility

Single Number Rating	Result
STC	29
R_w	29

B.10. Mismatched Double Leaf 7 mm Plywood + 10 mm Gypsum Plasterboard

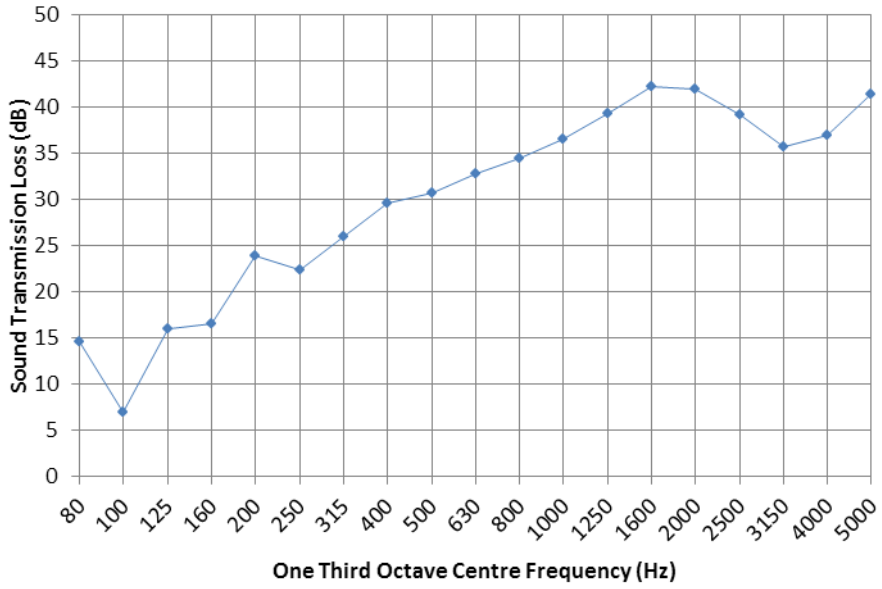

Figure B.28: Measured sound transmission loss of a mismatched double leaf 7 mm plywood + 10 mm gypsum plasterboard partition, measured in the large transmission loss facility

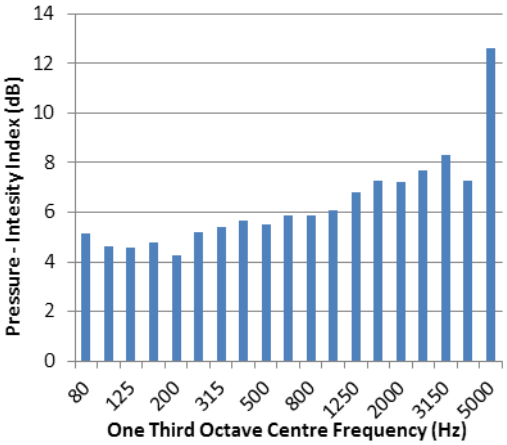

Figure B.29: Pressure-intensity index of intensity measurements for a mismatched double leaf 7 mm plywood + 10 mm gypsum plasterboard partition

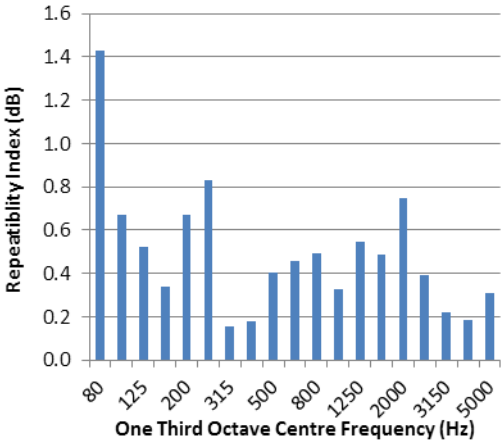

Figure B.30: Repeatability index of intensity measurements for a mismatched double leaf 7 mm plywood + 10 mm gypsum plasterboard partition

Table B.10: Single number ratings of a mismatched double leaf 7 mm plywood + 10 mm gypsum plasterboard partition, measured in large transmission loss facility

Single Number Rating	Result
STC	33
Rw	34

C. Detailed Results of Material Properties Tests

The results of the material properties test are presented in this section. The frequency dependent stiffness and damping loss factor measurements are presented. The empirical curves fitted to the data are also presented, along with the associated r^2 values.

C.1. 7 mm Plywood

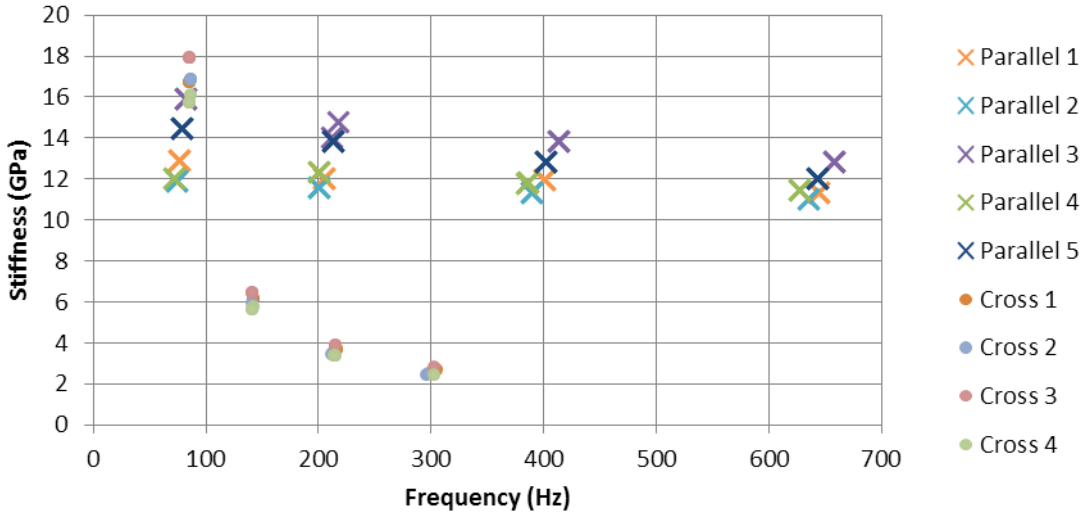

Figure C.1: Frequency dependent stiffness of 7 mm plywood, measured using free-free beam technique

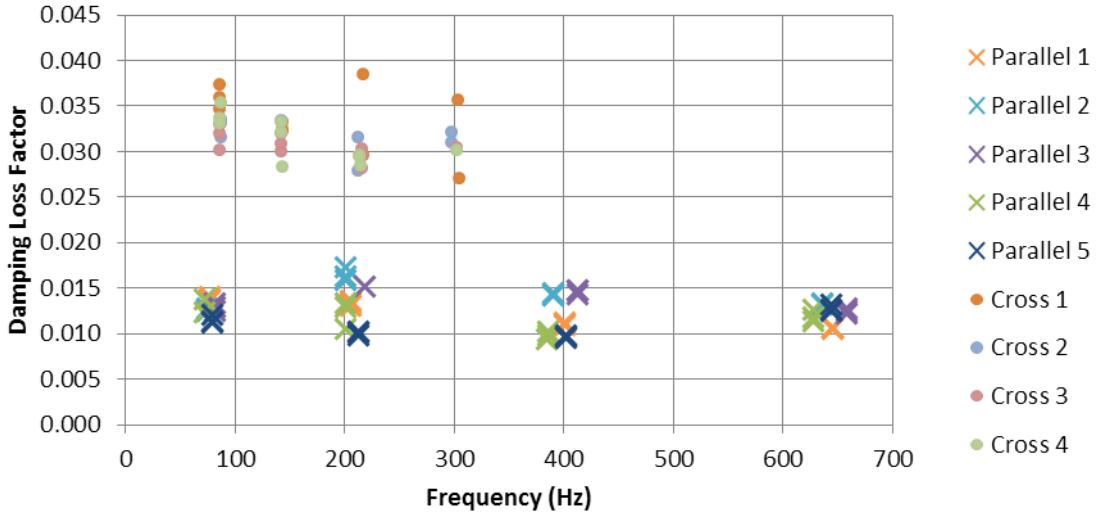

Figure C.2: Frequency dependent damping loss factor of 7 mm plywood, measured using free-free beam technique

Table C.1: Material properties of 7mm plywood

Damping Loss Factor – Cross Ply	0.032
Damping Loss Factor – Parallel to Ply	0.012
Geometric Mean of Damping Loss Factor	0.020
Stiffness – Cross Ply	8.1 GPa
Stiffness – Parallel to Ply	12.6 GPa
Geometric Mean of Stiffness Values	10.1 GPa
Surface Density	3.7 kg/m2
Poisson's Ratio (Assumed)	0.3

Table C.2: Exponential curve for 7 mm plywood stiffness measurements; parameters of curve and goodness of fit data.

Cross Ply – Exponential Equation	$E_{cp}(f) = 57.8e^{-0.015f}$ GPa
Cross Ply – r^2 value	0.96
Parallel to Ply – Exponential Equation	$E_{cp}(f) = 13.53e^{-0.00022f}$ GPa
Parallel to Ply – r^2 value	0.22

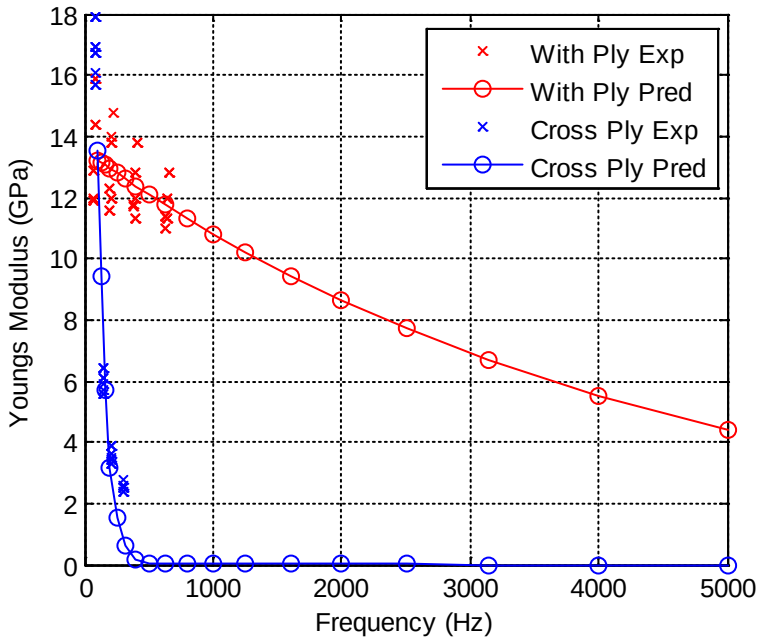

Figure C.3: Predicted stiffness of 7 mm plywood at 100 Hz – 5000 Hz one third octave band centre frequencies

C.2. 9 mm Plywood

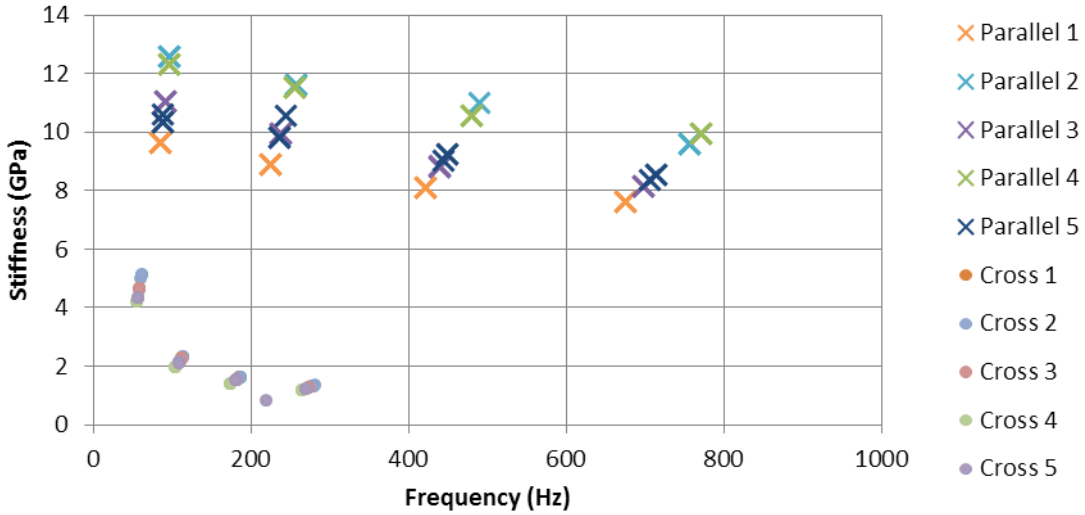

Figure C.4: Frequency dependent stiffness of 9 mm plywood, measured using free-free beam technique

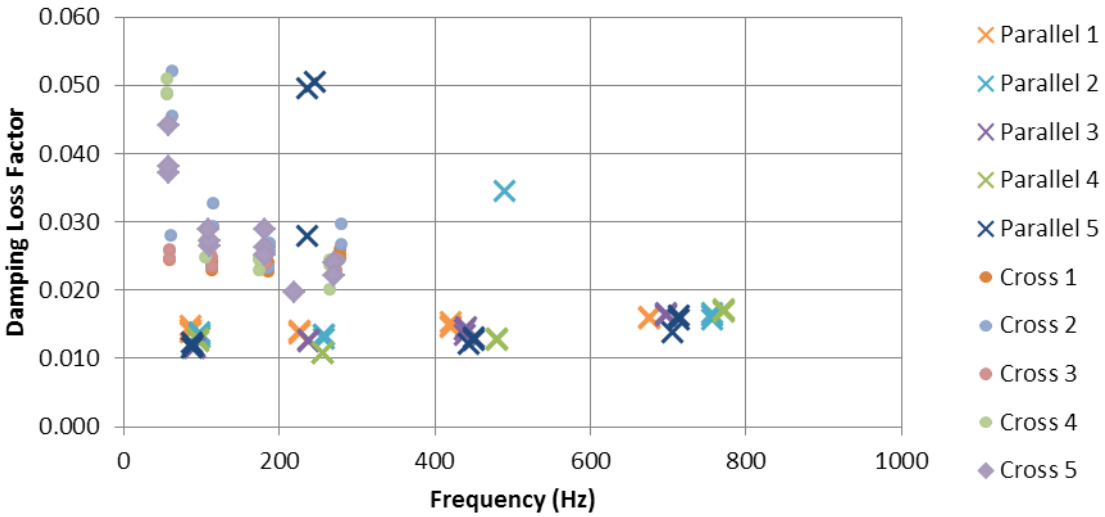

Figure C.5: Frequency dependent damping loss factor of 9 mm plywood, measured using free-free beam technique

Figure C.4. and Figure C.4. show the low frequency behaviour of the 9 mm plywood beams. An expanded frequency range is presented in Figure C.6.and Figure C.7. The two smaller beam lengths are 0.3 m and 0.4 m.

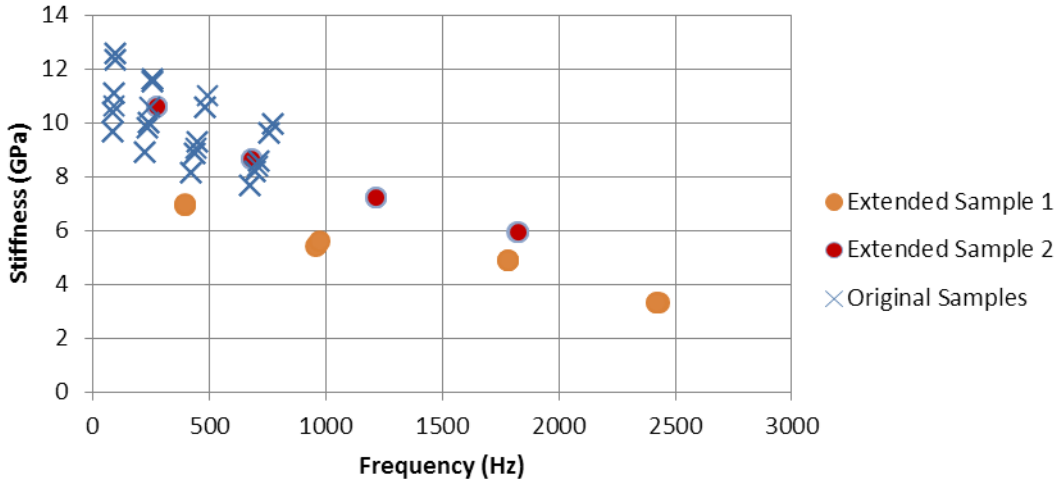

Figure C.6: Dynamic stiffness of 9 mm plywood beam in parellel to ply direction, measured over expanded frequency range.

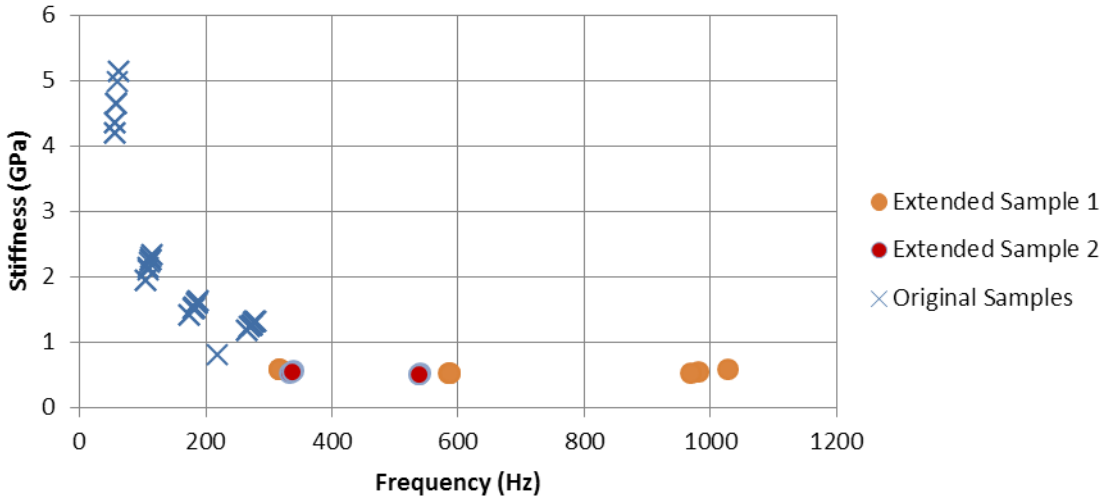

Figure C.7: Dynamic stiffness of 9 mm plywood beam in cross ply direction, measured over expanded frequency range.

Table C.3: Average stiffness and damping loss factor of 9 mm plywood

Damping Loss Factor – Cross Ply	0.028
Damping Loss Factor – Parallel to Ply	0.016
Geometric Mean of Damping Loss Factor	0.021
Stiffness – Cross Ply	2.2 GPa
Stiffness – Parallel to Ply	8.5 GPa
Geometric Mean of Stiffness Values	4.2 GPa
Surface Density	4.3 kg/m^2
Poisson's Ratio (Assumed)	0.3

Table C.4: Exponential curve for 9 mm plywood stiffness measurements; parameters of curve and goodness of fit data.

Cross Ply – Exponential Equation	$E_{cp}(f) = 2.81e^{-0.00083f}$ GPa
Cross Ply – r^2 value	0.15
Parallel to Ply – Exponential Equation	$E_{cp}(f) = 11.1e^{-0.00083f}$ GPa
Parallel to Ply – r^2 value	0.67

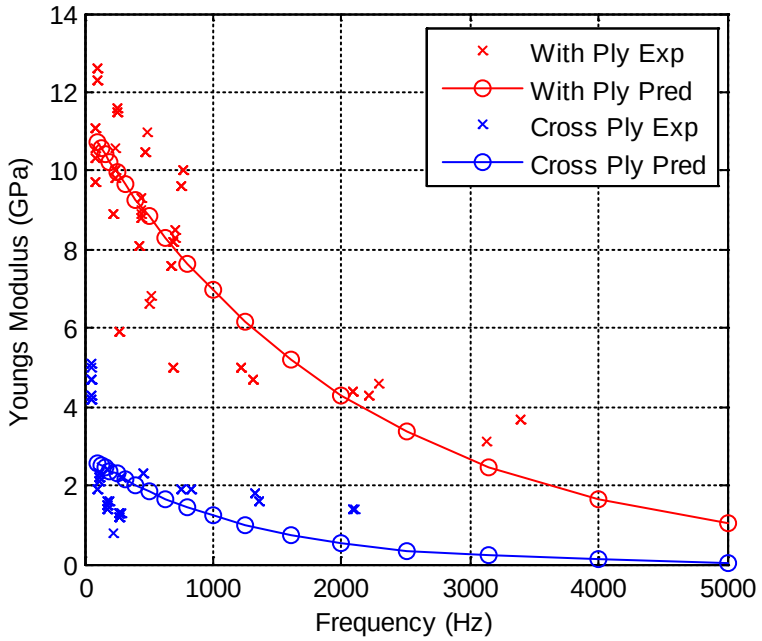

Figure C.8: Predicted stiffness pf 9 mm plywood at 100 Hz – 5000 Hz one third octave band centre frequencies

C.3. 12 mm Plywood

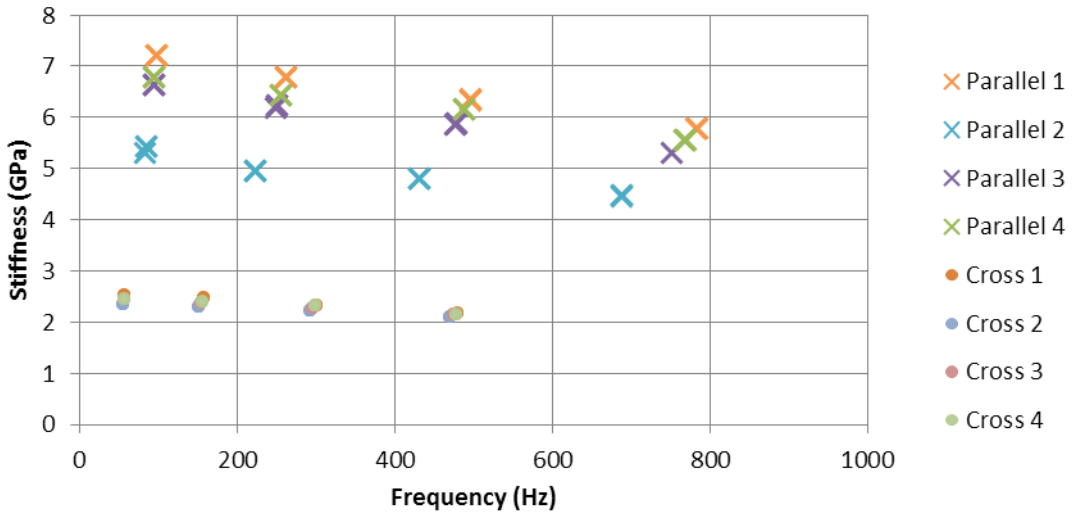

Figure C.9: Frequency dependent stiffness of 12 mm plywood, measured using free-free beam technique

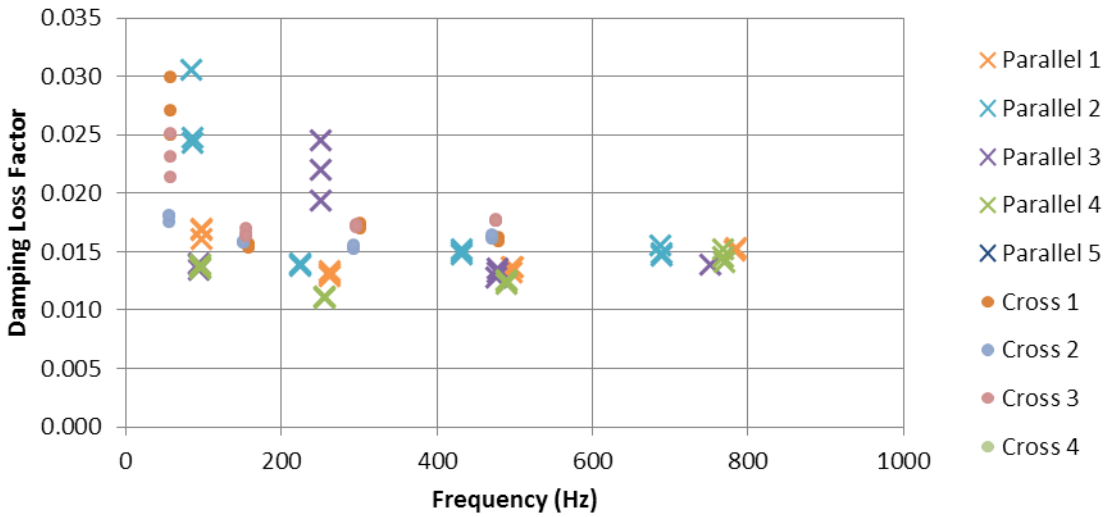

Figure C.10: Frequency dependent damping loss factor of 12 mm plywood, measured using free-free beam technique

Figure C.9. and Figure C.10. show the low frequency behaviour of the 12 mm plywood beams. An expanded frequency range is presented in Figure C.11. and Figure C.12.. The two smaller beam lengths are 0.3 m and 0.4 m.

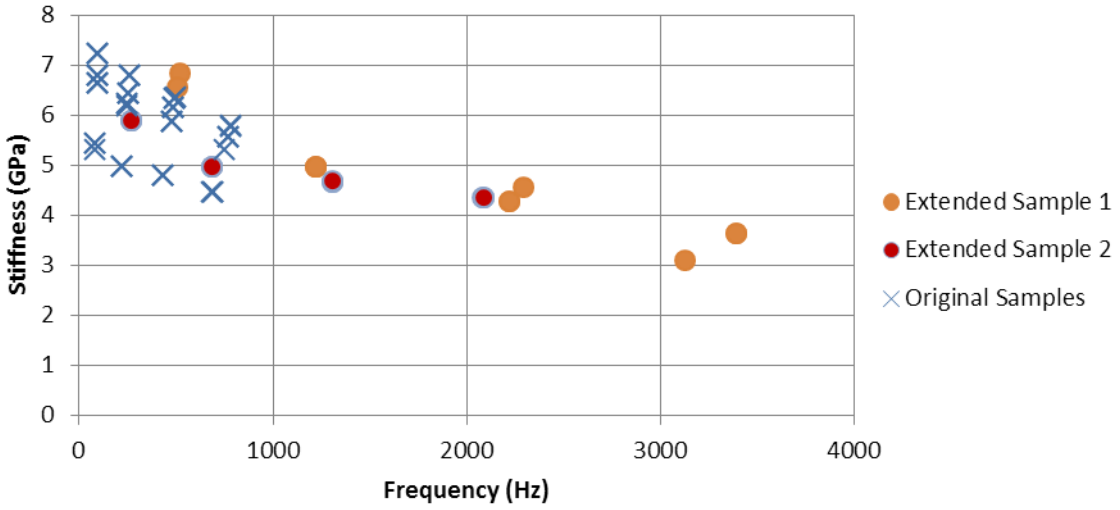

Figure C.11: Dynamic stiffness of 12 mm plywood beam in parellel to ply direction, measured over expanded frequency range.

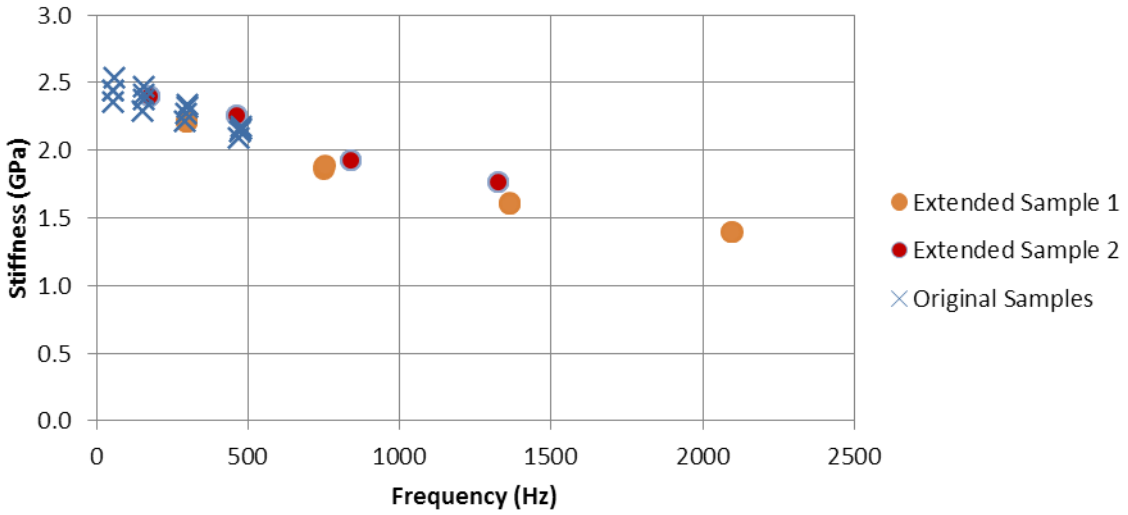

Figure C.12: Dynamic stiffness of 12 mm plywood beam in cross ply direction, measured over expanded frequency range.

Table C.9: Average material properties of 12 mm plywood

Damping Loss Factor – Cross Ply	0.018
Damping Loss Factor – Parallel to Ply	0.015
Geometric Mean of Damping Loss Factor	0.016
Stiffness – Cross Ply	2.2 GPa
Stiffness – Parallel to Ply	5.6 GPa
Geometric Mean of Stiffness Values	3.5 GPa
Surface Density	5.7 kg/m^2
Poisson's Ratio (Assumed)	0.3

Table C.10: Exponential curve for 12 mm plywood stiffness measurements; parameters of curve and goodness of fit data.

Cross Ply – Exponential Equation	$E_{cp}(f) = 2.48e^{-0.00029f}$ GPa
Cross Ply – r^2 value	0.94
Parallel to Ply – Exponential Equation	$E_{cp}(f) = 6.39e^{-0.00019f}$ GPa
Parallel to Ply – r^2 value	0.60

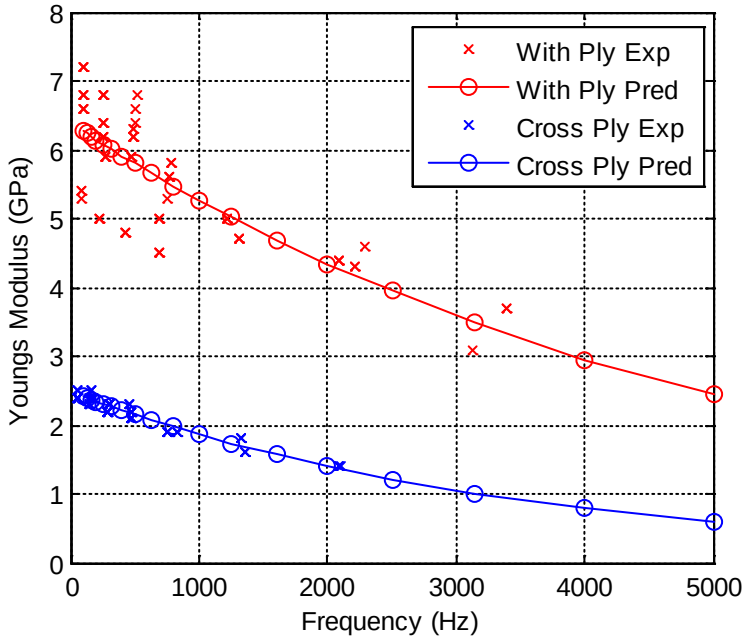

Figure C.13: Predicted stiffness of 12 mm plywood at 100 Hz – 5000 Hz one third octave band centre frequencies

C.4. 15 mm Plywood

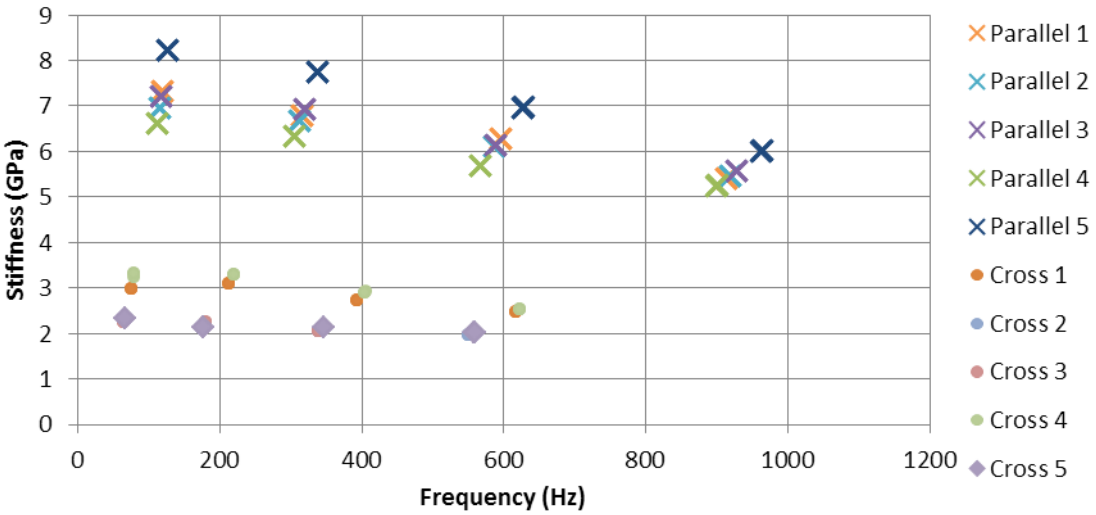

Figure C.14: Frequency dependent stiffness of 15 mm plywood, measured using free-free beam technique

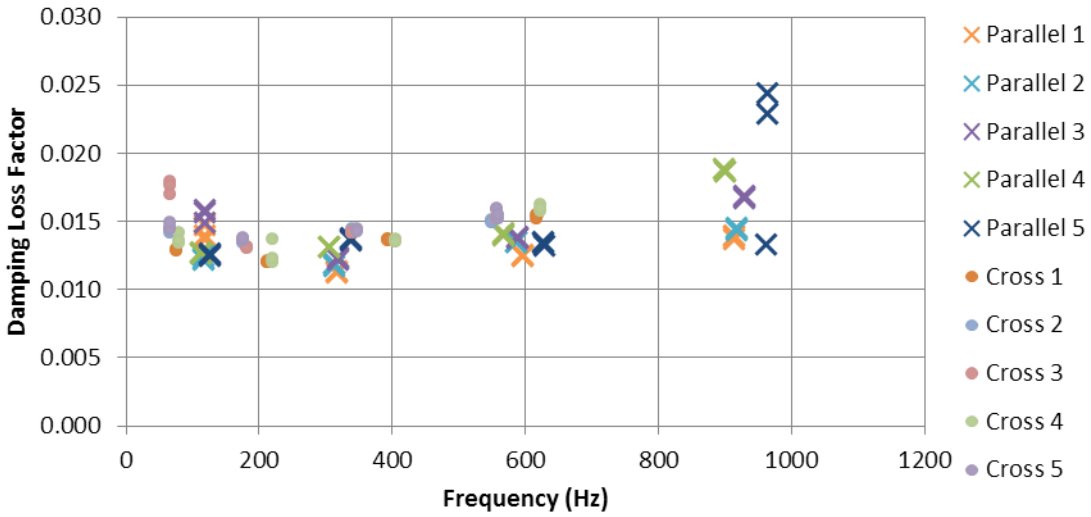

Figure C.15: Frequency dependent damping loss factor of 15 mm plywood, measured using free-free beam technique

Table C.11: Average stiffness and damping loss factor of 15 mm plywood

Damping Loss Factor – Cross Ply	0.014
Damping Loss Factor – Parallel to Ply	0.014
Geometric Mean of Damping Loss Factor	0.014
Stiffness – Cross Ply	2.5 GPa
Stiffness – Parallel to Ply	6.5 GPa
Geometric Mean of Stiffness Values	4.0 GPa
Surface Density	7.7 kg/m^2
Poisson's Ratio (Assumed)	0.3

C.5. 17 mm Plywood

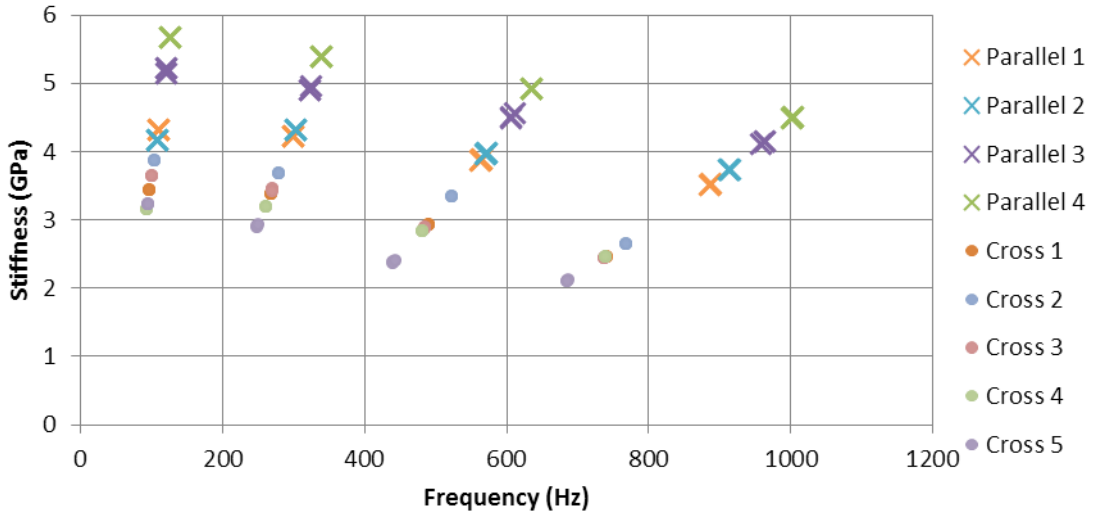

Figure C.16: Frequency dependent stiffness of 17 mm plywood, measured using free-free beam technique

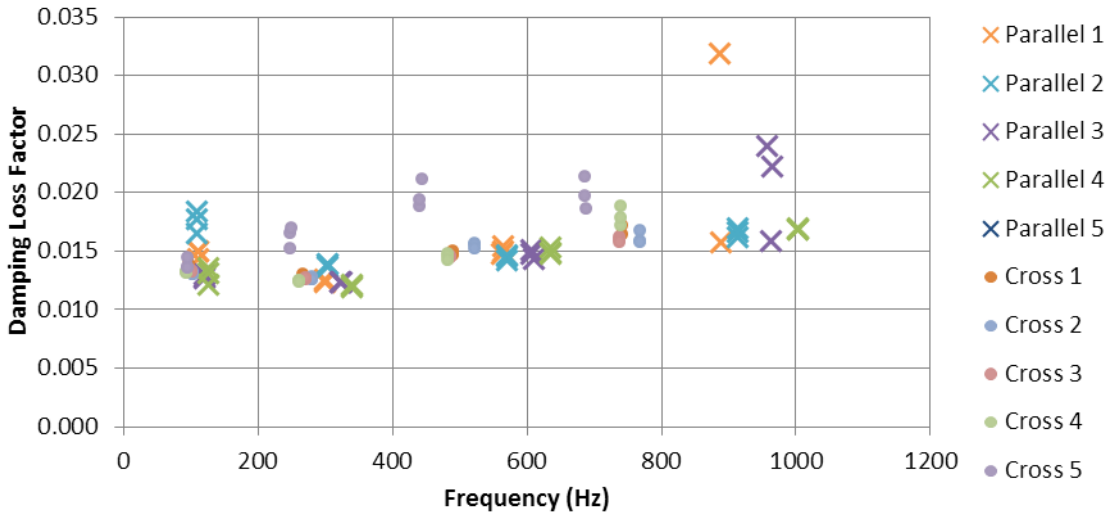

Figure C.17: Frequency dependent damping loss factor of 17 mm plywood, measured using free-free beam technique

Table C.12: Average stiffness and damping loss factor of 17 mm plywood

Damping Loss Factor – Cross Ply	0.015
Damping Loss Factor – Parallel to Ply	0.015
Geometric Mean of Damping Loss Factor	0.015
Stiffness – Cross Ply	3.0 GPa
Stiffness – Parallel to Ply	4.5 GPa
Geometric Mean of Stiffness Values	3.7 GPa
Surface Density	7.7 kg/m^2
Poisson's Ratio (Assumed)	0.3

Table C.13: Exponential curve for 17 mm plywood stiffness measurements; parameters of curve and goodness of fit data.

Cross Ply – Exponential Equation	$E_{cp}(f) = 3.71e^{-0.00055f}$ GPa
Cross Ply – r^2 value	0.65
Parallel to Ply – Exponential Equation	$E_{cp}(f) = 4.96e^{-0.00021f}$ GPa
Parallel to Ply – r^2 value	0.25

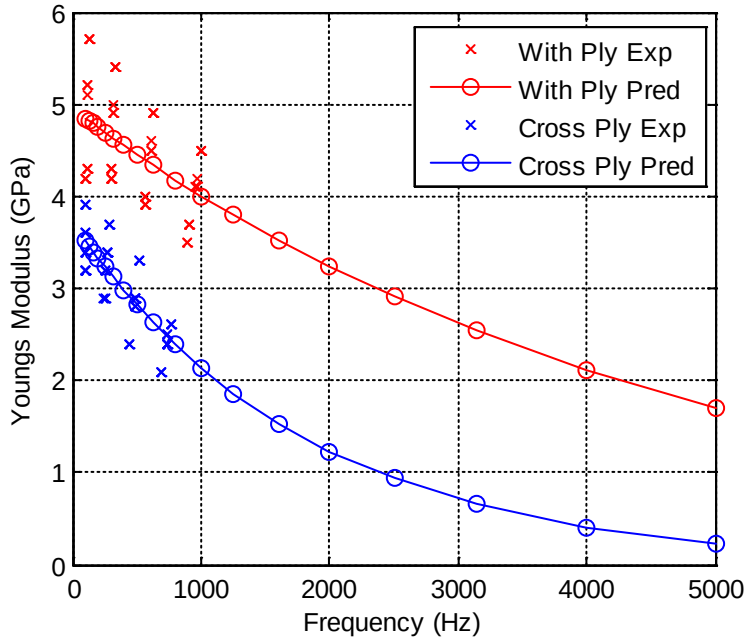

Figure C.18: Predicted stiffness of 17 mm plywood at 100 Hz – 5000 Hz one third octave band centre frequencies

C.6. 19 mm Plywood

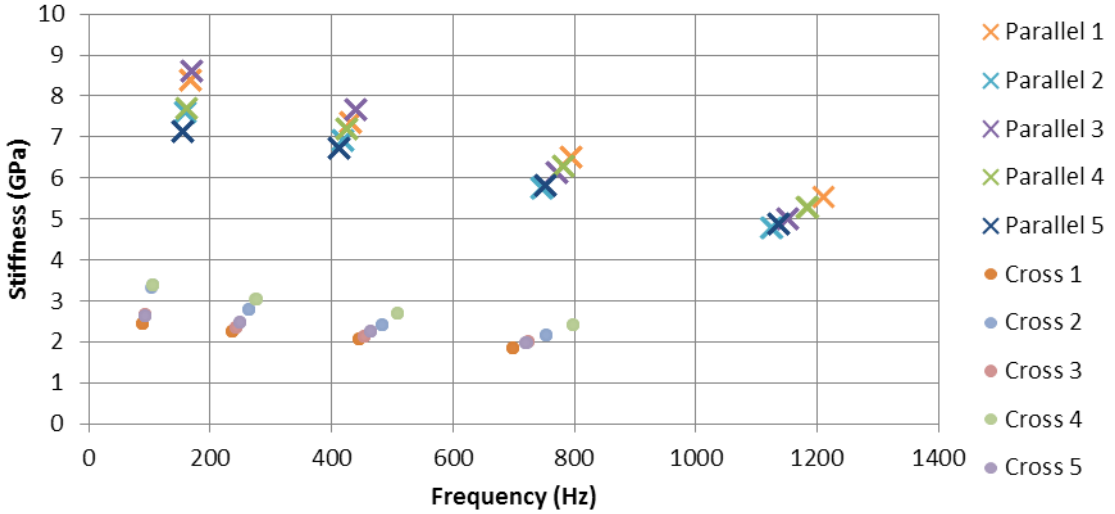

Figure C.19: Frequency dependent stiffness of 19 mm plywood, measured using free-free beam technique

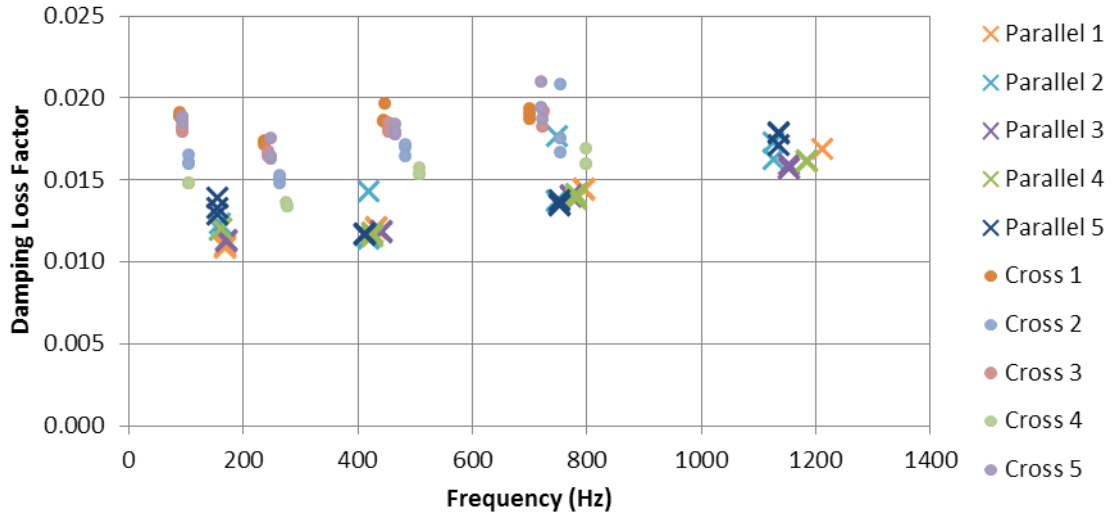

Figure C.20: Frequency dependent damping loss factor of 19 mm plywood, measured using free-free beam technique

Table C.14: Average stiffness and damping loss factor of 19 mm plywood

Damping Loss Factor – Cross Ply	0.017
Damping Loss Factor – Parallel to Ply	0.014
Geometric Mean of Damping Loss Factor	0.015
Stiffness – Cross Ply	2.5 GPa
Stiffness – Parallel to Ply	6.6 GPa
Geometric Mean of Stiffness Values	4.1 GPa
Surface Density	9.1 kg/m^2
Poisson's Ratio (Assumed)	0.3

Table C.15: Exponential curve for 19 mm plywood stiffness measurements; parameters of curve and goodness of fit data.

Cross Ply – Exponential Equation	$E_{cp}(f) = 2.95e^{-0.00048f}$ GPa
Cross Ply – r^2 value	0.43
Parallel to Ply – Exponential Equation	$E_{cp}(f) = 8.56e^{-0.00044f}$ GPa
Parallel to Ply – r^2 value	0.86

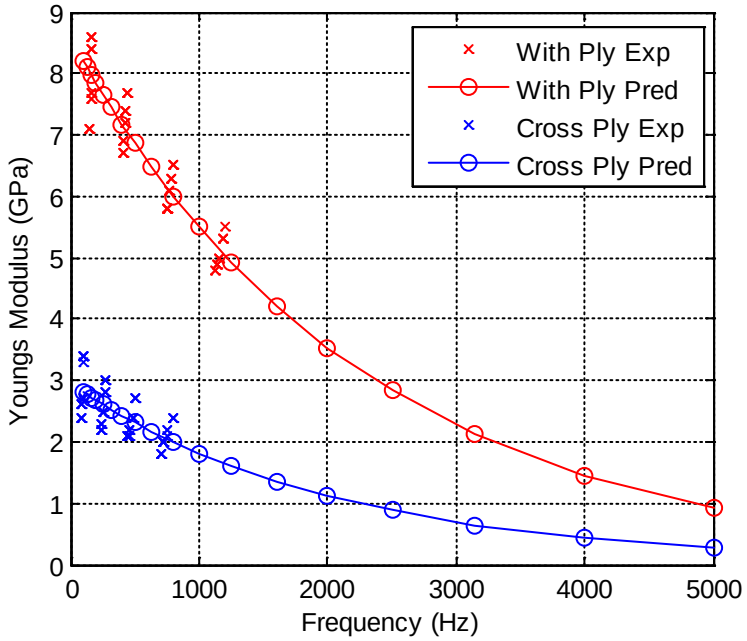

Figure C.21: Predicted stiffness of 19 mm plywood at 100 Hz – 5000 Hz one third octave band centre frequencies

C.7. 21 mm Plywood

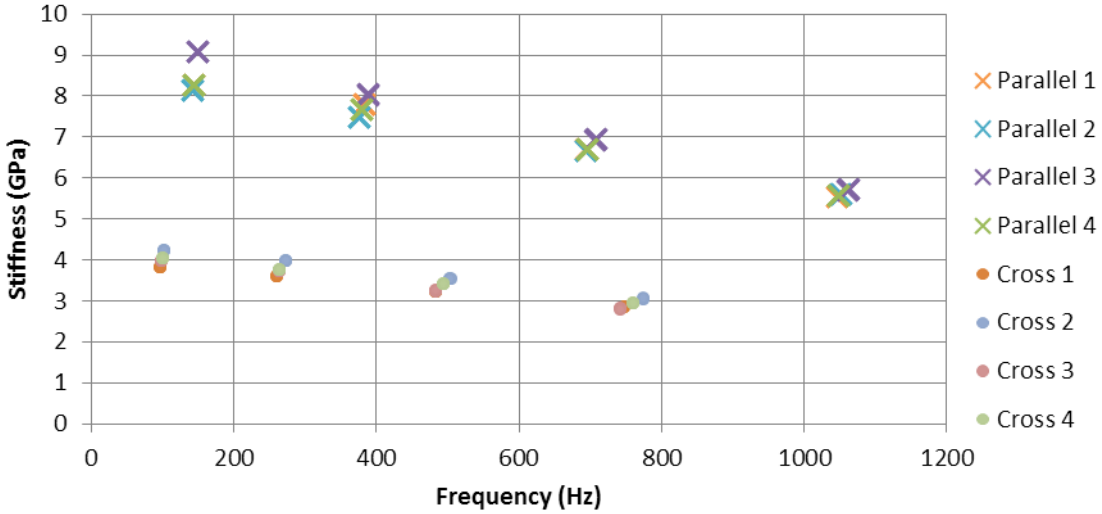

Figure C.22: Frequency dependent stiffness of 21 mm plywood, measured using free-free beam technique

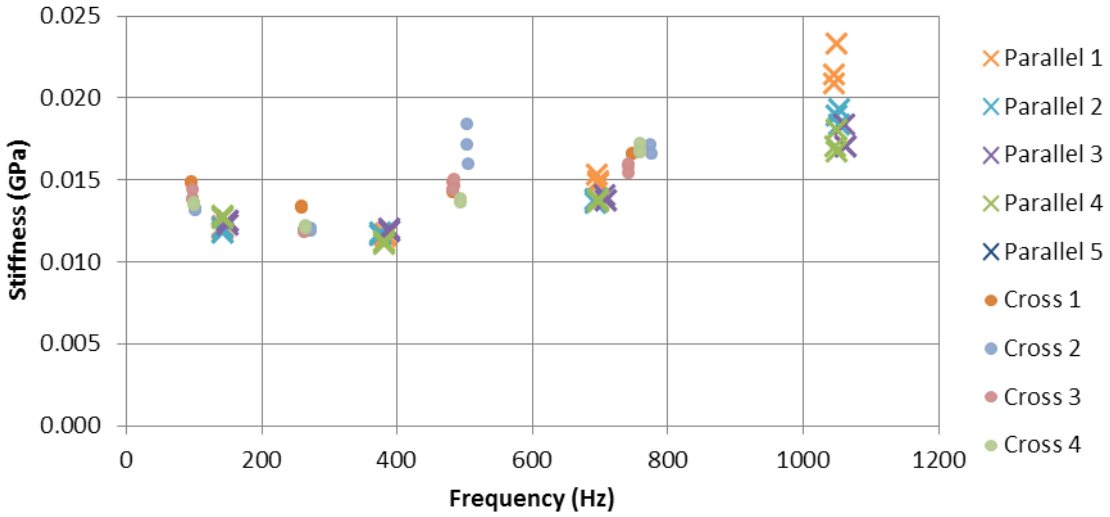

Figure C.23: Frequency dependent damping loss factor of 21 mm plywood, measured using free-free beam technique

Figure C.22. and Figure C.23. show the low frequency behaviour of the 12 mm plywood beams. An expanded frequency range is presented in Figure C.24. and Figure C.25. The two smaller beam lengths are 0.3 m and 0.4 m.

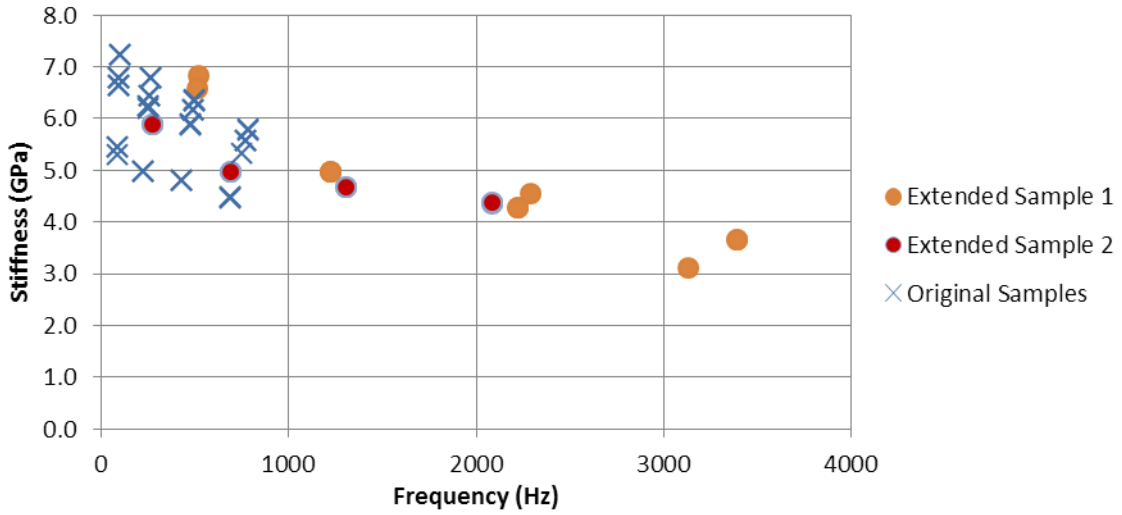

Figure C.24: Dynamic stiffness of 21 mm plywood beam in parellel to ply direction, measured over expanded frequency range.

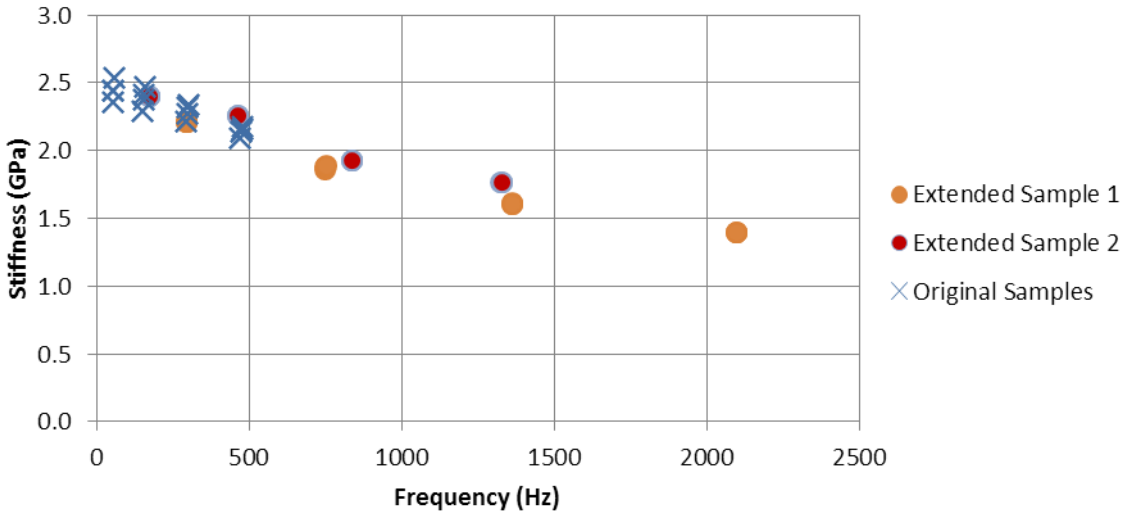

Figure C.25: Dynamic stiffness of 21 mm plywood beam in cross ply direction, measured over expanded frequency range.

Table C.16: Average stiffness and damping loss factor of 21 mm plywood

Damping Loss Factor – Cross Ply	0.014
Damping Loss Factor – Parallel to Ply	0.014
Geometric Mean of Damping Loss Factor	0.014
Stiffness – Cross Ply	2.9 GPa
Stiffness – Parallel to Ply	6.0 GPa
Geometric Mean of Stiffness Values	4.2 GPa
Surface Density	10.7 kg/m^2
Poisson's Ratio (Assumed)	0.3

Table C.17: Exponential curve for 21 mm plywood stiffness measurements; parameters of curve and goodness of fit data.

Cross Ply – Exponential Equation	$E_{cp}(f)3.63e^{-0.00035f}$ GPa
Cross Ply – r^2 value	0.77
Parallel to Ply – Exponential Equation	$E_{cp}(f) = 7.83e^{-0.00032f}$ GPa
Parallel to Ply – r^2 value	0.72

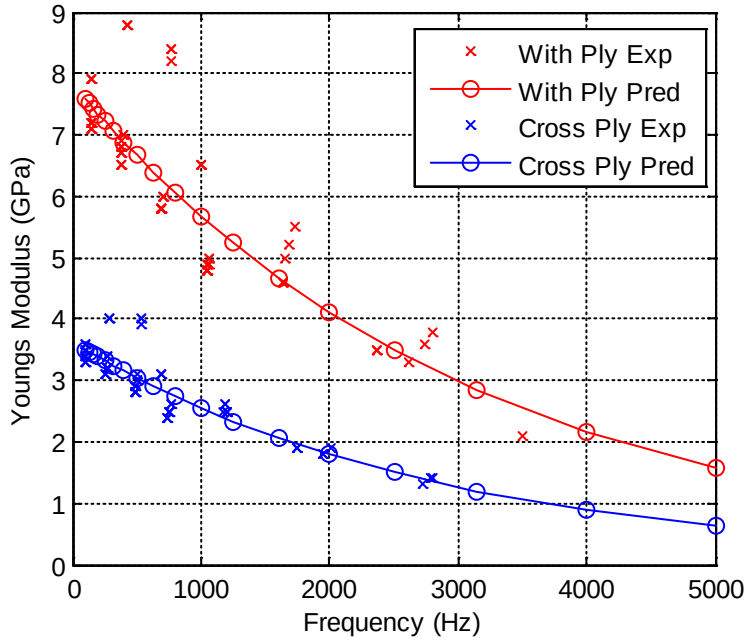

Figure C.26: Predicted stiffness of 21 mm plywood at 100 Hz – 5000 Hz one third octave band centre frequencies

C.8. Damped 12 mm Plywood

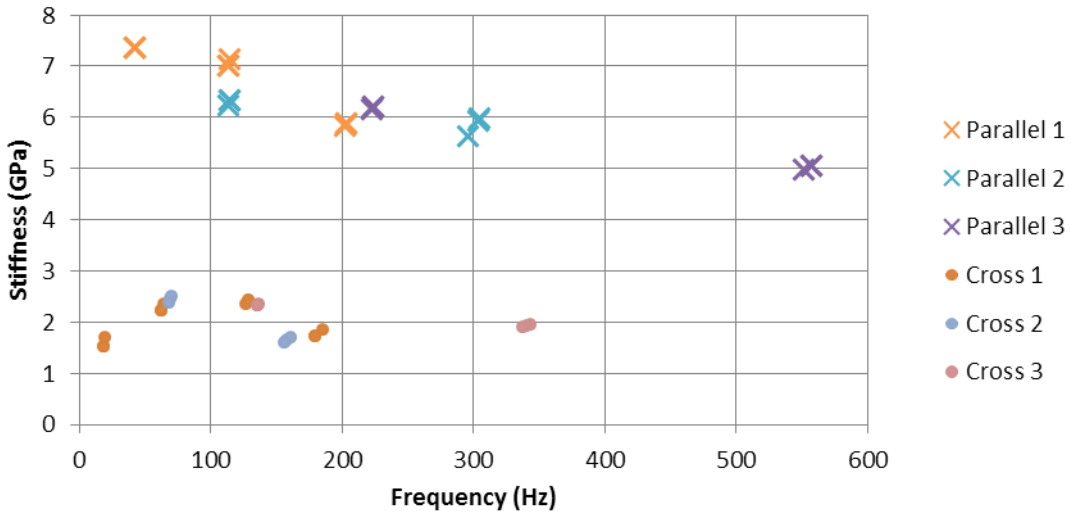

Figure C.27: Frequency dependent stiffness of damped 12 mm plywood, measured using free-free beam technique

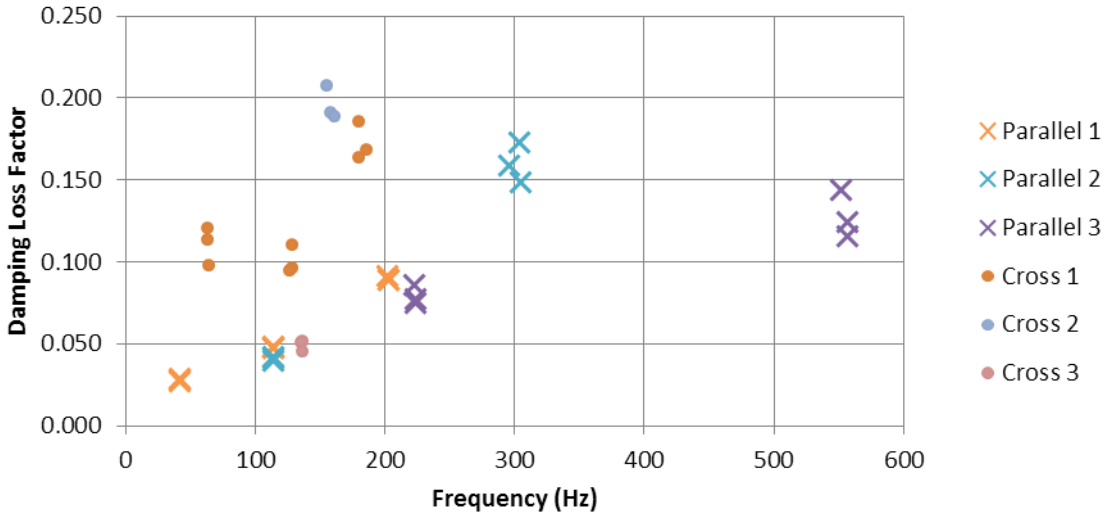

Figure C.28: Frequency dependent damping loss factor of damped 12 mm plywood, measured using free-free beam technique

Table C.18: Material properties of damped 12 mm plywood

Damping Loss Factor – Cross Ply	0.125
Damping Loss Factor – Parallel to Ply	0.082
Geometric Mean of Damping Loss Factor	0.101
Stiffness – Cross Ply	1.4 GPa
Stiffness – Parallel to Ply	6.2 GPa
Geometric Mean of Stiffness Values	2.9 GPa
Surface Density	3.8 kg/m2
Poisson's Ratio (Assumed)	0.3

Table C.19: Exponential curve for 7 mm plywood stiffness measurements; parameters of curve and goodness of fit data.

Cross Ply – Exponential Equation	$E_{cp}(f) = 57.8e^{-0.015f}$ GPa
Cross Ply – r^2 value	0.96
Parallel to Ply – Exponential Equation	$E_{cp}(f) = 13.53e^{-0.00022f}$ GPa
Parallel to Ply – r^2 value	0.22

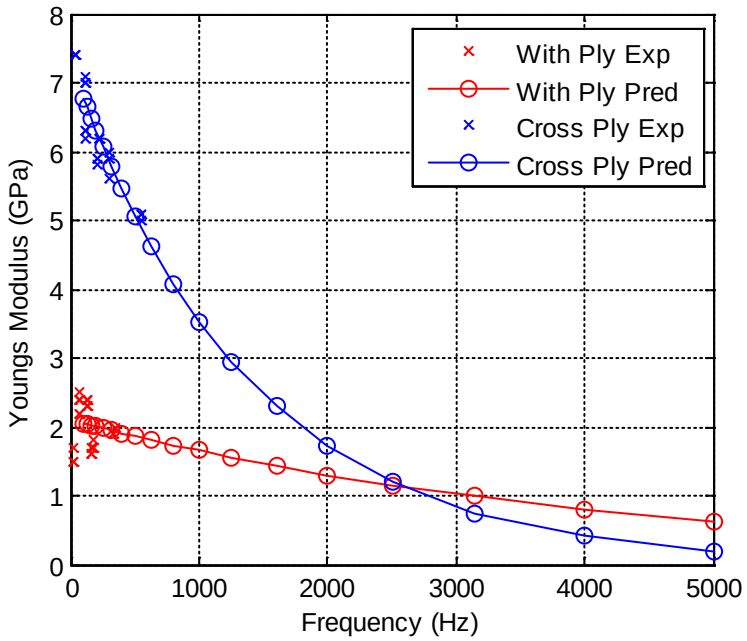

Figure C.29: Predicted stiffness of 7 mm plywood at 100 Hz – 5000 Hz one third octave band centre frequencies